

System-level metabolic effects of trematode infections in rodent models

Inauguraldissertation

zur

Erlangung der Würde eines Doktors der Philosophie

vorgelegt der

Philosophisch-Naturwissenschaftlichen Fakultät

der Universität Basel

von

Jasmina Saric

aus Neuhausen am Rheinflall

Schaffhausen

Basel 2010

Genehmigt von der Philosophisch-Naturwissenschaftlichen Fakultät auf Antrag von
Prof. Dr. Jürg Utzinger and Prof. Dr. Ian Wilson.

Basel, den. 14.10.2008

Prof. Dr. Eberhard Parlow
Dekan der Philosophisch-Naturwissenschaftlichen Fakultät

To my Family

„C'est l'esprit qui mène le monde”

Antoine de Saint-Exupéry

„Es ist der Geist, der die Welt bewegt“

Antoine de Saint-Exupéry

Table of contents

◆ Summary	12
◆ Zusammenfassung	16
◆ Acknowledgments	20
◆ Scientific partners	24
1 Introduction	28
1.1 Food-borne trematodiasis	28
1.1.1 General aspects	28
1.1.2 Echinostomiasis	30
1.1.3 Fascioliasis	32
1.2 Schistosomiasis	34
1.3 The metabolic profiling approach	37
1.4 Spectroscopy	39
1.4.1 NMR spectroscopy	39
1.4.2 Magic Angle Spinning	42
1.4.3 Mass Spectrometry	42
1.5 Chemometric analysis	44
1.5.1 Principal components analysis	44
1.5.2. Partial least squares analysis	45
1.5.3. Statistical total correlation spectroscopy	47
1.6 References	49
2 Goal and specific objectives	54

3	Species variation in the faecal metabolome gives insight into differential gastrointestinal function	56
3.1	Abstract	57
3.2	Introduction	57
3.3	Material and Methods	58
3.3.1	Faecal Sample Collection.	58
3.3.2	Exploration of Metabolic Variation across Species	59
3.3.3	Exploration of Metabolic Variation with Age	59
3.3.4	Effect of Sample Preparation and Storage on the Metabolic Profile.	59
3.3.5	¹ H NMR Spectroscopic Analysis of faecal Samples	60
3.3.6	Data Analysis	60
3.4	Results	62
3.4.1	Composition of Metabolite Profiles	62
3.4.2	Impact of Species, Age/Time and Sample Preparation on the Metabolic Profile	62
3.4.3	Species Differences in Metabolic Profiles between Rat, Mouse and Man	63
3.4.4	Age-Related Metabolic Changes in Aqueous Faecal Extracts	67
3.4.5	Effect of Sample Preparation and Storage Conditions on Metabolic Profile on Faecal Extracts	70
3.5	Discussion	72
3.5.1	Inter-Species Differences in the Faecal Metabolite Profile	72
3.5.2	Influence of Age/Time on the Faecal Metabolite Profile	74
3.6	Acknowledgment	76
3.7	References	77

4	Use of <i>Echinostoma</i> spp. in studies on chemotherapy and metabolic profiling	82
4.1	Abstract	83
4.2	Introduction	84
4.3	Use of <i>Echinostoma caproni</i> in trematocidal drug discovery and development	86
4.3.1	Evaluation of Echinostomicidal activity <i>in vivo</i>	86
4.3.2	Drug sensitivity assay with <i>Echinostoma caproni in vitro</i>	87
4.3.3	Scanning electron microscopy (SEM) studies	88
4.3.4	Spectroscopy	90
4.4	Metabonomic investigation on <i>Echinostoma caproni</i> in the mouse model	90
4.4.1	What is metabonomics?	90
4.4.2	Experimental protocol	94
4.4.3	Biomarker identification and diagnostic potential of biofluids in an <i>Echinostoma caproni</i> infection	94
4.4.4	Biomarker identification in tissue <i>via</i> MAS ¹ H NMR spectroscopy	100
4.4.5	Changes in the intestinal profiles	103
4.4.6	Integrative metabonomics: an approach to understand host-parasite-gut microbiota interactions	106
4.5	Concluding remarks	108
4.6	Acknowledgements	109
4.7	References	110
5	Metabolic profiling of an <i>Echinostoma caproni</i> infection in the mouse for biomarker discovery	122
5.1	Abstract	123
5.2	Author Summary	124
5.3	Introduction	125
5.4	Materials and Methods	126
5.6	Results	131

Table of contents

5.7 Discussion	144
5.8 Acknowledgments	150
5.9 Author Contributions	150
5.10References	151
6 Trematode-induced modulation of CNS metabolic profiles	158
6.1 Abstract	159
6.2 Introduction	160
6.3 Materials and methods	161
6.4 Results	166
6.6 Discussion	171
6.7 Acknowledgment	178
6.8 References	179
7 Discussion	184
7.1 Potential biological matrices for diagnosis	185
7.2 Specificity of biomarkers	187
7.3 Analytical tools	189
7.4 Systems integration	190
7.5 Trematode impact on the host central nervous system	190
7.6 Immune response from a metabolic view	192
7.7 Conclusion	193
7.8 Future research	195
7.9 References	196
◆ Curriculum Vitae	202





◆ Summary

Background: Trematode infections impose a great burden on the developing world by impairing life quality, productivity and life span of an individual. The prerequisite for efficient treatment and control of the diseases is the use of a quick and sensitive diagnostic tool which could replace the multi-diagnostic approach that is still used. The metabolic profiling approach implies the use of spectroscopic tools such as nuclear magnetic resonance (NMR) spectroscopy and mass spectrometry (MS) on potentially interesting biofluids and tissues, and is coupled with multivariate mathematical data modelling. It has been applied to many different field of research, such as biochemistry, medical sciences, drug pathway discovery, non-communicable diseases, nutrition and psychological disorders, and has been established as an efficient method for biomarker recovery and pathway deciphering. There is growing interest in metabolic profiling in systems biology. The first attempt to bring together metabolic profiling with the epidemiology of neglected tropical diseases was in mid-2002, when urine samples were obtained from more than 500 individuals in a rural Western part of Côte d'Ivoire. However, it was impossible to extract any meaningful information with regard to specific parasitic infection. The high degree of metabolic variation of the studied population in terms of age, genetic and nutritional background and the fact that the majority of individuals harboured three or more parasites concurrently might explain this observation.

My thesis outline was put forward once the metabolic profiles of selected parasitic infections in suitable rodent models, namely *Schistosoma mansoni* and *Trypanosoma brucei brucei* in the mouse, and *Schistosoma japonicum* in the hamster, were established as an alternative to directly exploring human populations in order to ascertain if characteristic biomarkers of infection could be found for single host-parasite scenarios. The success of these experimental investigations encouraged further studies, including the extension of metabolic profiling to other host-parasite models, in order to gain insight into specificity of biomarkers and to reveal the diagnostic potential of this metabolic profiling approach.

Goal and objectives: The overarching goal of this Ph.D. project was to deepen our understanding of trematode-induced metabolic changes in selected rodent models, and to critically assess the potential of a metabolic profiling approach applied to biofluids and tissue samples for biomarker recovery that may contain diagnostic and prognostic properties.

The specific objectives were (i) to optimise faecal sample preparation for subsequent ^1H NMR spectroscopy, and to assess metabolic variation in faecal samples with regard to species (i.e. human, rat and mouse), gender and age, (ii) to assess longitudinally the biochemical changes

in urine, plasma and faecal water of *E. caproni*-infected mice, and to compare the diagnostic capacity of different biofluids collected from infected and uninfected control mice, (iii) to gain information about *E. caproni*-induced changes in selected tissue samples e.g. (liver, kidney, spleen, ileum, jejunum and colon) of infected mice and correlate identified biomarkers with the previously extracted markers in the biofluids, which might reveal infection-related systems level changes (iv) to evaluate the remote and direct impact of three different trematodes (*E. caproni*, *F. hepatica*, *S. mansoni*) on the rodent host neural metabolic composition.

Methods: *E. caproni*- and *S. mansoni*-infected mice and uninfected control mice and *F. hepatica*-infected rats and uninfected control rats were kept in the animal facilities of the Swiss Tropical Institute under environmentally-controlled conditions (temperature, 22°C; relative humidity, 60-70%; light/dark cycle, 12/12 hours). Animals were acclimatized for 1-2 weeks prior to infection, in order to avoid stress-induced deviations of the metabolic profiles. Urine, plasma and stool were usually sampled on a weekly basis for high resolution ^1H nuclear magnetic resonance (NMR) spectroscopic analysis and tissues removed (liver, kidney, splee, gut, brain) upon dissection of the animals at the end of each experiment for ^1H magic angle spinning (MAS) analysis. Biofluids were stored at -40°C and tissues at -80°C pending NMR analysis.

^1H NMR spectroscopy was applied for acquisition of all biofluids and brain extracts, whereas for all other tissues, ^1H MAS NMR, a semi-solid technique, was performed. Multivariate statistical methods were implemented on all spectral data, after pre-processing, in particular principal components analysis (PCA) and partial least squares-discriminant analysis (PLS-DA) with incorporation of orthogonal signal filtration in a MATLAB environment were utilised. Assignments of the spectral peaks were made from the literature and confirmed *via* statistical total correlation spectroscopy (STOCSY), or *via* standard 2-dimensional (2D) NMR experiments conducted on selected samples.

Findings: Comparing the diagnostic templates, all three biofluids showed interesting deviations between uninfected control and *E. caproni*-infected mice. Urine and plasma were considered as most suitable biofluids due to the large number of potential biomarkers identified and because faecal water showed high fluctuations in the metabolic concentrations over time and a high degree of variation from one animal to another which was significantly higher than in urine and plasma. More detailed metabonomic investigations were performed

with *E. caproni* to assess systems impact on the mouse host. Resulting changes in the metabolic profiles of biofluids and tissue samples were correlated with each other, and revealed new insights into the biological pathomechanisms of this trematode, e.g. impact on gut microbial species and a trematode-induced imbalance of the transporter system in the gut. Whereas *E. caproni* did not induce any biochemical changes in the neural profile, rats infected with *F. hepatica*, and mice infected with *S. mansoni* showed strong deviations from uninfected control animals. *F. hepatica*-induced changes in the rat brain nucleotide metabolism was correlated to certain cytokine levels, e.g. IFN- γ , IL-5 and IL-13, and was consistent with modulation of the immune mechanisms. This finding provides a rationale for deeper analysis into the interaction of parasitic worms with the central nervous system of the host organism.

Conclusion and outlook: The remaining questions which still need to be addressed revolve around how to transfer the technology of biomarker detection into human populations, whereas the main obstacles pose the effect of multiparasitism on biomarkers, the specificity and cross-species transferability. However, we are confident that this will be resolved with more thorough biomarker evaluation, cross-species comparisons, co-infection models in suitable rodents and well selected and monitored human populations with single-infections. With the additional acquisition of highly specific biomarkers of disease *via* MS-based methods, a database of single infection markers in rodents can be completed and offer a quantity of possible biomarker-candidates also in humans. Succeeding the leap from rodent to human, metabolic profiling could lead to a novel diagnostic tool, replacing the multi-diagnostic assay for the broad panel of tropical diseases.



◆ Zusammenfassung

Hintergrund: Trematoden-Infektionen stellen eine enorme Belastung für die Bevölkerung in Entwicklungsländern dar, durch eine Einschränkung der körperlichen und geistigen Fähigkeiten, der Produktivität und der individuellen Lebenserwartung. Eine akkurate und praktische Diagnostikmethode, welche die herkömmliche Multidiagnostik für Tropenkrankheiten, ersetzen könnte, ist die Voraussetzung für eine effiziente Behandlung und Infektionskontrolle.

Das Erstellen von metabolischen Profilen basiert auf der Analyse von biologischen Matrizen mit spektroskopischen Methoden, vor allem der nuklearen magnetischen Resonanzspektroskopie (NMR) und Massenspektrometrie (MS), welche mit multivariaten statistischen Datenanalysen gekoppelt werden.

Die Technik des metabolischen Profilierens wurde schon in vielen Naturwissenschaftlichen Disziplinen erfolgreich angewandt, vor allem in der Biochemie, Medizin, Pharmazie, Ernährung und Psychologie. Das metabolische Profilieren konnte als effiziente Methode für Biomarker Extraktion und Entschlüsselung von metabolischen Netzwerken etabliert werden und erfährt daher steigendes Interesse in der Systembiologie.

Der erste Versuch metabolisches Profilieren in einer epidemiologischen Studie über vernachlässigte tropische Krankheiten einzubauen wurde im Jahre 2002 unternommen. Es wurden 500 Urinproben in einem ländlichen Gebiet im Westen der Elfenbein Küste gesammelt und mittels ^1H NMR Spektroskopie analysiert. Die Interpretation der Daten gestaltete sich jedoch schwierig, da der Grossteil der Bevölkerung eine hohe inter-individuelle Variabilität in Bezug auf Alter, genetischem und ernährungsbedingtem Hintergrund aufweist und aufgrund der Tatsache, dass die meisten Individuen mit mindestens drei Parasiten infiziert waren.

Der Rahmen meiner Doktorarbeit wurde festgesetzt, nachdem die metabolischen Profile ausgewählter Parasiteninfektionen in passenden Nagetier-Modellen (*Schistosoma mansoni* und *Trypanosoma brucei brucei* in der Maus, und *Schistosoma japonicum* im Hamster), etabliert waren. Der Erfolg dieser drei Studien ermutigte uns die Profilierungsmethode auf andere Wirts-Parasiten Modelle auszuweiten, um einen Einblick in die Spezifität von Biomarkern zu gewinnen und um das diagnostische Potential der Methode zu evaluieren.

Allgemeines Ziel und spezifische Ziele: Das Hauptziel dieser Doktorarbeit war, einen tieferen Einblick in metabolische Veränderungen nach einer Trematodeninfektion im Nagetierwirt zu gewinnen. Das diagnostische und prognostische Potential, welches die neue Technologie der metabolischen Charakterisierung von biologischen Matrizen um Biomarker zu gewinnen birgt, sollte kritisch beurteilt werden.

Die spezifischen Ziele waren (i) Optimierung der Stuhlproben Präparation für ^1H NMR Spektroskopie und eine Untersuchung der Variabilität der Proben in Bezug auf Spezies (Mensch, Maus und Ratte), Geschlecht und Alter; (ii) Untersuchung von biochemischen Veränderungen in Urin, Plasma und Stuhlproben von *Echinostoma caproni*-infizierten Mäusen während des gesamten Infektionsverlaufs um die diagnostische Kapazität der drei biologischen Matrizen zu vergleichen; (iii) Erhalten von Information über *E. caproni*-induzierte Veränderungen in ausgewählten Geweben (Leber, Niere, Milz, Ileum, Jejunum und Kolon) um die darin gefundenen Biomarker mit den vorherig extrahierten Veränderungen in den Bioflüssigkeiten zu korrelieren um die holistische Auswirkung des Wurmparasiten im Wirtstier beschreiben zu können; und (iv) Evaluation von direkten und indirekten Auswirkungen von drei verschiedenen Trematoden (*E. caproni*, *Fasciola hepatica*, *S. mansoni*) auf das Zentrale Nervensystem (ZNS) des Nagetierwirts.

Methoden: *E. caproni*- und *S. mansoni*-infizierte Mäuse and nichtinfizierte Kontroll-Mäuse und *F. hepatica*-infizierte Ratten und uninfectierte Kontroll-Ratten wurden in den Tierräumen des Schweizerischen Tropeninstituts unter kontrollierten Bedingungen gehalten (Temperatur: 22°C; relative Feuchtigkeit: 60-70%; hell/dunkel Zyklus: 12/12 Stunden). Die Tiere wurden vor der Infektion für 1-2 Wochen akklimatisiert um Stress-induzierte Abweichungen der metabolischen Profile zu vermeiden. Urin, Plasma und Stuhlproben wurden üblicherweise einmal pro Woche für ^1H NMR Spektroskopie gesammelt und die Organe (Leber, Niere, Milz, Darm und Hirn) wurden während der Sektion für ^1H Magic Angle Spinning (MAS) Analysen entnommen. Urin, Plasma und Stuhlproben wurden bei -40°C und die Gewebe bei -80°C gelagert bis zu NMR Analyse.

Alle Bioflüssigkeiten und Hirnextrakte wurden mittels ^1H NMR Spektroskopie gemessen, während die Daten der Gewebe mittels ^1H MAS NMR, einer semi-soliden Technik, generiert wurden.

Alle prozessierten Daten wurden mit multivariaten statistischen Methoden analysiert, inklusive der Principal Components Analysis (PCA) und der Partial Least Squares-

Diskriminante Analyse (PLS-DA) mit inkorporiertem orthogonalem Signal Filter in MATLAB. Die spektralen Regionen wurden mittels Literatur bestimmt und mittels Statistical Total Correlation Spectroscopy (STOCSY) oder 2-dimensionalen (2D) NMR Experimenten bestätigt, welche an ausgewählten Proben durchgeführt wurden.

Resultate: Der Vergleich von Urin, Plasma und Stuhlproben auf diagnostische Tauglichkeit offenbarte interessante Unterschiede zwischen *E. caproni*-infizierten und nicht-infizierten Mäusen. Während Urin und Plasma als potentielle diagnostische Kandidaten, aufgrund einer hohen Quantität an gefundenen potentiellen Biomarkern und einer angemessenen biologischer Stabilität in Frage kommen, wurden Stuhlproben als am wenigsten geeignet eingestuft, da sie sowohl eine hohe Zeit-abhängige als auch inter-individuelle Variabilität zwischen den Mäusen aufweisen. Um ein detaillierteres metabolisches Gesamtbild von dem Effekt der *E. caproni*-Infektion zu erhalten, wurden die erhaltenen Veränderungen aller analysierten Kompartimente (Gewebe, Urin, Plasma und Stuhlproben) gemeinsam in Betracht gezogen. Dieses Gesamtbild eröffnete neue Einblicke auf die biologischen Auswirkungen des Parasiten, wie zum Beispiel den Einfluss auf die Zusammensetzung der Darmbakterien oder eine Trematoden-induzierte Inhomöostase des intestinalen Transportsystems.

Untersuchungen an Hirnextrakten von Mäusen, die mit *E. caproni* infiziert waren, zeigten keine Veränderungen, während die *S. mansoni*- und *F. hepatica*-Infektion in den entsprechenden Tiermodellen (Maus bzw. Ratte) einen deutlichen Einfluss auf das neuronale metabolische Profil nach sich zog. Die Veränderung in der zerebralen Nukleotid Komposition, verursacht durch den Leberegel *F. hepatica*, konnte mit den Konzentrationen bestimmter Zytokine (IFN- γ , IL-5 und IL-13) korreliert werden und scheint zugunsten von *F. hepatica* einen immunmodulatorischen Effekt auszuüben. Dies verdeutlicht wie fundamental die Untersuchung eines Parasiten-induzierten Effekts auf das Zentralnervensystem des Wirts ist.

Schlussfolgerung und Ausblick: Es bleibt immer noch zu klären wie einfach oder schwierig sich diese neu erworbenen Technik der Biomarker Identifikation auf humane Populationen übertragen lässt. Die hauptsächlichen Schwierigkeiten liegen hierbei an der Auswirkung der Multiplen-Infektionen auf die Marker sowie auf die Spezifität und Inter-Spezies Übertragbarkeit. Mit einer rigorosen Evaluation von potentiellen Markern für Diagnostik, Inter-Spezies Vergleichen, Ko-Infektionen im geeigneten Nagetiermodell und ausgewählten

Human Populationen mit Mono-Infektionen, kann man diese Hindernisse ausräumen. Mit dem Ausbau der Technologie mittels Hochauflösungs MS können zusätzlich hochspezifische Biomarker detektiert werden, wie z. B. Parasiten-sekretierte Enzyme, die normalerweise in sehr niedrigen Konzentrationen im Plasma oder den Exkrementen des Wirtes vorliegen und daher *via* NMR Spektroskopie nicht nachweisbar sind. Dies würde die Palette der Biomarker Kandidaten erweitern und gleichzeitig das Problem der Spezies-Übertragbarkeit lösen, da solche Marker nicht Wirtsabhängig sind.

Sobald die Übertragbarkeit auf den Menschen etabliert ist, könnte eine solche Biomarker Identifikations Strategie zu einer neuen Diagnostik Methode führen, welche, andernfalls als die herkömmlichen multiplen Nachweismethoden, multiple Fingerprints in einem Test kombiniert, und somit die wichtigsten Infektionskrankheiten abdeckt.

◆ Acknowledgments

Meeting Dr. Stefanie Granado by co-incidence at the Centre Suisse de Recherche Scientifique at Côte d'Ivoire in 2004 who kindly let me accompany her to Interviews about "palludism" determined my doctoral application at the Swiss Tropical Institute. Applying directly to the heart of the institution, Director Marcel Tanner and his, just as kind-hearted secretary Christine Walliser, I landed in Prof. Jürg Utzinger's group, who acted as my main supervisor for three years. Jürg, always encouraging, enthusiastic and trusting, made me put in most effort to thank him for my freedom and own responsibility. To be supervised by Jürg meant to be treated as an equal, scientifically reasonable person, worth to interact with and to listen to. I'm deeply grateful to him to have introduced me to the scientific world, at first the Department of Public Health and Epidemiology which is home to hugely inspiring people, doing fieldwork under challenging conditions at Côte d'Ivoire, Chad, Ethiopia, Laos or China. Dr. Barbara Matthys, Dr. Peter Steinmann, Dr. Tobias Ephraim Erlanger, Dr. Bianca Plüss, Daniel Weibel, D. Borna I. Müller, Dr. Salome Dürr, Dr. Rhea Tschopp, Thomas Fürst, Stefanie Knopp, Prof. Christian Lengeler, Prof. Jakob Zinstag, Tipi Mak, but also Irène Küpfer, Dr. Penelope Vounatsou, Ricarda Merkle, Margrit Slaoui, Werner Rudin and Lukas Camenzind left one or the other strong impression on me with their modesty, friendliness and courage and make STI such a special and warm place. I'm especially thankful to Prof. Jennifer Keiser for giving mental support the STI-laboratories and for being always a very practical and objective advisor, and also to Guy Riccio, Prof. Hans Peter Beck, Dr. Jacques Chollet and Prof. Reto Brun for their kindness and support.

My other scientific world was not quite what I expected. Applied at STI with the intention to do field work, I found myself at Imperial College London, standing at the reception of the Sir Alexander Fleming Building waiting for Dr. Yulan Wang who intended to guide me through a "Metabonomics" workshop. The first moment, we looked at each other a bit suspiciously but it didn't take me long to enjoy her hospitality and good sense of humour. Yulan became a dear friend over the past 3 years, and I can't thank her enough for her patience in the lab, her expert advice and her support in everyday life, and even though she's now Prof. Wang in far away Wuhan, she stays close.

Jia Li was supposed to be my collaborating student and the one person I would work closest with, for a long time. After three years of Ph.D. we have gone through a work intense time at STI, a winter of microbiology in Cork, feeling the Ireland blues, oral presentations in Strasbourg, many hotpots and a respectable amount of shared publications.

Acknowledgments

My first impression that this person might be too young and too different to become a real friend didn't prove true. I admire Jia's patience, wisdom and her scientific professionalism and I hope to stay close work wise and personally for many more years.

My second supervisor was Prof. Elaine Holmes. First she let me into her group, then in her house. I can't quite remember how I got to live with her for almost three years, but thanks to her, I felt home in both, the group at Imperial College and in the house in Hammersmith. There are many words describing Elaine but I cannot think of any but good ones. Her sharp mindedness, intelligence and her spirit come along with generosity, tolerance and lovability and make her an exceptional character and a role model for me in scientific as well as personal aspects.

The Department of Biomolecular Medicine at Imperial College seems to attract a special kind of people, which are highly capable, professional, brave, creative, and witty. Dr. Christina Legido-Quigley, Dr. Francois P. Martin, Dr. Olivier Cloarec, Dr. Tsz M. Tsang, Dr. Magda Bictash, Jake M. Pearce, Dr. Ivan Yap, Dr. Olaf Beckonert, Dr. Matthias Rantalainen, Dr. Timothy Ebbels, Dr. Kirill Veselkov, Dr. Jake G. Bundy, Dr. Richard Barton, Dr. Elizabeth Want, Dr. Andrew Clayton, Dr. Ruey L. Loo, Dr. Muireanne Cohen, Dr. Toby Athersuch, Dr. Hector Keun, Nahid Ashby, Prof. John Lindon, Prof. Nigel Gooderham and finally Prof. Jeremy Nicholson who brought this impressive group into existence, make it a pleasure to be a part of it.

Although Macclesfield and Cork were missing the London internationality, it is always a pleasure to interact intellectually with Prof. Ian Wilson whose *esprit* and nice madness are enlightening AstraZeneca and with Dr. Julian Marchesi whose enthusiasm was a candle in the Irish December weather. I also thank the people in both facilities for their support; Prof. Georgios Theodoridis, Dr. Eleni Gika, Dr. Frieda Teichert and Filippos Michopoulos at AstraZeneca and Dr. Pauline Scanlan and Dr. Sharon Lawton at University College Cork and, last but not least Prof. Stefan Dirnhofer at Basel University who did the Histological survey for the parasite-animal models with Austrian diligence.

Financial support I am greatly thankful for the financial support from the Reisefonds of the University of Basel which enabled me to attend the Gordon Conference on Parasite-Host interaction in June 2008 in Newport US, which definitely opened new future research perspectives. I also thank the Dissertationsfonds of the University of Basel for contributing to the print costs of the thesis.





◆ **Scientific partners**

Swiss Tropical Institute: The planning of the parasite rodent models, the establishment of the infection and the sample collection have been performed in the laboratories of STI, within the research groups of Prof. Jürg Utzinger and Prof. Jennifer Keiser at the Department of Epidemiology and Public Health, and the Department of Medical Parasitology and Infection Biology, respectively. *E. caproni* metacercariae have been kindly provided by Prof. Bernard Fried; Lafayette College, Easton, PA, United States of America and *F. hepatica* metacercariae have been purchased from Gordon Graham, UK.

Imperial College: The present Ph.D. project was conducted in intense collaboration with Prof. Elaine Holmes and Prof. Jeremy K. Nicholson who acts as head of the Department of Biomolecular Medicine at Imperial College London. Biofluids and tissues from all parasite-rodent models were taken to IC, where sample preparation and data acquisition *via* ^1H NMR spectroscopic experiments has been performed in the spectrometer facilities of the Department of Biomolecular Medicine. Multivariate statistical analysis programs were accessed *via* departmental licenses and applied on the NMR spectra after pre-processing of the data with in-house developed scripts in a MATLAB environment.

Astrazeneca: To complete the NMR-spectral data set of the *E. caproni*- and the *F. hepatica*-infection models with MS-derived biomarkers, I spent some very inspiring and learning-intensive weeks at AstraZeneca at the Macclesfield site under supervision and support of Prof. Ian Wilson.

University College Cork: Additional studies on the impact of *E. caproni* and *F. hepatica* infections on the host gut microbial composition have been done *via* polymerase chain reaction (PCR) and denaturing gradient gel electrophoresis (DGGR) with help of Dr. Julian Marchesi and his group members at the Department of Microbiology at the University College Cork (UCC), Cork, Ireland.

Basel University: Prof. Stefan Dirnhofer at the Institute for Pathology at Basel University, finally provided us with his histological know-how by analyzing various tissues for our experiments in shortest time, and made the production of the slices even possible.



Scientific collaboration [<http://maps.google.co.uk/>]





1 Introduction

1.1 Food-borne trematodiasis

1.1.1 General aspects

Infections with food-borne trematodes have been reported worldwide, but the highest prevalence are found in Southeast Asian countries (e.g. Thailand, Laos and the Philippines) (Keiser and Utzinger, 2007b). A map of the distribution of the main food-borne trematodes is shown in Figure 1.1 (Keiser and Utzinger, 2007b). More than 10% of the world's population is at risk of food-borne trematodiasis and the estimated number of infections in 2004 was 40 million (WHO, 1995). Endemic regions face infection-related losses in productivity and actual working hours, impaired mental development in schoolchildren and a lowered life quality in general (Dickson *et.al.*, 2000; Fried *et.al.*, 2004; Keiser and Utzinger, 2004; Urbani and Palmer, 2001). Food-borne trematodiasis are not only a direct burden on the human population, but also pose, as zoonotic diseases, a remarkable veterinarian problem and are, hence, responsible for huge economic loss (Anantaphruti, 2001; Gajadhar *et.al.*, 2006).

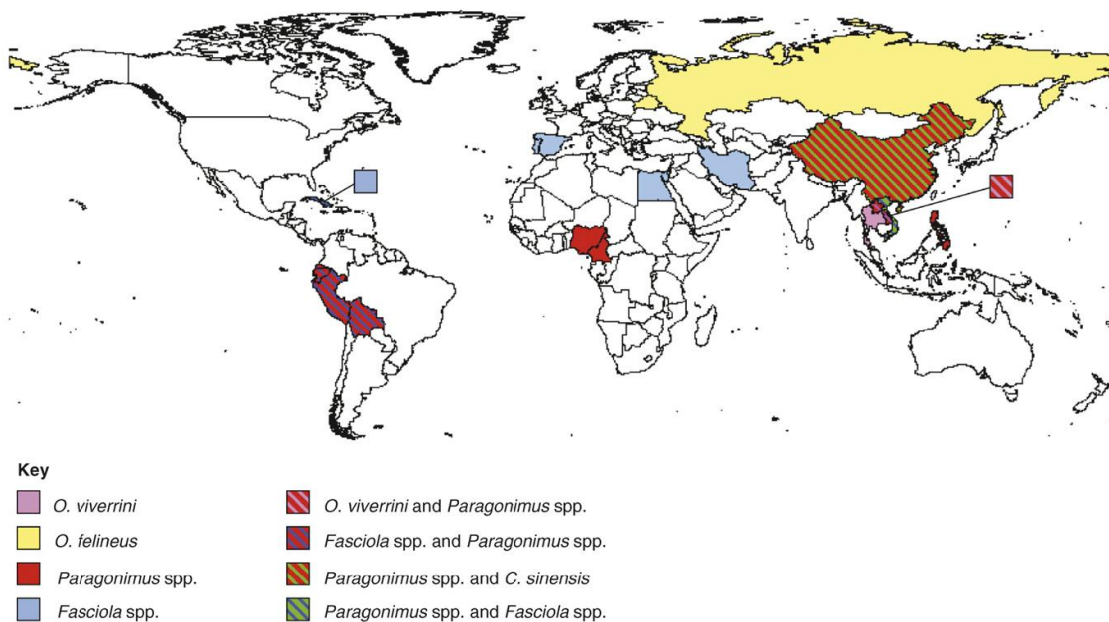


Figure 1.1. Map of distribution of the major food-borne trematodes [Keiser 2007]

Despite efforts to reduce infection prevalence, food-borne trematodiasis is far away from being controlled, much less eliminated, but rather is being considered as an emerging global health problem (Chai *et.al.*, 2007; Mas-Coma *et.al.*, 2005; Saijuntha *et.al.*, 2007).

Food-borne trematodiasis belongs to the so-called neglected tropical diseases (NTDs) (Hotez *et.al.*, 2006; Sripa, 2008). The NTDs include currently 14 diseases, most of them listed also by the World Health Organisation (WHO), such as Chagas disease, cholera, dengue haemorrhagic fever, human African trypanosomiasis, leishmaniasis, leprosy and schistosomiasis. NTDs are particularly rampant in rural settings in developing countries characterised by poor sanitation and health care. Importantly, the majority of the NTDs have been controlled or have been eliminated locally in industrialised countries and do not have an epidemic or pandemic capacity due to their geographical restriction.

The epidemiology and global distribution of food-borne trematodiasis has changed in the last decades. Hygiene education, more efficient drug treatment with broad-spectrum anthelmintic drugs, the use of chemical fertilisers and food control contributed to reduced infections in urban industrialized Asian cities, whereas increasing population density with lack of improved sanitation, increasing production of fish in aquaculture and sustained malnutrition lead to increased burden in some endemic regions, and opened up new endemic locations (Keiser and Utzinger, 2004; Keiser and Utzinger, 2005).

Trematodes belong to the phylum of plathelminthes, characterised by a flat shape, bilateral symmetry, lack of segmentation and the presence of an oral and ventral sucker. Most trematodes are endoparasitic, hermaphroditic worms with complex life cycles, often including several intermediate and one (or several) definitive host(s). The classification of the flukes is mainly based on the physiological location in the host organism, which include liver (*Fasciola* spp., *Clonorchis* spp. and *Opisthorchis* spp.), blood (*Schistosoma* spp.), lung (*Paragonimus* spp.) and the gut, which offers habitat for a reported 70 species (Fried *et.al.*, 2004) amongst which are *Echinostoma* spp. and *Fasciolopsis* spp..

The effects of food-borne trematodes on their host mainly depend on the location of the mature worms, but also on infection intensity, whereby with low numbers of worms the host remains asymptomatic, large infection burdens induce a high morbidity. Most noticed infections induce inflammation and eosinophilia due to constant irritation by the eggs or the worm itself, inducing acute and chronic pathology. The main symptoms of intestinal fluke infections, caused by *Echinostoma* spp., include diarrhoea, ulceration of the bowels mucosa

and abdominal pain. The liver flukes (*C. sinensis*, *F. hepatica*, and *O. viverrini*) can directly damage the liver tissue and induce jaundice. Furthermore, the development of a cholangiocarcinoma has been associated with chronic infection with *C. sinensis* and *O. viverrini* (Srivatanakul, Sriplung et al. 2004). *Paragonimus* spp., residing in the lung, cause chest pain, remittent fever and a chronic productive cough containing the eggs of the parasite (Liu *et.al.*, 2008).

Diagnosis of a food-borne trematode infection is based on examination of stool (or sputum in the case of *Paragonimus* spp.) samples under a microscope for detection of parasite eggs, the polymerase chain reaction (PCR), immunological and molecular methods, such as the enzyme-linked immunosorbent assay (ELISA), whereby PCR and ELISA show a high level of cross-reactivity between different trematode species and require trained personnel and relatively sophisticated and costly equipment (Bergquist *et.al.*, 2009; Bergquist, 2008; Kumar *et.al.*, 2008; Muller *et.al.*, 2007). Detection of parasite eggs in faeces, on the other hand can be unreliable, as eggs are missed out particularly in early stages of infection or at light infection intensity (Keiser and Utzinger, 2004; Upatham and Viyanant, 2003).

1.1.2 Echinostomiasis

Human echinostomiasis poses a burden in Southeast Asia and the Far East, mainly where high prevalences of infection have been reported. A study in the Indonesian Lake Lindu Valley revealed average infection-prevalences of 42.6% amongst the population (Carney, Sudomo 1980). Reports of infection-prevalences from Taiwan range from 11% to 65% (Carney 1991), whereas an average prevalence of 5% was reported in the Chinese Guangdong and Fujian provinces ((Li, 1991). Transmission is related to the consumption of raw or undercooked freshwater food and the use of night soil (human excrements) as fertilizer in fishponds which goes hand-in-hand with socio-economic factors including malnutrition, poverty and lack of hygiene education. Furthermore, population explosion leads to an increased aquaculture and a growing free-food market, hence wider distribution of metacercariae-infected aquatic food products. Control of the disease is also difficult, as the human cycle operates along with a separate, silvatic lifecycle, which keeps inflectional reservoirs maintained (e.g. intermediate hosts and eggs in freshwater bodies) (Graczyk and

Fried, 1998; Toledo and Fried, 2005). Adult echinostomes live in the intestine and bile duct of a wide variety of vertebrate hosts, mainly aquatic and semi-aquatic mammals and birds.

E. caproni, which is used in the present experimental set-up, inhabits the ileum and jejunum in the small intestinal part of the mouse host and undergoes an anterior shift towards jejunum/duodenum with growing age, e.g. 8 weeks (Fried and Huffman, 1996).

The life cycle of *E. caproni* is shown in Figure 1.2 The life cycle follows the typical pattern of the food-borne trematodes, and includes two intermediate hosts. Fertilized eggs are released by the main host faeces into freshwater bodies (1) where they develop into miracidiae (3) after approximately 2 weeks at temperatures between 22 and 28°C. The miracidiae hatch preferably in the late morning hours and actively penetrate the foot region of the first intermediate host, which is an aquatic snail (4), the main species of which belong to *Biomphalaria* spp. and *Lymnaea* spp. (Huffman and Fried, 1990). After transformation into sporocysts (4A) and then rediae (4B) in the heart region, and migration to the digestive gland-gonade complex, the developing cercariae (4C, 5) emerge from the first intermediate host and infect the kidney region of the second intermediate host, which can be the same or other snail species or *Rana* tadpoles (grown freshwater fish, respectively). The developing metacercarial cysts (6), in turn, are taken up with consumption of the second intermediate host by the main host (Huffman and Fried, 1990), in which the metacercariae encyst in the duodenum (7). Juvenile and adult *E. caproni* reside in ileum and jejunum, and shift with age towards duodenum (8). The maturation and residence of the fluke in the gut of the main host can induce pathology, particularly with high infection-burdens. Human echinostomiasis is characterised by diarrhoea, abdominal pain, eosinophilia, edema and anorexia, particularly among individuals with heavy infection intensity and can damage the intestinal mucosa, by causing catarrhal inflammation and erosions. Light infections, on the other hand, induce mainly gastric pain and anaemia (Graczyk and Fried, 1998). The presence of the fluke in the small intestinal part (e.g. ileum, jejunum) of the host can result in gut architectural changes in the mouse, such as villi fusion, erosion and crypt hyperplasia (Toledo and Fried, 2005) as well as intestinal dilation (Balfour *et.al.*, 2001). A number of compounds are available with echinostomicidal activity, whereby praziquantel is the most effective. The benzimidazoles, (e.g. albendazole and mebendazole) also have some effect (Cross and Basaca-Sevilla, 1986; Keiser and Utzinger, 2004; Pungpark *et.al.*, 1984). A panel of new active substances has been tested at the Swiss Tropical Institute in *in vitro* and *in vivo* studies.

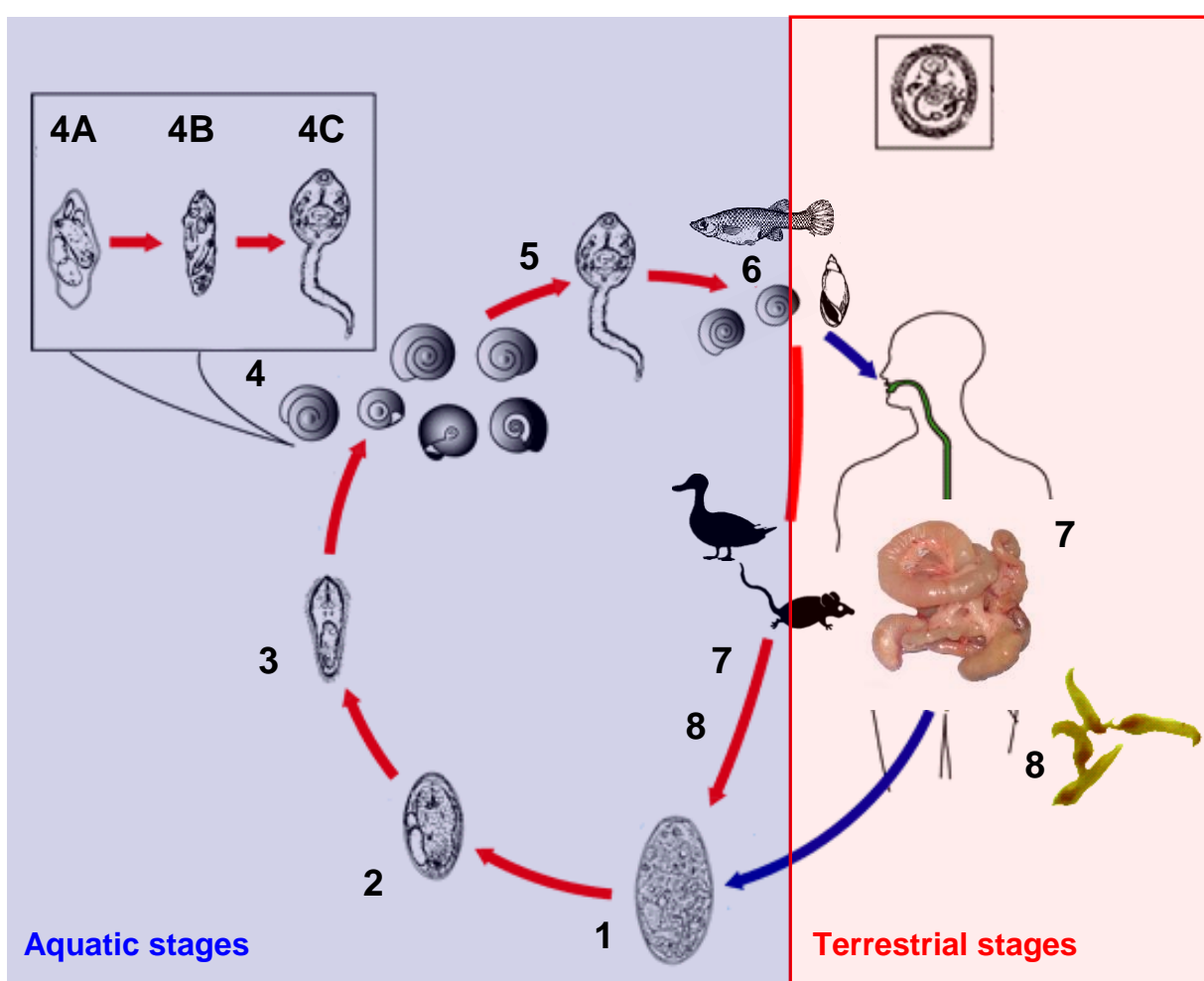


Figure 1.2. Life cycle of *E. caproni* [adapted from CDC; <http://www.dpd.cdc.gov/dpdx/HTML/Fasciolopsiasis.htm>; accessed September 2008]

Tribendimidine, the synthetic peroxide, OZ78 and two derivatives of artemisinin (i.e. artesunate and artemether), achieved high worm burden reductions after a single oral dose administered to *E. caproni*-infected mice (Keiser *et.al.*, 2006a; Keiser *et.al.*, 2006c; Keiser *et.al.*, 2006d). This high efficacy holds promise for the development of alternative drug treatments and emphasise broader experimental examination including clinical trials.

1.1.3 Fascioliasis

Fascioliasis a worldwide veterinarian, and to a lesser extent human problem and is caused mainly by infection with *F. gigantica* and *F. hepatica*. Whilst the former is geographically restricted to South America and Africa, the latter shows a broader geographical distribution. An estimated 2.4 million people suffer from fascioliasis and 180 million individuals live in

endemic regions (Mas-Coma, 1998). Like most food-borne trematode infections, also fascioliasis has changed its distribution pattern in the last decades, particularly due to migration, urbanisation and new irrigation programmes (Keiser and Utzinger, 2005; Mas-Coma *et.al.*, 1999). Most human infections are reported from the Andean highlands of Peru and Bolivia, Iran and Egypt (Bjorland *et.al.*, 1995; Haseeb *et.al.*, 2002; Stork *et.al.*, 1973).

The importance of fascioliasis as veterinarianian problem in countries with high dependence on livestock production cannot be overemphasised, as infected sheep and cattle suffer from anorexia, anaemia and weight loss, which in turn leads to a massive productivity loss of milk, meat and wool.

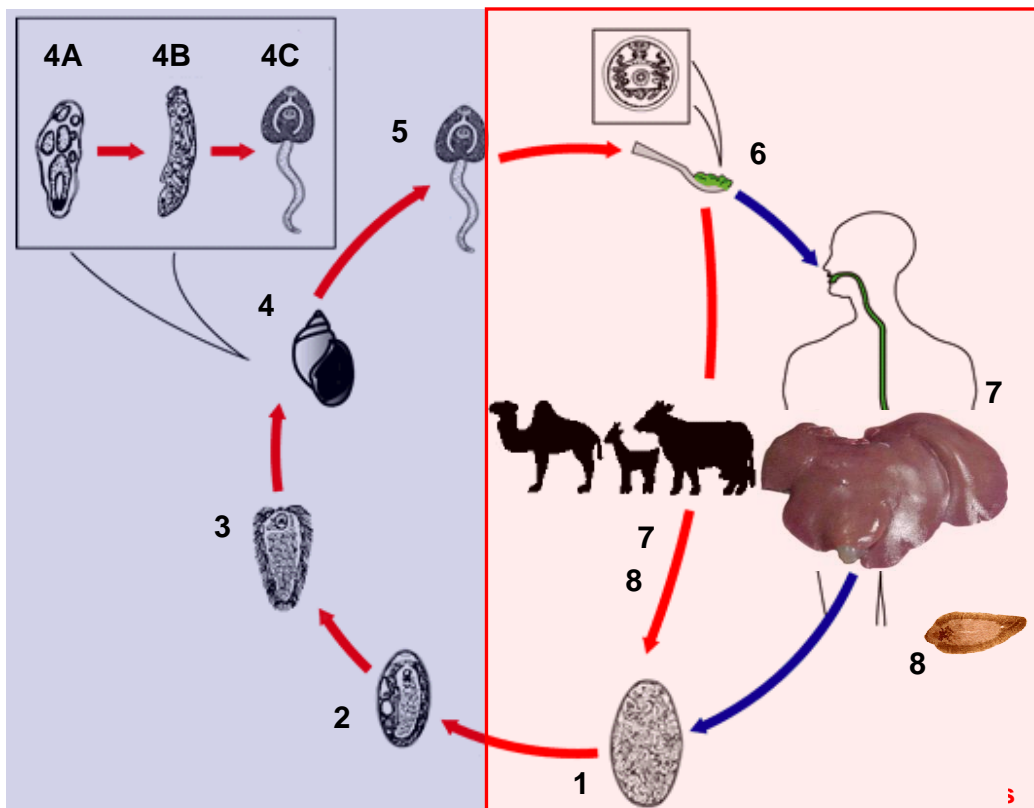


Figure 1.3. Life Cycle of *F. hepatica* [adapted from CDC; <http://www.dpd.cdc.gov/dpdx/HTML/Fascioliasis.htm>; accessed September 2008]

The life cycle of *F. hepatica* (Figure 1.3) deviates slightly from that of *Echinostoma* spp. and is simpler as it only includes one intermediate host snail, e.g. *Galba truncatula* (Flynn *et.al.*, 2007). Encystment of the free-swimming cercariae (5) happens on freshwater vegetation, e.g. lettuce or watercress, where the infective stage, the metacercariae (6), is taken up by the

mammalian host. The metacercariae encyst in the intestinal lumen (7), penetrate the gut wall and enter the perivisceral cavity, where they start migrating towards the liver (8). Once the juvenile flukes reach the liver, they burrow through the hepatic tissue for 5-7 weeks and feed on the parenchymal cells, which causes massive mechanical liver damage including extensive haemorrhages and fibrosis. Residence of the adult worms in the bile ducts induces anaemia and hyperplasia (Lim *et.al.*, 2007). Infection with *F. hepatica* is characterised by two different stages of pathology; whereas the acute stage is induced by the inflammation of the liver, as reaction to the migration of the larval stages and includes epigastric pain, fatigue and fever (Saba *et.al.*, 2004). The second, or biliary stage, is caused by the residence of the mature fluke in the bile ducts and their waste products and are characterised by jaundice, abdominal pain and biliary cholic.

The current drug of choice against *F. hepatica* and *F. gigantica* infection is triclabendazole. Emetine as an alternative treatment can resolve in serious adverse effects and albendazole and mebendazole did not show activity against the liver fluke (Keiser and Utzinger, 2004). Artemether and OZ78 were also assessed for *in vivo* activity against *F. hepatica* in a series of experiments, and showed promising results (Keiser *et.al.*, 2008; Keiser *et.al.*, 2006b; Keiser and Utzinger, 2007a). Most interestingly, single administrations of both drugs in rats infected with *F. hepatica* triclabendazole-resistant strains showed 100% clearance of the worms (Keiser *et.al.*, 2007).

1.2 Schistosomiasis

It is estimated, that 779 million people are at risk of schistosomiasis and a 207 million individuals are infected with one or possibly two of the five human pathogens, namely *S. haematobium*, *S. intercalatum*, *S. japonicum*, *S. mansoni* and *S. mekongi* (Chitsulo *et.al.*, 2000; Manzella *et.al.*, 2008a; Manzella *et.al.*, 2008b; Steinmann *et.al.*, 2006). The global burden due to schistosomiasis has been estimated at 1.7 up to 4.5 million disability-adjusted life years (DALYs) (Brooker and Utzinger, 2007; Hotez *et.al.*, 2006). The geographical distribution of schistosomiasis covers 74 countries, mainly in Africa and Asia (Chitsulo *et.al.*, 2000) (Figure 1.4).

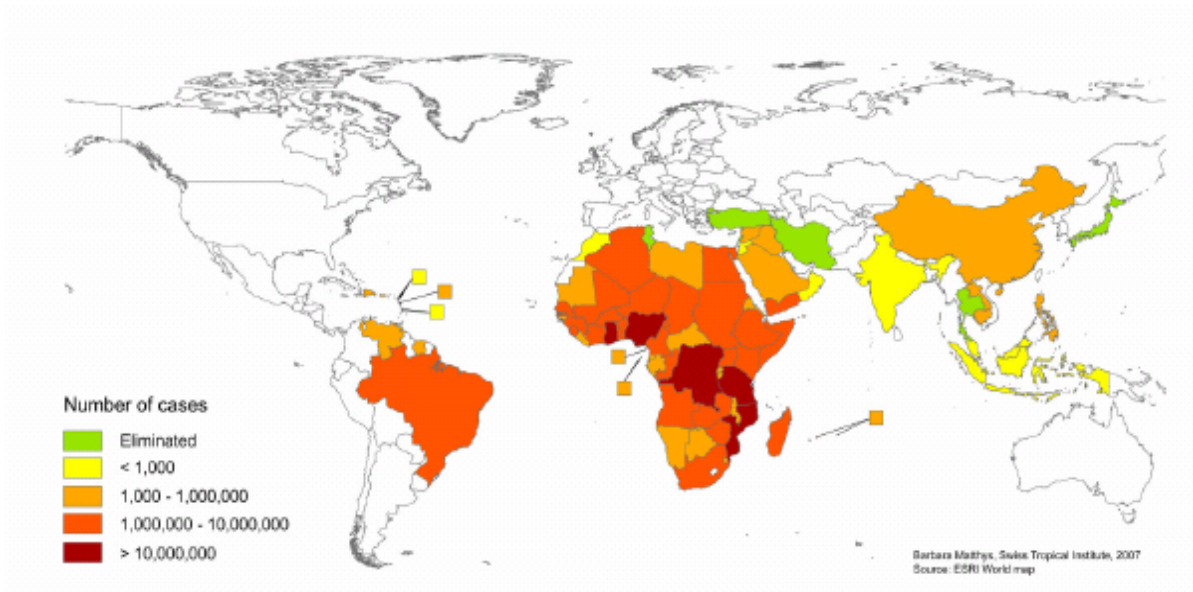


Figure 1.4. Global geographical distribution of schistosomiasis [Steinmann et.al., 2006]

Similar to the distribution of *F. hepatica*, also *S. mansoni* underwent an increase in the last decades mainly due to water resources development projects (small and large dams and irrigation schemes) to meet the agricultural need of the growing population density (Chitsulo *et.al.*, 2000).

Undetected, sub-clinical infection with schistosomes can lead to non-specific manifestations, which impose a burden on the individual, including impaired cognitive development of children, undernutrition and growth stunting, infertility, increased susceptibility to co-infection, energy decrease and a resulting decrease in work output (King and Dangerfield-Cha, 2008).

The main difference between the life cycle of schistosomiasis (Figure 1.5) and the food-borne trematodes, is the transmission to the main host. After the miracidiae hatch from the eggs (1,2), they penetrate the intermediate host snail, which is a *Biomphalaria* species (3) in the case of *S. mansoni*, and develop into cercariae with a bifurcated tail (5). After evasion from the snail into freshwater bodies, the cercariae are able to actively penetrate the skin of the main host (6), where they undertake a body migration passing the lung and moving further to the liver where they transform into schistosomula (7). This last premature stage continues migration *via* blood circulation (8) to the liver, where they mature into adults (9) and finally reach their determined tissue of residence such as the mesenteric veins for *S. mansoni* adults where oviposition commences (10).

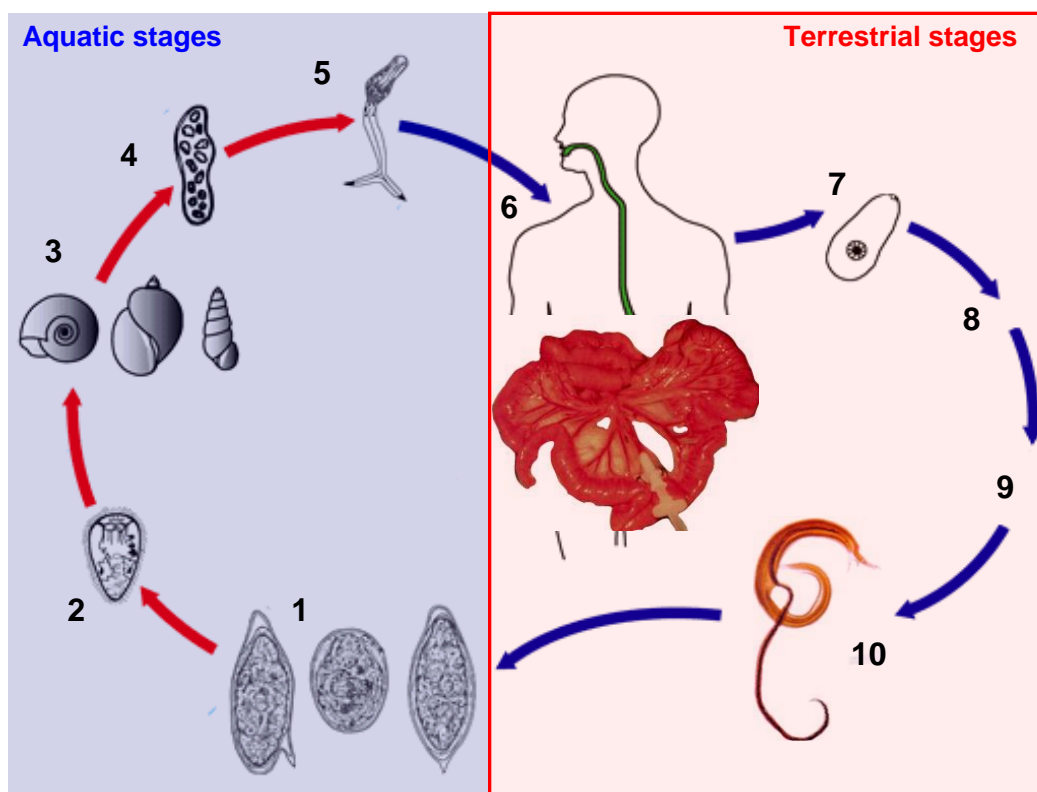


Figure 1.5. Life cycle of *S. mansoni* [adapted from CDC; <http://www.dpd.cdc.gov/dpdx/HTML/Schistosomiasis.htm>; accessed September 2009]

In contrast to other trematodes, which are hermaphrodites, the schistosome sexual reproduction organs are distributed to male and female individuals. The female has a thinner and longer shape and is constantly embedded in the gynaecophoric channel which the male forms (Gryseels *et.al.*, 2006). In the African species (*S. mansoni* and *S. haematobium*), the female produces hundreds of eggs per day, whereas the oriental species, *S. japonicum* has a 10-fold higher egg output, which is an important issue for understanding the pathophysiology of schistosomiasis.

The different stages of the schistosome induce different pathological reactions. The penetration of the host skin by the cercariae can induce urticarial rash and itching. The so-called “Katayama fever” represents the acute form of schistosomiasis and is caused by the migration of the immature worms. Fever, eosinophilia, fatigue and non-productive cough reflect the induced systemic hypersensitivity reaction (Gryseels *et.al.*, 2006). Chronic infection establishes due to egg output of the female. Eggs can get trapped in various body compartments, such as liver, spleen, cerebrospinal system and can, due to their metabolic

activity e.g. secretion of proteolytic enzymes, induce inflammatory reactions followed by tissue necrosis and granuloma formation around the eggs. Tissue replacement by fibrotic deposits implicates tissue architectural changes and impairment of blood flow (Gryseels *et.al.*, 2006; Manzella *et.al.*, 2008a).

Praziquantel is the drug of choice against schistosomiasis, whereas derivatives of artemisinin are active against the immature stages (Utzinger *et.al.*, 2007). There are ongoing drug studies to extend the arsenal of treatments against schistosomiasis (Xiao *et.al.*, 2007), which are urgently required as it is dangerous to rely on only one drug, particularly in terms of resistance development.

1.3 The metabolic profiling approach

Metabonomics is a “quantitative measurement of time-related multiparametric metabolic responses of multicellular systems to pathophysiological stimuli or genetic modification” (Nicholson *et.al.*, 1999)

The combination of spectroscopic methods with a multivariate statistical approach has opened up a complete new way of understanding systems based on biochemical conditions and introduced a complementary chapter to the other main –omics sciences; namely genomics, proteomics and transcriptomics (Holmes *et.al.*, 2008b; Lindon *et.al.*, 2006; Nicholson, 2006; Nicholson *et.al.*, 2005). Starting off successfully with biomarker extraction in models of toxicity or infection (Allwood *et.al.*, 2008; Coen *et.al.*, 2003; Martin *et.al.*, 2006; Saric *et.al.*, 2008; Wang *et.al.*, 2004; Wang *et.al.*, 2008; Wang *et.al.*, 2006), psychological disturbances (Allwood *et.al.*, 2008; Denkert *et.al.*, 2006; Holmes *et.al.*, 2006; Tsang *et.al.*, 2006), nutritional deviations (Holmes *et.al.*, 2008a) or non-communicable diseases, such as heart disease (Ordovas and Mooser, 2006), the metabolic profiling approach has proven to be highly efficient, reproducible and to offer a myriad of new biological insights. The amount of possible matrices is almost as wide as the fields the approach can be possibly applied and include biofluids (urine, plasma, faecal water, cell extracts), semi-solids, such as sperm or bacterial colonies, tissue, bone/cartilage and also synthetic material. The basic metabolic profiling approach is so well established and robust nowadays, that the extracted biochemical knowledge can be integrative completed with data from additional analytical platforms, such as PCR, degrading gel electrophoresis (DGGE) (Li *et.al.*, 2008) or

ELISA in order to link gut microbial changes and deviating cytokine levels (unpublished data) respectively, to underlying metabolic conditions.

Amongst all spectroscopic techniques, ^1H nuclear magnetic resonance (NMR) spectroscopy has proved to produce the quantitatively highest amount of definable metabolic markers. Thus far this technique has been used for decades in structural biochemistry and molecular biology for matrices with very low component diversity, and has mainly served the purpose of molecular structural identification (Fiorito *et.al.*, 2008). Only with the development of multivariate statistical analysis methods did it become possible to deal with inter-group differences between the spectra of urine, plasma or tissue, which contain thousands of partially overlapping resonances. Other spectroscopic techniques commonly used for metabolic profiling include MS, which has an inherent higher sensitivity than NMR spectroscopy and is most efficient when coupled to preceding separation methods, such as high-performance and ultra-performance liquid-chromatography (HPLC-MS/UPLC-MS) and gas chromatography (GS-MS) or capillary electrophoresis (CE-MS). Although, MS is not yet as well-established for biomarker recovery purposes as ^1H NMR spectroscopy, it is essential for structure elucidation and it also bears the potential to become a crucial tool in the recovery of potentially highly specific, but low abundant markers of disease, such as parasite-derived enzymes.

The multivariate statistical methods, also referred to as “chemometrics” are capable in dealing with large or high-dimensional datasets, which are a typical feature of metabonomics and other –omics sciences (Eriksson *et.al.*, 2004; Eriksson *et.al.*, 2001; Trygg *et.al.*, 2007). The most popular approaches are the linear projection methods principal components analysis (PCA) and projection to latent structures (PLS) analysis, which are able to deal with complex biological datasets and also handle noise and incomplete data structures. PCA belongs to the unsupervised multivariate methods, which means that there is no prior class-assumption included in the analysis, whereas PLS is a supervised method and delivers a quantitative value of how well the created model fits into the assumption of class. Although there are various methods of multivariate analyses (e.g. Bayesian statistics, neural networks, etc.) PCA, PLS and further development of these two methods, such as the hierarchical PCA (H-PCA) and hierarchical PLS (H-PLS) or orthogonal PLS (O-PLS) have established as main tools for metabolic profiling.

1.4 Spectroscopy

1.4.1 NMR spectroscopy

Certain isotopic nuclei possess an inherent magnetic moment, called spin, which is the crucial prerequisite for NMR spectroscopy. When isotopes with spin are brought into a magnetic field, they will absorb and then re-emit electromagnetic energy in the range of radio wavelengths, whereby the interaction of spin and magnetic field determine the frequency at which the radio frequency is absorbed and can vary due to magnetic field strength, type of nucleus and the electronic environment surrounding the isotope. Nuclei without spin ($I=0$) are called NMR silent and have got only one energy level, whereas ^1H , ^{13}C and ^{31}P and possess a net spin of $I=1/2$ which can manifest as 2 different energy levels (Figure 1.6 A) following the equation $2I+1$. In isotope populations with spin $1/2$, when placed in an external magnetic field, slightly more isotopes will align with the magnetic field, which is the lower energy state than alignment against the magnetic field and the resulting difference in population is defined as “Boltzmann distribution”. NMR spectroscopy manipulates and acquires data out of the resulting bulk magnetisation vector (Figure 1.6 B), which makes it a relatively insensitive technique. Once the nuclei are brought into the centre of the magnetic field, and are aligned, a radiofrequency pulse is applied which flips the bulk magnetisation vector from z-axis 90° down to the x-axis (Figure 1.6 C) (Claridge, 1999).

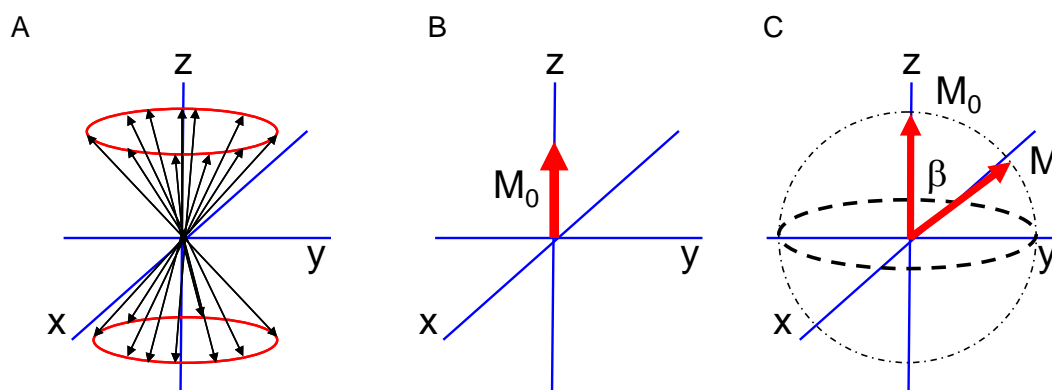


Figure 1.6. Basic alignment of nuclei in a static magnetic field and subsequent oscillation of the bulk magnetisation vector after the application of a radio frequency pulse

The actual phenomenon of magnetic resonance results from the relaxation of the nuclei back to their original state and is recorded initially as a free induction decay (time domain data) which is converted into frequency data by Fourier transformation for the purpose of interpretation (Figure 1.7).

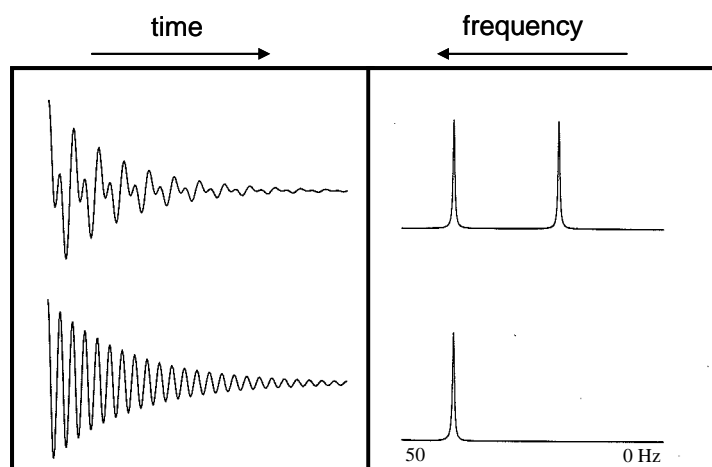


Figure 1.7. To obtain an interpretable NMR spectrum, the initial time-domain signal must be converted into frequency-domain spectral signals by Fourier transform algorithms

Two types of relaxation back to equilibrium, give a measure of the size of the molecule, where large molecules relax faster than small compounds. T_1 is the spin-lattice relaxation time and measures how fast the disturbed nucleus can reach equilibrium with the constant magnetic field B_0 and involves transfer of energy with surrounding nuclei. T_2 , the spin-spin relaxation indicates the time it takes for an excited nucleus to decay to its zero energy state along the x-y plane.

The chemical shift, spin-spin coupling and the peak intensities represent other spectral and molecular descriptors. The chemical shift is a relative scale and is expressed in parts per million (ppm), and calculated by $\delta = [\gamma (\text{solute in Hz}) - \gamma (\text{reference in Hz}) \times 10^6] / [\text{spectrometer frequency in Hz}]$. The reference substance is usually chosen as sodium 3-trimethylsilyl [2,2,3,3- $^2\text{H}_4$] propionate (TSP) and set arbitrarily to 0 ppm. Each nucleus experiences a slightly different effect of the applied external magnetic field according to its exact chemical and electrical environment since the electron cloud surrounding each nucleus exerts a small shielding effect against B_0 . Thus protons that are surrounded by a dense electron cloud will be more shielded from the magnetic field and will appear at a relatively upfield shift. Therefore, each nuclear environment is unique resulting in the generation of characteristic spectral signatures for each molecule.

Spin-spin coupling or J-coupling is based on the interaction of neighbouring NMR active nuclei and reveals structural details of the molecular composition. The characteristic multiplicities of peaks, follow the n+1 rule, for example a proton with no neighbouring (n=0) protons over 1-3 bonds will be shown as singlet in the spectra, whereas a proton, surrounded by 2 other protons, will manifest as a triplet (Figure 1.8).

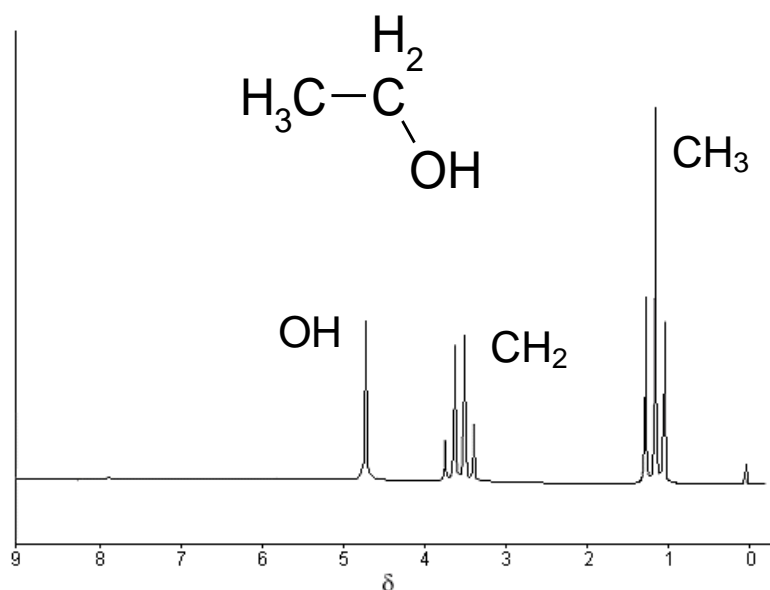


Figure 1.8. Peak multiplicity of ethanol based on the $n+1$ rule for the impact of neighbouring protons

Since NMR is based on quantum mechanics, the peak intensities are directly proportional to the number of nuclei with same neighbouring conditions.

Two-dimensional (2D) NMR spectroscopic methods are a key tool in structure elucidation, and include homo-nuclear assays, such as ^1H - ^1H 2D J-resolved spectroscopy (JRES), which shows the exact multiplicity of each peak, correlation spectroscopy (COSY) (Ernst, 1986) and total correlation spectroscopy (TOCSY) (Bax, 1984). Both the latter methods indicate interaction of the same nuclei in one molecule, but whereas COSY shows only J-coupling between pairs of nuclei that are adjacent, e.g. up to 3 bonds away, TOCSY extracts correlation for all homonuclei within one spin system.

Heteronuclear experiments between different NMR active nuclei generate information connected between two different NMR active isotopes. For example heteronuclear multiple quantum correlation experiment (HMQC) can be used to identify a direct coupling of protons to carbons. The information extracted from HMQCs is often combined with heteronuclear multiple bond experiments (HMBC) which are complementary experiments and reveal weak J-couplings, e.g. protons which are bound to a certain carbon over 2, 3 or 4 bonds. Applying both the experiments can give an enormous amount of extra information about molecular structures where assignment based on the simpler homonuclear experiments is difficult.

NMR spectroscopy is very efficient. A standard one-dimensional spectrum can be acquired and interpreted within a few minutes. Moreover, the technique is non-destructive and requires only small sample sizes (e.g. mg for tissue and 20 μl for original liquid samples).

Many of the peaks in the commonly used biomatrices are already defined and if not, structural analysis *via* 2D NMR methods or *via* coupling with MS and other spectroscopic methods allow identification of unknown regions. All these factors, and the ease of the sample preparation and the low relative cost for individual samples, have made NMR spectroscopy a most powerful tool in metabolic profiling. Drawbacks of this spectroscopic platform are the high initial cost of equipment and the inherently lower sensitivity, compared to other spectroscopic methods, such as MS.

1.4.2 Magic Angle Spinning

Apart from biomarker extraction from biofluids, which serves, in particular in this thesis project, diagnostic purposes, the analysis of tissue can contribute to understanding of drug pathways (Yap *et.al.*, 2006), organ malfunction (Tate *et.al.*, 2000) and entire systems by linking several physiological compartments (Martin *et.al.*, 2006). Solid state analysis NMR spectroscopy has been revolutionised by MAS. This method is not sample-destructive and can overcome the problems of restricted motion, chemical shift anisotropy and physical heterogeneity, which direct NMR analysis of semi-solid tissues has to face (Garrod *et.al.*, 1999; Waters *et.al.*, 2000). The restricted motion of the molecules in a solid structure impedes the total averaging of the dipolar coupling (D) and the shift anisotropy to zero, which is expressed as broad NMR resonances. Both these factors depend on the angle between the static magnetic field and the inter-nuclear vector, in the form $3\cos^2\theta - 1$, and rotating a solid sample with the magic angle of 54.7° which averages the equation to zero, enables a high-resolution spectra with sharp lines and splittings to be obtained (Andrew, 1962).

1.4.3 Mass Spectrometry

Although NMR spectroscopy has its advantages over MS in metabolic profiling, due to better evaluated methods of biomarker recovery and a higher reproducibility, MS-technologies have gained more and more importance as highly complementary structure elucidation tool in coupling with chromatographic separation methods (Gika *et.al.*, 2007; Lenz *et.al.*, 2005; Lenz and Wilson, 2007; Wilson *et.al.*, 2005) and also as pathway decoder in simple biological systems, such as protozoan (Kamleh *et.al.*, 2008) organisms. With its high inherent sensitivity MS holds promise to add low abundant but highly specific biomarkers to

the already established pool of NMR recovered discriminatory compounds and construct more specific fingerprints of pathological states.

Mass spectrometers should fulfil certain prerequisites, which include the generation of ions from the analyte, in a first step, followed by their separation in an analyser according to mass. For structure elucidation purposes it is advantageous to have an additional ion fragmentation-analyser system, whereas for metabolic profiling purposes, e.g. quantitative screening of metabolites, a reduced amount of data is easier to handle and thus no further fragmentation of ions would be performed. A detector measures mass and abundance of the emerging ions and data can be processed. The mainly applied source of ionisation in metabonomics is electrospray (ESI), which is based on the application of a strong electric field that interacts with the passing analyte and forms highly charged droplets that desorb in form of multiple charged ions, which in turn improves sensitivity. The analyser systems are diverse and the more recent developments lean towards higher sensitivity, such as the time-of-flight analysers, where bundled ions are accelerated before detection. Also Orbitrap Fourier transform (FT)-MS (FT-MS) delivers ultra-high mass resolution by using hydrophilic interaction chromatography (HILIC) columns, which separate out the lipid fractions before the rest metabolic composition enters the MS (Kamleh *et.al.*, 2008).

The outcome of such an MS acquisition is exemplified in Figure 1.9, where the mass spectrum of methanol is shown.

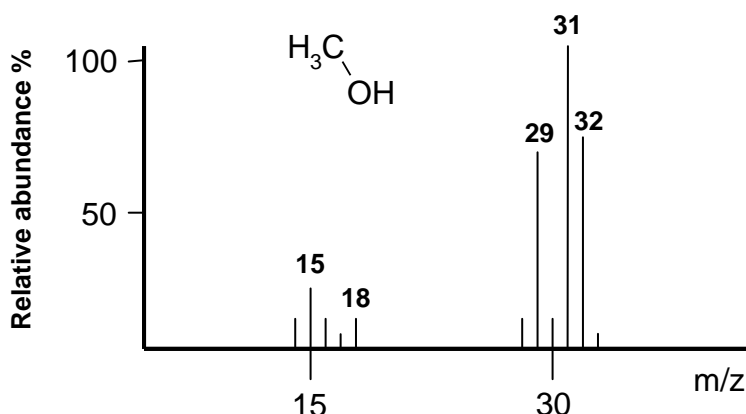


Figure 1.9. Mass to charge distribution of methanol and its fragments

Usually the molecular ion implies the molecular weight and appears at the highest m/z ratio, e.g. 32 in the case of methanol. The intensity at 15 indicates the defragmented methyl group whereas the mass difference of 17 can be related to the loss of a hydroxyl group.

MS is only as efficient as its previous separation. LC and GC are the preferred separation methods apart from the manual solid phase extraction and all three methods are based on the same mechanistic principles of the interaction of the mobile phase, which has to be separated (liquid or gas), with a stationary phase, which is the column matrix. The physico-chemical characteristics of a compound determine the strength of interaction between the different molecules in a sample and the column matrix and are expressed in retention time which indicates the emerging of the compound from the matrix.

1.5 Chemometric analysis

1.5.1 *Principal components analysis*

The principal component analysis (PCA) is normally the first approach to be applied to a multivariate data set, and consists of a single X-matrix, organised in n rows (observations, in this case individual urine spectra) and k columns (descriptors, i.e. for this data set spectral shift regions). In the PCA all spectral information for a given object is compressed into a single data point and projected on to a scores plot revealing general information about the distribution of the data, e.g. clustering, time trajectories and eventual outliers. The concomitant loadings plot contains the metabolic information responsible for individual differences in space and is directly applicable to the scores plot (Figure 1.10).

The PCA projects every observation as single point into an n -dimensional space, whereby every single descriptor, e.g. the integral belonging to a certain chemical shift region, represents one dimension, and determines the localisation of the observation in the metabolic hyperspace. The resulting swarm of points needs to be mean centred in order to facilitate direct comparison of variables (Fig. 1.11 a, b) before applying a first principal component (PC) analysis chosen to visualise the maximum variability in the data set (Fig. 1.11 c). The following PCs are always orthogonal to the previous PC (d) and explain less and less variance with every step. Two PCs define a hyperplane (Fig. 1.11 e) onto which the points or observations can be projected in order to generate the scores plot (Figure 1.11 f).

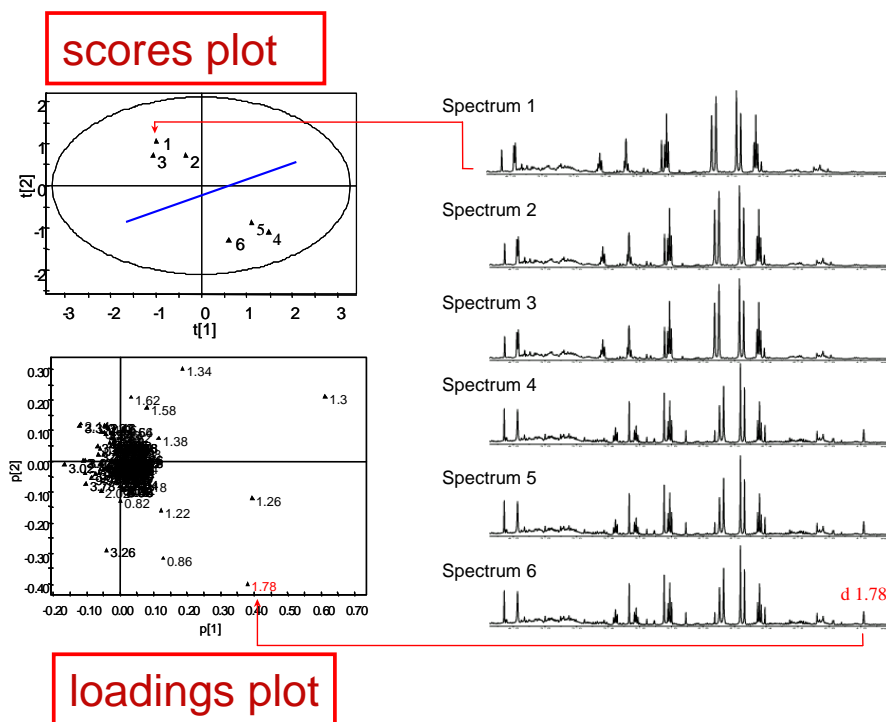


Figure 1.10. Explanatory capacity of PCA, adapted from original by Dr. Tsz M. Tsang

The number of PCs for each data set will be as many as the variables within the data set, but the lower PCs will contain only noise. Thus the number of PCs calculated in each model will depend upon two parameters, fit the goodness of fit of the model (R^2X), and the predictive ability of the model (Q^2X), and is chosen at an optimal region where both values are as high as possible. The former shows how robust the set of data is, e.g. if one point is taken out, how probable it would be that it is going to be at the same place by projecting it back. The latter indicates the probability that the location of a new data point can be predicted correctly.

1.5.2. Partial least squares analysis

PLS analysis correlates the spectral content (usually in the X-matrix) to additional quantitative information, such as physiological or pathological measures (e.g. packed cell volume, bodyweight, etc.) or infection intensity, which is outlined in a measurement response or y-matrix and fitted to X by maximising the covariance between the two matrices (Eriksson *et.al.*, 2004; Eriksson *et.al.*, 2001; Trygg, 2002; Trygg *et.al.*, 2007). Furthermore, PLS can also act in a qualitative way, and be applied as discriminant analysis, where a 0/1 dummy matrix indicates class relationship.

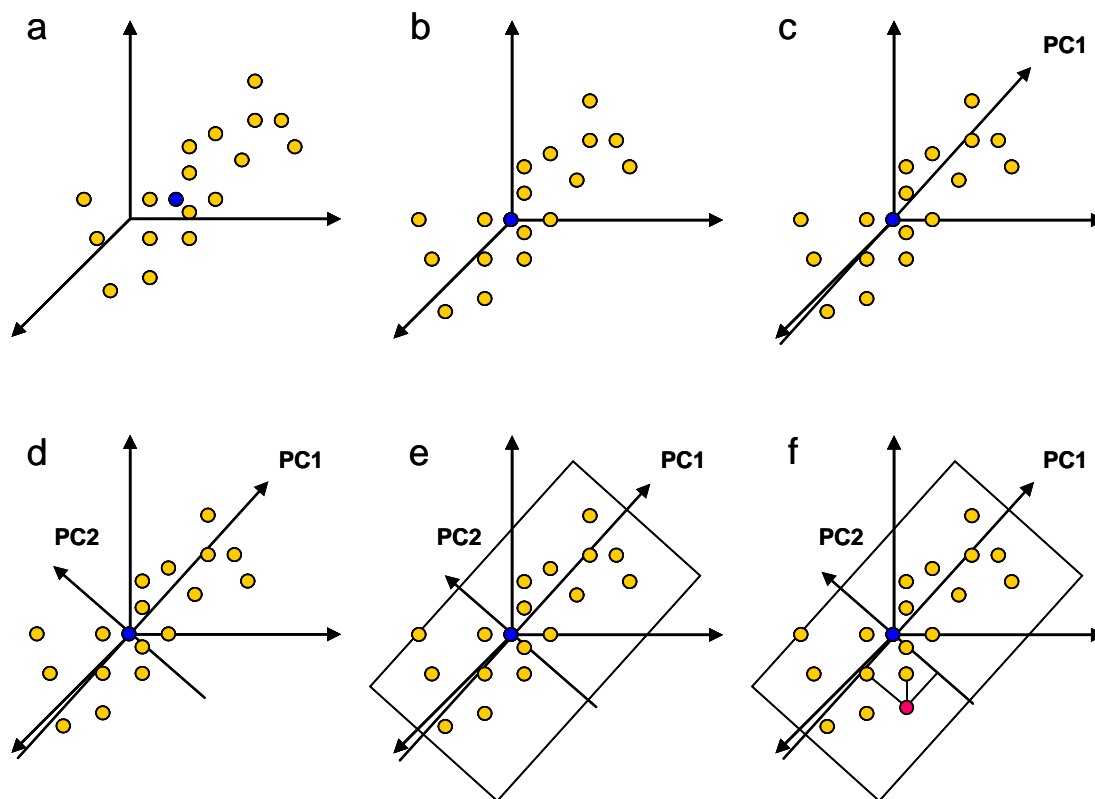


Figure 1.11. Geometrical demonstration of the basic PCA principle

Although PLS-DA is applied frequently to biological data sets in order to get a measure of model predictability, PLS bears an inherent risk of delivering false biomarkers, as it can potentially relate x-internal variation to the y-dataset and thus construct artificial causalities. Thus supervised methods are usually constructed using a training set and then the resultant model tested with a validation set (observations which have been removed prior to modelling the training set). This process is known as cross validation and is often performed internally within an algorithm, for example in the Umetrics software every 7th observation is left out and back predicted. Another way to avoid this false link is the addition of an orthogonal component to the X-dataset which comprehends all X-internal variation and removes it from correlation analysis with the Y-matrix. Orthogonal PLS is generally applied in biomarker detection assays rather than PLS. Geometrically, the main difference between PLS and PCA is that data points are projected in two hyperspaces instead of one. Location in X (predictor space) and Y (response space) is based on the information in the two different data matrices, and the aim of the statistical analysis is to search for positional correlation between them.

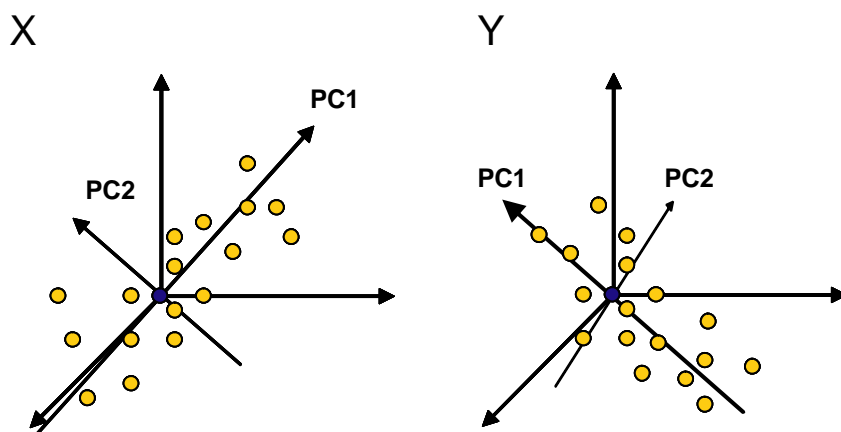


Figure 1.12. Approximation of PCs in X in a partial least squares analysis happens with considering correlation to the second matrix Y and *vice versa*

The first PC in X and Y is calculated to give the best approximation of each swarm of points, but also to contain an optimal correlation between the two point locations (Figure.1.12). The second components aim to approximate and optimize the positional correlations between X and Y-hyperplane, whereas in X the second component has to be orthogonal to the first but not in Y.

1.5.3. Statistical total correlation spectroscopy

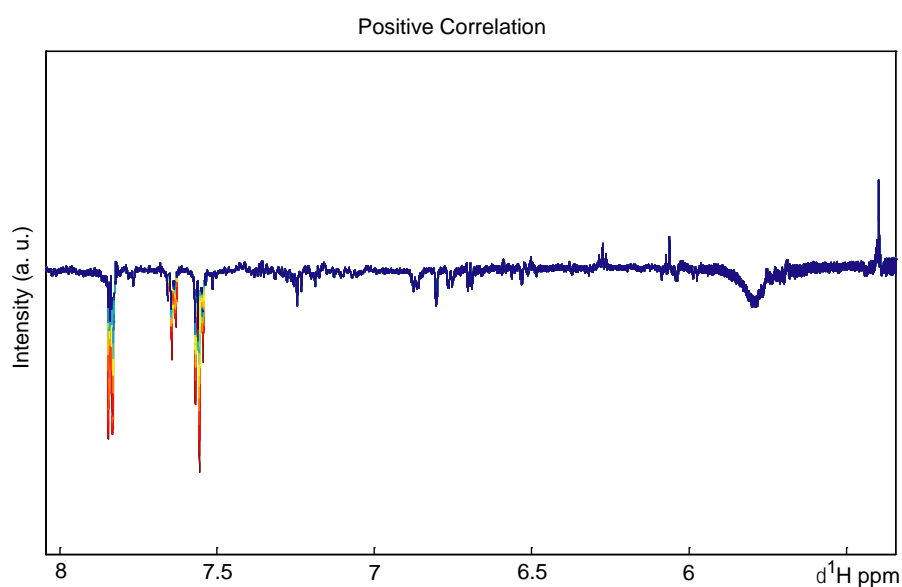


Figure 1.13. Statistical total correlation spectroscopy, revealing structural or pathway relation

Statistical total correlation spectroscopy is a multivariate approach to resolve molecular structure for one molecule or to indicate biological relationships between compounds (e.g. biological or physical relationship) and is based on the correlation of intensities or datapoints over multiple spectra (Cloarec *et.al.*, 2005). In Figure 1.13, for example, STOCSY analysis on the apex of the hippurate triplet at chemical shift 7.55, revealed strong correlations with all other hippurate chemical shifts (7.64 (triplet), 7.84 (doublet) and 3.97 (doublet)), - here only the aromatic region is shown. STOCSY offers an alternative to 2D NMR techniques in structure elucidation, which suffer resolution problems, compared to 1D spectra, thus cannot deal with low abundant metabolites or metabolic resonances hidden by overlapped and particularly dense chemical shift regions. STOCSY deals with the digitised spectra rather and is not restricted by visual means and internuclear proximity. Thus it has become an essential tool for structure elucidation in metabolic profiling and is also applicable to paired data sets as heteronuclear-STOCSY (HET-STOCSY), such as parallel acquisitions of two different magnetic active nuclei.

Statistically, the correlation matrix (C) used for STOCSY is calculated by $C=1/(n-1) X_1^T X_2$, whereas X_1 and X_2 are built by the autoscaled matrices of $n \times v_1$ and $n \times v_2$, respectively (n = number of spectra; v = number of variables in the spectra for each matrix).

1.6 References

- Allwood J.W., Ellis D.I., Goodacre R. 2008. Metabolomic technologies and their application to the study of plants and plant-host interactions. *Physiol Plant* **132**(2):117-35.
- Anantaphruti M.T. 2001. Parasitic contaminants in food. *Southeast Asian J Trop Med Public Health* **32 Suppl 2**:218-28.
- Andrew E.R.E., R. G.;. 1962. Principle of high resolution NMR in solids. *Disc. Farad. Soc.* **34**:38.
- Balfour C.D., Rossi M., Fried B. 2001. Effects of a 100 metacercarial cyst inoculum on the host-parasite relationship of *Echinostoma caproni* and ICR mice. *J Helminthol* **75**(4):321-4.
- Bax A. 1984. Topics in ¹³C NMR spectroscopy.
- Bergquist R., Johansen M.V., Utzinger J. 2009. Diagnostic dilemmas in helminthology: what tools to use and when? *Trends Parasitol* **25**(4):151-6.
- Bergquist R.J., M. V.; Utzinger, J. 2008. Diagnostic dilemmas in helminthology: what tools to use and when? *Trends in Parasitology--Opinion submitted*.
- Bjorland J., Bryan R.T., Strauss W., Hillyer G.V., McAuley J.B. 1995. An outbreak of acute fascioliasis among Aymara Indians in the Bolivian Altiplano. *Clin Infect Dis* **21**(5):1228-33.
- Brooker S., Utzinger J. 2007. Integrated disease mapping in a polyparasitic world. *Geospat Health* **1**(2):141-6.
- Chai J.Y., Han E.T., Guk S.M., Shin E.H., Sohn W.M., Yong T.S., Eom K.S., Lee K.H., Jeong H.G., Ryang Y.S. and others. 2007. High prevalence of liver and intestinal fluke infections among residents of Savannakhet Province in Laos. *Korean J Parasitol* **45**(3):213-8.
- Chitsulo L., Engels D., Montresor A., Savioli L. 2000. The global status of schistosomiasis and its control. *Acta Trop* **77**(1):41-51.
- Claridge T. 1999. High-resolution NMR techniques in organic chemistry.
- Cloarec O., Dumas M.E., Craig A., Barton R.H., Trygg J., Hudson J., Blancher C., Gauguier D., Lindon J.C., Holmes E. and others. 2005. Statistical total correlation spectroscopy: an exploratory approach for latent biomarker identification from metabolic ¹H NMR data sets. *Anal Chem* **77**(5):1282-9.
- Coen M., Lenz E.M., Nicholson J.K., Wilson I.D., Pognan F., Lindon J.C. 2003. An integrated metabolomic investigation of acetaminophen toxicity in the mouse using NMR spectroscopy. *Chem Res Toxicol* **16**(3):295-303.
- Cross J.H., Basaca-Sevilla V. 1986. Studies on *Echinostoma ilocanum* in the Philippines. *Southeast Asian J Trop Med Public Health* **17**(1):23-7.
- Denkert C., Budczies J., Kind T., Weichert W., Tablack P., Sehouli J., Niesporek S., Konsgen D., Dietel M., Fiehn O. 2006. Mass spectrometry-based metabolic profiling reveals different metabolite patterns in invasive ovarian carcinomas and ovarian borderline tumors. *Cancer Res* **66**(22):10795-804.
- Dickson R., Awasthi S., Williamson P., Demellweek C., Garner P. 2000. Effects of treatment for intestinal helminth infection on growth and cognitive performance in children: systematic review of randomised trials. *BMJ* **320**(7251):1697-701.
- Eriksson L., Antti H., Gottfries J., Holmes E., Johansson E., Lindgren F., Long I., Lundstedt T., Trygg J., Wold S. 2004. Using chemometrics for navigating in the large data sets of genomics, proteomics, and metabolomics (gpm). *Anal Bioanal Chem* **380**(3):419-29.

-
- Eriksson L., Johansson E., Kettaneh-Wold N., Trygg J., Wikstrom C. 2001. Multi and megavariate data analysis. Umetrics Academy.
- Ernst R.R.B., G.; Wokaun, A. 1986. Principles of nuclear magnetic resonance in one and two dimensions.
- Fiorito F., Herrmann T., Damberger F.F., Wuthrich K. 2008. Automated amino acid side-chain NMR assignment of proteins using (13)C- and (15)N-resolved 3D [(1)H, (1)H]-NOESY. *J Biomol NMR* **42**(1):23-33.
- Flynn R.J., Mannion C., Golden O., Hacariz O., Mulcahy G. 2007. Experimental Fasciola hepatica infection alters responses to tests used for diagnosis of bovine tuberculosis. *Infect Immun* **75**(3):1373-81.
- Fried B., Graczyk T.K., Tamang L. 2004. Food-borne intestinal trematodiasis in humans. *Parasitol Res* **93**(2):159-70.
- Fried B., Huffman J.E. 1996. The Biology of the intestinal trematode Echinostoma caproni. *Adv Parasitol* **38**:311-68.
- Gajadhar A.A., Scandrett W.B., Forbes L.B. 2006. Overview of food- and water-borne zoonotic parasites at the farm level. *Rev Sci Tech* **25**(2):595-606.
- Garrod S., Humpfer E., Spraul M., Connor S.C., Polley S., Connelly J., Lindon J.C., Nicholson J.K., Holmes E. 1999. High-resolution magic angle spinning 1H NMR spectroscopic studies on intact rat renal cortex and medulla. *Magn Reson Med* **41**(6):1108-18.
- Gika H.G., Theodoridis G.A., Wingate J.E., Wilson I.D. 2007. Within-day reproducibility of an HPLC-MS-based method for metabonomic analysis: application to human urine. *J Proteome Res* **6**(8):3291-303.
- Graczyk T.K., Fried B. 1998. Echinostomiasis: a common but forgotten food-borne disease. *Am J Trop Med Hyg* **58**(4):501-4.
- Gryseels B., Polman K., Clerinx J., Kestens L. 2006. Human schistosomiasis. *Lancet* **368**(9541):1106-18.
- Haseeb A.N., el-Shazly A.M., Arafa M.A., Morsy A.T. 2002. A review on fascioliasis in Egypt. *J Egypt Soc Parasitol* **32**(1):317-54.
- Holmes E., Loo R.L., Stamler J., Bictash M., Yap I.K., Chan Q., Ebbels T., De Iorio M., Brown I.J., Veselkov K.A. and others. 2008a. Human metabolic phenotype diversity and its association with diet and blood pressure. *Nature* **453**(7193):396-400.
- Holmes E., Tsang T.M., Tabrizi S.J. 2006. The application of NMR-based metabonomics in neurological disorders. *NeuroRx* **3**(3):358-72.
- Holmes E., Wilson I.D., Nicholson J.K. 2008b. Metabolic phenotyping in health and disease. *Cell* **134**(5):714-7.
- Hotez P.J., Molyneux D.H., Fenwick A., Ottesen E., Ehrlich Sachs S., Sachs J.D. 2006. Incorporating a rapid-impact package for neglected tropical diseases with programs for HIV/AIDS, tuberculosis, and malaria. *PLoS Med* **3**(5):e102.
- Huffman J.E., Fried B. 1990. Echinostoma and echinostomiasis. *Adv Parasitol* **29**:215-69.
- Kamleh A., Barrett M.P., Wildridge D., Burchmore R.J., Scheltema R.A., Watson D.G. 2008. Metabolomic profiling using Orbitrap Fourier transform mass spectrometry with hydrophilic interaction chromatography: a method with wide applicability to analysis of biomolecules. *Rapid Commun Mass Spectrom* **22**(12):1912-8.
- Keiser J., Brun R., Fried B., Utzinger J. 2006a. Trematocidal activity of praziquantel and artemisinin derivatives: in vitro and in vivo investigations with adult Echinostoma caproni. *Antimicrob Agents Chemother* **50**(2):803-5.

-
- Keiser J., Rinaldi L., Veneziano V., Mezzino L., Tanner M., Utzinger J., Cringoli G. 2008. Efficacy and safety of artemether against a natural *Fasciola hepatica* infection in sheep. *Parasitol Res* **103**(3):517-22.
- Keiser J., Shu-Hua X., Tanner M., Utzinger J. 2006b. Artesunate and artemether are effective fasciolicides in the rat model and in vitro. *J Antimicrob Chemother* **57**(6):1139-45.
- Keiser J., Shu-Hua X., Utzinger J. 2006c. Effect of tribendimidine on adult *Echinostoma caproni* harbored in mice, including scanning electron microscopic observations. *J Parasitol* **92**(4):858-62.
- Keiser J., Utzinger J. 2004. Chemotherapy for major food-borne trematodes: a review. *Expert Opin Pharmacother* **5**(8):1711-26.
- Keiser J., Utzinger J. 2005. Emerging foodborne trematodiasis. *Emerg Infect Dis* **11**(10):1507-14.
- Keiser J., Utzinger J. 2007a. Artemisinins and synthetic trioxolanes in the treatment of helminth infections. *Curr Opin Infect Dis* **20**(6):605-12.
- Keiser J., Utzinger J. 2007b. Food-borne trematodiasis: current chemotherapy and advances with artemisinins and synthetic trioxolanes. *Trends Parasitol* **23**(11):555-62.
- Keiser J., Utzinger J., Tanner M., Dong Y., Vennerstrom J.L. 2006d. The synthetic peroxide OZ78 is effective against *Echinostoma caproni* and *Fasciola hepatica*. *J Antimicrob Chemother* **58**(6):1193-7.
- Keiser J., Utzinger J., Vennerstrom J.L., Dong Y., Brennan G., Fairweather I. 2007. Activity of artemether and OZ78 against triclabendazole-resistant *Fasciola hepatica*. *Trans R Soc Trop Med Hyg* **101**(12):1219-22.
- King C.H., Dangerfield-Cha M. 2008. The unacknowledged impact of chronic schistosomiasis. *Chronic Illn* **4**(1):65-79.
- Kumar N., Ghosh S., Gupta S.C. 2008. Early detection of *Fasciola gigantica* infection in buffaloes by enzyme-linked immunosorbent assay and dot enzyme-linked immunosorbent assay. *Parasitol Res* **103**(1):141-50.
- Lenz E.M., Bright J., Knight R., Westwood F.R., Davies D., Major H., Wilson I.D. 2005. Metabonomics with ¹H-NMR spectroscopy and liquid chromatography-mass spectrometry applied to the investigation of metabolic changes caused by gentamicin-induced nephrotoxicity in the rat. *Biomarkers* **10**(2-3):173-87.
- Lenz E.M., Wilson I.D. 2007. Analytical strategies in metabonomics. *J Proteome Res* **6**(2):443-58.
- Li M., Wang B., Zhang M., Rantalainen M., Wang S., Zhou H., Zhang Y., Shen J., Pang X., Wei H. and others. 2008. Symbiotic gut microbes modulate human metabolic phenotypes. *Proc Natl Acad Sci U S A* **105**(6):2117-22.
- Li X. 1991. Food-borne parasitic zoonoses in the People's Republic of China. *Southeast Asian J Trop Med Public Health* **22 Suppl**:31-5.
- Lim J.H., Kim S.Y., Park C.M. 2007. Parasitic diseases of the biliary tract. *AJR Am J Roentgenol* **188**(6):1596-603.
- Lindon J.C., Holmes E., Nicholson J.K. 2006. Metabonomics techniques and applications to pharmaceutical research & development. *Pharm Res* **23**(6):1075-88.
- Liu Q., Wei F., Liu W., Yang S., Zhang X. 2008. Paragonimiasis: an important food-borne zoonosis in China. *Trends Parasitol* **24**(7):318-23.
- Manzella A., Ohtomo K., Monzawa S., Lim J.H. 2008a. Schistosomiasis of the liver. *Abdom Imaging*.
- Manzella A., Ohtomo K., Monzawa S., Lim J.H. 2008b. Schistosomiasis of the liver. *Abdom Imaging* **33**(2):144-50.

-
- Martin F.P., Verdu E.F., Wang Y., Dumas M.E., Yap I.K., Cloarec O., Bergonzelli G.E., Corthesy-Theulaz I., Kochhar S., Holmes E. and others. 2006. Transgenomic metabolic interactions in a mouse disease model: interactions of *Trichinella spiralis* infection with dietary *Lactobacillus paracasei* supplementation. *J Proteome Res* **5**(9):2185-93.
- Mas-Coma M.S., Esteban J.G., Bargues M.D. 1999. Epidemiology of human fascioliasis: a review and proposed new classification. *Bull World Health Organ* **77**(4):340-6.
- Mas-Coma S., Bargues M.D., Valero M.A. 2005. Fascioliasis and other plant-borne trematode zoonoses. *Int J Parasitol* **35**(11-12):1255-78.
- Mas-Coma S.B., M. D.; Esteban, J. G. 1998. Fascioliasis.
- Muller B., Schmidt J., Mehlhorn H. 2007. PCR diagnosis of infections with different species of Opisthorchiidae using a rapid clean-up procedure for stool samples and specific primers. *Parasitol Res* **100**(4):905-9.
- Nicholson J.K. 2006. Global systems biology, personalized medicine and molecular epidemiology. *Mol Syst Biol* **2**:52.
- Nicholson J.K., Holmes E., Wilson I.D. 2005. Gut microorganisms, mammalian metabolism and personalized health care. *Nat Rev Microbiol* **3**(5):431-8.
- Nicholson J.K., Lindon J.C., Holmes E. 1999. 'Metabonomics': understanding the metabolic responses of living systems to pathophysiological stimuli via multivariate statistical analysis of biological NMR spectroscopic data. *Xenobiotica* **29**(11):1181-9.
- Ordovas J.M., Mooser V. 2006. Metagenomics: the role of the microbiome in cardiovascular diseases. *Curr Opin Lipidol* **17**(2):157-61.
- Pungpark S., Bunnag D., Harinasuta T. 1984. Albendazole in the treatment of opisthorchiasis and concomitant intestinal helminthic infections. *Southeast Asian J Trop Med Public Health* **15**(1):44-50.
- Saba R., Korkmaz M., Inan D., Mamikoglu L., Turhan O., Gunseren F., Cevikol C., Kabaalioglu A. 2004. Human fascioliasis. *Clin Microbiol Infect* **10**(5):385-7.
- Saijuntha W., Sithithaworn P., Wongkham S., Laha T., Pipitgool V., Tesana S., Chilton N.B., Petney T.N., Andrews R.H. 2007. Evidence of a species complex within the food-borne trematode *Opisthorchis viverrini* and possible co-evolution with their first intermediate hosts. *Int J Parasitol* **37**(6):695-703.
- Saric J., Li J.V., Wang Y., Keiser J., Bundy J.G., Holmes E., Utzinger J. 2008. Metabolic Profiling of an *Echinostoma caproni* Infection in the Mouse for Biomarker Discovery. *PLoS Negl Trop Dis* **2**(7):e254.
- Sripa B. 2008. Concerted action is needed to tackle liver fluke infections in Asia. *PLoS Negl Trop Dis* **2**(5):e232.
- Steinmann P., Keiser J., Bos R., Tanner M., Utzinger J. 2006. Schistosomiasis and water resources development: systematic review, meta-analysis, and estimates of people at risk. *Lancet Infect Dis* **6**(7):411-25.
- Stork M.G., Venables G.S., Jennings S.M., Beesley J.R., Bendezu P., Capron A. 1973. An investigation of endemic fascioliasis in Peruvian village children. *J Trop Med Hyg* **76**(9):231-5 passim.
- Tate A.R., Foxall P.J., Holmes E., Moka D., Spraul M., Nicholson J.K., Lindon J.C. 2000. Distinction between normal and renal cell carcinoma kidney cortical biopsy samples using pattern recognition of (1)H magic angle spinning (MAS) NMR spectra. *NMR Biomed* **13**(2):64-71.
- Toledo R., Fried B. 2005. Echinostomes as experimental models for interactions between adult parasites and vertebrate hosts. *Trends Parasitol* **21**(6):251-4.

-
- Trygg J. 2002. O2-PLS for qualitative and quantitative analysis in multivariate calibration. *J Chemom* **16**:283-93.
- Trygg J., Holmes E., Lundstedt T. 2007. Chemometrics in metabonomics. *J Proteome Res* **6**(2):469-79.
- Tsang T.M., Huang J.T., Holmes E., Bahn S. 2006. Metabolic profiling of plasma from discordant schizophrenia twins: correlation between lipid signals and global functioning in female schizophrenia patients. *J Proteome Res* **5**(4):756-60.
- Upatham E.S., Viyanant V. 2003. Opisthorchis viverrini and opisthorchiasis: a historical review and future perspective. *Acta Trop* **88**(3):171-6.
- Urbani C., Palmer K. 2001. Drug-based helminth control in Western Pacific countries: a general perspective. *Trop Med Int Health* **6**(11):935-44.
- Utzinger J., Xiao S.H., Tanner M., Keiser J. 2007. Artemisinins for schistosomiasis and beyond. *Curr Opin Investig Drugs* **8**(2):105-16.
- Wang Y., Holmes E., Nicholson J.K., Cloarec O., Chollet J., Tanner M., Singer B.H., Utzinger J. 2004. Metabonomic investigations in mice infected with *Schistosoma mansoni*: an approach for biomarker identification. *Proc Natl Acad Sci U S A* **101**(34):12676-81.
- Wang Y., Utzinger J., Saric J., Li J.V., Burckhardt J., Dirnhofer S., Nicholson J.K., Singer B.H., Brun R., Holmes E. 2008. Global metabolic responses of mice to *Trypanosoma brucei brucei* infection. *Proc Natl Acad Sci U S A* **105**(16):6127-32.
- Wang Y., Utzinger J., Xiao S.H., Xue J., Nicholson J.K., Tanner M., Singer B.H., Holmes E. 2006. System level metabolic effects of a *Schistosoma japonicum* infection in the Syrian hamster. *Mol Biochem Parasitol* **146**(1):1-9.
- Waters N.J., Garrod S., Farrant R.D., Haselden J.N., Connor S.C., Connelly J., Lindon J.C., Holmes E., Nicholson J.K. 2000. High-resolution magic angle spinning (1)H NMR spectroscopy of intact liver and kidney: optimization of sample preparation procedures and biochemical stability of tissue during spectral acquisition. *Anal Biochem* **282**(1):16-23.
- WHO. 1995. Control of foodborne trematode infections. Report of a WHO study group. *WHO Technical Report Series*(849).
- Wilson I.D., Nicholson J.K., Castro-Perez J., Granger J.H., Johnson K.A., Smith B.W., Plumb R.S. 2005. High resolution "ultra performance" liquid chromatography coupled to oa-TOF mass spectrometry as a tool for differential metabolic pathway profiling in functional genomic studies. *J Proteome Res* **4**(2):591-8.
- Xiao S.H., Keiser J., Chollet J., Utzinger J., Dong Y., Endriss Y., Vennerstrom J.L., Tanner M. 2007. In vitro and in vivo activities of synthetic trioxolanes against major human schistosome species. *Antimicrob Agents Chemother* **51**(4):1440-5.
- Yap I.K., Clayton T.A., Tang H., Everett J.R., Hanton G., Provost J.P., Le Net J.L., Charuel C., Lindon J.C., Nicholson J.K. 2006. An integrated metabonomic approach to describe temporal metabolic dysregulation induced in the rat by the model hepatotoxin allyl formate. *J Proteome Res* **5**(10):2675-84.





2 Goal and specific objectives

The overarching goal of this Ph.D. project was to deepen our understanding of trematode-induced metabolic changes in selected rodent models, and to critically assess the biomarker recovery potential of a metabolic profiling approach applied to biofluids and tissue samples that may contain diagnostic and prognostic properties.

1. To optimise sample preparation for subsequent ^1H NMR spectroscopy, and to assess metabolic variation in samples with regard to species (i.e. human, rat and mouse), gender and age.
2. To assess longitudinally the biochemical changes in urine, plasma and water of *E. caproni*-infected mice, and to compare the diagnostic capacity of different biofluids collected from infected and uninfected mice.
3. To gain information about *E. caproni*-induced changes in selected tissue samples e.g. (liver, kidney, spleen, ileum, jejunum and colon) of infected mice and correlate identified biomarkers with the previously extracted markers in the biofluids, which might reveal infection-related systems level changes.
4. To evaluate the remote and direct impact of three different trematodes (*E. caproni*, *F. hepatica*, *S. mansoni*) on the rodent host neural metabolic composition.



3 Species variation in the faecal metabolome gives insight into differential gastrointestinal function

Jasmina Saric,^{†,‡} Yulan Wang,[‡] Jia Li,^{†,‡} Muireann Coen,[‡] Jürg Utzinger,[†] Julian R. Marchesi,[§] Jennifer Keiser,[†] Kirill Veselkov,[‡] John C. Lindon,[‡] Jeremy K. Nicholson,[‡] and Elaine Holmes^{*‡}

[†] Department of Public Health and Epidemiology, Swiss Tropical Institute, P.O. Box, CH-4002 Basel, Switzerland

[‡] Department of Biomolecular Medicine, Division of Surgery, Oncology, Reproductive Biology and Anaesthetics (SORA), Faculty of Medicine, Imperial College London, Sir Alexander Fleming Building, South Kensington, London SW7 2AZ, United Kingdom

[§] Alimentary Pharmabiotic Centre and Department of Microbiology, University College Cork, College Road, Cork, Ireland

*Corresponding author: Professor Elaine Holmes, Department of Biomolecular Medicine, Division of Surgery, Oncology, Reproductive Biology and Anaesthetics (SORA), Faculty of Medicine, Imperial College London, Sir Alexander Fleming Building, South Kensington, London SW7 2AZ, United Kingdom. Tel.: +44 20 7594-3220; Fax: +44 20 7594-3226. E-mail: elaine.holmes@imperial.ac.uk

This article has been published in
Journal of Proteome Research **2008**, 7: 352-360

3.1 Abstract

The metabolic composition of faecal extracts provides a window for elucidating the complex metabolic interplay between mammals and their intestinal ecosystems, and these metabolite profiles can yield information on a range of gut diseases. Here, the metabolites present in aqueous faecal extracts of humans, mice and rats were characterised using high-resolution ^1H NMR spectroscopy coupled with multivariate pattern recognition techniques. Additionally, the effects of sample storage and preparation methods were evaluated in order to assess the stability of faecal metabolite profiles, and to optimize information recovery from faecal samples. Finally, variations in metabolite profiles were investigated in healthy mice as a function of time. Inter-species variation was found to be greater than the variation due to either time or sample preparation. Although many faecal metabolites were common to the three species, such as short chain fatty acids and branched chain amino acids, each species generated a unique profile. Relatively higher levels of uracil, hypoxanthine, phenylacetic acid, glucose and aromatic amino acids were present in the rat, with β -alanine being unique to the rat and glycerol being unique to the human. Human faecal extracts showed a greater inter-individual variation than the two rodent species, reflecting the natural genetic and environmental diversity in human populations. Faecal composition in healthy mice was found to change over time, which might be explained by altered gut microbial presence or activity. The systematic characterization of faecal composition across humans, mice and rats, together with the evaluation of inherent variation, provides a baseline for future studies seeking to determine faecal biomarkers of disease and/or response to dietary or therapeutic interventions.

3.2 Introduction

There is growing awareness both of the beneficial role the gut microbiota can play in maintaining homeostasis in human health and of the adverse association of certain microbial species with diseases as diverse as cardiovascular diseases and autism.¹⁻⁶ This link has led to renewed interest in the characterization of the microbial content in the mammalian intestine. Several studies have used faecal material as a medium for assessing the presence of diseases, such as chronic pancreatitis, inflammatory bowel disease (IBD) and colon cancer.⁷⁻¹¹ Moreover, the potential anti-carcinogenic activity of microbial metabolites present in feces, particularly short chain fatty acids (SCFAs), has been investigated by exposing cultured cells to faecal extracts.¹²

High-resolution ^1H NMR spectroscopy of biofluids such as urine and plasma can be used to generate diagnostic information relating to many physiological and pathological conditions, particularly when used in conjunction with pattern recognition methods.¹³⁻¹⁷ Recent studies have shown that ^1H NMR spectral profiles of faecal extracts carry diagnostic information for diseases, including Crohn's disease and ulcerative colitis.⁸ However, unlike urine and plasma which are relatively well-characterised in terms of their metabolite composition and extent of inter-species variation,^{18,19} temporal variation and the effect of sample preparation in the faecal metabolite profile have not yet been assessed.

Here, we characterise inter-species differences between humans, mice and rats in the content and temporal stability of the faecal metabolite profiles, and explore the effect of different faecal sample preparation methods. Our rationale for choosing mice and rats is that these vertebrates are widely used in disease model studies. The ultimate objective of this study is to provide a baseline for future investigations applying faecal profiling to monitor the effect of dietary and pharmaceutical interventions, changes in lifestyles and progression and regression of diseases.

3.3 Material and Methods

3.3.1 Faecal Sample Collection.

A single stool specimen of 12 healthy humans (6 women and 6 men; age: 31.8 ± 10.2 years, range: 24-51 years) was obtained from a previous metabonomic study, cross comparing IBD patient subgroups (e.g., Crohn's disease, ulcerative colitis) and healthy controls,⁸ and measured using ^1H NMR spectroscopy. This study was approved by the medical ethics committee of the Cork University Hospital (Cork, Ireland) and written informed consent was obtained from each participant.

Female NMRI mice and female Wistar rats were purchased from RCC (Itingen, Switzerland) and kept in groups of 4 at the animal facilities of the Swiss Tropical Institute (Basel, Switzerland), as described elsewhere.²⁰ In brief, the animals were approximately 6-week-old when faecal sample collection commenced, and the average body weight of mice and rats was 25.6 g and 87.4 g respectively. Animals had free access to water and rodent food from Eberle NAFAG (Gossau, Switzerland). Faecal samples were acquired between 08:00 and 10:00 to minimize variation introduced by diurnal rhythm. The experiments were

approved by the local government of Basel (permission nos. 2070 and 2081), and handling of the animals and collection of feces was according to Swiss national regulations.

A second rat strain of 8 Sprague-Dawley (SD; CrI:CD(SD)IGS BR) males (age: 7 weeks; weight: 175.5-200 g) was obtained from Charles River Laboratories (Wilmington, MA, USA). The animals were provided with food and water *ad libitum*. All in-life studies were reviewed and approved by the Institutional Animal Care and Use Committee.

3.3.2 Exploration of Metabolic Variation across Species

The inter-species variation was assessed in human spectra ($n = 12$), the Wistar female rat group ($n = 10$) and finally, female NMRI mice ($n = 12$). Both rats and mice were 9-week-old at the time of sampling.

3.3.3 Exploration of Metabolic Variation with Age

The biochemical variation in faecal metabolite profiles was evaluated in two groups of NMRI female mice ($n_1 = 10$; $n_2 = 12$), in Wistar female rats ($n = 10$) and male SD rats ($n = 8$). The first batch of 10 mice was tested for metabolic differences between sample collection at the age of 6 weeks (baseline) and 53 days later. A more detailed time course study was performed in a second batch of 12 mice where faecal samples were obtained at 8 different time points beginning when the animals were 6 weeks of age and ending at week 11 (sampling days: 1, 3, 7, 10, 14, 21, 28 and 35). Faecal samples obtained from 10 female Wistar rats were prepared under the same conditions and assessed over a 23-day period (starting at the age of 6 weeks). Additionally the stability of faecal composition was assessed over a 24-hour time frame (consistent with a typical acclimatization period in metabolism cages) in 8 male SD rats.

3.3.4 Effect of Sample Preparation and Storage on the Metabolic Profile.

The effects of lyophilization, sonication and filtration on the composition and stability of the faecal metabolite profile were assessed in feces of the Wistar rat group. Full experimental details are given in the supplementary material. Human samples were compared in terms of storage and spectra were acquired from the same faecal sample before and after freezing.

3.3.5 ^1H NMR Spectroscopic Analysis of faecal Samples

For the human samples, 200-300 g of stool was mixed with 400 μl of phosphate buffered saline (PBS; 1.9 mM Na_2HPO_4 , 8.1 mM NaH_2PO_4 , 150 mM NaCl , pH 7.4), containing 10% deuterium oxide (D_2O), which acts as a field frequency lock for the spectrometer, and 0.01% sodium 3-(trimethylsilyl) [2,2,3,3- $^2\text{H}_4$] propionate (TSP) (pH 7.4), which was used as a chemical shift reference (δ 0.0). The resulting samples were centrifuged at 14,000 g_{av} for 10 min to remove particulates. ^1H NMR spectra were acquired for each sample using a Bruker DRX 600 NMR spectrometer operating at 600.13 MHz for ^1H equipped with 5 mm broad band probe (Bruker; Rheinstetten, Germany). A standard 1-dimensional (1-D) solvent suppressed NMR spectrum was acquired for each sample using the pulse sequence [RD- 90° - t_1 - 90° - t_m - 90° -ACQ]. Water suppression was achieved by irradiation of the water peak during the recycle delay (RD = 2 s), and mixing time (t_m = 100 ms). The 90° pulse length was adjusted to approximately 10 μs and t_1 was set to 3 μs . The spectral width was 20 ppm and a total of 64 transients were collected into 32k data points for each spectrum.

The faecal spectral data for rats and mice were acquired with the same pulse program and parameters used for human faecal extracts, but with 128 scans, to compensate for the lower sample weight available in the rodent models (see supplement and material for further details).

Metabolite assignments were made by reference to the literature²¹⁻²⁶ and by using statistical total correlation spectroscopy (STOCSY) with an in-house developed script (Dr. O. Cloarec, Imperial College London).²⁷ Assignments were confirmed with standard two-dimensional (2-D) ^1H - ^1H correlation spectroscopy (COSY), total correlation spectroscopy (TOCSY), ^1H - ^{13}C heteronuclear single quantum correlation (HSQC) and heteronuclear multiple bond correlation (HMBC), performed on selected samples. The COSY and TOCSY acquisition parameters, described in detail elsewhere,^{28,29} were measured on a 600 MHz NMR spectrometer, whereas the ^1H - ^{13}C HSQC and HMBC spectra³⁰⁻³² were acquired on a Bruker Avance 800 NMR spectrometer (Rheinstetten, Germany) operating at 800.13 MHz.

3.3.6 Data Analysis

The NMR spectra were corrected for phase and baseline distortions using an in-house MATLAB script (Dr. T. Ebbels, Imperial College London). Spectra were normalized to total unit area (excluding the region containing the residual water resonance δ 4.7-4.9) and

imported into MATLAB for multivariate analysis. Interpretation of the data was based on principal component analysis (PCA) and orthogonal projection to latent structure-discriminant analysis (O-PLS-DA)³³ of the spectra, in conjunction with visual analysis. PCA provides visualization of clustering, systematic variation (e.g., time-related changes) and outliers by projecting a swarm of coordinates into an n -dimensional hyperspace referred to as a scores plot. Each coordinate represents one individual NMR spectrum, the position of which is determined by its summed spectral intensity ratio. This is plotted on a plane defined by the highest variance of the swarm of points.³⁴ Each principal component (PC) is a linear combination of the original spectral descriptors. Since the first PC relates to the maximum variance in the data set, subsequent PCs are all orthogonal to the preceding PC and explain progressively less of the variance.

The O-PLS-DA model approach gives information about systematic differences in the data related to the biological ‘class’ and allows maximum discrimination between two or more classes. As with PCA, the data can be displayed as scores plots indicating similarity between samples, but additionally the method generates correlation coefficient plots enabling interpretation of the discriminating features in the spectral data. These coefficients plots are colored according to the significance of correlation to ‘class’ (e.g., species, time, etc.) with red representing high significance and blue encoding for low significance. Back-scaling to the covariance matrix is used to maintain the original spectral structure to facilitate interpretability of the coefficient plots.³³ These methods are adapted from the standard O-PLS method defined by Trygg et al.³⁵

The O-PLS-DA models were constructed using NMR spectral data as the X -matrix and class information as the Y -matrix. One orthogonal component was used to remove variation unrelated to class and a 7-fold cross validation of the data was carried out to measure the robustness of the model. The plots were performed in MATLAB with an in-house developed script (Dr. O. Cloarec, Imperial College London).³³ The significance of the differences between two classes in O-PLS-DA was assessed by a correlation coefficient. We designated a cut-off value of 0.53; higher coefficients indicate statistical significance ($p \leq 0.05$) of any given metabolite in discriminating between two classes when considering a group size of 12.

Finally, integration over selected peak regions as determined by the highest weighting coefficients in the model assessing time related variation was performed in MATLAB using a previously published method,³⁶ modified by K. Veselkov. The pair wise comparison of

metabolic changes at time points of interest was performed using a Mann-Whitney test with Bonferroni adjustment for p values in multiple comparisons.

3.4 Results

3.4.1 *Composition of Metabolite Profiles*

Faecal extracts for all three species were characterised by ^1H NMR spectroscopy and the metabolites identified are summarized in Table 3.1. Faecal spectra from the mouse, rat and human shared several similarities in profile as the direct comparison of the 1-D ^1H NMR spectra in Figure 3.1A-C shows. For example, all spectra contained visible resonances from SCFAs (n-butyrate, propionate and acetate), the branched chain amino acids (BCAA; i.e., valine, isoleucine and leucine), glutamate, aspartate, tyrosine and phenolics. An example of metabolite assignment for a mouse faecal extract is provided in a typical 2-D TOCSY spectrum in Figure 3.2.

3.4.2 *Impact of Species, Age/Time and Sample Preparation on the Metabolic Profile*

Three different sources of variation (i.e., species, age/time and sample preparation) and their impact on the faecal metabolome were considered in this study. Differences in the faecal metabolite profiles relating to sample preparation methods were minor in comparison with the variation in profile attributable to species or age/time. A detailed summary of the effect of sample preparation methods on metabolite profile variability is given in the supplementary material. A global PCA of the aqueous faecal extracts shows the relative contribution of species and age/time differences to the variation in the faecal profiles (Figure 3.3A). The most influential factor in describing the variation in the data set was species, which was differentiated in the first PC explaining 77.4% of the total variance in the data, followed by age/time which was differentiated in the second PC. Spectra of faecal samples from mice, humans and rats formed distinct clusters. Whilst the spectra of faecal samples from mice and rats formed relatively tight clusters in both the PCA and PLS-DA scores plots, the human faecal samples were distinct from the other two species and more dispersed, reflecting greater variation in the inter-sample metabolic composition.

A closer assessment of the human control group revealed some degree of differentiation between samples from men and women, due to higher levels of SCFAs (particularly acetate

and *n*-butyrate) in male faecal extracts. Age did not introduce any systematic variation into the faecal profiles (see supplementary material). Samples from humans and mice showed the clearest differentiation in the first PC with those from rats lying in between, in a separate cluster (Figure 3.3A). Thus, all three species had biochemically distinct faecal extract NMR profiles with the greatest similarity demonstrated between mice and rats, and the second closest group pairing being rats and humans. The particular metabolites which predominantly introduced variation into the spectral profile according to species or age difference are examined in the following sections.

3.4.3 Species Differences in Metabolic Profiles between Rat, Mouse and Man

In addition to common metabolic features, several marked inter-species differences were observed and are summarized in Table 3.1. Human faecal samples were characterised by lower levels of lactate and various amino acids, such as phenylalanine, alanine, threonine, glucose and the BBCAs. Glucose resonances were only visible in 4 of the 12 human samples and were associated with the presence of uracil and fumarate, which were otherwise not detectable by visual inspection. In addition, the faecal profile in several human individuals contained glycerol (Figure 3.1A) which was not observed in either of the rodent species, and relatively higher concentrations of acetate and propionate (Figure 3.3B). Higher levels of glucose, hypoxanthine, phenylacetic acid, fumarate, tyrosine uracil and glycine were found in rats and resonances from β -alanine were only visible in the rat (Figure 3.1C).

From a direct comparison between female NMRI mice and female Wistar rats using the supernatant of sonicated slurry, higher levels of uracil, glutamate, *n*-butyrate, propionate and acetate occurred in the rat, whereas alanine and the BCAAs were present in lower levels which is highlighted in the O-PLS-DA plot (Figure 3.3C). Relatively low levels of 3-hydroxy-phenylpropionic acid (3HPPA) were present in approximately 50% of the samples obtained from mice, whereas this metabolite was only observed in one human and one rat faecal sample.

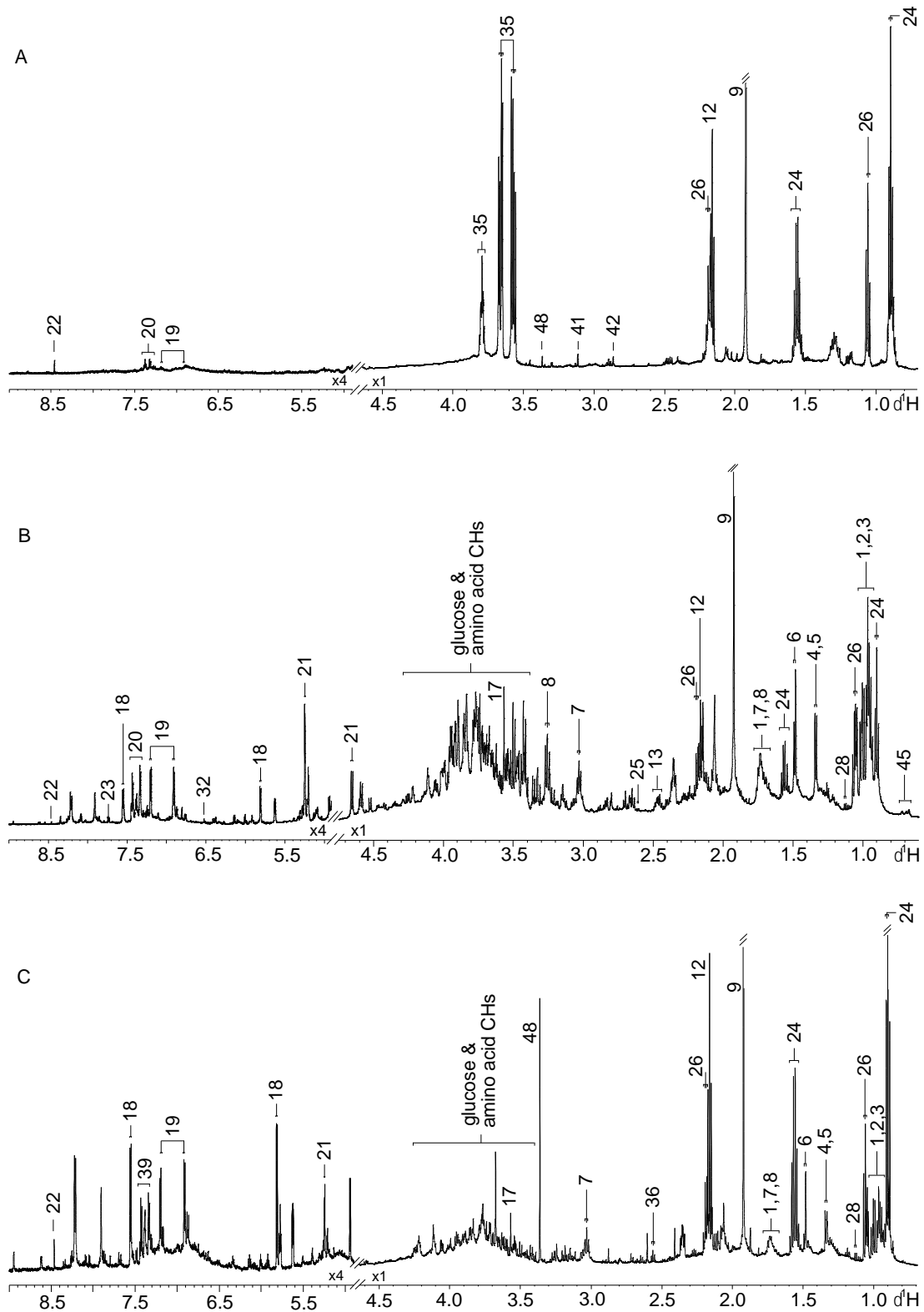


Figure 3.1. 1-D ^1H NMR spectra of (A) human, (B) mouse and (C) rat faecal water. The numbers refer to the metabolites presented in Table 3.1.

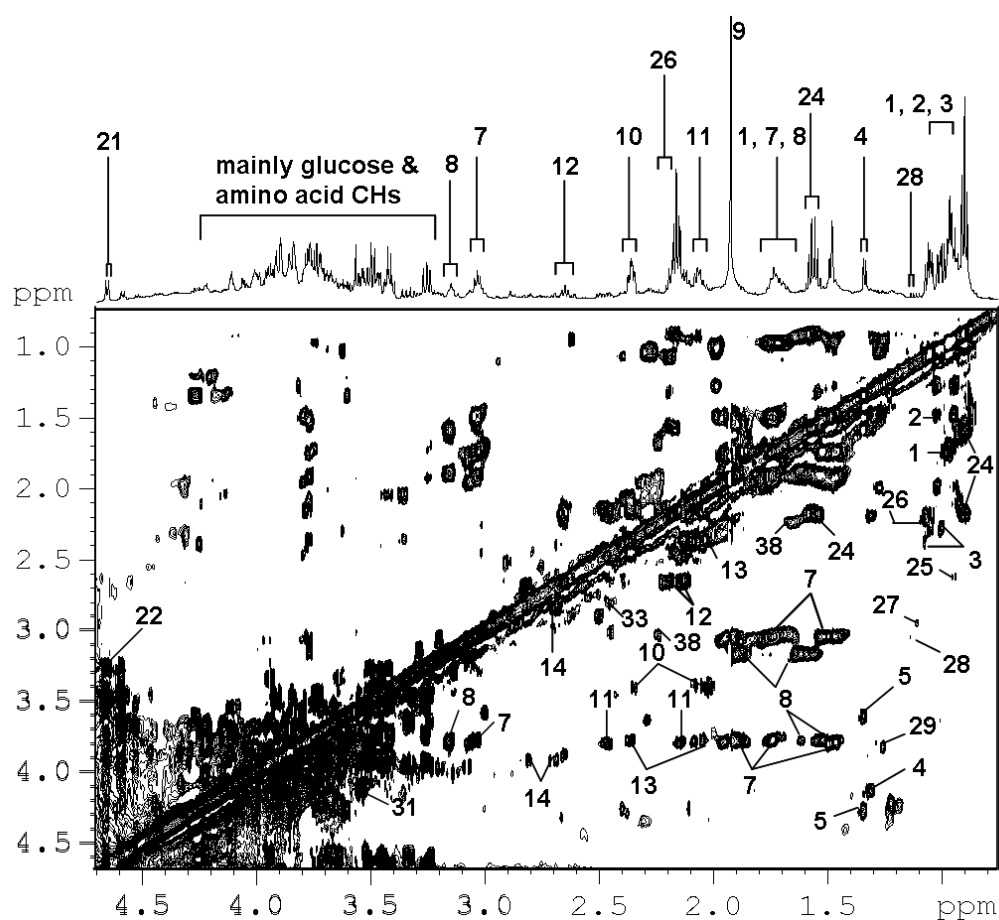


Figure 3.2. 600 MHz ^1H - ^1H 2-D TOCSY spectra of a faecal extract from a female NMRI mouse. Keys: 1, leucine; 2, iso-leucine; 3, valine; 4, lactate; 5, threonine; 7, lysine; 8, arginine; 10, proline; 11, glutamate; 12, methionine; 13, glutamine; 14, aspartate; 22, formate; 24, n-butyrate; 25, α -ketoisocaproate; 26, propionate; 27; α -keto- β -methyl-N-valerate; 28, α -ketoisovalerate; 29, α -hydroxyisovalerate; 31, myoinositol.

The C18 axial methyl signals from bile acids were found in all three species but the identity of the bile acids differed between the species. Rats and mice excreted higher levels of taurocholic/tauro- β -muricholic acid with the latter being relatively higher in mice as described previously,³⁷ whereas deoxycholic acid was the prominent bile acid prevalent in human faecal samples (Figure 3.3D) which is consistent with previous studies.^{38,39} However, in 50% of the human faecal samples the C18 bile acid methyl signal was obscured by a broad envelope of resonances that distorted the spectral baseline in this region which made detailed assignment difficult.

Species variation in the faecal metabolome

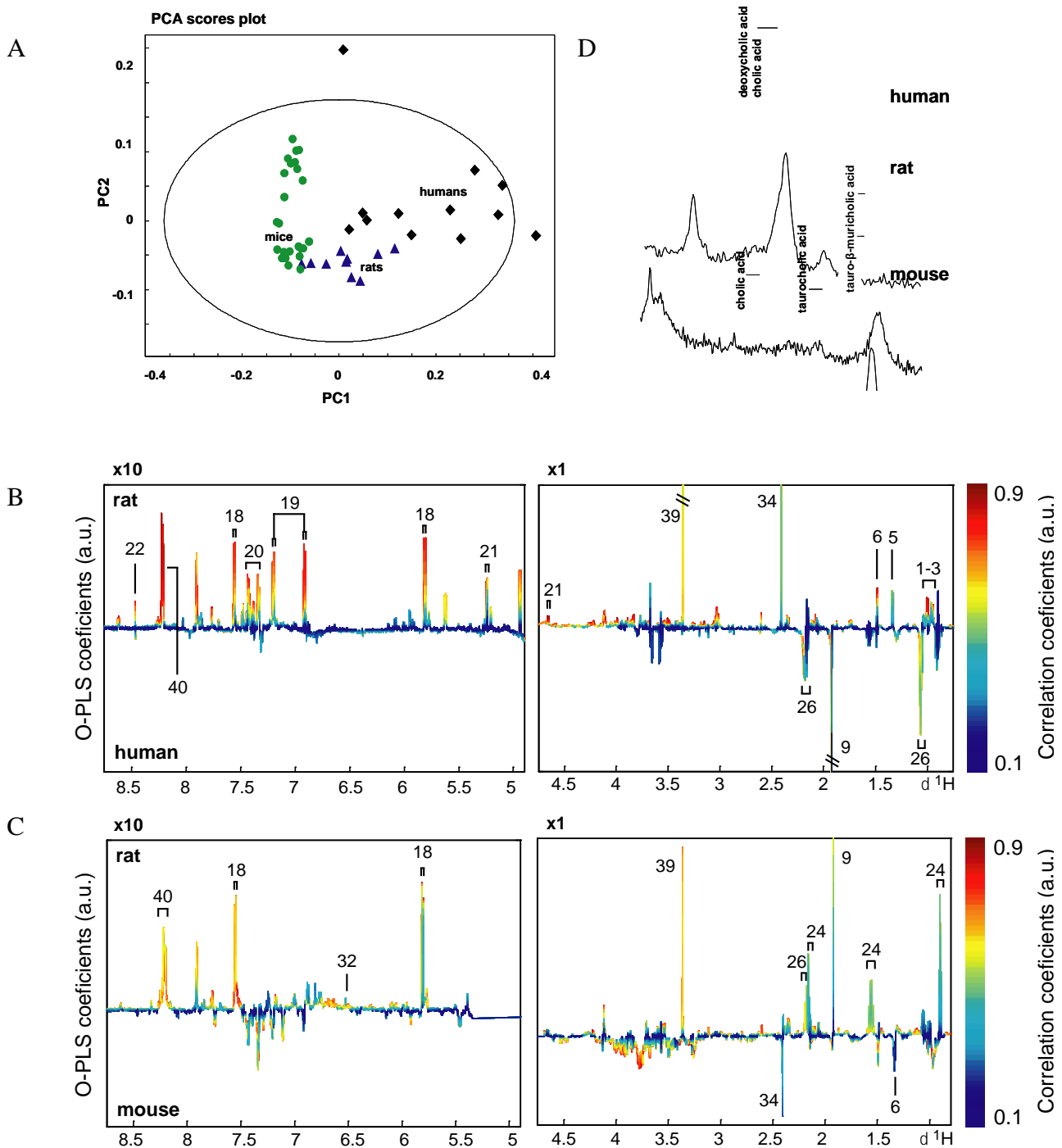


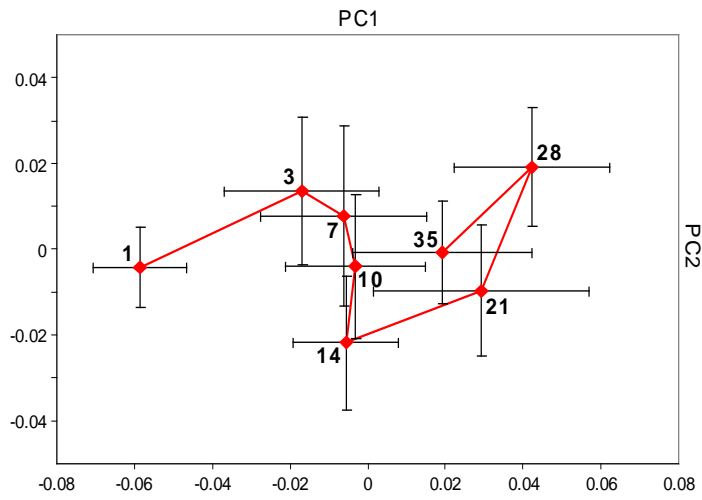
Figure 3.3. (A) Diagram showing the relative effects of two different sources of variation (species and age/time). PCA scores plots of faecal samples analyzed showing differentiation between species (first PC) and time (second PC). The outlier in the human group (male, 26-year-old), is due to higher levels of the SCFAs and a shift at the acetate region (δ 1.92); (B) O-PLS-DA coefficient plots of rats *versus* humans, and (C) rats *versus* mice. The color scale indicates the significance of metabolite variations between the two classes and its maximum is model-dependent. The numbers refer to the metabolites listed in Table 3.1; (D) comparison of the bile acids in all three species for region δ 0.63-0.78 ppm.

3.4.4 Age-Related Metabolic Changes in Aqueous Faecal Extracts

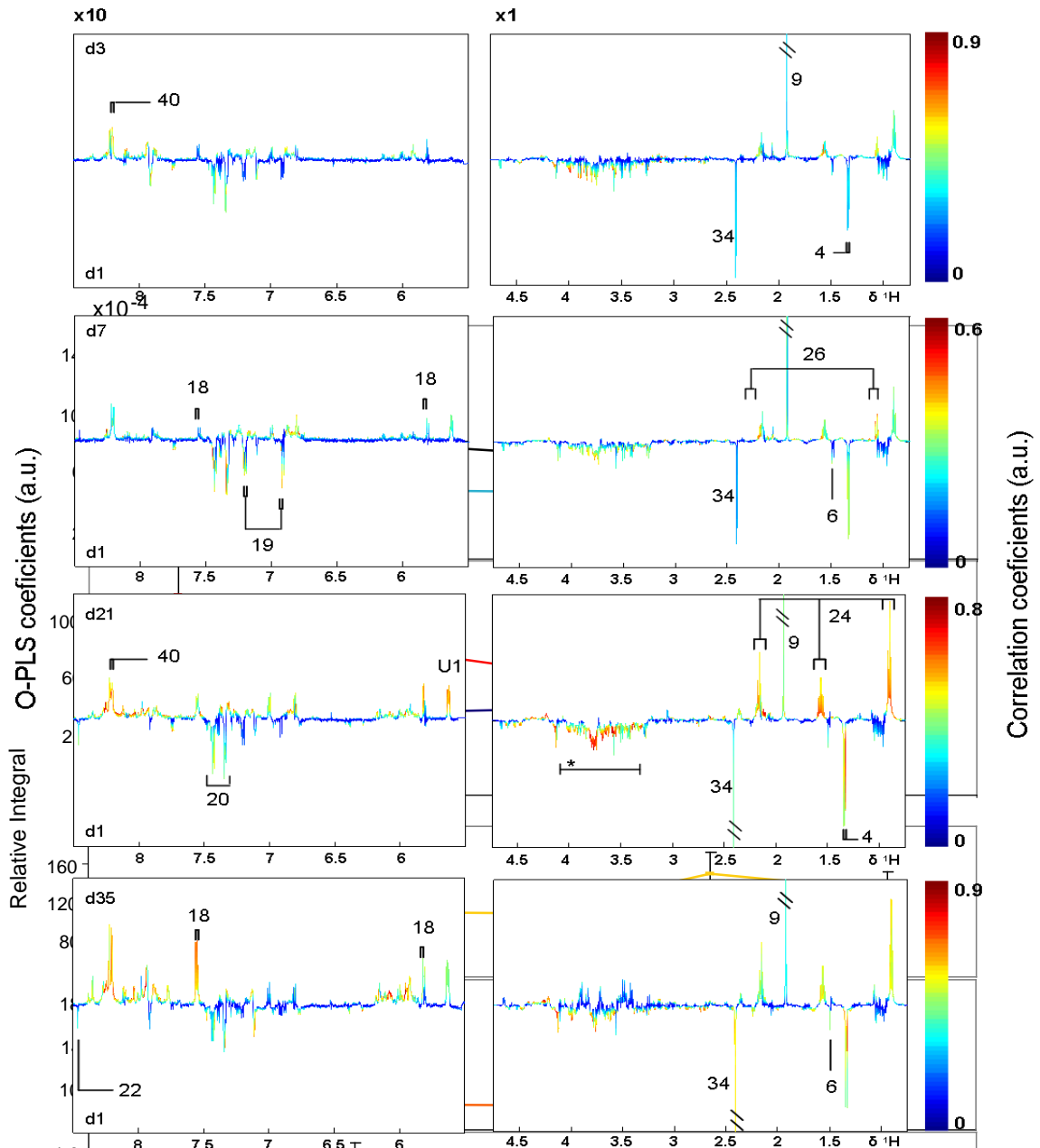
The biochemical variation in faecal metabolite profile of the first group of 10 NMRI female mice revealed highly significant changes in the metabolic profile. In comparison to the baseline samples, those obtained 53 days later showed a marked decrease in various amino acids, including aromatic amino acids (phenylalanine and tyrosine), BCAAs (valine, leucine and isoleucine), lysine, aspartate, glutamate, alanine, methionine and glycine. Apart from the change in the relative amino acid concentrations, there was a significant decrease in lactate and an increase in uracil with time. The sum of the metabolic changes over time in the second group of 12 mice were visualized in a PCA trajectory (Figure 3.4A) which showed substantial, time-dependent movements between days 1 and 35, particularly along the first PC. To obtain a deeper understanding of the significantly changing metabolites, an O-PLS-DA model was calculated for a series of pair wise comparisons between day 1 with days 3, 7, 21 and 35 (Figure 3.4B). Significantly lower levels of phenylalanine were observed at all time points when compared with day 1 (coefficient 0.69-0.81), whilst tyrosine underwent a significant decrease at days 7 (coefficient 0.67) and 21 (coefficient 0.72). Lactate was decreased from day 7 with significance increasing at later time points (coefficient 0.57-0.71). Amongst the metabolites which increased compared to day 1, were three SCFAs (n-butyrate, propionate and acetate), which showed a significant change comparing either of the later time points with day 1. The coefficients ranged from 0.56-0.63 for acetate, 0.65-0.76 for propionate and 0.64-0.81 for butyrate. Threonine and hypoxanthine were significantly differentiated by class at day 35 (coefficients 0.82 and 0.79, respectively), whilst threonine showed the same coefficient of 0.82 already at day 21. Uracil was significantly increased at days 3 and 35 when compared to day 1, but not at the intermediate time points (coefficients 0.62 and 0.71). Resonances from several of the metabolites which showed time-dependent variations were integrated using an automated curve fitting program, and the relative concentration in relation to the total spectral integral determined (Figure 3.4C). The p-values were assessed using a nonparametric 1-way analysis of variance (Mann-Whitney) test in MATLAB. Uracil increased significantly at days 21 and 35 compared to day 1 ($p < 0.001$), similar to hypoxanthine which increased at three different days, 3, 21 and 35 compared to day 1 ($p < 0.01$). Succinate underwent a significant decrease after 35 days ($p < 0.001$), whilst lactate decreased already after 5 days ($p < 0.05$) and maintained its significance over the course of the experiment.

Species variation in the faecal metabolome

A



B



C

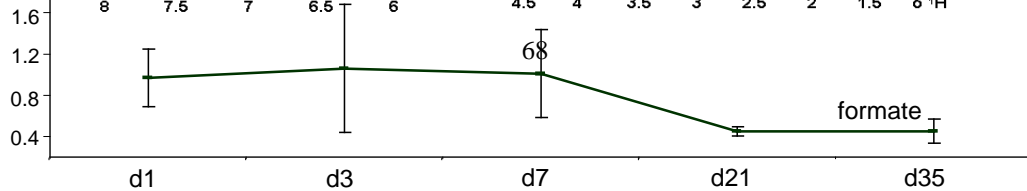


Figure 3.4. (A) PCA trajectory plot of faecal spectra obtained from the mean values for a group of 12 female NMRI mice over a 5-week study period. Mice were 6-week-old at the onset of the experiment. Each point in the plot represents average values of the first and second PC at a certain time point of faecal collection, e.g., at days 1, 3, 7, 10, 14, 21, 28 and 35. The error bars along the first PC and the second PC are expressed by 2 standard deviations of the mean; (B) O-PLS-DA coefficient plots, comparing day 1 of animal handling (class 1) with either of the later time points (class 2). The numbers refer to the metabolites in Table 3.1; * resonances from sugars and amino acid CH groups; (C) Normalised integrals of 5 selected regions with corresponding metabolite identity, proportional to concentrations of metabolites in a solution, (black, hypoxanthine , blue, uracil; red, lactate; marine, succinate; yellow, butyrate; orange, glucose; green, formate) changed significantly during the experiment. The error bars are defined by two standard deviations of the mean. Significant changes are given in the text.

An additional comparison of day 3 with days 21 and 35 also revealed statistical significant differences ($p < 0.001$). Formate decreased after 21 and 35 days ($p < 0.001$), whilst butyrate increased already after day 3, compared to day 1 ($p < 0.01$) and maintained significance at all later time points. Glucose showed an inconsistent picture. Days 3 and 7 were significantly lower, compared to day 1 ($p < 0.05$), whilst a day 1 to day 35 comparison did not differ at all. Comparing days 5 and 19 to day 33 showed statistical difference ($p < 0.01$). The data (Figure 3.1) are expressed as mean \pm 2 standard deviations of the mean.

Although time-dependent trends in increasing acetate and propionate were evident, accurate integration of these resonances was not possible due to extreme inter-sample variation which resulted in an inhomogenous pattern of resonance overlap with n-butyrate and other metabolites in the case of propionate and acetate.

Faecal samples obtained from 10 female Wistar rats obtained at the age of 6 weeks and 23 days later, were assessed and demonstrated time-related changes in the profile. A decrease in the amino acids phenylalanine, tyrosine, glycine, alanine and the BCAA was observed, which was consistent with the findings in mice. However, unlike the mouse model, the levels of SCFAs and uracil did not change significantly with increasing age of the rats. Rat faecal profiles proved to be stable in lyophilized samples over a short period of time, e.g., 24 h.

3.4.5 Effect of Sample Preparation and Storage Conditions on Metabolic Profiles on Faecal Extracts

Differences in the faecal metabolite profiles relating to sample preparation methods were minor in comparison with the variation in profile attributable to species or age/time. The effects of freezing, lyophilization and two different sterilization methods and their associated variability are detailed in the supplementary files. In brief, the processes of freezing and lyophilization increased the BCAA levels and lyophilization decreased the SCFAs. Of the two assessed sterilization methods (sonication and filtration) only sonication had an observable effect in comparison with the untreated sample. Like lyophilization, sonication led to lower relative contribution of the SCFAs to the spectral profile.

Species variation in the faecal metabolome

	Metabolite	Proton group	$\delta^1\text{H}$ (ppm)	Species
1	leucine	α -CH, γ -CH, δ -CH ₃ , δ -CH ₃	3.72(t), 1.69(m), 0.97(d), 0.94(d)	m = r > h
2	iso-leucine	α -CH, β -CH, γ -CH ₂ , δ -CH ₃ , δ -CH ₃	3.68(d), 1.93(m), 1.25(m), 1.47(m), 0.99(d), 1.02(d)	m = r > h
3	valine	α -CH, β -CH, γ -CH ₃ , γ -CH ₃	3.62(d), 2.28(m), 0.98(d), 1.03(d)	m = r > h
4	lactate	α -CH, β -CH ₃	4.11(q), 1.33(d)	m = r > h
5	threonine	α -CH, β -CH, γ -CH ₃	3.60(d), 4.26(m), 1.33(d)	r > h**
6	alanine	α -CH, β -CH ₃	3.81(q), 1.48(d)	m > r > h
7	lysine	α -CH, β -CH ₂ , γ -CH ₂ , δ -CH ₂ , ϵ -CH ₂	3.77(t), 1.92(m), 1.73(m), 1.47(m), 3.05(t)	
8	arginine	α -CH, β -CH ₂ , γ -CH ₂ , δ -CH ₂ ,	3.76(t), 1.89(m), 1.59(m), 3.17(t)	
9	acetate	CH ₃	1.92(s)	h > r > m
10	proline	α -CH, β -CH ₂ , γ -CH ₂ , δ -CH ₂	4.15(t), 2.05(m), 2.38(m), 2.00(m), 3.39(t)	r > h**
11	glutamate	α -CH, β -CH ₂ , γ -CH ₂	3.78(m), 2.06(m), 2.36(m)	
12	methionine	α -CH, β -CH ₂ , γ -CH ₂ , δ -CH ₃	3.87(m), 2.10(m), 2.65(dd), 2.15(s)	
13	glutamine	α -CH, β -CH ₂ , γ -CH ₂ ,	3.78(m), 2.15(m), 2.46(m)	
14	aspartate	α -CH, β -CH ₂	3.92(m), 2.70(m), 2.81(m)	
15	asparagine	α -CH, β -CH ₂	4.01(m), 2.87(dd), 2.96(dd)	
16	ethanolamine	NH-CH ₂ , HO-CH ₂	3.15(t), 3.78(t)	
17	glycine	CH ₂	3.55(s)	r > h = m
18	uracil	CH, CH	5.81(d), 7.59(d)	r > m > h
19	tyrosine	CH, CH	7.23(d), 6.91(d), 2.93(t), 3.25(t)	r > m > h
20	phenylalanine	2,6-CH, 3,5-CH, 4-CH, ArCH ₂ , NH ₂ CH	7.44(m), 7.39(m), 7.33(m), 3.17(dd), 3.30(dd), 3.99(dd)	m > r > h
21	glucose	1-CH, 2-CH, 1-CH, ring protons	5.23(d), 3.25 (m), 4.67 (m), 3.35-4.0 (m)	r > m > h
22	formate	CH ₃	8.46 (s)	r = m > h
23	tryptophan	4-CH, 7-CH, 2-CH, 5,6-CH, 5,6-CH, NH ₂ CH, CH ₂	7.79(d), 7.56(d), 7.34(s), 7.29(t), 7.21(t), 4.06(dd), 3.49(dd), 3.31(dd)	
24	butyrate	CH ₃ , α -CH ₂ , β -CH ₂	0.9(t), 2.16(t), 1.56(m)	r = h > m
25	α -ketoisocaproate	CH ₂ , CH, 2xCH ₃	2.61(d), 2.1(m), 0.94(d)	
26	propionate	CH ₂ , CH ₃	2.19(q), 1.06(t)	h > r > m
27	α -keto- β -methyl-N-valerate	CH, CH ₂ , CH ₂ , terminal-CH ₃ , β CCH ₃	2.93(m), 1.7(m), 1.46(m), 0.9(t), 1.1(d)	
28	α -ketoisovalerate	CH, 2xCH ₃	3.02(m), 1.13(d)	
29	α -hydroxyisovalerate	α -CH, β -CH, CH ₃ , CH ₃	3.85(d), 2.02(m), 0.79(d), 0.84(d)	
30	urocanate	CHCOOH, CH(ring), C ₅ , C ₃	6.4(d), 7.13(d), 7.41(s), 7.89(s)	
31	myoinositol	1,3-CH, 2-CH	3.53(dd), 4.06(t)	
32	fumarate	CH ₃	6.53 (s)	
33	3-hydroxyphenyl propionic acid	CH ₂ , CH ₂ COOH, ring protons	2.47 (t), 2.85 (t), 6.8 (m)	
34	succinate	2x CH ₁	2.42 (s)	m > r > h**
35	glycerol	half CH ₂ , half CH ₂ , C ₂ --H	3.56 (dd), 3.64 (dd), 3.87 (m)	h*
36	β -alanine	NCH ₁ , CH ₂ COOH	3.19 (t), 2.56 (t)	r*
37	bile acid			
38	5-aminovalerate	CH ₂ NH ₂ , CH ₂ COOH, CH	3.02 (t), 2.24 (t), 1.65 (m)	
39	phenylacetic acid	CH ₂ , ring protons	3.52 (s), 7.29 (t), 7.36 (t)	r > m > h
40	hypoxanthine	ring protons	8.11 (s), 8.099 (s)	r > m > h
41	malonate	CH ₁	3.133(s)	h*
42	trimethylamine	CH ₃	2.88(s)	
43	3-hydroxyphenyl propionic acid	CH ₂ , CH ₂ COOH, ring protons	2.47 (t), 2.85 (t), 6.8 (m)	
44	5-aminovalerate	CH ₂ NH ₂ , CH ₂ COOH, CH	3.02 (t), 2.24 (t), 1.65 (m)	
45	bile acid		0.7 (m)	
46	myoinositol	1,3-CH, 2-CH	3.53(dd), 4.06(t)	
47	urocanate	CHCOOH, CH(ring), C ₅ , C ₃	6.4(d), 7.13(d), 7.41(s), 7.89(s)	
48	methanol	CH	3.36(s)	

Table 3.1. List of metabolites found in three species, human (h), mouse (m) and rat (r). *specific for one species; </> relatively lower/higher amount of the metabolite found in feces in species comparison; **shows trend but is not significant to the p-value

3.5 Discussion

In order to establish their diagnostic biomarker utility, detailed examination of readily accessible biofluids that can be collected in a non-invasive fashion should be pursued. Although faecal extracts might not represent the first choice of most analyses for metabolic profiling, the intimate connection of the faecal metabolites with the gut microbiota is undeniable. Furthermore with the growing appreciation of the importance of the gut microbes in mammalian disease¹⁻⁶ it is now time to evaluate variations in metabolite composition between humans and widely used experimental animals.

Extracts of faecal water hold promise as a biological medium for diagnosing disease⁸⁻¹² and can help to characterise the symbiotic metabolic relationship between the mammalian host and its associated microbiome. However, the utility of a biofluid or tissue extract, and the reliability of candidate biomarkers identified in that medium are partially dependent on the normal physiological variation in biochemical composition and on the stability of the metabolic profile. The biochemical composition in aqueous faecal extracts obtained from three different mammalian species, including temporal/age variation and the effect of sample preparation, have been investigated in the current study with a view to assessing the reliability of feces as a medium for identifying biomarkers of disease. Species age/time and sample preparation methods were all found to be sources of variation in the metabolic profile of faecal extracts, in decreasing order of magnitude of effect. The sample preparation method used exerted minimal influence on the spectral profile, and the magnitude of variation induced by different methods was negligible in comparison to species differences. It can therefore be assumed that information and data relating to the identification of candidate biomarkers for pathological conditions or therapeutic interventions will be transferable across studies and laboratories.

3.5.1 *Inter-Species Differences in the Faecal Metabolite Profile*

The faecal metabolite profiles of the three species investigated (humans, rats and mice) shared some similarities but also contained metabolite patterns that were unique to each species. Metabolites that were conserved across the three species included many of the amino acids and the SCFAs (n-butyrate, propionate and acetate), whereas glycerol was unique to humans

and β -alanine was specific for rats. Unsurprisingly the variation in the faecal profiles from human samples was much greater than for either mice or rats which were largely homogeneous and formed tight clusters in the PCA scores plots (Figure 3.3A). The greater diversity in the human profiles is also reflective of exposure to greater environmental gut microbiome variation and host genetic variation than laboratory animals kept genetically uniform and under environmentally-controlled conditions. The inhomogeneity of the human samples is found to be influenced by the gender of the participants but not by age (range: 24-51 years). This result mirrors the difference in the relative degree of variation typically observed in urinary metabolite profiles.¹⁹ Faecal excretion of relatively high concentrations of SCFAs, predominantly acetate, in men has not to our knowledge previously been reported. In fact, contrary to these findings Wolever and colleagues (1996)⁴⁰ reported that serum acetate:propionate ratios did not differ between men and women. Whilst some human metabolites like the BCAAs, lysine, asparagine and the SCFAs (acetate, n-butyrate and propionate) were found in all analysed human samples in similar relative concentrations, other components such as the bile acids were highly variable in concentration and presence. Interestingly, uracil, glucose and fumarate appeared to co-vary in the human samples but this was not the case in either of the rodent species investigated. The glucose and pyrimidine transporters in the small intestine share a similar distribution and mode of action.¹⁹ In addition to showing the greatest dispersion, human samples were also most divergent from the other groups, with rats and mice being the most similar to each other in profile. Rat faecal profiles were characterised by relatively higher concentrations of uracil and the aromatic amino acids tyrosine and phenylalanine, in comparison with the two other species. Particularly high uracil levels in the rat were associated with the presence of β -alanine which was not observed in either human or mouse faecal samples. Both components are intermediates in the degradation of cytosine (Figure 3.5).⁴¹ The high levels of β -alanine and cytosine in the rat faecal samples suggest a higher presence of potential inhibitors of the uracil transporters in the jejunum of the rat, which actively transports uracil from mucosa to serum. It could be shown that phenylalanine, which was also increased in the rat faecal sample, acts as a fully competitive inhibitor of the uracil transporter.⁴² The degradation of uracil to β -alanine by certain intestinal bacteria may account for the relative higher levels of β -alanine found in rat feces.^{43,44}

3.5.2 Influence of Age/Time on the Faecal Metabolite Profile

The O-PLS-DA models, differentiating samples obtained sequentially over a 5-week period on the basis of time, were significant with reasonably strong Q^2 values (0.48-0.88).

These results indicate that the faecal profile was not stable over the duration of the study. The PCA trajectory (Figure 3.4A) also supports this observation, showing an initial deviation from the metabolic starting position in the first week of the study and then a period of relative stability followed by another deviation in biochemical composition of faecal content 3 weeks after the initial sampling point.

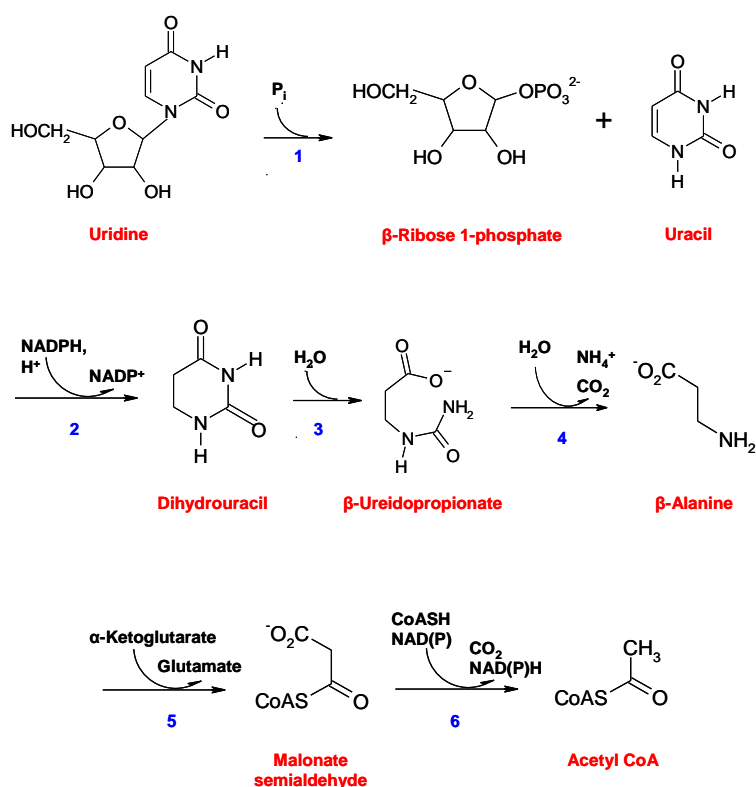


Figure 3.5. Degradative pathway of uracil: Key for enzymes: 1, uridine phosphorylase; 2, dihydropyrimidine dehydrogenase; 3, dihydropyrimidinase; 4, 3-ureidopropionase; 5, 3-alanine-pyruvate transaminase; 6, malonate semialdehyde dehydrogenase.

Although the global trend in time-related variation in the faecal metabolome was clear, the inter-animal variation was relatively high as demonstrated by the error bars in the PCA scores plot in Figure 3.4A. The metabolic components predominantly associated with this temporal

variation included the SCFAs (acetate, propionate and n-butyrate) which increased with time along with tyrosine and uracil, whereas alanine and succinate decreased over the study duration. Both rats and mice showed similar temporal variation in the faecal metabolite profile. However, the metabolic profile was relatively stable in rats over short periods (up to 24 h), particularly when lyophilized samples were used. Since the relative contributions of the SCFAs are reduced following the lyophilization process, this is consistent with the SCFAs showing higher temporal variation than other faecal components. The mice were approximately 6-week-old at the beginning of the experiment. Female mice typically become sexually mature when aged between 6 and 7 weeks,⁴⁵⁻⁴⁸ therefore some of the initial metabolite changes in the first week may be related to the onset of sexual maturity since this is known to have an effect on the composition of the microbiota. However, this is unlikely to account for the metabolic changes evolving after day 14 of the study (corresponding to mice aged approximately 8 weeks). Also, since the nature of changes in specific metabolites over time were largely consistent throughout the total duration of the study, with the exception of lactate, succinate and threonine, the initial perturbations in metabolite profile changes are more likely to derive from a shift in the gut microbiota presence or activity which is independent of the onset of sexual maturity.^{47,48}

As demonstrated in other publications, the variation in the biochemical composition of feces caused by age/time or inter-individual differences are small compared to the variation induced by diseases such as Crohn's disease, ulcerative colitis or bowel cancer.⁷⁻⁹ The characterization of variation in the 'normal' faecal metabolome presented here, and the indication of the more stable metabolic components of the faecal profile, should facilitate establishing the degree of confidence with which future disease-related studies can be interpreted in assessing systemic metabolic changes induced by nutritional interventions (e.g., pre- or probiotic administration), as well as lifestyle choices.

3.6 Acknowledgment.

The authors thank Dr. Olivier Cloarec for providing the MATLAB script for O-PLS-DA and STOCSY analysis. This work received financial support from Imperial College London, Department of Biomolecular Medicine, the Swiss National Science Foundation (project no. PPOOB--102883) and Science Foundation Ireland. The authors also acknowledge Nestlé for provision of funds for Y.W.

3.7 References

- (1) Guarner, F.; Malagelada, J. R. *Lancet* **2003**, 361, 512-519.
- (2) Ordovas, J. M.; Mooser, V. *Curr. Opin. Lipidol.* **2006**, 17, 157-161.
- (3) Ley, R. E.; Turnbaugh, P. J. *Nature* **2006**, 444, 1022-1023.
- (4) Nicholson, J. K.; Holmes, E.; Wilson I. D. *Nat Rev Microbiol.* **2005**, 3, 431-438.
- (5) Parracho, H. M.; Bingham, M. O.; Gibson, G. R.; McCartney, A. L. *J. Med Microiol.* **2005**, 54, 987-991.
- (6) Juste, C. *Bull. Cancer.* **2005**, 92, 708-721.
- (7) Naruse, S.; Ishiguro, H.; Ko, S. B.; Yoshikawa, T.; Yamamoto, T.; Yamamoto, A.; Futakuchi, S.; Goto, H.; Saito, Y.; Takahashi, S. *J Gastroenterol.* **2006**, 41, 901-908.
- (8) Marchesi, J. R.; Holmes, E.; Khan, F.; Scanlan, P.; Shanahan, F.; Wilson, I. D.; Wang, Y. *J. Proteome Res.* **2007**, 6, 546-551.
- (9) Angriman, I.; Scarpa, M.; D'Inca, R.; Basso, D.; Ruffolo, C.; Polese, L.; Sturniolo, G. C.; D'Amico, D. F.; Plebani, M. *Clin. Chim. Acta* **2007**, 381, 63-68.
- (10) Tonus, C.; Neupert, G.; Sellinger, M. *World J. Gastroenterol.* **2006**, 12, 7007-7011.
- (11) Ahlquist, D. A.; Skoletsky, J. E.; Boynton, K. A.; Harrington, J. J.; Mahoney, D. W.; Piercall, W. E.; Thibodeau, S. N.; Shuber, A. P. *Gastroenterology* **2000**, 119, 1219-1227.
- (12) Glei, M.; Hoffmann, T.; Kuster, K.; Hollmann, J.; Lindhauer, M. G.; Pool-Zobel, B. *J. Agric. Food Chem.* **2006**, 54, 2088-2095.
- (13) Nicholson, J. K.; Lindon, J. C.; Holmes, E. *Xenobiotica* **1999**, 29, 1181-1189.
- (14) Nicholson, J. K.; Connelly, J.; Lindon, J. C.; Holmes, E. *Nat. Rev. Drug Discov.* **2002**, 1, 153-161.
- (15) Lenz, E. M.; Wilson, I. D. *J. Proteome Res.* **2007**, 6, 443-458.
- (16) Wang, Y. L.; Holmes, E.; Nicholson, J. K.; Cloarec, O.; Chollet, J.; Tanner, M.; Singer, B. H.; Utzinger, J. *Proc. Natl. Acad. Sci. U.S.S.* **2004**, 101, 12676-12681.
- (17) Lindon, J. C.; Holmes, E.; Nicholson, J. K. *Pharm. Res.* **2006**, 23, 1075-1088.

- (18) Robertson, D. G.; Reily, M. D.; Lindon, J. C.; Holmes, E.; Nicholson, J. K. *Compr. Toxicol.* **2002**, 14, 583-610.
- (19) Bollard, M. E.; Stanley, E. G.; Lindon, J. C.; Nicholson, J. K.; Holmes, E. *NMR Biomed.* **2005**, 18, 143-162.
- (20) Keiser, J.; Utzinger, J.; Tanner, M.; Dong, Y.; Vennerstrom, J. *J. Antimicrob. Chemother.* **2006**, 58, 1193-1197.
- (21) Foxall, P. J. D.; Spraul, M.; Farrant, R. D.; Lindon, L. C.; Neild, G. H.; Nicholson, J. K. *J. Pharm. Biomed. Anal.* **1993**, 11, 267-276.
- (22) Bailey, D.; Davies, M. J.; Routier, F. H.; Bauer, C.; Feeney, J.; Hounsell, E. F. *Carbohydr. Res.* **1997**, 300, 289-300.
- (23) Schneider, M. U.; Demling, L.; Domschke, S.; Heptner, G.; Merkel, I.; Domschke, W. *Hepatogastroenterology* **1985**, 32, 210-215.
- (24) Bene, B. C. *Physiol. Chem. Phys.* **1980**, 12, 241-247.
- (25) Cuvillier, O.; Alonso, C.; Wieruszkeski, J. M.; Brassart, C.; Strecker, G.; Bouquelet, S.; Michalski, J. C. *Glycobiology* **1995**, 5, 281-289.
- (26) Righetti, C.; Peroni, D. G.; Pietrobelli, A.; Zancanaro, C. *J. Pediatr. Gastroenterol. Nutr.* **2003**, 36, 498-501.
- (27) Cloarec, O.; Dumas, M. E.; Craig, A.; Barton, R. H.; Trygg, J.; Hudson, J.; Blancher, C.; Gaugier, D.; Lindon, J. C.; Holmes, E.; Nicholson, J. K. *Anal. Chem.* **2005**, 77, 1282-1289.
- (28) Hurd, R. E. *J. Magn. Reson.* **1990**, 87, 422-428.
- (29) Bax, A.; Davis, D. G. *J. Magn. Reson.* **1985**, 65, 355-360.
- (30) Bodenhausen, G.; Ruben, D. *J. Chem. Phys. Lett.* **1980**, 69, 185-189.
- (31) Bax, A.; Summers, M. F. *J. Am. Chem. Soc.* **1986**, 108, 2093-2094.
- (32) Summers, M. F.; Marzilli, L. G.; Bax, A. *J. Am. Chem. Soc.* **1986**, 108, 4285-4294.
- (33) Cloarec, O.; Dumas, M. E.; Trygg, J.; Craig, A.; Barton, R. H.; Lindon, J. C.; Nicholson, J. K.; Holmes, E. *Anal. Chem.* **2005**, 77, 517-526.
- (34) Eriksson, L.; Johansson, E.; Kettaneh-Wold, N.; Trygg, J.; Wikstrom, C.; Wold, S. *Multi and megavariate data analysis*, **2001**.

- (35) Trygg, J. J. *Chemom.* **2002**, 16, 283-293.
- (36) Crockford, D. J.; Keun, H. C.; Smith, L. M.; Holmes, E.; Nicholson, J. K. *Anal. Chem.* **2005**, 77, 4556-4562.
- (37) Martin, F. P. J.; Dumas, M. E.; Wang, Y. L.; Legido-Quigley, C.; Yap, I. K. S.; Tang, H. R.; Zirah, S.; Murphy, G. H.; Cloarec, O.; Lindon, J. C.; Sprenger, N.; Fay, L. B.; Kochhar, S.; van Bladeren, P.; Holmes, E.; Nicholson, J. K. *Mol Syst. Biol.* **2007**, 3, 1-16.
- (38) Kiyohisa, U.; Takashi, S.; Seiko, N.; Kikuji, I.; Haruto, T.; Kazuo, K.; Hiroyuki, N.; Nobuo, Y.; Kazuo, Y. *Lipids* **1999**, 34, 269-273.
- (39) Carey, J. B.; Watson, C. J. *J. Biol. Chem.* **1955**, 216, 847-850.
- (40) Wolever, T. M. S.; Fernandes, J.; Rao, A. V. *J. Nutr.* **1996**, 126, 2790-2797.
- (41) Wasternack, C. *Pharmacol. Ther.* **1980**, 8, 629-651.
- (42) Katgely, B. W.; Bridges, R. J.; Rummel, W. *Biochim. Biophys. Acta* **1986**, 862, 429-434.
- (43) Andersen, G.; Andersen, B.; Dobritzsch, D.; Schnakerz, K. D.; Piskur, J. *FEBS J.* **2007**, 274, 1804-1817.
- (44) West, T. P. *Antonie van Leeuwenhoek* **2001**, 80, 163-167.
- (45) Sprumont, P. *Cell Tissue Res.* **1978**, 188, 409-426.
- (46) Woodmansey, E. J. *J. Appl. Microbiol.* **2007**, 102, 1178-1186.
- (47) Hopkins, M. J.; Sharp, R.; Macfarlane, G. T. *Dig. Liver Dis.* **2002**, 34 (Suppl. 2), S12-S18.
- (48) Andrieux, C.; Membre, J. M.; Cayuela, C.; Antoine, J. M. *Scand. J. Gastroenterol.* **2002**, 37, 792-798.





4 Use of *Echinostoma* spp. in studies on chemotherapy and metabolic profiling

Jasmina Saric,^{†,‡} Jia Li,^{†,‡} Yulan Wang,[‡] Elaine Holmes,[‡] Jürg Utzinger,[†] and Jennifer Keiser,^{†,*}

[†] Department of Public Health and Epidemiology, Swiss Tropical Institute, P.O. Box, CH-4002 Basel, Switzerland

^{†,*} Department of Medical parasitology and Infection Biology, Swiss Tropical Institute, P.O. Box, CH-4002 Basel, Switzerland

[‡] Department of Biomolecular Medicine, Division of Surgery, Oncology, Reproductive Biology and Anaesthetics (SORA), Faculty of Medicine, Imperial College London, Sir Alexander Fleming Building, South Kensington, London SW7 2AZ, United Kingdom

*Corresponding author: Professor Jennifer Keiser, Department of Medical parasitology and Infection Biology, Swiss Tropical Institute, P.O. Box, CH-4002 Basel, Switzerland.

Tel.: +41 61 284-8218; Fax: +41 61 284-8101. E-mail: jennifer.keiser@unibas.ch

4.1 Abstract

In this chapter we briefly summarize the use of echinostomes in chemotherapeutic studies, and provide a comprehensive overview of metabolic profiling using an *Echinostoma caproni*-mouse model. *In vitro* and *in vivo* assays with *Echinostoma* spp. are suitable means for screening of anthelmintic drugs. Indeed, these models have been utilized for more than three decades and play an important role for discovery and development of novel drugs and treatment options against major trematode infections. Rapid diagnosis of infection and monitoring of disease progression and resolution are of pivotal importance for personalized health care and disease control at the population level. Spectroscopic profiling of the host metabolism, in combination with multivariate statistical methods, is a powerful approach for biomarker discovery that give rise for diagnosis and prognosis of infection and disease stages, and for subtle monitoring control interventions. The comparison of biofluids and tissue samples obtained from mice experimentally infected with *E. caproni* and from non-infected control animals revealed a high number of biomarkers in different kinds of biofluids (e.g., blood plasma, faecal water and urine). Several tissues also showed significant metabolic changes after a chronic infection with *E. caproni*. Whilst urine and blood plasma are obvious and convenient choices for diagnostic purposes, the study on tissue samples complemented the information extracted from biofluids and aided in a deeper understanding of biochemical mechanisms of disease.

4.2 Introduction

This chapter reviews the use of echinostomes in chemotherapeutic studies and in metabolic profiling. Chemotherapy is one of the main pillars for the control of food-borne trematode infections, including echinostomiasis. However, the current chemotherapeutic arsenal is limited to two drugs; namely (i) triclabendazole for the treatment of fascioliasis, and (ii) praziquantel against clonorchiasis, opisthorchiasis, paragonimiasis, and intestinal fluke infections⁴. Disposing of only two drugs for diseases that affect at least 40 million individuals, with some 750 million people at risk (more than 10% of the world's population) is potentially dangerous. Moreover, food-borne trematodiasis is emerging²² and there is considerable concern regarding the development of drug-resistant parasite strains as unexpectedly low cure rates have been observed in clonorchiasis patients following praziquantel administration⁶¹. A vaccine against food-borne trematodiasis is not expected to arrive for at least another decade or so. Changing human behavior as a means to reduce transmission of the diseases is a formidable challenge due to cultural habits (e.g., consumption of raw fish and other aquatic products)⁶². Hence, development of novel trematocidal drugs is of great importance in the period while praziquantel and triclabendazole remain effective. An *Echinostoma*-mouse model holds promise in trematocidal drug discovery and development, and metabolic profiling can serve as a platform for biomarker discovery with diagnostic, prognostic, and drug/vaccine target potential.

In the next part we summarize studies that have utilized *Echinostoma* spp. as a drug discovery tool. Emphasis is placed on *in vivo*, *in vitro*, and scanning electron microscopic (SEM) investigations. Spectroscopy is another interesting tool that has been applied in drug discovery and development⁶³. However, whilst spectroscopy has been widely used in drug research and development (R&D) for antiparasitic drugs⁶⁴ to our knowledge, it has not been specifically applied to echinostomiasis. Advances in the technology of spectroscopy lend themselves to profiling the metabolic response of the host organism to parasite invasion. Hence, the third part of the chapter is focused on illuminating the role of the spectroscopic strategies in profiling host-parasite and host-parasite-drug interactions. The main focus of its application to *E. caproni* has been to establish a comprehensive metabolic response of the mouse to an *E. caproni* infection⁶⁵, and to compare the biochemical profiles in the biofluids and tissues of infected with non-infected control mice.

Use of *Echinostoma* spp. in studies

Table 4.1 Use of the *E. caproni*-mouse model for chemotherapeutic studies

Year, Reference	Model	Treatment	Dose (mg/kg)	Worm burden reduction (%)
1971, ⁶⁶	<i>E. miyagawai</i> in mice	Male fern extract	1 x 400	64.5
		Acriquine	1 x 300	86
		Dichlorophen	1 x 200	80
		Trichlorophen	1 x 200	84
		Chloxyl	1 x 100	100
		Bithionol	1 x 100	100
		Phenasal	1 x 100	100
		Piperazine salt of phenasal	1 x 100	100
		Brotianide	1 x 75	100
		Niclofolan	1 x 10	100
		Nitroxynil	1 x 25	100
1975, ⁶⁷	<i>E. caproni</i> in mice	Oxyclozanide	1 x 50	100
		Rafoxanide	1 x 50	100
		Tribromsalan	1 x 100	100
		Niclosamide	1 x 200	100
		Hexachlorophene	1 x 200	100
1979, ⁶⁸	<i>E. caproni</i> in mice	Bithionol	1 x 300	80
		Flubendazole	1 x 200	0
		Thiabendazole	5 x 200	100
		Oxybendazole	5 x 200	0
1980 ⁶⁹	<i>E. caproni</i> in mice	Cambendazole	5 x 200	5
		Fenbendazole	5 x 200	20
		Parbendazole	5 x 200	50
		Mebendazole	5 x 200	100
1986 ⁹	<i>E. ilocanum</i> in rats and gerbils	Mebendazole	50 mg per animal	100
		Clorsulon	1 x 100	100
1995 ⁷⁰	<i>E. caproni</i> in ICR mice	Rafoxanide	1 x 50	100
		Mebendazole	1 x 1000	No effect
		Arprinocid	1 x 100	No effect
1998 ⁷¹	<i>E. caproni</i> in BALB/c mice	Albendazole	1 x 100	Not reported
2006 (Keiser et al., 2006b)	<i>E. caproni</i> in NMRI mice	Tribendimidine	1 x 125	100
2006 (Keiser et al., 2006d)	<i>E. caproni</i> in NMRI mice	OZ78	1 x 1000	100
2006 (Keiser et al., 2006a)	<i>E. caproni</i> in NMRI mice	Artemether	1 x 1100	100
	<i>E. caproni</i> in NMRI mice	Artesunate	1 x 700	100
	<i>E. caproni</i> in NMRI mice	Artemisinin	1 x 1500	99
	<i>E. caproni</i> in NMRI mice	Arteether	1x 1300	75
	<i>E. caproni</i> in NMRI mice	Praziquantel	1 x 50	100

4.3 Use of *Echinostoma caproni* in trematocidal drug discovery and development

4.3.1 Evaluation of *Echinostomicidal* activity *in vivo*

Rodents infected with *Echinostoma* spp. are suitable models for anthelmintic studies, justified as follows. First, it is relatively straightforward to maintain the life cycle in the laboratory. In the case of *E. caproni*, for example, mice are used as the definitive host and *Biomphalaria glabrata* snails as first and second intermediate host¹². In contrast, studies utilizing *Clonorchis sinensis*, one of the most important liver flukes⁷², require rats as the definitive host, as well as the digestion of infected fish material to obtain metacercariae⁷³, and hence the life cycle is considerably more challenging to maintain in the laboratory. Second, *E. caproni* has a short development period of only 10-14 days in rodents¹². This model therefore produces rapid results and is more cost-effective than host-parasite models with a longer development and a more complex life cycle. Moreover, the *Echinostoma*-mouse model is not only useful for anthelmintic studies on echinostomes, but can also serve as a pre-screen to test for *in vivo* trematocidal activity of compounds. However, it should be kept in mind that the feeding behavior (echinostomes do not feed on blood) and the location of *Echinostoma* spp. in the definitive host differ from the major food-borne trematodes, the liver flukes (e.g. *C. sinensis*, *Fasciola hepatica*, and *Opisthorchis viverrini*) and the lung flukes (*Paragonimus* spp.). So for example, depending on the pharmacologic characteristics (e.g. absorption and distribution) of the drug, the *in vivo* drug efficacy between the individual fluke infections might vary.

Table 4.1 summarizes *in vivo* studies that employed *Echinostoma* spp. for drug screening studies. The first investigation we could identify dates back to 1971⁶⁶. The majority of studies employed *E. caproni* in the mouse, but also *E. ilocanum* in rats and gerbils⁹, and *E. miyagawai* in mice⁶⁶ were utilized. Drug efficacy was analyzed as early as 24 hours post-treatment⁶⁷. High activities against *E. caproni* and *E. miyagawai* were observed with single oral doses of chloxyl, phenasan, niclosamide, niclofolan and hexachlorofen^{66,67}.

Some of these drugs were commonly used in the first half of the 20th century to treat infections with different food-borne trematodes in humans; however, patients often suffered from severe adverse events^{74, 75}. Four studies analyzed the echinostomicidal effect of different benzimidazoles. Several of the benzimidazoles (e.g., thiabendazole) showed no activity even after long treatment courses or when administered at high doses^{69, 70}.

On the other hand, complete worm burden reductions were observed in two studies with multiple treatment courses of mebendazole^{9, 69}. Praziquantel, tribendimidine, artemisinin and two of its derivatives (artemether and artesunate), and the synthetic trioxolane OZ78 were tested recently in the *E. caproni*-mouse model^{76, 77}. A single 50 mg/kg oral dose of praziquantel resulted in 100% worm burden reduction. High doses of artesunate (700 mg/kg), OZ78 (1000 mg/kg), artemether (1100 mg/kg), and artemisinin (1500 mg/kg) were required to yield cure rates of 99-100%. The need for high doses of artemisinin and two of its main derivatives to achieve high efficacy in the *E. caproni*-mouse model might be explained with *E. caproni* being a non-hematophagous feeder. Hence, this intestinal fluke does not degrade hemoglobin to generate free heme, which is a possible activator/receptor for the artemisinins¹. Indeed, previous studies found that considerably lower doses of the artemisinins and synthetic trioxolanes administered to rats infected with *F. hepatica*, or mice infected with the blood fluke *Schistosoma mansoni* resulted in high worm burden reductions (Keiser, 2006d, Utzinger et al. 2007). Finally, tribendimidine is considered a promising broad spectrum anthelmintic drug, which has recently been approved by Chinese food and drug regulatory authorities⁷⁸. Complete worm burden reductions were achieved in the *E. caproni*-mouse model following the administration of a single 125 mg/kg oral dose or higher⁷⁷.

4.3.2 Drug sensitivity assay with *Echinostoma caproni* *in vitro*

Several studies have examined the echinostomicidal properties of different drugs *in vitro*^{67, 76, 79}. Since echinostomes have a short development period *in vivo*, these trematodes can be obtained within a couple of days for subsequent *in vitro* studies. Another advantage of this model is that mice tolerate high infection intensities with echinostomes, leading to a large quantity (up to 100) of worms that can be recovered from the intestine of mice¹³. In contrast, only a low number of flukes can be obtained from other food-borne trematode-rodent models, e.g., *F. hepatica*-rat model delivers, on average ~5-8 flukes⁸⁰. For *in vitro* chemotherapeutic studies, echinostomes were recovered from mice 11-14 days post-infection and incubated in the presence of the compound to be analyzed in NCTC 135 culture medium, or Hanks' balanced salt solution (HBSS), supplemented with antibiotics. Worms were observed for up to five days and mortality recorded^{67, 76, 79}. Drug effects might also be assessed by motility disturbances (e.g., activity or paralysis), or morphological changes such as relaxation, shrinkage, curling, tegumental disruption, or worm disintegration.

Excysted juvenile *Echinostoma* worms ⁸¹ might also prove useful for *in vitro* chemotherapeutic studies. Assays with juvenile *E. caproni* obtained from metacercariae, treated in a trypsin-bile salts excystation medium at 39°C ⁸¹1997), for example, do not require the definitive host, hence are ethically sound, rapid to obtain, and inexpensive.

4.3.3 Scanning electron microscopy (SEM) studies

The tegument of trematodes is one of the most susceptible sites of damage following chemotherapy, and drug effects are readily examined by the evaluation of treated worm specimen by SEM. Indeed, SEM analysis deepens our knowledge of the sites and mechanisms of action of anthelmintics ⁸². Structural changes in the tegument following drug administration can be analyzed by means of SEM under *in vitro* and *in vivo* conditions. Tegumental responses are often analyzed with increasing incubation periods *in vitro* or progressing time post-treatment *in vivo*. While surface structures of normally developed control specimens of *E. caproni* have been studied in detail using SEM ⁸³, thus far only one study has evaluated the effect of drugs on this intestinal fluke by the same tool ⁷⁷. Fig 4.1 depicts the oral sucker (OS) and the ventral sucker (VS) of an adult *E. caproni* specimen recovered from an untreated control mouse. For comparison, Fig 4.2 shows an *E. caproni* trematode recovered from a mouse treated with a single 150 mg/kg oral dose of tribendimidine (Figs 4.2a and 4.2b), and 700 mg/kg artesunate (Figs 4.2c and 4.2d). Typical features of drug-induced damage included a reduced opening of the oral sucker (Figs 4.2a, 4.2b and 4.2d), focal damage of the tegument as eruption (Fig 4.2c), furrowing, or sloughing (no image shown).

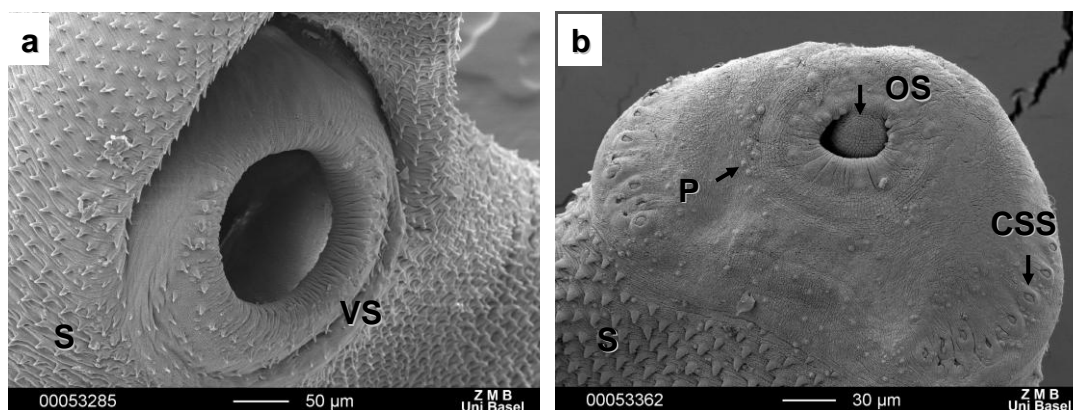


Figure 4.1. Previous page: SEM observation of an *E. caproni* trematode recovered from a mouse 14 days after an experimental infection. **(a)** Ventral sucker (VS), and tegumental spines (S), **(b)** Anterior part with oral sucker (OS), papillae (P), collar spine sockets (CSS), and spines (S)

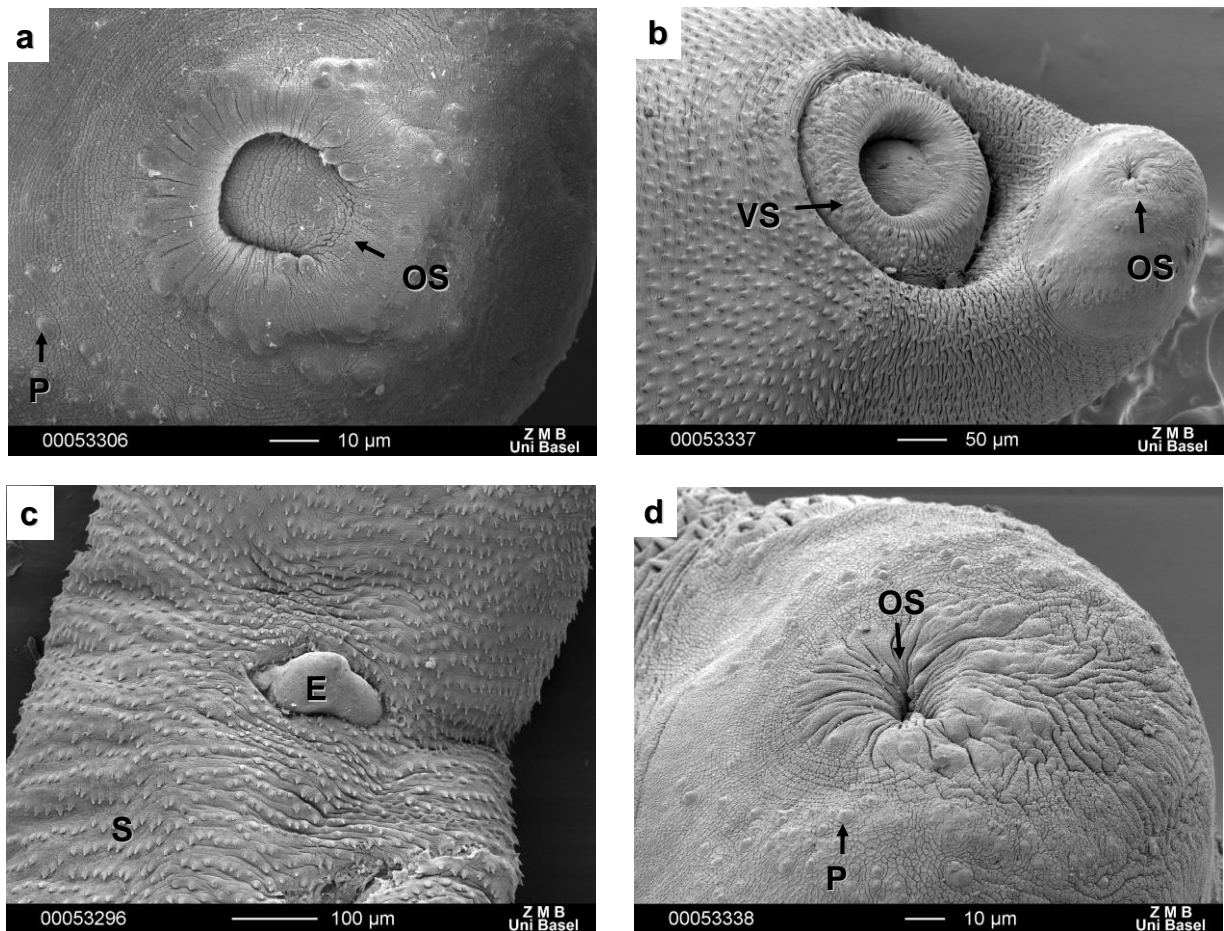


Figure 4.2. SEM observation of an *E. caproni* trematodes recovered from mice following treatment with tribendimidine **(a, b)**, and artesunate **(c, d)**. **(a)** Reduced opening of oral sucker (OS) 4 h after administration of a single 150-mg kg⁻¹ oral dose of tribendimidine. (P) papillae. **(b)** Reduced opening of oral sucker (OS) 8 h after administration of a single 150-mg kg⁻¹ oral dose of tribendimidine. (VS) ventral sucker. **(c)** Eruption (E), and tegumental spines (S) on the ventral midbody surface 4 h after administration of a single 700 mg kg⁻¹ oral dose of artesunate. **(d)** Reduced opening of oral sucker (OS) 8 h after administration of a single 700-mg kg⁻¹ oral dose of artesunate. (P) papillae

4.3.4 Spectroscopy

Both nuclear magnetic resonance (NMR) spectroscopy and mass spectrometry (MS) have been used to elucidate the mechanism of action of antiparasitic drugs. The general pre-metabonomics applications of NMR and MS include structural identification of possible target proteins and pathway steps for new drug developmental angles, and the monitoring of drug degradation⁸⁴⁻⁸⁶. For example, it was demonstrated that the antibiotics pentalenolactone and koningic acid inhibit the glycosomal enzyme of *Trypanosoma brucei*. NMR analysis was able to indicate that these compounds bind to the cysteine residue of the active site of the enzyme⁸⁷. Other examples include the investigation of the inhibition of the merozoite surface protein in *Plasmodium falciparum* by suramin and its analogues⁸⁸, the interaction of antiparasitic guanyl hydrazones with the cell membrane of *Trypanosoma cruzi*⁶³, and the evaluation of methylene blue as an antimalarial drug candidate against drug-resistant parasite strains⁶⁴.

Further extension of spectroscopy has allowed direct application to profiling metabolic changes in the tissues and biofluids of host organisms infected with parasites. The advent of postgenomic disciplines such as transcriptomics, proteomics, metabonomics, and lipidomics has opened up a wealth of new possibilities in characterizing the response of an organism to physiological and pathological challenges (Nicholson et al. 2002), and has facilitated the increasingly popular ‘systems biology’ approach. A clear role for genomics, proteomics (see chapter 9) and metabonomics has been established in parasitology with respect to diagnostics, characterizing host-parasite interactions, and in monitoring and evaluating therapeutic responses to intervention.

4.4 Metabonomic investigation on *Echinostoma caproni* in the mouse model

4.4.1 What is metabonomics?

Metabonomics, also known as metabolomics and metabolic profiling^{41, 89}, involves the generation of multivariate profiles or fingerprints of biological samples using multivariate statistics, applied to high-resolution analytical methods such as NMR spectroscopy, MS and capillary electrophoretic chromatography. The approach has been used for the characterization of metabolic phenotypes of healthy, diseased and treated subjects⁹⁰, and the diagnosis and monitoring of a wide variety of clinical and physiological conditions, ranging

from cardiovascular disease ⁵¹ to nutritional intervention ⁹¹. Although gas chromatography (GC)-MS, capillary electrophoresis chromatography, and infrared spectroscopy have all been used successfully as metabonomics tools, applications in parasitology have been limited largely for NMR-based studies with one or two liquid chromatography (LC)-MS examples beginning to emerge. Studies by Vasta and colleagues have used high performance thin layer chromatographic analyses to examine metabolic profiling in mice infected with *E. caproni*. Significant changes were discovered in the neutral lipid profiles in both feces and urine of mice infected with *E. caproni* relative to the uninfected controls (Vasta, Fried and Sherma 2008).

In the current chapter we will focus on NMR-based metabolite profiling with a brief discussion of the current capability and potential of LC-MS for diagnosing and characterizing parasite infections with particular consideration to *E. caproni*.

NMR spectroscopy. NMR has been an important tool in analytic and organic chemistry for several decades. Early studies on biofluids (typically urine and blood) were performed using visual means of interpreting molecular changes in the spectra. However, in 1989 a breakthrough occurred in spectral analysis involving the application of computer-based methods for data reduction and assessing similarity/dissimilarity between various spectra (Nicholson and Wilson 1989), and NMR-spectroscopy (especially ¹H NMR spectroscopy) became an efficient and convenient analytical tool used in a diversity of medical and biological fields, and currently represents an important tool in systems biology ⁹².

NMR spectroscopy measures the interaction of nuclei with an applied electronic magnetic field. The frequency or position of the chemical shift scale will be determined by the electron cloud surrounding a particular nucleus which provides a shielding effect from the magnetic field. Hence, the exact resonance of a nucleus is related to its chemical environment, and therefore gives information regarding chemical structure of a molecule. In addition, neighboring nuclei interact *via* bonding electrons, and hence carry information regarding the neighboring nuclei. Coupled nuclei, show multiplicity of peaks, which is determined by the number of protons on the adjacent atoms and is given by $n+1$ peaks, where n is the number of neighboring spin-coupled nuclei. Furthermore, the intensity of a resonance peak in NMR spectra is proportional to the concentration of nuclei present in a particular chemical

environment. Therefore, NMR spectroscopy can provide quantitative information as well as structural information on the metabolites or compounds in a biological sample. For methodological details the reader is referred to Claridge (1999).

Mass spectrometry. The initial application of MS to metabolic profiling originated from cell culture systems and plant studies (Fiehn 2002). Nowadays MS is increasingly utilized in the metabolic profiling of biofluids, because of its inherently high sensitivity, and its ability to target different classes of molecules in the metabolic spectrum, depending on the chosen type of MS platform and the characteristic of the sample. Thus MS is a highly complementary technique to NMR. MS is ideally coupled with a previous, separation of the mixture *via* LC or solid phase extraction. LC-MS is the most popular method of metabolic profiling after NMR spectroscopy^{93, 94}, but also GS-MS and MS-MS finds increasing application. In practice, the combination of multiple analytical platforms will provide the most precise information, because every single technique contributes a unique set of data shaping the overall metabolic picture^{95, 96}.

For MS analysis of biological matrices, after appropriate chromatographical separation, the fraction is introduced into the ionisation source, where the molecules gain (positive ionisation mode) or lose (negative ionisation mode) one ion, and are further separated by MS according to the mass-to-charge ratio (m/z) of the ions. Where hard ionisation sources are used the molecular fragments can provide structural information as well as an accurate relative molecular mass, which can be useful in molecular assignment. The data generated consist of a chromatographic retention time and a mass to charge (m/z) ratio and thus there is significantly less overlap with metabolite signals generated by LC-MS than one-dimensional (1D) NMR analysis since the data are already dispersed in two dimensions. However, analytical drift in either the chromatographic conditions or the m/z value can be problematic and several algorithms have been produced to address the peak or signal alignment. An additional factor which requires consideration in MS analysis is the fact that differential ion suppression effects across samples can produce artefacts and render quantification of metabolites difficult.

Chemometric tools. Spectra from biological samples, such as blood, urine, faecal water, and tissues generally contain several thousands of resonances, which are partly overlapping and thus can observe important information. In order to extract the maximum information from the large amount of raw, complex data, multivariate statistical methods are used for data reduction and to visualize the data in simple graphs.

Prior to multivariate analysis a series of pre-processing steps are usually applied to the spectral data to enable more accurate interpretation. These include procedures such as peak alignment and registration, smoothing, centring of baselines, and normalization of each spectrum to a constant sum such that concentration differences between samples can be removed.

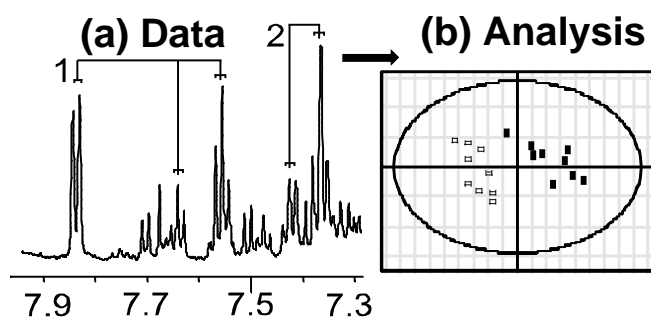


Figure 4.3. Schematic of sample acquisition and data handling; (a) acquisition of metabolite profiles followed by (b) mathematical modelling of the data to establish pre- (*filled square*) and postinfection (*open square*) phenotypes for each parasite. Key: 1, hippurate; 2, phenylacetyl glycine

There are two basic types of multivariate statistical methods: (i) unsupervised, and (ii) supervised approaches. Unsupervised methods are generally used for reducing the complexity and the volume of the data and use no prior knowledge of class or measure of response. Following data reduction approaches according to defined algorithms, the data are displayed as co-ordinates in a 2- or 3-dimensional (2D or 3D) plot, which can be examined to obtain information on outliers, trends and similarities within the data. The most widely applied unsupervised method is principal component analysis (PCA) (Fig 4.3). In contrast with unsupervised methods, the main feature of supervised methods is to use knowledge of class membership to optimise the difference between two or more classes. Thus in this context supervised methods are generally used to predict the biological ‘state’ of an organism, e.g., infected or non-infected. For supervised methods, cross-validation is necessary by using a part of the data as “training set” in order to construct the model and the remaining part of the data as a “test set” to validate the model. Some of the main supervised methods are soft independent modelling of classification analogy (SIMCA), partial least squares (PLS) analysis⁵⁴ and, more recently, also Bayesian methods⁹⁷. At its simplest these linear projection methods allow rearrangement of the original variables (in this case spectral data

points) to form a new component which describes the maximum direction or dimension of variation in the data. Subsequent components are calculated to be orthogonal and describe progressively less variation. Thus a plot of the first two or three components allows visualization of similarity between objects (in this case biological samples) based on their spectral composition.

Further improvement in data modelling can also be obtained by implementation of a mathematical filter, such as orthogonal signal correction, to remove systematic variation in the data set that is unrelated to the property of interest. For example, in determining whether an animal is infected, systematic variation introduced by age or sex differences may compromise the model. Orthogonal PLS discriminant analysis (O-PLS-DA)⁹⁸ has been used successfully to remove the influence of such potential sources of variation.

4.4.2 *Experimental protocol*

Here we use NMR spectroscopy to characterise the metabolic features of an *E. caproni*-mouse model and to illustrate our metabolic profiling strategy. A standard metabonomic protocol for exploring the effects of parasite infection is summarized in Fig 4.4. Briefly, urine, plasma and stool from *E. caproni*-infected, and age- and sex-matched uninfected mice were collected at weekly intervals over a 33-day time course, and measured using conventional ¹H NMR spectroscopy. Each NMR experiment required approximately 5 min to acquire. At the end of the experiment all animals were sacrificed and tissues (liver, kidney, spleen, ileum, jejunum, and colon) were obtained for ¹H magic angle spinning (MAS) NMR analysis. All samples were stored frozen at -80°C prior to analysis by ¹H NMR spectroscopy or MS. A suite of multivariate statistical methods beginning with unsupervised methods, such as PCA, and progressing to supervised approaches, such as PLS-DA, were used to analyze the spectra.

4.4.3 *Biomarker identification and diagnostic potential of biofluids in an Echinostoma caproni infection*

Characteristic spectral profiles of several mammalian biofluids are already well established, including those of urine, plasma and faecal water extracts⁹⁹⁻¹⁰⁴. Urine and plasma have already been assessed for their diagnostic potential in various single parasite-rodent models including *Schistosoma mansoni*¹⁰⁵, *Schistosoma japonicum*¹⁰⁶, *Trypanosoma brucei brucei*⁹⁶, *Trichinella spiralis*¹⁰⁷ and *Plasmodium berghei* (Li et al. submitted).

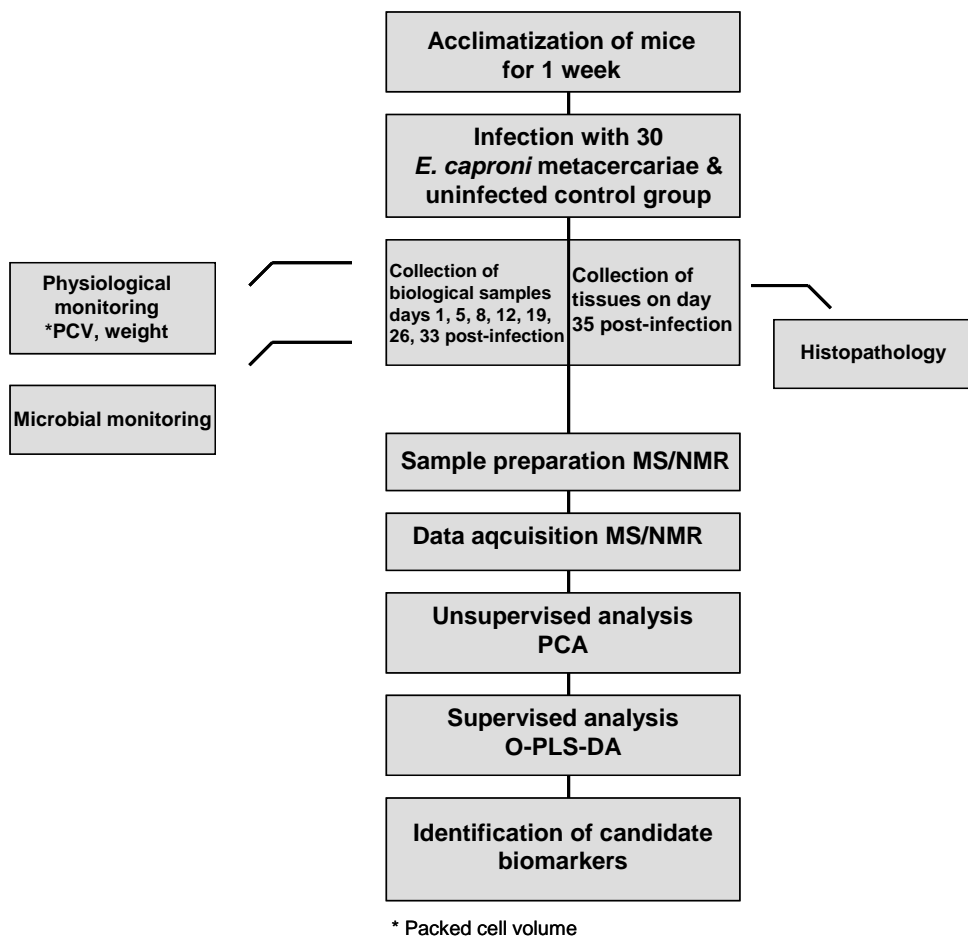


Figure 4.4. Schematic draft of the experimental protocol used to acquire biological samples from mice infected with *E. caproni* for metabolic profiling

More recently, faecal water composition in relation to physiological variation and characterization has been assessed in more detail^{108, 109}.

These biofluids are relatively straightforward to obtain in a minimally invasive manner, and are present in reasonably large quantities. Hence, these biofluids can serve as suitable biological matrices for disease diagnostics. Furthermore, urine, plasma and stool are to some extent representative of the organism as a whole, as they reflect to a high degree malfunctions and impaired homeostasis in metabolic composition. Typical metabolites detected in each of these three types of biological samples are listed in Table 4.2. In the *E. caproni*-mouse model, all three biological samples were found to alter with infection and progressive changes in the spectral profiles were monitored over time. Alterations in the metabolic composition of the samples reflect the response of the host organism as it strives to compensate for the invasion of the parasite and maintain homeostatic control.

Plasma. The strongest differentiation of the *E. caproni*-infected group of mice occurred between days 12 and 26 post-infection, and the most striking differences related to increases in the concentrations of lipoproteins, triacylglycerols, and saturated and unsaturated fatty acids after day 12 post-infection. This observation is consistent with the well documented degradation of biological membranes by this intestinal fluke ¹¹⁰. Other infection-related changes included a depletion of the branched chain amino acids (BCAAs; e.g., leucine, isoleucine, and valine) and choline/glycerophosphocholine.

Urine. Urine has been emphasised to represent an ideal diagnostic template ^{111, 112}, as it collects the waste products of the whole organism, and can reflect the metabolic status of an individual to a high degree. Some urinary biomarkers can be directly related to kidney failure, organ damage, nutrient uptake, microbial composition, etc. ^{91, 113}. Urine is relatively easy to obtain and probably the best metabolically characterised biological template at all ^{99, 102-104}.

E. caproni-infected mice showed decreased levels of 2-ketoisocaproate, which could be due to the depletion of leucine in plasma, which acts as precursor in a transamination reaction ¹¹⁴. Significantly lower levels of urinary taurine was a consistent feature in infected mice and is likely to derive from the high level of lipid degradation in the gut, caused by *E. caproni*, thus creating a higher demand for lipid digestion. As taurine is involved in bile acid conjugation and fat emulsification, it is likely that the urinary depletion of the compound is due to the higher demand. Taurine is conjugated with chenodeoxycholic acid and cholic acid in the liver, where primary bile salts are formed and excreted in urine. Deconjugation of taurine happens *via* gut bacterial species, after the lipids formed a micellar form together with the bile salts, in order to cross the intestinal wall. Hepatic taurine is then absorbed by the blood circulation ¹¹⁵.

It is conceivable that an infection with intestinal flukes results in changes in the bacterial composition due to the close proximity and direct influence of *E. caproni*. Indeed, the most prevalent alterations in the urine profile were the relative concentrations of gut microbial synthesized compounds, such as decreased 2-ketoisocaproate, acetate, hippurate, and increased phenylacetylglycine, *p*-cresol glucuronide and, trimethylamine. The specific change in *p*-cresol glucuronide is likely to reflect an alteration in either the presence or activity of *Clostridium* subspecies, as *p*-cresol is a known metabolite of both, *C. difficile* and *C. scatologenes* ^{116, 117}.

Table 4.2. List of metabolites found in urine (ur), plasma (pl) and stool (st) of 7-8 week-old mice (NMRI strain, female mice)

Metabolite	Coupling pattern (Hz)	δ (ppm)	Biofluid
2-hydroxyisobutyrate	2xCH ₃	1.36 (s)	ur
2-hydroxyisovalerate	α -CH, β -CH, γ -CH ₃ , γ' -CH ₃	3.85(d), 2.02(m), 0.79(d), 0.84(d)	st
2-ketoisocaproate	α -CH, β -CH, γ -CH ₃ , γ' -CH ₃	3.85(d), 2.02(m), 0.79(d), 0.84(d)	ur, st
2-ketoisovalerate	CH, 2xCH ₃	3.02(m), 1.13(d)	pl, st
2-oxoglutarate	β -CH ₂ , γ -CH ₂	3.02(t), 2.5 (t)	ur
3-aminopropionate (β -alanine)	NCH ₂ , CH ₂ COOH	3.19 (t), 2.56 (t)	st
3-hydroxybutyrate	half α -CH ₂ , half α -CH ₂ , β -CH, γ -CH ₃	2.32 (m), 2.42 (m), 4.16 (m), 1.21 (d)	pl
3-hydroxyphenyl propionic acid	α -CH ₂ , β -CH ₂ , 2-CH	2.47 (t), 2.85 (t), 6.8 (m)	st
3-methyl-2-oxovalerate	β -CH, half γ -CH ₂ , half γ -CH ₂ , γ -CH ₃ , β -CH ₃	2.93(m), 1.7(m), 1.46(m), 0.9(t), 1.1(d)	st
5-aminovalerate	5-CH ₂ , 2-CH ₂ , 3,4-CH ₂	3.02 (t), 2.24 (t), 1.65 (m)	st
acetate	CH ₃	1.91(s)	pl, ur, st
acetoacetate	α -CH ₂ , γ -CH ₃ ,	2.29 (s), 3.45 (s)	pl
alanine	α -CH, β -CH ₃	3.81(q), 1.48(d)	pl, ur, st
allantoin	CH	5.4 (s)	pl, ur
arginine	α -CH, β -CH ₂ , γ -CH ₂ , δ -CH ₂ ,	3.76(t), 1.89(m), 1.59(m), 3.17(t)	st
asparagine	α -CH, half β -CH ₂ , half β -CH ₂	4.01(m), 2.87(dd), 2.96(dd)	st
aspartate	α -CH, half β -CH ₂ , half β -CH ₂ ,	3.92(m), 2.70(m), 2.81(m)	st
bile acids	CH ₃	0.7 (m)	st
butyrate	α -CH ₂ , β -CH ₂ , γ -CH ₃	2.16(t), 1.56(m), 0.9(t)	st
choline	3xCH ₃ , α -CH ₂ , β -CH ₂	3.21 (s), 4.07 (m), 3.52 (m)	pl
citrate	1-CH ₂ , 3-CH ₂	2.69 (d), 2.54 (d)	pl, ur, st
creatine	CH ₃ , CH ₂	3.04 (s), 3.93 (s)	pl, ur, st
creatinine	CH ₃ , CH ₂	3.05 (s), 4.06 (s)	ur
dihydroxythymine	CH ₂ , CH, CH ₃	3.17 (m), 2.47 (m), 1.07 (d)	pl
dimethylamine	2xCH ₃	2.71 (s)	ur
dimethylglycine	2xCH ₃ , CH ₂	2.89(s), 3.71(s)	ur
ethanolamine	NH-CH ₂ , HO-CH ₂	3.15(t), 3.78(t)	st
formate	CH	8.45 (s)	pl, ur, st
fumarate	CH	6.53 (s)	st, ur
glutamate	α -CH, β -CH ₂ , γ -CH ₂	3.78(m), 2.06(m), 2.36(m)	st
glutamine	α -CH, β -CH ₂ , γ -CH ₂	3.78(m), 2.15(m), 2.46(m)	st
glycerol	half α , γ -CH ₂ , half α , γ -CH ₂ , β -CH	3.56 (dd), 3.64 (dd), 3.87 (m)	st
glycerophosphocholine	3xCH ₃ , half α -CH ₂ , half α -CH ₂ , half β -CH ₂ , half β -CH ₂ , γ -CH ₂	3.23 (s), 4.32 (t), 3.6(dd), 3.68(t), 3.89(m), 3.72(dd)	pl
glycine	CH ₂	3.55(s)	st
glycolate	CH ₂	3.94 (s)	ur
guanidinoacetate	CH ₂	3.8 (s)	ur
hippurate	CH ₂ , 2,6-CH, 3,5-CH, 4-CH	3.97 (d), 7.84 (d), 7.55 (t), 7.64 (t)	ur
hypoxanthine	3-CH, 7-CH	8.099 (s), 8.11 (s)	st
indoxylsulfate	5-CH, 6-CH, 4-CH, 7-CH	7.2 (t), 7.27 (t), 7.51 (d), 7.7 (d)	ur
isoleucine	α -CH, β -CH, half γ -CH ₂ , half γ -CH ₂ , δ -CH ₃ , β -CH ₃ ,	3.68(d), 1.93(m), 1.25(m), 1.47(m), 0.99(d), 1.02(d)	pl, st
lactate	CH, CH ₃	4.12(q), 1.33(d)	pl, ur, st
leucine	α -CH, β -CH ₂ , γ -CH, δ -CH ₃ , δ -CH ₃	3.72(t), 1.96(m), 1.63(m), 1.69(m), 0.91(d), 0.94(d)	pl, st
lysine	α -CH, β -CH ₂ , γ -CH ₂ , δ -CH ₂ , ϵ -CH ₂	3.77(t), 1.92(m), 1.73(m), 1.47(m), 3.05(t)	st

Table 4.2. (continued)

Metabolite	Coupling pattern (Hz)	δ (ppm)	Biofluid
mannitol	α -CH ₂ , β -CH, γ -CH	3.78(m), 3.88(dd), 3.68(dd)	ur
methanol	CH ₃	3.36 (s)	pl
methionine	α -CH, β -CH ₂ , γ -CH ₂ , CH ₃	3.87(m), 2.10(m), 2.65(dd), 2.15(s)	pl, st
methyl crotonate	CH, CH ₃ , CH ₃	5.65(s), 1.70(s), 1.71(s)	ur
methylamine	CH ₃	2.61 (s)	ur
methylguanidine	CH ₃	2.83 (s)	ur
myoinositol	1,3-CH, 2-CH, 5-CH, 4,6-CH	3.53(dd), 4.06(t), 3.28(t), 3.63(t)	st
<i>N</i> -methyl-nicotinamide	CH ₃ , 6-CH, 2-CH, 5-CH, 4-CH	4.48 (s), 8.97 (d), 9.28 (s), 8.19 (t), 8.9 (d)	ur
<i>p</i> -cresolglucuronide	2-CH, 6-CH, 3-CH, 5-CH,	7.06(d), 7.23(d), 2.3(s), 5.07(d)	ur
phenylacetic acid	CH ₂ , 2,6-CH, 3,5-CH	3.52 (s), 7.29 (t), 7.36 (t)	st
phenylacetylglycine	2,6-CH, 3,5-CH, 4-CH, ArCH ₂ , NCH ₂	7.43 (m), 7.36 (s), 7.37 (m), 3.75 (d), 3.68 (s)	ur
phenylalanine	2,6-CH, 3,5-CH, 4-CH, CH ₂ , CH	7.44(m), 7.39(m), 7.33(m), 3.17(dd),3.30(dd), 3.99(dd)	st
proline	α -CH, half β -CH ₂ , half β -CH ₂ , γ -CH ₂ , δ -CH ₂	4.15(dd), 2.05(m),2.38(m), 2.00(m), 3.39(m)	st
propionate	CH ₂ , CH ₃	2.19(q), 1.06(t)	st
pyridoxamine-5-phosphate	OCH ₂ , CH ₂ N, CH ₃	7.67 (s),4.34 (s), 2.48 (s)	ur
<i>scyllo</i> -inositol	6xCH	3.35 (s)	pl
succinate	2x CH ₂	2.41 (s)	ur, st
taurine	CH ₂ N, CH ₂ S	3.27 (t), 3.43 (t)	ur
threonine	α -CH, β -CH, γ -CH ₃	3.60(d), 4.26(m), 1.33(d)	st
trimethylamine	3xCH ₃	2.88 (s)	ur
trimethylamine- <i>N</i> -oxide	3xCH ₃	3.27 (s)	ur
tryptophan	4-CH, 7-CH, 2-CH, 5-CH, 6-CH, α -CH, half β -CH ₂ , half β -CH ₂	7.79(d), 7.56(d), 7.34(s), 7.29(t), 7.21(t), 4.06(dd), 3.49(dd),3.31(dd)	st
tyrosine	2,6-CH, 3,5-CH, CH ₂ , α -CH	7.23(d), 6.91(d), 2.93(t), 3.25(t)	st
uracil	5-CH, 6-CH	5.81(d), 7.59(d)	t
ureidopropanoate	α -CH ₂ , β -CH ₂	2.38 (t), 3.3 (t)	ur
urocanate	α -CH, β -CH, 5-CH, 2-CH	6.4(d), 7.13(d), 7.41(s), 7.89(s)	ur, st
valine	α -CH, β -CH, γ -CH ₃ , γ' -CH ₃	3.62(d), 2.28(m), 0.98(d), 1.03(d)	pl, st
α -glucose	1-CH, 2-CH, 3-CH, 4-CH, 5-CH, half 6- CH ₂ , half 6-CH ₂	5.24(d), 3.56 (dd), 3.7(t), 3.4(t), 3.83(m), 3.72(dd), 3.85(m)	pl, ur, st
β -glucose	1-CH, 2-CH, 3-CH, 4-CH, 5-CH, half 6- CH ₂ , half 6-CH ₂	4.65(d), 3.25 (dd), 3.47(t), 3.4(t), 3.47(ddd), 3.78(dd), 3.9(dd)	pl, ur, st
lipids fractions	CH ₃	0.84 (t)	pl
	(CH ₂) _n	1.25 (m)	pl
	β -CH ₂ CH ₂ CO	1.57 (m)	pl
	CH ₂ C=C	1.97 (m), 2.00 (m)	pl
	CH ₂ CO	2.23 (m)	pl
	C=CCH ₂ C=C	2.69 (m), 2.71 (m), 2.72 (m)	pl
	CH=CH	5.23 (m), 5.26 (m), 5.29 (m)	pl

p-cresol is taken up by the blood stream where it binds to serum proteins and is later excreted, after conjugation with glucuronic acid in the liver and kidney¹¹⁸. Other bacteria in the gut degrade dietary choline and carnitine to trimethylamine (TMA) which is then oxidized further in the liver to trimethylamine-*N*-oxide (TMAO)^{119, 120}. Again, an *E. caproni*-induced change of the microbial community is suggested by the disturbance of the TMA and TMAO equilibrium in urine and the subsequent depletion of choline/glycerophosphocholine in the plasma.

The results generated by multivariate data analysis can be ordered chronologically to display the metabolic response in a host-parasite model over the duration of the time course of infection. This can be a useful tool in characterizing the stage of an infection and may provide useful information in determining a therapeutic strategy for disease management. An example of such a response or “trajectory” is depicted in Fig 4.5, which illustrates the evolving response in the urine profile. Key features include decreased levels of hippurate, 2-ketoisocaproate, and taurine, and subsequent increases in trimethylamine, *p*-cresol glucuronide, TMAO, and phenylacetyl glycine.

Stool. As with the urine profiles, the faecal water samples from mice infected with *E. caproni* were characterised by alteration in gut microbial metabolites. Spectra from faecal extracts contained bile acids, the short chain fatty acids (SCFAs) butyrate, acetate, and propionate, and the amino acids including lysine, arginine, tryptophan and glutamine, amongst others which were also present in plasma and/or urine (Table 4.2).

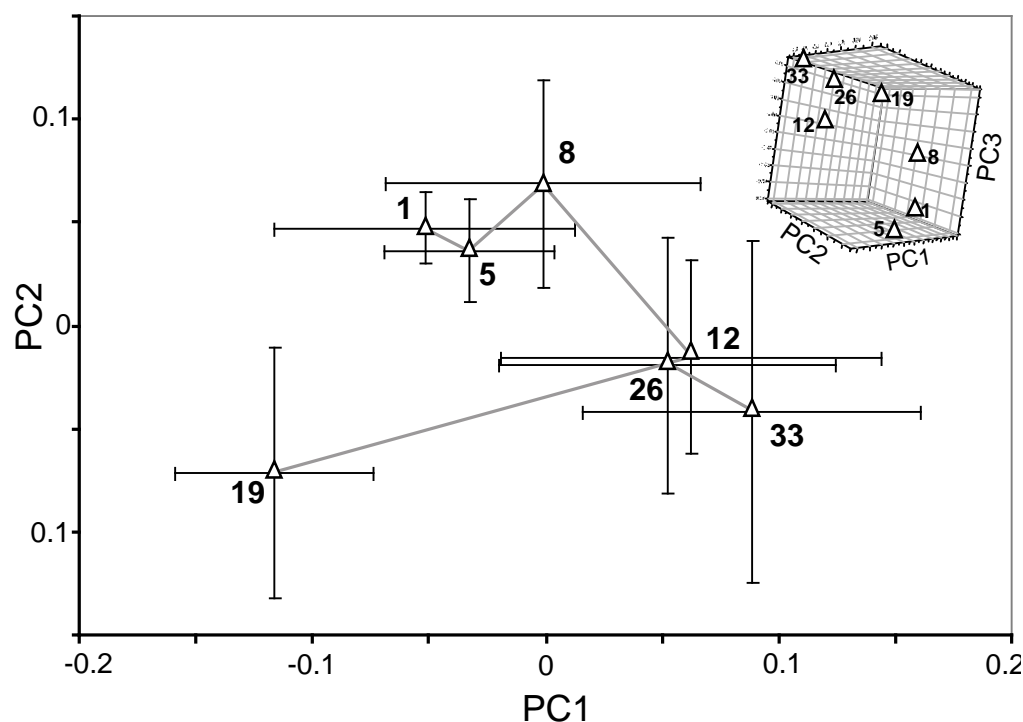


Figure 4.5. 2D and 3D time trajectory of urine samples from *E. caproni*-infected mice obtained from the mean PC1 and PC2 values over a 33-day time period. Biological samples were collected at seven time points postinfection (e.g., days 1, 5, 8, 12, 19, 26, and 33). The error bars reflect two standard deviations of the mean

Nearly all changes observed in the faecal samples due to an experimental infection with *E. caproni* can be attributed to a changed gut microbial composition. The SCFAs (e.g., propionate, butyrate, and acetate) are produced by colonic bacteria *via* fermentation, and undergo a decrease in the faecal samples of infected animals compared to the non-infected control group. Acetate is the main SCFA in the colon, and is, together with propionate, taken up into the peripheral blood circulation where they have antagonistic functions in cholesterol synthesis, e.g., acetate increases, whilst propionate is known to decrease synthesis. Butyrate is the main source of energy for the colonic mucosa¹²¹. The changed gut microbiota is also reflected in the increased concentration of 5-aminovalerate in infected animals, which is normally degraded by a *Clostridium* subspecies (e.g., *C. aminovalericum*) to propionate and acetate^{122, 123}. The increase of the metabolite could indicate a depletion of this sub-strain. Increased levels of the BCAAs in stool are due to malabsorption caused by the parasite.

Utility of biofluids as a matrix for diagnostics. Based on our findings with the *E. caproni*-mouse model, the combination of all three assessed biofluids would deliver the most comprehensive metabolic fingerprint, and would reflect the overall picture of the infection impact, most accurately (Saric et al. submitted). However, in reality it is more conceivable to select the most suitable template and to further optimize it, since collection of all three biofluids in human populations may not always be practical. Comparing the three biofluids in terms of their biomarker potential, plasma would be the diagnostic matrix of choice in terms of biomarker quantity. Urine also has good potential, with 10 identified biomarkers and this biofluid is particularly convenient for sample collection. Faecal samples would be the least suitable template, as the inter- and intra-individual variation in healthy individuals is already considerable, which might be due to the extremely variable dynamics over time and diversity of bacterial strains in general.

4.4.4 Biomarker identification in tissue via MAS ¹H NMR spectroscopy

MAS NMR spectroscopy allows solid and semi-solid tissues to be profiled (Andrew 1959). The utility of this technology lies mainly in the evaluation in disease mechanisms in animal models, since it is a necessarily invasive approach. However, under some circumstances, e.g., differentiation of benign and malignant tumors, it is a potentially valuable clinical tool. Since candidate biomarkers identified in biofluids such as urine or plasma can originate from different tissues or organs, direct analysis of these tissues can provide a better understanding

of the etiology of the biomarker. Each tissue has a characteristic and unique metabolic profile reflecting the different cellular structures and functions specific to that tissue.

Kidney. The heterogeneous structure of the kidney is reflected in the region specific metabolic profiles. The cortex and medulla both contain various amino acids, e.g., glutamate/glutamine, aspartate, lysine, threonine, the aromatic amino acids phenylalanine, tyrosine, and the BCAAs (Fig 4.6A). However, characteristic for the renal medulla is the presence of higher concentrations of various osmolytes, like taurine, betaine, *myo*- and *scyllo*-inositol, together with glucose, choline, glycerophosphocholine (GPC), phosphocholine, and creatine. Analysis of *E. caproni*-infected and non-infected control animals showed no difference in the biochemical composition of the renal medulla, whilst the cortex manifested in increase of alanine, glutamate, aspartate, and *scyllo*-inositol in infected animals. GPC was found to be in lower concentrations in the renal cortex of infected mice, which could reflect the decrease of the metabolite in the plasma, but could also indicate a changed ionic cellular environment, e.g., NaCl, as GPC uptake into cells is known to be increased in case of high tonicity outside the cell membrane^{124, 125}. Other osmotically active substances like betaine and inositols, e.g. *scyllo*-inositol, are found in kidney, but also in other organs such as the brain or liver are known to change inversely with the GPC concentration. In fact, infection with *E. caproni* appeared to be positively associated with *scyllo*-inositol concentrations in the cortical part of the kidney. Amino acid re-absorption occurs predominantly in the proximal tubules of the kidney. The dicarboxylic amino acids glutamate and aspartate have separate carrier molecules, whilst alanine belongs to the neutral amino acids, which are carried by specific transporters^{126, 127}.

It is probable that the resulting immune response, initiated by the infection, plays a central role in the renal amino acid changes, namely cytokines and antigen-antibody complexes, which circulate through the kidney. In the literature, the immunological consequence of an infection with *E. caproni* seems to be inconsistent, based on the varying ratio of T-helper cell subgroups (e.g., T_H1/T_H2), which is partially responsible for the establishment of an infection, and induces different groups of cytokines and immunoglobulin¹²⁸. However, both, antibody-antigen complexes as well as cytokines are known to be involved in pathological processes in the kidney, and are likely to induce minor biochemical changes.

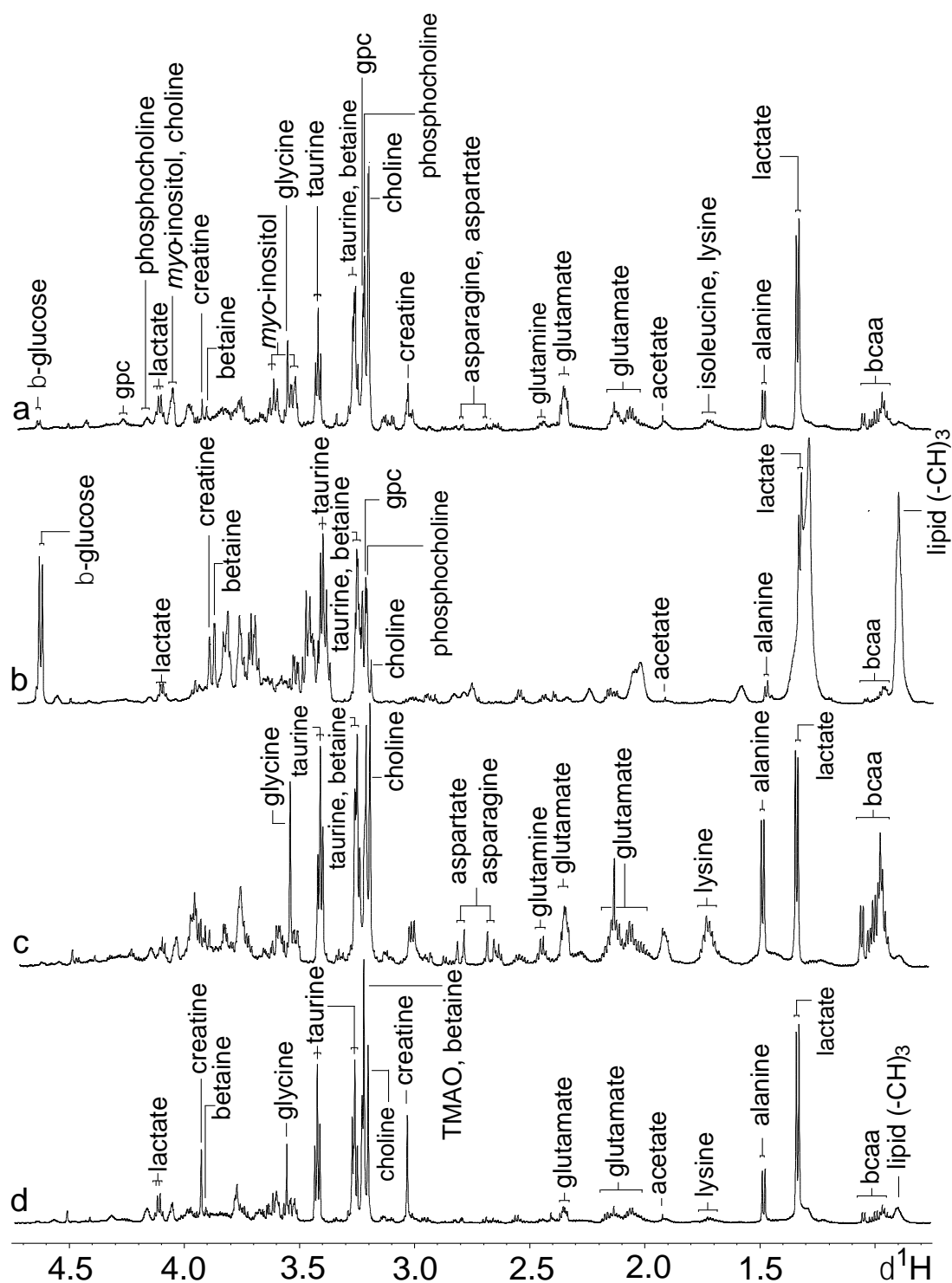


Figure 4.6. Typical 600-MHz ^1H -1D spectra of four selected tissues of an uninfected control mouse, aged 11 weeks; (a) kidney cortex), (b) liver, (c) spleen, and (d) ileum. Key: gpc, glycerophosphocholine; bcaa, branched chain amino acids

Secretory products of *E. caproni*, could hypothetically act as renal stimulator as well, but due to low concentration in plasma the compounds would be below detection limit of NMR and were therefore not detected.

Liver. Phosphocholine and betaine were present in significantly higher concentrations in the liver of *E. caproni*-infected mice. However, choline and GPC levels, which are in the same pathway, remained unaffected. We speculate that the increased amount of free amino acids and triacylglycerols in plasma is taken up into the hepatic cell in the form of phosphatidylcholine, degraded to GPC and subsequently to choline with the same rate of turnover. In a further degradation step choline is converted to betaine (irreversible) and phosphocholine, which are present in relatively higher levels in the liver of infected mice, compared to the non-infected control animals^{129, 130}.

Spleen. In accordance with the studies of Brunet et al.¹²⁸, where the mesenteric lymph nodes showed immunologic activity as response to an infection with *E. caproni*, but not the spleen, no infection-related changes in metabolic composition were observed in the spleen.

4.4.5 Changes in the intestinal profiles

The metabolic monitoring of the gut is of particular interest after an infection with an intestinal fluke for obvious reasons. On the one hand, there is well documented structural damage following an infection with *E. caproni*, whereby the most obvious histopathological changes in the host derived from the direct action of the fluke, which remains after excystation in ICR mice, for 8 weeks in the jejunum and ileum of the small intestinal part, and then shifts to duodenum and jejunum, which is more anterior¹³.

On the other hand, analysis of the biofluids indicated a strong infection-induced effect on the host microflora. Indeed, it is unthinkable that a parasitic worm, living in such proximity to the microbial community, would not influence the dynamics of the microorganisms in one way or another, which in turn bears potential consequences for the intestinal tissue in particular, and the whole organism in general.

Jejunum and ileum are functionally and histologically quite similar, with the main difference that the ileum contains the highest density of the Peyer's patches, which are immunologically active sites. The jejunum is larger in diameter, and hence its overall absorptive capacity is higher than that of the ileum. Digestion is completed in the small intestine and the products and fluids are absorbed. In contrast, the colon (large intestine) bears

the highest density of bacteria and is the major site for fermentation of dietary carbohydrates to SCFAs (e.g., butyrate, acetate, and propionate). Acetate is known to increase the colonic blood flow and is the main SCFA in the colon. It enters the blood circulation and can be taken up by muscle cells (e.g. longitudinal muscle of the small intestine) in order to generate energy, whilst propionate is taken up by the liver cells as substrate for gluconeogenesis. Butyrate is the main energy source for colonocytes¹²¹. Comparing the spectral profiles of the two parts of the small intestine (jejunum and ileum) with the large intestine, the SCFAs account for the main difference. Butyrate and propionate were only found in colon spectra, whilst acetate was a feature of all three regions of the gut, but was found in much higher relative concentrations in colon than in ileum/jejunum. The characteristic spectral composition for non-infected tissues for ileum is illustrated in Figs 4.6D and 4.7.

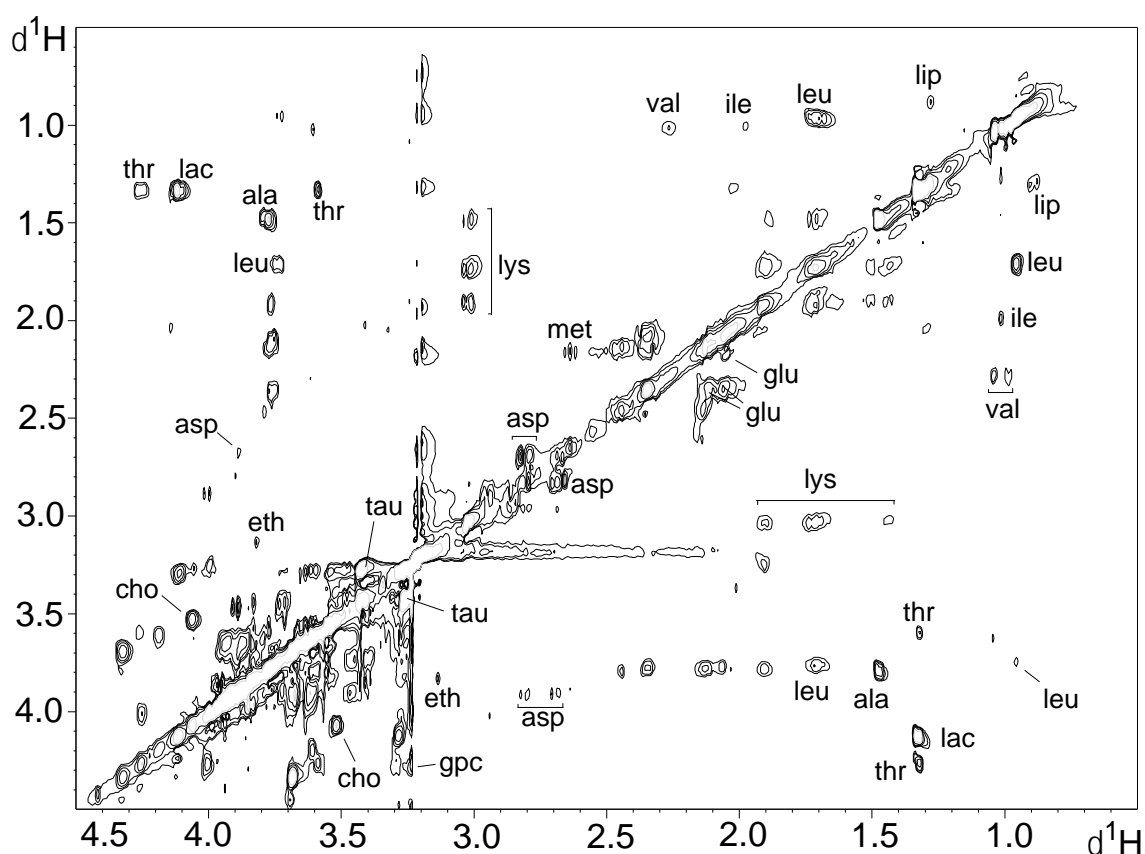


Figure 4.7. MAS 600 MHz ^1H - ^1H 2D TOCSY spectra of ileum from an uninfected control mouse. Key: ala, alanine; asp, asparagine; cho, choline; eth, ethanolamine; glu, glutamate; gpc, glycerophosphocholine; lac, lactate; leu, leucine; lip, lipid; lys, lysine; met, methionine; tau, taurine; thr, threonine; val, valine

All three parts of the gut showed significantly different metabolite profiles between infected and non-infected animals with the greatest effect on ileum where a disturbance of the intestinal transport (e.g. a disturbed Na^+ electrochemical gradient) was evident. Increased tissue concentration of glucose was found in the ileum, which is consistent with the documented increase in serum mucosal flux induced by pro-inflammatory cytokines such as IL-1 α , IL-6, and IL-8, which leads to an increased uptake of glucose into the ileal cells *via* the sodium-glucose linked co-transporter (SGLT1)^{126, 127}. The high uptake rate of glucose resulted in lower concentrations of glycine in infected animals, due to a glucose competitive mechanism¹³¹. Further metabolic change included a decrease in tissue concentration of ascorbate, alanine, glutamine, aspartate, isoleucine, and valine, in the ileum of infected animals 36 days post-infection. This may be associated with inhibition of transporters, including SLC1A1 (excitatory amino acid carrier), B⁰AT1/SLC6A19 (neutral amino acid transport system), and SVCT1 (ascorbic acid transporter) which are known to regulate the uptake of anionic amino acids (aspartate), neutral amino acids, and the ascorbate, respectively¹²⁷. Additionally, the *E. caproni*-induced hypertrophy leads to an increased consumption of glutamine in the intestinal, over-proliferating cells and thus contributes to the depletion of glutamine stores in the ileum^{15, 132}.

The two aromatic amino acids tyrosine and phenylalanine were increased in jejunum, but even though they share the same mechanism of re-absorption as the other neutral amino acids, which were depleted in ileum, their increase appears to contradict to a higher demand in the jejunal tissue, rather than a disturbed electrochemical gradient.

The observed decrease on *myo*-inositol signals in the metabolic profiles results from mechanic disruption of the intestinal mucosa cells. *Myo*-inositol, taurine and betaine are small organic solutes, which are kept in the cell to maintain osmotic homoeostasis. This is obviously important in intestinal epithelia cells due to the digestive activities, which can potentially induce a hypertonic condition^{133, 134}. Increased levels of trimethylamine were observed in the colon of infected animals, which together with increased urinary excretion, would appear to indicate a general increase in the production of this metabolite^{119, 120}.

4.4.6 Integrative metabonomics: an approach to understand host-parasite-gut microbiota interactions

The direct impact of a pathological agent on an individual tissue can be ascertained by histology or by measurement, for example, of inflammatory markers. However, pathologies rarely target single organs and in order to achieve an accurate mechanistic understanding of how a disease progresses, it is usually necessary to evaluate the response of an organism across several physiological compartments. The application of metabolic profiling allows the extraction of latent information derived from numerous biofluid and tissue matrices and by integration of this knowledge can deliver a holistic framework of responses at a global systems level.

***Echinostoma caproni*-induced consequences on osmotic micro-environment and cross-cellular transport.** Various osmotically active substances showed changes in relative concentrations during the course of an *E. caproni* infection, such as betaine which increased in the liver, *scyllo*-inositol (increased), and GPC in the kidney (decreased), and *myo*-inositol in jejunum which decreased. All those metabolites serve as osmotic regulators in the tissue cells, whereas GPC is the only osmolyte in which uptake into the cell is induced by high NaCl levels. Thus the lower GPC levels could be either due to the changed tonicity (NaCl to water ratio) or directly relatable to the depletion of plasma concentrations. However, its decrease seems to induce an increased intracellular concentration of *scyllo*-inositol in the renal tubes, which is known to change concentration inversely to GPC. The decrease of *myo*-inositol in the ileum is probably due to mechanic disruption of the intestinal mucosa cells, rather than due to osmotic necessity, as this would imply a higher uptake of an osmolyte to increase the cell influx of liquid and subsequently nutrients.

In the gut, it appears that the Na⁺-dependent transport is disturbed, which may be due to disruption of the NaCl concentration with the resulting changes in membrane potential and gradient, which regulate carrier-dependent as well as independent transport. The malabsorption of the anionic amino acids aspartate, ascorbate and the neutral amino acids alanine, isoleucine, and valine, perhaps indicates inhibition of specific Na⁺-dependent transporters, such as SLC1A1, SVCT1, and B⁰AT1/SLC6A19.

In the renal cortex increased tissue concentrations of aspartate, glutamate, and alanine showed an increased concentration. Specifically, Na⁺-dependent carrier molecules for transport of the

two dicarboxylic amino acids aspartate and glutamate seem to be impaired in the infection with *E. caproni*.

Holistic influence of the gut microbiota. Trimethylamine increased in urine and colon of *E. caproni*-infected mice, which implies an increased synthesis in infected animals, compared to the healthy state of the rodent. As compensation to this overproduction, both colonic uptake and urinary excretion are increased. A shift in the microbial composition toward bacterial species, which are able to degrade trimethylammonium compounds like choline, carnitine, or GPC to TMA with further oxidation to TMAO, could explain the increase of the TMA and TMAO in urine, as well as the depletion of choline and GPC in plasma. On the other hand, this microbial shift is unlikely to contribute to the changed concentrations of GPC in the kidney and phosphocholine in the liver, respectively, as the osmotic imbalance in the former and the higher rate of lipid degradation in the latter will outweigh the microbial contribution. Interestingly, the decrease of the SCFAs in the faecal samples of *E. caproni*-infected mice is not reflected in any of the assessed gut tissues, whereas, particularly in the case of colon, a reduced propionate, acetate and butyrate concentration would be expected to mirror the decrease in the feces. Acetate was the only urinary SCFA which demonstrated a subsequent depletion.

The presence of an intestinal fluke would be expected to have a considerable impact on the microbial community of the gut because of the proximity and thus direct interaction of the fluke and bacterial colonies. Yet, our integrated data suggest that the overall expression of metabolites, which are related to a changed gut microbiota, is not stronger compared to two previously assessed blood fluke-rodent models; indeed *S. mansoni*-infected mice and *S. japonicum*-infected hamsters showed the same urinary pattern of gut microbial modified metabolites, including changes in hippurate and trimethylamine^{105, 106}.

Metabolite flow through different physiological compartments. It is possible to monitor some of the metabolic changes across different physiological compartments. Most of these changes have their origin in the malabsorption of the ileum, such as isoleucine and valine, which are excreted in the feces in higher concentrations and thus, show lower levels in ileum and plasma. Also alanine and aspartate seem to be absorbed at lower rate in the ileum, but are increased in the kidney. Glucose, in contrast, shows increased levels in the ileum, which reflects in higher uptake from the blood circulation at the beginning of the infection. The marked decrease of plasmatic leucine, probably induces the relatively lower levels of 2-

ketoisocaproate in urine, as it is a transamination product of the former, in the urine ¹¹⁴. Finally, creatine is excreted in higher amounts in urine, reflecting the depletion in plasma.

A further use of metabolic profiling is the characterization of the parasite itself. The main biochemical components of *E. caproni* consisted of creatine, taurine, and betaine and the primary excretion products released in the intestinal are free fatty acids and sterols ¹³⁵. It is possible that the fluke-derived compounds affect the metabolic profile in the host. However, since we illustrate a protocol using an infection with the intestinal fluke with an average of 28 worms counted upon dissection of infected mice, the host weight to parasite mass ratio would be approximately 300:1, thus it is unlikely to see a contribution of those excretory products in the host organism.

4.5 Concluding remarks

The pressing need for novel trematocidal drugs has been emphasised ¹³⁶. We have summarized different studies that have demonstrated that the *E. caproni*-mouse model and *Echinostoma* cultured *in vitro* are useful tools for trematocidal drug discovery.

Metabolic profiling of an array of biological samples derived from mice infected with *E. caproni* demonstrates a novel angle for diagnosis in parasitology. A variety of disease-specific biomarkers have been demonstrated, and the approach is non-invasive and highly efficient. Furthermore, the potential of metabolic profiling to recover metabolic information in nearly every physiological compartment of a host organism allows cross-linking different pathological events and delivers a global picture of disease, which makes it a promising tool in systems biology for the purpose of infection diagnosis and eventually will provide opportunities for monitoring response to trematocidal agents.

4.6 Acknowledgements

J. Keiser (project no. PPOOA--114941) and J. Utzinger (project no. PPOOB—102883 and no. PPOOB-119129) are grateful to the Swiss National Science Foundation for personal career development grants. This investigation received further financial support from Imperial College London, and Nestlé provided personal funds for Y. L. Wang. The authors thank Kirill Veselkov for giving access to his peak alignment script in MATLAB. Last but not least we are grateful to Professor Bernard Fried and Professor Rafael Toledo for inviting us to write this chapter and for their careful read and copy-editing.

4.7 References

- Akoachere, M., Buchholz, K., Fischer, E., Burhenne, J., Heafeli, W. E., Schirmer, R. H., and Becker, K. 2005. *In vitro* assessment of methylene blue on chloroquine-sensitive and resistant *Plasmodium falciparum* strains reveals synergistic action with artemisins. *Antimicrobial Agents and Chemotherapy* 49: 4592-4597.
- Andrew, E. R., Bradbury, A., and Eades, R. G. 1959. Removal of dipolar broadening of nuclear magnetic resonance spectra of solids by specimen rotation. *Nature* 183: 1802-1803.
- Azzouz, S., Maache, M., Sanchez-Moreno, M., Petavy, A. F., and Osuna, A. 2007. Effect of alkyl-lysophospholipids on some aspects of the metabolism of *Leishmania donovani*. *Journal of parasitology* 93: 1202-1207.
- Balfour, C. D., Rossi, M., and Fried, B. 2001. Effects of a 100 metacercarial cyst inoculum on the host-parasite relationship of *Echinostoma caproni* and ICR mice. *Journal of Helminthology* 75: 321-324.
- Bang, J. W., Crockford, D. J., Holmes, E., Pazos, F., Sternberg, M. J., Muggleton, S. H., and Nicholson, J. K. 2008. Integrative top-down system metabolic modeling in experimental disease states via data-driven Bayesian methods. *Journal of Proteome Research* 7: 497-503.
- Barker, H. A., D'Ari, L., and Kahn, J. 1987. Enzymatic reactions in the degradation of 5-aminovalerate by *Clostridium aminovalericum*. *Journal of Biological Chemistry* 262: 8994-9003.
- Beckonert, O., Keun, H. C., Ebbels, T. M., Bundy, J., Holmes, E., Lindon, J. C., and Nicholson, J. K. 2007. Metabolic profiling, metabolomic and metabonomic procedures for NMR spectroscopy of urine, plasma, serum and tissue extracts. *Nature Protocols* 2: 2692-2703.
- Bender, D. A. 2002. *Introduction to nutrition and metabolism*, Boca Raton: CRC Press.
- Borges, M. N., and Figueroa-Villar, J. D. 2001. NMR interaction studies of aromatic guanyl hydrazones with micelles: model for mechanism of action of cationic antibiotics. *Biopolymers* 62: 9-14.

- Brunet, L. R., Joseph, S., Dunne, D. W., and Fried, B. 2000. Immune responses during the acute stages of infection with the intestinal trematode *Echinostoma caproni*. *Parasitology* 120: 565-571.
- Chai, J. Y., Murrell, K. D., and Lymbery, A. J. 2005. Fish-borne parasitic zoonoses: status and issues. *International Journal for Parasitology* 35: 1233-1254.
- Claridge, T. D. W. 1999. High-resolution NMR techniques in organic chemistry, Oxford: Elsevier.
- Clayton, T. A., Lindon, J. C., Everett, J. R., Charuel, C., Hanton, G., Le Net, J. L., Provost, J. P., and Nicholson, J. K. 2003. A hypothesis for a mechanism underlying hepatotoxin-induced hypercreatinuria. *Archives of Toxicology* 77: 208-217.
- Cook, G. C. 1971. Impairment of glycine absorption by glucose and galactose in man. *Journal of Physiology* 217: 61-70.
- Cross, J. H., and Basaca-Sevilla, V. 1986. Studies on *Echinostoma ilocanum* in the Philippines. *Southeast Asian Journal of Tropical Medicine and Public Health* 17: 23- 27.
- Dawson, R. M. 1955. The role of glycerylphosphorylcholine and glycerylphosphoryl-ethanolamine in liver phospholipid metabolism. *Biochemical Journal* 59: 5-8.
- De Aquino, T. M., Liesen, A. P., da Silva, R. E. A., Lima, V. T., Carvalho, C. S., de Faria, A. R., de Araujo, J. M., de Lima, J. G., Alves, A. J., de Melo, E. J. T., and Goes, A. J. S. 2008. Synthesis, anti-*Toxoplasma gondii* and antimicrobial activities of benzaldehyde-4-phenyl-3-thiosemicarbazones and 2-[(phenylmethylene)hydrazono]-4-oxo-3-phenyl-5-thiazolidineacetic acids. *Bioorganic and Medical Chemistry* 16: 446-456.
- Deras, I. L., Aubin, S. M. J., Blase, A., Day, J. R., Koo, S., Partin, A. W., Ellis, W. J., Marks, L. S., Fradet, Y., Rittenhouse, H., and Groskopf, J. 2008. PCA3: a molecular urine assay for predicting prostate biopsy outcome. *Journal of Urology* 179: 1587-1592.
- Ebbels, T. M. D., Holmes, E., Lindon, J. C., and Nicholson, J. K. 2004. Evaluation of metabolic variation in normal rat strains from a statistical analysis of ¹H NMR spectra of urine. *Journal of pharmaceutical and Biomedical analysis* 36: 823-833.
- Fiehn, O. 2002 Metabolomics-the link between genotypes and phenotypes. *Plant Molecular Biology* 48: 155-171.

- Fleck, S. L., Birdsall, B., Babon, J., Dluzewski, A. R., Martin, S. R., Morgan, W. D., Angov, E., Kettleborough, C. A., Feeney, J., Blackman, M. J., and Holder, A. A. 2003. Suramin and suramin analogues inhibit merozoite surface protein-1 secondary processing and erythrocyte invasion by the malaria parasite *Plasmodium falciparum*. *Journal of Biological Chemistry* 278: 47670-47677.
- Foxall, P. J. D., Spraul, M., Farrant, R. D., Lindon, L. C., Neild, G. H., and Nicholson, J. K. 1993b. 750 MHz ¹H NMR spectroscopy of human blood plasma. *Journal of Pharmaceutical and Biomedical Analysis* 11: 267-276.
- Fried, B., Irwin, S. W. B., and Lowry, S. F. 1990. Scanning electron microscopy of *Echinostoma trivolis* and *E. caproni* (Trematoda) adults from experimental infections in the golden hamster. *Journal of Natural History* 24: 433-440.
- Fried, B., and Huffman, J. E. 1996. The biology of the intestinal trematode *Echinostoma caproni*. *Advances in Parasitology* 38: 311-368.
- Fried, B., Schmidt, K. A., and Sorensen, R. E. 1997. *In vivo* and ectopic encystment of *Echinostoma revolutum* and chemical excystation of the metacercariae. *Journal of Parasitology* 83: 251-254.
- Halton, D. W. 2004. Microscopy and the helminth parasite. *Micron* 35: 361-390.
- Haswell-Elkins, M., and Levri, E. 2003. Food-borne trematodes. In *Manson's Tropical Diseases*, eds. G. C. Cook, and A. I. Zumla, pp. 1471-1486, London: Saunders.
- Horutz, K., and Fried, B. 1995. Effects of *Echinostoma caproni* infection on the neutral lipid content of the intestinal mucosa of ICR mice. *International Journal for Parasitology* 25: 653-655.
- Huffman, J. E., and Fried, B. 1990. *Echinostoma* and echinostomiasis. *Advances in Parasitology* 29: 215-269.
- Keiser, J., Brun, R., Fried, B., and Utzinger, J. 2006a. Trematocidal activity of praziquantel and artemisinin derivatives: *in vitro* and *in vivo* investigations on adult *Echinostoma caproni*. *Antimicrobial Agents and Chemotherapy* 50: 803-805.
- Keiser, J., and Utzinger, J. 2007a. Food-borne trematodiasis: current chemotherapy and advances with artemisinins and synthetic trioxolanes. *Trends in Parasitology* 23: 555-562.

- Keiser, J., and Utzinger, J. 2007b. Advances in the discovery and development of novel trematocidal drugs. *Expert Opinion on Drug Discovery* 2 (Suppl.): S9-S23.
- Keiser, J., and Utzinger, J. 2005. Emerging foodborne trematodiasis. *Emerging Infectious Diseases* 11: 1507-1514.
- Keiser, J., Xiao, S. H., and Utzinger, J. 2006b. Effects of tribendimidine on adult *Echinostoma caproni* harbore in mice, including scanning electron microscopic observations. *Journal of parasitology* 92: 858-862.
- Keiser, J., Xiao, S. H., Tanner, M., and Utzinger, J. 2006c. Artesunate and artemether are effective fasciolicides in the rat model and in vitro. *Journal of Antimicrobial Chemotherapy* 57: 1139-1145.
- Keiser, J., Utzinger, J., Tanner, M., Dong, Y., Vennerstrom, J. L. 2006d. The synthetic peroxide OZ78 is effective against *Echinostoma caproni* and *Fasciola hepatica*. *Journal of Antimicrobial Chemotherapy* 58: 1193-1197.
- Keun, H. C., Ebbels, T. M., Antti, H., Bollard, M. E., Beckonert, O., Schlotterbeck, G., Senn, H., Niederhauser, U., Holmes, E., Lindon, J. C., and Nicholson, J. K. 2002. Analytical reproducibility in ¹H NMR-based metabonomic urin analysis. *Chemical Research in Toxicology* 15: 1380-1386.
- Krotov, A. I., and Gusel'nikova, L. M. 1971. Use of white mice infected with *Echinostoma miyagawai* Ischii, 1932, for experimental therapy of intestinal trematodiasis. *Meditzinskaia Parazitologiiia I Parazitarnie Bolezni* 40: 679-682.
- Kwon, E. D., Zablocki, K., Peters, E. M., Jung, K. Y., Garcia-Perez, A., and Burg, M. B. 1996.
- Labow, B. I., and Souba, W. W. 2000. Glutamine. *World Journal of Surgery* 24: 1503-1513.
- Lämmli, G. 1968. Chemotherapy of trematode infections. *Advances in Chemotherapy* 3: 153-251.
- Leger, N., Nottoghem, M. J., and Cavier, R. 1973. Un test pharmacodynamique pour l'essai des douvicides. *Bulletin de la Societe de Pathologie Exotique et de ses Filiales* 66: 732-736.

- Leger, N., and Notteghem, M. J. 1975. The fasciolidal activity of a new compound, brotianide on *Echinostoma caproni* Richard, 1964. *Annales Pharmaceutiques Francaises* 33: 273-277.
- Lenz, E. M., Bright, J., Knight, R., Westwood, F. R., Davies, D., Major, H., and Wilson, I. D. 2005. Metabonomics with ^1H NMR spectroscopy and liquid chromatography-mass spectrometry applied to the investigation of metabolic changes caused by gentamicin-induced nephrotoxicity in the rat. *Biomarkers* 10: 173-187.
- Lesaffer, G., De Smet, R., Belpaire, F. M., Van Vlem, B., Van Hulle, M., Cornelis, R., Lameire, N., and Vanholder, R. 2003. Urinary excretion of the uraemic toxin *p*-cresol in the rat: contribution of glucuronidation to its metabolism. *Nephrology, Dialysis, Transplantation* 18: 1299-1306.
- Li, J. V., Wang, Y. L., Saric, J., Nicholson, J. K., Dirnhofer, S., Singer B. H., Tanner, M., Wittlin, S., Holmes, E., Utzinger, J. 2008. Global metabolic responses of NMRI mice to an experimental *Plasmodium berghei* infection. *Journal of Proteome Research* 7: 3948-3956.
- Lindon, J. C., Holmes, E., and Nicholson, J. K. 2001. Pattern recognition methods and applications in biomedical magnetic resonance. *Progress in NMR Spectroscopy* 39: 1-40.
- Lindon, J. C., Nicholson, J. K., and Wilson I. D., 2000. Directly coupled HPLC-NMR and HPLC-NMR-MS in pharmaceutical research and development. *Journal of chromatography B, Biomedical Sciences and Applications* 748: 233-258.
- Lun, Z. R., Gasser, R. B., Lai, D. H., Li, A. X., Zhu, X. Q., Yu, X. B., and Fang, Y. Y. 2005.
- Marchesi, J. R., Holmes, E., Khan, F., Kochhar, S., Scanlan, P., Shanahan, F., Wilson, I. D., and Wang, Y. L. 2007. Rapid and noninvasive metabonomic characterization of inflammatory bowel disease. *Journal of Proteome Research* 6: 546-551.

- Martin, F. P. J., Verdu, E. F., Wang, Y., Dumas, M. E., Yap, I. K. S., Cloarec, O., Bergonzelli, G. E., Corthesy-Theulaz, I., Kochhar, S., Holmes, E., Lindon, J. C., Collins, S. M., and Nicholson, J. K. 2006. Transgenomic metabolic interactions in a mouse disease model: interactions of *Trichinella spiralis* infection with dietary *Lactobacillus paracasei* supplementation. *Journal of Proteome Research* 5: 2185-2193.
- Maurer, K., Decere, M., and Fried, B. 1996. Effects of the anthelmintics clorsulon, rafoxanide, mebendazole and arprinocid on *Echinostoma caproni* in ICR mice. *Journal of Helminthology* 70: 95-96.
- Merchant, M. L., and Klein, J. B. 2007. Proteomics and diabetic nephropathy. *Seminars in Nephrology* 27: 627-626.
- Mitch, W. E., and Chan, W. 1979. α -Ketoisocaproate stimulates branched-chain amino acid transaminase in kidney and muscle. *American Journal of Physiology* 236:E514-E518.
- Miyakawa, H., Woo, S. K., Dahl, S. C., Handler, J. S., and Kwon, H. M. 1999. Tonicity-responsive enhancer binding protein, a rel-like protein that stimulates transcription in response to hypertonicity. *Proceedings of the National Academy of Sciences USA* 96: 2538-2542.
- Nicholson, J. K. 2006. Global systems biology, personalized medicine and molecular epidemiology. *Molecular Systems Biology* 2: 52.
- Nicholson, J. K., and Wilson, I. D. 1989. High resolution proton magnetic resonance spectroscopy of biological fluids. *Progress in NMR Spectroscopy* 21: 449-501.
- Nicholson, J. K., Lindon, J. C., and Holmes, E. 1999. 'Metabonomics': understanding the metabolic responses of living systems to pathophysiological stimuli via multivariate statistical analysis of biological NMR spectroscopic data. *Xenobiotica* 29: 1181-1189.
- Nicholson, J. K., Connelly, J., Lindon, J. C., Holmes, E. 2002. Metabonomics: a platform for studying drug toxicity and gene function. *Nature Reviews Drug Discovery* 1: 153-161.
- Nicholson, J. K., Foxall, P. J. D., Spraul, M., Farrant, R. D., and Lindon, J. C. 1995. 750 MHz ^1H and ^1H - ^{13}C NMR spectroscopy of human blood plasma. *Analytical Chemistry* 67: 793-811.

- Notteghem, M. J., Leger, N., and Cavier, R. 1979. Study of fluke-killing activity of flubendazole on *Echinostoma caproni* Richard, 1964. *Annales Pharmaceutiques Francaises* 37: 153-156.
- Notteghem, M. J., Leger, N., and Forget, E. 1980. Comparison of the fluke-killing activity of some compounds derivated from benzimidazole. *Annales Pharmaceutiques Francaises* 38: 61-63.
- Ohdoi, C., Nyhan, W. L., and Kuhara, T. 2003. Chemical diagnosis of Lesch-Nyhan syndrome using gas chromatography-mass spectrometry detection. *Journal of Chromatography B, Analytical Technologies in the Biomedical and Life Sciences* 792: 123-130.
- Ordovas, J. M., and Mooser, V. 2006. Metagenomics: the role of the microbiome in cardiovascular diseases. *Current Opinion in Lipidology* 17: 157-161.
- Ramsay, I. R., and Pullammanappallil, P. C. 2001. Protein degradation during anaerobic wastewater treatment: derivation of stoichiometry. *Biodegradation* 12: 247-257.
- Rim, H. J. 1984. Therapy of fluke infections in the past. *Arzneimittelforschung* 34: 1127-1129.
- Rochfort, S. 2005. Metabolomics reviewed: a new “omics” platform technology for systems biology and implications for natural product research. *Journal of natural Products* 68: 1813-1820.
- Saric, J., Li, J. V., Wang, Y. L., Keiser, J., Bundy, J. G., Holmes, E., and Utzinger, J. 2008. Metabolic profiling of an *Echinostoma caproni* infection in the mouse for biomarker discovery. *PLoS Neglected Tropical Diseases* 2:e254.
- Saric, J., Wang, Y. L., Li, J., Coen, M., Utzinger, J., Marchesi, J. R., Keiser, J., Veselkov, K., Lindon, J. C., Nicholson, J. K., and Holmes, E. 2008. Species variation in the faecal metabolome gives insight into differential gastrointestinal function. *Journal of Proteome Research* 7: 352-360.
- Schlotterbeck, G., Ross, A., Dieterle, F., and Senn, H. 2006. Metabolic profiling technologies for biomarker discovery in biomedicine and drug development. *Pharmacogenomics* 7: 1055-1075.

- Schmidt, J. 1998. Effects of benzimidazole anthelmintics as microtubule-active drugs on the synthesis and transport of surface glycoconjugates in *Hymenolepis microstoma*, *Echinostoma caproni*, and *Schistosoma mansoni*. *Parasitology Research* 84: 362-368.
- Schneck, J. L., Fried, B., and Sherma, J. 2004. Effects of tonicity on the release of neutral lipids in *Echinostoma caproni* adults and observations on lipids in excysted metacercariae. *Parasitology Research* 92: 285-288.
- Seibel, B. A., and Walsh, P. J. 2002. Trimethylamine oxide accumulation in marine animals: relationship to acylglycerol storage. *Journal of Experimental Biology* 205: 297-306.
- Selmer, T., and Adrei, P. I. 2001. *p*-Hydroxyphenylacetate decarboxylase from *Clostridium difficile*. A novel glycyl radical enzyme catalysing the formation of *p*-cresol. *European Journal of Biochemistry* 268: 1363-1372.
- Shukla-Dave, A., Roy, R., Bhadury, A. P., and Chatterjee, R. K. 2000. Effects of 2-deoxy-D-glucose on *Acanthocheilonema viteae*: rodent filariids as studied by multinuclear NMR spectroscopy. *Physiological Chemistry and Physics and Medical NMR* 32: 1-12.
- Smith, J. L., Wishnok, J. S., and Deen, W. M. 1994. Metabolism and excretion of methylamines in rats. *Toxicology and Applied Pharmacology* 125: 296-308.
- Thwaites, D. T., and Anderson, C. M. 2007. H⁺-coupled nutrient, micronutrient and drug transporters in the mammalian small intestine. *Experimental Physiology* 92: 603-619.
- Tinga, N., De, N., Vien, H. V., Chau, L., Toan, N. D., Kager, P. A., and Vries, P. J. 1999. Little effect of praziquantel or artemisinin on clonorchiasis in Northern Vietnam. A pilot study. *Tropical Medicine and International Health* 4: 814-818.
- Trygg, J., Holmes, E., and Lundstedt, T. 2007. Chemometrics in metabonomics. *Journal of Proteome Research* 6: 469-479.
- Trygg, J., and Wold, S. 2002. Orthogonal projections to latent structures (O-PLS). *Journal of Chemometrics* 16: 119-128.
- Utzinger, J., Xiao, S. H., Tanner, M., and Keiser, J. 2007. Artemisinins for schistosomiasis and beyond. *Current Opinion in Investigational Drugs* 8: 105-116.

- Vasta, J. D., Fried, B., and Sherma, J. 2008. High performance thin layer chromatographic analysis of neutral lipids in the urine of BALB/c mice infected with *Echinostoma caproni*. *Parasitology Research* 102: 625-629.
- Wang, Y. L., Holmes, E., Nicholson, J. K., Cloarec, O., Chollet, J., Tanner, M., Singer, B. H., and Utzinger, J. 2004. Metabonomic investigations in mice infected with *Schistosoma mansoni*: an approach for biomarker identification. *Proceedings of the National Academy of Sciences USA* 101: 12676-12681.
- Wang, Y., Lawler, D., Larson, B., Ramadan, Z., Kochhar, S., Holmes, E., and Nicholson, J. K. 2007. Metabonomic investigations of aging and caloric restriction in a life-long dog study. *Journal of Proteome Research* 6: 1846-1854.
- Wang, Y. L., Utzinger, J., Saric, J., Li, J V., Burckhardt, J., Dirnhofer, S., Nicholson, J. K., Singer, B. H., Brun, R., and Holmes, E. 2008. Global metabolic responses of mice to *Trypanosoma brucei brucei* infection. *Proceedings of the National Academy of Sciences USA* (in press).
- Wang, Y. L., Utzinger, J., Xiao, S. H., Xue, J., Nicholson, J. K., Tanner, M., Singer, B. H., and Holmes, E. 2006. System level metabolic effects of a *Schistosoma japonicum* infection in the Syrian hamster. *Molecular and Biochemical parasitology* 146: 1-9.
- Willson, M., Lauth, N., Perie, J., Callens, M., and Opperdoes, F. R. 1994. Inhibition of glyceraldehyde-3-phosphate dehydrogenase by phosphorylated epoxides and alpha-enones. *Biochemistry* 33: 214-220.
- Wong, J. M., de Souza, R., Kendall, C. W., Emam, A., and Jenkins, D. J. 2006. Colonic health: fermentation and short chain fatty acids. *Journal of Clinical Gastroenterology* 40: 235-243.
- Wright, E. M., Hirayama, B., Hazama, A., Loo, D. D., Supplisson, S., Turk, E., and Hager, K. M. 1993. The sodium/glucose cotransporter (SGLT1). *Society of General Physiologists Series* 48:229-241.
- Xiao, S. H., Keiser, J., Chollet, J., Utzinger, J., Dong, Y., Endriss, Y., Vennerstrom, J. L., and Tanner, M. *In vitro* and *in vivo* activities of synthetic trioxolanes against major human schistosome species. *Antimicrobial Agents and Chemotherapy* 51: 1440-1445.

- Xiao, S. H., Wu, H. M., Tanner, M., Utzinger, J., and Wang, C. 2005. Tribendimidine: a promising, safe and broad-spectrum anthelmintic agent from China. *Acta Tropica* 94: 1-14.
- Xiao, S. H., Xue, J., Tanner, M., Zhang, Y. N., Keiser, J., Utzinger, J., and Qiang, H. Q. 2008. Artemether, artesunate, praziquantel and tribendimidine administered singly at different dosages against *Clonorchis sinensis*: a comparative *in vivo* study. *Acta Tropica* 106: 54-59.
- Yancey, P. H., Clark, M. E., Hand, S. C., Bowlus, R. D., and Somero, G. N. 1982. Living with water stress: evolution of osmolyte systems. *Science* 217: 1214- 1222.
- Yu, L., Blaser, M., Andrei, P. I., Pierik, A. J., and Selmer, T. 2006. 4-Hydroxyphenylacetate decarboxylases: properties of a novel subclass of glyceryl radical enzyme systems. *Biochemistry* 45: 9584-9592.
- Zablocki, K., Miller, S. P., Garcia-Perez, A., and Burg, M. B. 1991. Accumulation of glycerophosphocholine (GPC) by renal cells: osmotic regulation of GPC:choline phosphodiesterase. *Proceedings of the National Academy of Sciences USA* 88: 7820-7824.
- Zeisel, S. H., Mar, M. H., Howe, J. C., and Holden, J. M. 2003. Concentrations of choline-containing compounds and betaine in common foods. *Journal of Nutrition* 133: 1302-1307.





5 Metabolic profiling of an *Echinostoma caproni* infection in the mouse for biomarker discovery

Jasmina Saric^{1,2}, Jia V. Li^{1,2}, Yulan Wang^{2‡}, Jennifer Keiser³, Jake G. Bundy², Elaine Holmes², Jürg Utzinger^{1*}

1 Department of Public Health and Epidemiology, Swiss Tropical Institute, Basel, Switzerland

2 Department of Biomolecular Medicine, Division of Surgery, Oncology, Reproductive Biology and Anaesthetics (SORA), Faculty of Medicine, Imperial College London, London, United Kingdom

3 Department of Medical Parasitology and Infection Biology, Swiss Tropical Institute, Basel, Switzerland

***Corresponding Author:** Jürg Utzinger, Department of Public Health and Epidemiology, Swiss Tropical Institute, P.O. Box, CH-4002 Basel, Switzerland. Tel.: +41 61 284-8129; Fax: +41 61 284-8105, E-mail: juerg.utzinger@unibas.ch

‡ Present Address: State Key Laboratory of Magnetic Resonance and Atomic and Molecular Physics, Wuhan Centre for Magnetic Resonance, Wuhan Institute of Physics and Mathematics, Wuhan, People's Republic of China

This article has been published in
PLoS Neglected Tropical Diseases **2008**, 2(7), e254

5.1 Abstract

Background. Metabolic profiling holds promise with regard to deepening our understanding of infection biology and disease states. The objectives of our study were to assess the global metabolic responses to an *Echinostoma caproni* infection in the mouse, and to compare the biomarkers extracted from different biofluids (plasma, stool, and urine) in terms of characterizing acute and chronic stages of this intestinal fluke infection.

Methodology/Principle Findings. Twelve female NMRI mice were infected with 30 *E. caproni* metacercariae each. Plasma, stool and urine samples were collected at 7 time points up to day 33 post-infection. Samples were also obtained from non-infected control mice at the same time points and measured using ^1H nuclear magnetic resonance (NMR) spectroscopy. Spectral data were subjected to multivariate statistical analyses. In plasma and urine, an altered metabolic profile was already evident 1 day post-infection, characterised by reduced levels of plasma choline, acetate, formate and lactate, coupled with increased levels of plasma glucose, and relatively lower concentrations of urinary creatine.

Conclusion/Significance. The current investigation is part of a broader NMR-based metabonomics profiling strategy and confirms the utility of this approach for biomarker discovery. In the case of *E. caproni*, a diagnosis based on all three biofluids would deliver the most comprehensive fingerprint of an infection. For practical purposes, however, future diagnosis might aim at a single biofluid, in which case urine would be chosen for further investigation, based on quantity of biomarkers, ease of sampling, and the degree of differentiation from the non-infected control group.

Keywords: *Echinostoma caproni*, diagnosis, NMR spectroscopy, metabonomics, biomarker, multivariate data analysis

5.2 Author Summary

Consumption of raw fish and other freshwater products can lead to unpleasant worm infections. Indeed, such worm infections are of growing public health and veterinary concern, but they are often neglected, partially explained by the difficulty of accurate diagnosis. In the present study we infected 12 mice with an intestinal worm (i.e., *Echinostoma caproni*) and collected blood, stool and urine samples 7 times between 1 and 33 days after the infection. At the same time points, blood, stool and urine were also sampled from 12 uninfected mice. These biofluid samples were examined with a spectrometer and data were analyzed with a multivariate approach. We observed important differences between the infected and the uninfected control animals. For example, we found an increased level of branched chain amino acids in the stool of infected mice and subsequent depletion in blood plasma. Additionally, we observed changes related to a disturbed intestinal bacterial composition, particularly in urine and stool. The combination of results from the three types of biofluids gave the most comprehensive characterization of an *E. caproni* infection in the mouse. Urine would be the biofluid of choice because the ease of sample collection and the high number and extent of changed metabolites.

5.3 Introduction

An estimated 40 million individuals are infected with food-borne trematodes and, in many parts of the world, the diseases caused by these infections are emerging [1]. Yet, food-borne trematodiasis are so-called neglected tropical diseases [2]. An infection with food-borne trematodes is acquired by the consumption of the larval stage of the parasite, present in aquatic food products (e.g., freshwater fish, crustacean, and water plants). Adult flukes reside either in the intestine (e.g., *Echinostoma* spp.), the lung (e.g., *Paragonimus* spp.), or the liver (e.g., *Clonorchis sinensis*, *Fasciola* spp., *Opisthorchis* spp.) and can lead to various forms of pathology [2,3].

A light infection with the intestinal fluke *Echinostoma* spp. in humans causes no marked deviation from the healthy state in the majority of cases, whereas the clinical symptoms due to a heavy infection include abdominal pain, violent diarrhea, anorexia, easy fatigue, and changes in the intestinal architecture, such as intestinal erosions, damage of intestinal mucosa, and catarrhal inflammation [4]. Histopathological investigations in mice and humans infected with *Echinostoma* spp. have revealed atrophied, fused and eroded villi, and a crypt hyperplasia in both lightly and heavily infected subjects [5-7].

At present, the most widely used diagnosis for infections with *Echinostoma* spp. and other food-borne trematodes, is by means of microscopic examination of stool samples for the presence of parasite eggs. However, light infection intensities, particularly at the onset of disease are often missed by this diagnostic approach. In addition, the detection of echinostome eggs in stool samples varies greatly due to species-dependent differences in egg laying capacity. Other means for diagnosis of food-borne trematode infections include immunological and molecular tests, such as the enzyme-linked immunosorbent assay (ELISA) [8] or polymerase chain reaction (PCR) [9], which depend on specificity of antigens and primers, respectively.

In the current study we applied a combination of ^1H nuclear magnetic resonance (NMR) spectroscopy and multivariate statistical analysis to identify candidate biomarkers of an *E. caproni* infection and disease states in the mouse, by metabolic profiling of blood plasma, stool, and urine samples. *E. caproni* is a suitable trematode model that has been widely and effectively used in the laboratory for drug screening, and to deepen our understanding of the immunology and pathology of echinostomes and other food-borne trematodes in the

vertebrate host [10-12]. NMR spectroscopy delivers a snapshot of the metabolite composition in biofluids, tissues and even bone/cartilage, and has found a large array of applications in biology and medicine, such as the detection and differentiation of coronary heart disease [13], and biomarker identification in schizophrenia patients [14]. The systemic metabolic profile of a biological sample is of special interest, because it can be characteristic of the entire organism, and hence finds increasing application in systems biology [15]. The use of multivariate statistical methods to analyze and interpret complex spectral datasets makes it possible to deal with large sample data banks, and to detect differences between physiologically or pathologically distinct states. Candidate biomarkers can be identified from these models, taking into consideration intra-group variations, sample preparation methods, and spectral data acquisition. Thus far, we have characterised the global metabolic responses to several parasitic infections in rodents, namely (i) *Schistosoma mansoni* in the mouse [16], (ii) *S. japonicum* in the hamster [17], (iii) *Trichinella spiralis* in the mouse [18], (iv) *Trypanosoma brucei brucei* in the mouse [19], and (v) *Plasmodium berghei* in the mouse (J.V. Li et al., unpublished data), mainly based on the urine and/or blood plasma metabolite profiles. Here we extend these initial host-parasite models to consider the relative merit of using biomarkers derived from a combined biological sample profile, and apply a metabolic profiling strategy for the first time to a food-borne trematode.

5.4 Materials and Methods

***E. caproni*-mouse model and animal husbandry.** Our experiments were carried out in accordance with Swiss cantonal and national regulations on animal welfare (permission no. 2081). Female NMRI mice (n = 24) were purchased from RCC (Itingen, Switzerland), and housed in groups of 4 in macrolon cages under environmentally-controlled conditions (temperature: ~25°C; humidity: ~70%; light-dark cycle: 12-12 h). Mice had free access to commercially available rodent food from Nafag (Gossau, Switzerland) and community tap water supply.

Mice were 5 to 6-week-old at the onset of the experiments and had an average weight of 25.5 g (standard deviation (SD) = 0.9 g). Half of the mice remained uninfected throughout the study and served as controls. The other 12 mice were orally infected with 30 *E. caproni* metacercariae each (provided by B. Fried; Lafayette College, Easton, PA, United States of

America) [20] on designated study day 0, which took place 1 week after arrival of animals to provide sufficient acclimatization time, and hence minimize stress-related impact on the metabolic profiles. Upon dissection of mice at the end of the experiment, however it was found that no infection had been established in 4 animals. Therefore these 4 mice were excluded from any further analysis.

Collection of biofluids. Blood plasma, stool and urine samples were collected over a 33-day time course at 7 distinct sampling points (days 1, 5, 8, 12, 19, 26, and 33 post-infection), representative of different stages in the life of the *E. caproni* fluke, including acute and chronic infection stages. Collection was carried out between 08:00 and 10:00 hours in order to avoid potential variation of metabolite concentrations due to diurnal fluctuations. Stool and urine samples were collected into Petri dishes by gently rubbing the abdomen of the mice, and were immediately transferred into separate Eppendorf tubes and kept at -40°C . Blood samples (40-50 μl) were collected from the tail tip of each mouse into haematocrit tubes with sodium [Na] heparin-coat. Tubes were placed in a centrifuge (model 1-15, Sigma; Osterode am Harz, Germany) operated at 4,000 g for 4 min in order to separate plasma from red blood cells. The packed cell volume (PCV), i.e., length of red blood cells column in the microcapillary versus total length of blood sample column, was determined and expressed as percentage. Subsequently, the plasma fraction (~ 20 μl) was transferred into a separate Eppendorf tube and kept at -40°C . Animals were weighed at each sampling point, using a Mettler balance (model K7T; Greifensee, Switzerland).

Mice were killed 36 days post-infection, using CO_2 . The small intestine was removed, and adult worms recovered from the ileum and jejunum and counted. Biological samples and an *E. caproni* specimen were forwarded to Imperial College London (United Kingdom) on dry ice and stored at -40°C prior to processing for ^1H NMR spectroscopic data acquisition.

Preparation of biofluids and *E. caproni* homogenate. Urine samples were prepared with a phosphate buffer (pH 7.4) containing 50% D_2O (Goss Scientific Instruments; Chelmsford, United Kingdom) as a field frequency lock and 0.01% sodium 3-(trimethylsilyl) [2,2,3,3- $^2\text{H}_4$] propionate (TSP) (Cambridge Isotope Laboratories Inc.; Andover, MA, United States of America), as a chemical shift reference (δ 0.0). An aliquot of 25 μl of urine was added to 25 μl phosphate buffer. Plasma samples were prepared by adding 30 μl of 0.9% saline made up in 50% D_2O into the Eppendorf tubes containing ~ 20 μl of plasma. Because of the limited

volumes of urine and plasma, samples were transferred into 1.7 mm micro NMR-tubes (CortecNet; Paris, France) using a micro-syringe.

Stool samples were prepared with the same buffer as for urine but using 90% D₂O to reduce the water content. Two pellets of stool were mashed with 700 µl buffer and sonicated for 30 min to inactivate gut bacteria and achieve biochemical stability in the sample. The samples were then centrifuged at 13,000 g for 2 min, and 550-600 µl of the supernatant was transferred into a new Eppendorf tube and stored at -40°C. Shortly before data acquisition, the stool supernatant was defrosted, centrifuged and transferred into NMR tubes of 5 mm outer diameter.

A tissue extraction was performed on the *E. caproni* specimen for ¹H NMR spectroscopic analysis. The adult *E. caproni* fluke was mashed in 1 ml of chloroform with a glass mortar and pestle. A total of 1 ml of methanol and 1 ml of water were added, and this mixture was transferred into a glass tube. Another 0.5 ml of each liquid was used to rinse the mortar and transferred into the same glass tube. The mixture was centrifuged at 2,500 g for 30 min. The aqueous and the chloroform phases were transferred into a new glass tube each, chloroform was evaporated over night and the aqueous phase was lyophilized. Prior to ¹H NMR data acquisition, the powder obtained from the aqueous phase was resolved in 550 µl phosphate buffer (90% D₂O), whereas the dry mass of the chloroform fraction was dissolved in deuterated chloroform (CDCl₃).

Acquisition of spectral data. ¹H NMR spectra from plasma, stool, and urine samples, and the *E. caproni* homogenate were recorded on a Bruker DRX 600 NMR spectrometer, operating at 600.13 MHz for proton frequency (Bruker; Rheinstetten, Germany). A Bruker 5 mm triple resonance probe with inverse detection was used, employing a standard NMR 1-dimensional (1D) experiment with pulse sequence [recycle delay (RD)-90°-*t*₁-90°-*t*_m-90°-ACQ], setting *t*₁ to 3 µs, and using a mixing time (*t*_m) of 150 ms. Water suppression was achieved with irradiation of the water peak during the RD set to 2 s and mixing time. The 90° pulse length was adjusted to ~10 µs. A total of 256 transients were collected into ~32,000 data points for each spectrum with a spectral width of 20 ppm. For plasma, two additional pulse programs were applied, namely Carr-Purcell-Meiboom-Gill (CPMG), and diffusion edited spectroscopy (DOESY) [21] to focus on the low and high molecular weight components of the plasma profile, respectively. All free induction decays (FIDs) were multiplied by an exponential function equivalent to a 0.3 Hz line-broadening factor prior to Fourier transformation.

Assignments of the spectral peaks were made from literature values [22-25] and confirmed *via* statistical total correlation spectroscopy (STOCSY) in MATLAB [26] and *via* standard 2-dimensional (2D) NMR experiments conducted on selected samples, including correlation spectroscopy (COSY), total correlation spectroscopy (TOCSY), and J-resolved NMR spectra [27,28].

Data processing and analysis. Data processing was as follows. First, spectra were corrected for phase and baseline distortions with an in-house developed MATLAB script. Second, the region containing the water/urea resonances (i.e., δ 4.2-6.3 in urine, δ 4.4-5.2 in plasma, and δ 4.7-5.5 in stool extracts) was excluded. Third, the spectra were normalized over the total remaining spectral area. Analysis of the spectral data was performed with principal component analysis (PCA) [29], projection to latent structure discriminant analysis (PLS-DA) and orthogonal (O)-PLS-DA [30]. PCA was used to explore any intrinsic similarity between samples. PCA models cannot be over-fitted since no prior information on infection status is included in the model. PLS-DA was then used to apply knowledge of infection status to optimize separation of classes and recovery of candidate biomarkers [30]. O-PLS-DA includes an orthogonal data filter in the PLS-DA and was used to further improve the extraction of infection-related biomarkers by removing the influence of systematic variation not related to infection status. The weight of contribution of the peaks is indicated by the color scale, whereby red symbolizes relatively high correlation with infection and blue indicates relatively low or no correlation. The metabolites which contributed the greatest weight to the O-PLS-DA coefficient plot were identified. The NMR spectral data were used as the *X*-matrix and class information (infected or non-infected control) as the *Y*-matrix to build the O-PLS-DA models. A model consisting of one PLS component and one orthogonal component was generated using 7-fold cross validation. Finally, in order to more accurately profile the temporal behavior of the discriminatory metabolites characterizing an *E. caproni* infection, computational integration was performed. Resonances from several of the metabolites in each sample, which showed infection-dependent variations, were integrated using an automated curve fitting program. The relative concentration in relation to the total spectral integral, subsequent to removal of the water resonance, was determined. This was performed in MATLAB using a previously published method [31], and further modified by a colleague (K. Veselkov; Imperial College London, UK). The p-values for the metabolites were assessed using a non-parametric 1-way analysis of variance (Mann-Whitney U) test in MATLAB.

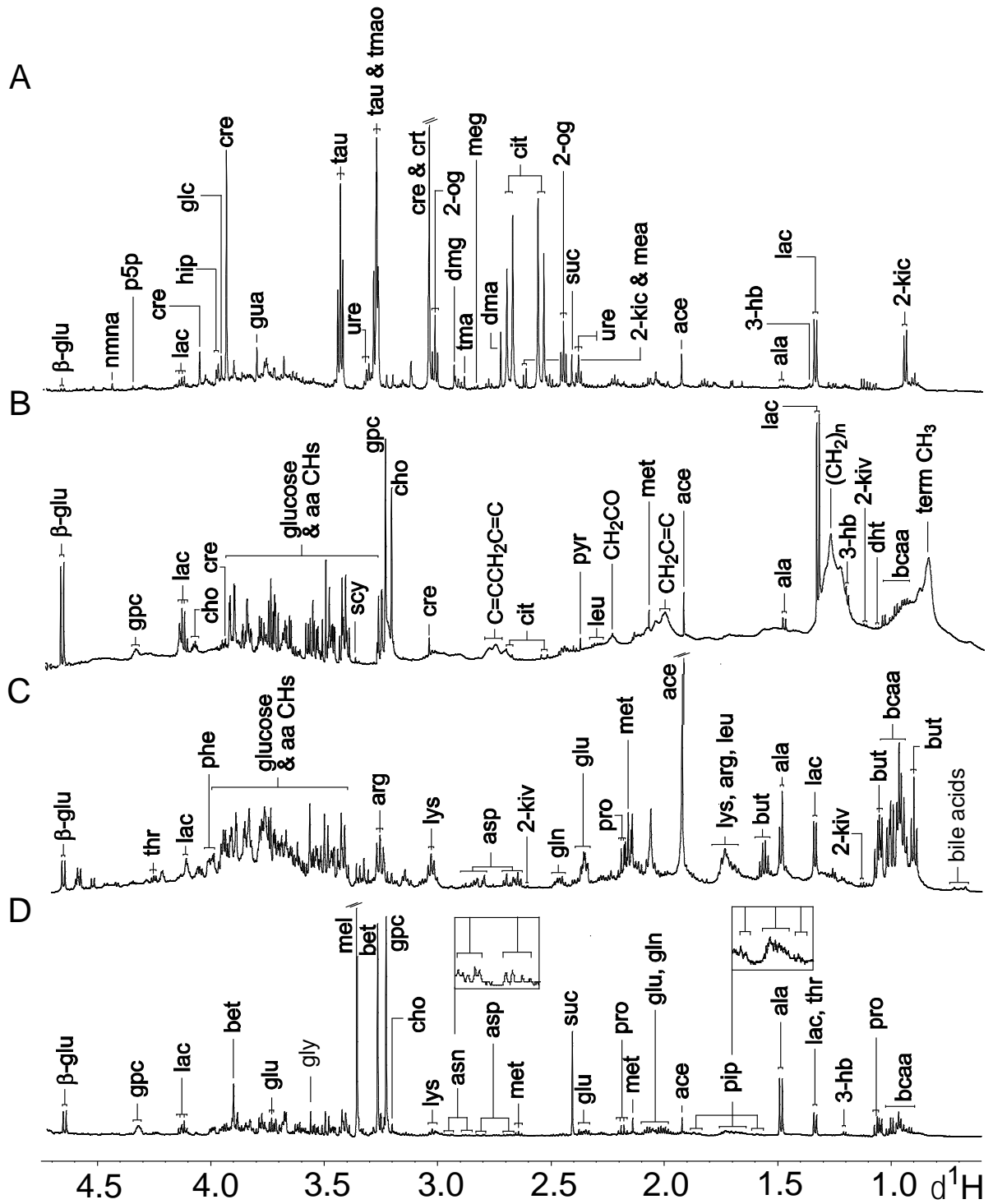


Figure 5.1. Previous page: Aliphatic region of a representative 600 MHz ¹H-NMR 1D spectra of biological samples obtained from an uninfected control mouse, aged 7-8 weeks. Spectra of urine (A), plasma (B), and faecal water (C) are shown. Additionally, the same region was displayed for the extract of an individual *E. caproni* fluke (D). Key: 2-og, 2-oxoglutarate; 3-hb, 3-hydroxybutyrate; 2-kic, 2-ketoisocaproate; 2-kiv, 2-ketoisovalerate; β-glu, β-glucose; aa, amino acids; ace, acetate; ala, alanine; arg, arginine; asn, asparagine; asp, aspartate; bcaa, branched chain amino acids; bet, betaine; but, butyrate; cit, citrate; cho, choline; cre, creatine; crt, creatinine; dht, dihydroxythymine; dma, dimethylamine; dmg, dimethylglycine; glc, glycolate; gln, glutamine; glu, glutamate; gly, glycine; gpc, glycerophosphocholine; gua, guanidinoacetate; hip, hippurate; lac, lactate; leu, leucine; lys, lysine; mea, methylamine; meg, methylguanidine; mel, methanol; met, methionine; nmna, N-methylnicotinamide; phe, phenylalanine; pip, pipercolate; pro, proline; p5p, pyridoxamine-5-phosphate; pyr, pyruvate; scy, scyllo-inositol; suc, succinate; tau, taurine; thr, threonine; tma, trimethylamine; tmao, trimethylamine-N-oxide; ure, ureidopropanoate.

5.6 Results

Physiological monitoring of mice. *E. caproni*-infected mice showed no visible sign of ill-health over the course of the experiment. The mean weight and mean PCV of *E. caproni*-infected (n = 8) and non-infected control mice (n = 12) did not differ at any of the time points investigated. The PCV values maintained a constant level throughout the experiment (49.6-55.1%). Upon dissection and worm count, an infection was confirmed in 8 out of the 12 mice (average worm count 26.5, SD = 12.0, range: 10-44 worms). The 4 animals with no established infection were excluded from further analyses.

Composition of metabolite profiles. Prior to assessing the metabolic effects of an *E. caproni* infection, the ¹H NMR spectra of plasma, stool, and urine samples obtained from non-infected mice were characterised and found to be inherently different in composition. All three types of biofluids contained lactate, alanine, glucose, and acetate. Unique to the urine metabolic profile was the presence of hippurate, indoxylsulfate, urocanate, taurine, trimethylamine-N-oxide (TMAO), 2-oxoglutarate, ureidopropanoate, and 2-ketoisocaproate, amongst others (Figure 5.1A, Figure 5.2A and Table 5.1). The plasma spectral profiles were characterised by the predominance of various lipids and lipoprotein fractions, along with resonances from creatine, and several amino and organic acids (Figure 5.1B, Figure 5.2B and Table 5.2). Apart from the standard 1D acquisition, applied on all biofluids, a CPMG and DOESY pulse

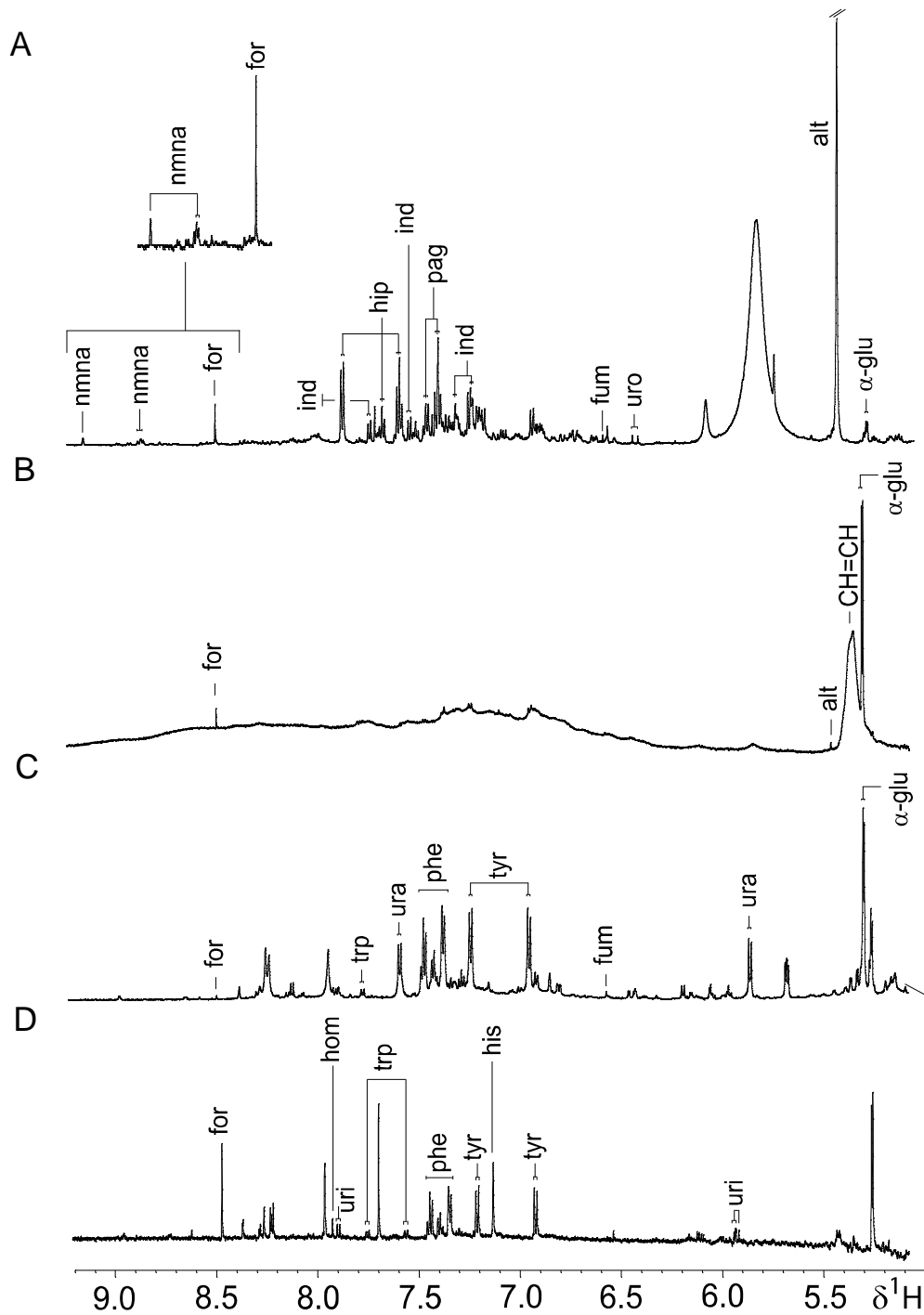


Figure 5.2. Aromatic region of representative 600 MHz ^1H -NMR 1D spectra of biological samples obtained from an uninfected control mouse, aged 7-8 weeks. Spectra of urine (A), plasma (B), and faecal water (C) are shown. Additionally, the same region of a 600 MHz ^1H NMR 1D spectrum of *E. caproni* extract is depicted (D). Key: α -glu, α -glucose; alt, alantoin; for, formate; fum, fumarate; hip, hippurate; his, histidine; hom, homocarnosine; ind, indoxylsulfate; nmna, *N*-methyl-nicotinamide; pag, phenylacetyl-glycine; phe, phenylalanine; trp, tryptophan; tyr, tyrosine; ura, uracil; uri, uridine; uro, urocanate.

sequence was used in plasma profiling, to represent low and high molecular weight metabolites, respectively. Characteristic metabolic features of the stool extracts were bile acids and short chain fatty acids (SCFAs), such as butyrate, and propionate. In addition, other amino acids, such as tryptophan, lysine, arginine, and glutamine were more visible in stool spectra, compared to urine and plasma (Figure 5.1C, Figure 5.2C and Table 5.3)

In order to establish whether excretory products of the parasite itself were likely to contribute to any of the biofluids analyzed, a standard 1D spectrum of an adult *E. caproni* was acquired. The spectrum of the parasite differed from the biofluids obtained from the mouse host in content of homocarnosine, histidinol, uridine, pipercolate, and betaine (Figure 5.1D, Figure 5.2D), although betaine has been observed in ¹H NMR spectra of urine in previous studies [32]. Tables 5.1-5.4 summarize key metabolites found in urine, plasma, and stool extracts of mice, and in the *E. caproni* homogenate, respectively.

Multivariate analysis and global metabolic trajectories. In both PCA and PLS-DA scores plots of the urinary metabolite profiles, a clear separation of *E. caproni*-infected and non-infected control mice was already visible 1 day post-infection. This separation was maintained in all later time points except day 5. Metabolic trajectories were constructed for each type of biofluids by taking the mean position in the principal component (PC) scores plot for each group of mice (*E. caproni*-infected and non-infected controls) separately, and connecting the coordinates chronologically to establish any systematic change in metabolic composition over the time course of the experiment. The control group showed no significant movement over the study duration (data not shown), whereas in the infected group, day 19 was significantly separated from all other days post-infection, and the whole time course of infection showed a shift from the upper left to the lower right quadrant (Figure 5.3A), whereby days 1 and 5 post-infection differed significantly from the sampling end point (day 33).

The plasma spectra of *E. caproni*-infected mice showed marked differences at days 1, 12, 26, and 33 post-infection, with the best discriminatory model at day 12 post-infection (goodness of prediction (Q^2) according to PCA = 0.97; Q^2 (PLS-DA) = 0.89). Comparing the 3 different pulse programs applied, plasma time trajectories, showed similar behavior. The control trajectories were generally clustered, indicating stability of the metabolite composition over the study period. However, the standard 1D trajectory showed a slight difference between early and late time points (e.g., day 1 was separated in space from days 19 to 33).

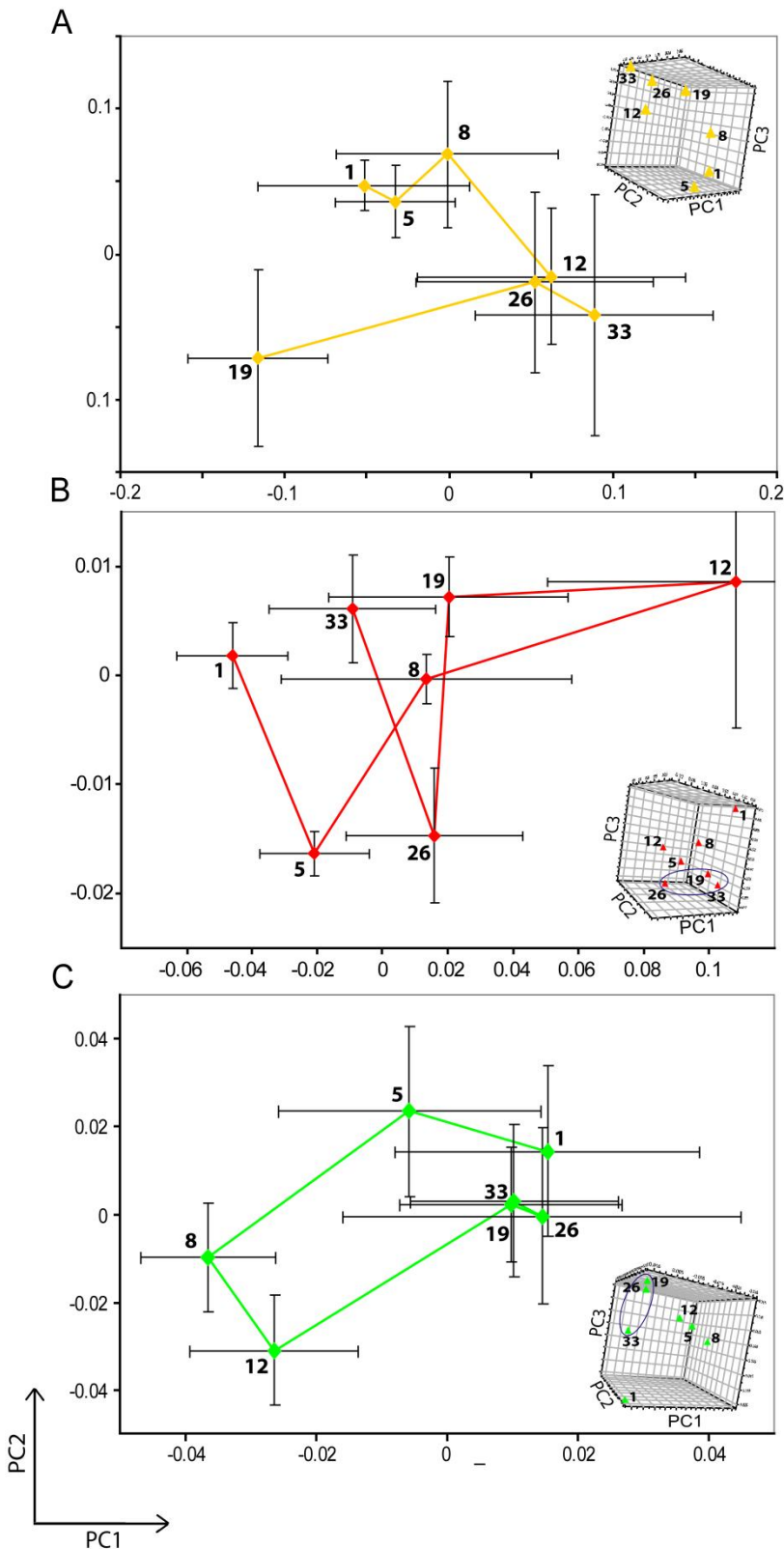


Figure 3. PCA trajectory plot of urine (A), plasma (B), and faecal water spectra (C) obtained from the mean PC1 and PC2 values for the *E. caproni*-infected mice over a 33-day period. The collection of the biofluids was performed at days 1, 5, 8, 12, 19, 26, and 33 post-infection. The ellipses in the 3D plots (Figures 3B and C) are for illustration purposes only, and are not based on statistical boundaries.

Table 5.1. Next page: List of metabolites found in urine over a 33-day study period in NMRI female mice. The arrows show whether the metabolic change, associated with an *E. caproni* infection, is significantly increased (↑) or decreased (↓) in infected mice compared to non-infected control mice and the numbers, next to the arrows indicate the day of maximum significance. The p-values for the changing metabolites were assessed using a non-parametric 1-way analysis of variance (Mann-Whitney U) test in MATLAB, based on the integrals of the selected peaks and were all in the range of 0.001 to 0.05.

Metabolic profiling of an *Echinostoma caproni* infection

Metabolite	Maximal time of metabolic change	Chemical moiety	Chemical shift in ppm and multiplicity
2-hydroxyisobutyrate		2xCH ₃	1.36(s)
2-ketoisocaproate	↓ (d12)	CH ₂ , CH, 2xCH ₃	2.61(d), 2.10(m), 0.94(d)
2-oxoglutarate		β-CH ₂ , γ-CH ₂	3.02(t), 2.50(t)
acetate	↓ (d8)	CH ₃	1.91(s)
alanine		α-CH, β-CH ₃	3.81(q), 1.48(d)
allantoin		CH	5.40(s)
citrate		1-CH ₂ , 3-CH ₂	2.69(d), 2.54(d)
creatine	↓ (d8)	CH ₃ , CH ₂	3.04(s), 3.93(s)
creatinine		CH ₃ , CH ₂	3.05(s), 4.06(s)
dimethylamine		2xCH ₃	2.71(s)
dimethylglycine		2xCH ₃ , CH ₂	2.89(s), 3.71(s)
formate		CH	8.45(s)
fumarate		CH	6.53(s)
α-glucose	↑ (d1); ↓ (d12)*	1-CH, 2-CH, 3-CH, 4-CH, 5-CH, half 6-CH ₂ , half 6-CH ₂	5.24(d), 3.56(dd), 3.70(t), 3.40(t), 3.83(m), 3.72(dd), 3.85(m)
β-glucose	↑ (d1); ↓ (d12)*	1-CH, 2-CH, 3-CH, 4-CH, 5-CH, half 6-CH ₂ , half 6-CH ₂	4.65(d), 3.25(dd), 3.47(t), 3.40(t), 3.47(ddd), 3.78(dd), 3.90(dd)
glycolate		CH ₂	3.94(s)
guanidinoacetate		CH ₂	3.80(s)
hippurate	↓ (d33)	CH ₂ , 2,6-CH, 3,5-CH, 4-CH	3.97(d), 7.84(d), 7.55(t), 7.64(t)
indoxylsulfate		5-CH, 6-CH, 4-CH, 7-CH	7.20(t), 7.27(t), 7.51(d), 7.70(d)
lactate		CH, CH ₃	4.12(q), 1.33(d)
mannitol	↑ (d12)	2xα-CH ₂ , 2xβ-CH, 2xγ-CH	3.78(m), 3.88(dd), 3.68(dd)
methyl crotonate		β-CH, γ-CH ₃ , γ'-CH ₃	1.66(s), 1.70(s), 1.71(s)
methylamine		CH ₃	2.61(s)
methylguanidine		CH ₃	2.83(s)
N-methyl-nicotinamide		CH ₃ , 6-CH, 2-CH, 5-CH, 4-CH	4.48(s), 8.97(d), 9.28(s), 8.19(t), 8.90(d)
p-cresolglucuronide	↑ (d12)	2,6-CH, 3,5-CH	7.06(d), 7.23(d), 2.30(s), 5.07(d)
phenylacetylglucine	↑ (d26)	2,6-CH, 3,5-CH, Ph-CH ₂ , N-CH ₂	7.43(m), 7.37(m), 3.75(d), 3.68(s)
pyridoxamine-5-phosphate		OCH ₂ , CH ₂ N, CH ₃	7.67(s), 4.34(s), 2.48(s)
succinate	↑ (d33)	2xCH ₂	2.41(s)
taurine	↓ (d19)	CH ₂ N, CH ₂ S	3.27(t), 3.43(t)
trimethylamine	↑ (d12)	3xCH ₃	2.88(s)
trimethylamine-N-oxide	↑ (d12)	3xCH ₃	3.27(s)
ureidopropanoate		α-CH ₂ , β-CH ₂	2.38(t), 3.3(t)
urocanate		α-CH, β-CH, 5-CH, 2-CH	6.40(d), 7.13(d), 7.41(s), 7.89(s)

Metabolic profiling of an *Echinostoma caproni* infection

Table 5.2. List of plasma metabolites found in mice over a 33-day study period. Arrows indicate significantly changing substances comparing plasma of *E. caproni*-infected mice with non-infected control mice (↑, increased; ↓, decreased in infected animals) and the numbers in brackets indicate the day of maximum significance. *glucose was the only metabolite found, which changed its directionality with time, i.e., it increased significantly after one day of infection and at day 8 post-infection was present in significantly lower concentrations, compared to uninfected control mice. The p-values for the changing metabolites were assessed using a non-parametric 1-way analysis of variance (Mann-Whitney U) test in MATLAB, based on the integrals of the selected peaks and were all in the range of 0.001 to 0.05.

Metabolite	Maximal time of metabolic change	Chemical moiety	Chemical shift in ppm and multiplicity
2-ketoisovalerate		CH, 2xCH ₃	3.02(m), 1.13(d)
3-hydroxybutyrate		half α-CH ₂ , half α-CH ₂ , β-CH, γ-CH ₃	2.32(m), 2.42(m), 4.16(m), 1.21(d)
acetate	↑ (d12)	CH ₃	1.91(s)
acetoacetate		α-CH ₂ , γ-CH ₃	2.29(s), 3.45(s)
alanine		α-CH, β-CH ₃	3.81(q), 1.48(d)
allantoin		CH	5.40(s)
choline	↓ (d33)	3xCH ₃ , α-CH ₂ , β-CH ₂	3.21(s), 4.07(m), 3.52(m)
citrate		1-CH ₂ , 3-CH ₂	2.69(d), 2.54(d)
creatine	↓ (d12)	CH ₃ , CH ₂	3.04(s), 3.93(s)
dihydroxythymine		CH ₂ , CH, CH ₃	3.17(m), 2.47(m), 1.07(d)
formate	↑ (d12)	CH	8.45(s)
α-glucose	↑ (d1); ↓ (d12)*	1-CH, 2-CH, 3-CH, 4-CH, 5-CH, half 6-CH ₂ , half 6-CH ₂	5.24(d), 3.56(dd), 3.70(t), 3.40(t), 3.83(m), 3.72(dd), 3.85(m)
β-glucose	↑ (d1); ↓ (d12)*	1-CH, 2-CH, 3-CH, 4-CH, 5-CH, half 6-CH ₂ , half 6-CH ₂	4.65(d), 3.25(dd), 3.47(t), 3.40(t), 3.47(ddd), 3.78(dd), 3.90(dd)
Glycerophosphocholine	↓ (d12)	3xCH ₃ , half α-CH ₂ , half α-CH ₂ , half β-CH ₂ , half β-CH ₂ , γ-CH ₂	3.23(s), 4.32(t), 3.60(dd), 3.68(t), 3.89(m), 3.72(dd)
isoleucine	↓ (d33)	α-CH, β-CH, half γ-CH ₂ , half γ-CH ₂ , δ-CH ₃ , β-CH ₃	3.68(d), 1.93(m), 1.25(m), 1.47(m), 0.99(d), 1.02(d)
lactate		CH, CH ₃	4.12(q), 1.33(d)
leucine	↓ (d33)	α-CH, β-CH ₂ , γ-CH, δ-CH ₃ , δ-CH ₃	3.72(t), 1.96(m), 1.63(m), 1.69(m), 0.91(d), 0.94(d)
methionine		α-CH, β-CH ₂ , γ-CH ₂ , CH ₃	3.87(m), 2.10(m), 2.65(dd), 2.15(s)
scyllo-inositol		6xCH	3.35(s)
valine	↓ (d33)	α-CH, β-CH, γ-CH ₃ , γ'-CH ₃	3.62(d), 2.28(m), 0.98(d), 1.03(d)
lipid fraction	↑	CH ₃	0.84(t)
lipid fraction	↑	(CH ₂) _n	1.25(m)
lipid fraction	↑	β-CH ₂ CH ₂ CO	1.57(m)
lipid fraction	↑	CH ₂ C=C	1.97(m), 2.00(m)
lipid fraction	↑	CH ₂ CO	2.23(m)
lipid fraction	↑	C=CCH ₂ C=C	2.69(m), 2.71(m), 2.72(m)
lipid fraction	↑	CH=CH	5.23(m), 5.26(m), 5.29(m)

Metabolic profiling of an *Echinostoma caproni* infection

Table 5.3. Metabolites found in faecal water of mice over a 33-day study period. Arrows indicate differences in the spectral profiles between *E. caproni*-infected mice and non-infected control mice (↑, increased; ↓, decreased in infected animals) and the numbers in brackets show the day post-infection of maximum concentration difference of the respective metabolite. The p-values for the changing metabolites were assessed using a non-parametric 1-way analysis of variance (Mann-Whitney U) test in MATLAB, based on the integrals of the selected peaks and were all in the range of 0.001 to 0.05.

Metabolite	Maximal time of metabolic change	Chemical moiety	Chemical shift in ppm and multiplicity
2-hydroxyisovalerate		α -CH, β -CH, γ -CH ₃ , γ' -CH ₃	3.85(d), 2.02(m), 0.79(d), 0.84(d)
2-ketoisocaproate		CH ₂ , CH, 2xCH ₃	2.61(d), 2.10(m), 0.94(d)
2-ketoisovalerate		CH, 2xCH ₃	3.02(m), 1.13(d)
3-aminopropionic acid		α -CH ₂ , β -CH ₂	2.56(t), 3.19(t)
3-hydroxyphenylpropionate		α -CH ₂ , β -CH ₂ , 2-CH	2.85(t), 2.47(m), 6.80(m)
2-oxoisoleucine		CH, half γ -CH ₂ , half γ -CH ₂ , δ -CH ₃ , β -CH-CH ₃	2.93(m), 1.70(m), 1.46(m), 0.90(t), 1.10(d)
5-aminovalerate	↑ (d26)	5-CH ₂ , 2-CH ₂ , 3,4-CH ₂	3.02(t), 2.24(t), 1.65(m)
acetate	↓ (d12)	CH ₃	1.91(s)
alanine	↓ (d12)	α -CH, β -CH ₃	3.81(q), 1.48(d)
arginine		α -CH, β -CH ₂ , γ -CH ₂ , δ -CH ₂	3.76(t), 1.89(m), 1.59(m), 3.17(t)
asparagine		α -CH, half β -CH ₂ , half β -CH ₂	4.01(m), 2.87(dd), 2.96(dd)
aspartate		α -CH, half β -CH ₂ , half β -CH ₂	3.92(m), 2.70(m), 2.81(m)
bile acids		CH ₃	0.70(m)
butyrate	↓ (d26)	α -CH ₂ , β -CH ₂ , γ -CH ₃	2.16(t), 1.56(m), 0.90(t)
ethanolamine		NH-CH ₂ , HO-CH ₂	3.15(t), 3.78(t)
formate		CH	8.45(s)
fumarate		CH	6.53(s)
α -glucose		1-CH, 2-CH, 3-CH, 4-CH, 5-CH, half 6-CH ₂ , half 6-CH ₂	5.24(d), 3.56(dd), 3.70(t), 3.40(t), 3.83(m), 3.72(dd), 3.85(m)
β -glucose		1-CH, 2-CH, 3-CH, 4-CH, 5-CH, half 6-CH ₂ , half 6-CH ₂	4.65(d), 3.25 (dd), 3.47(t), 3.40(t), 3.47(ddd), 3.78(dd), 3.90(dd)
glutamate		α -CH, β -CH ₂ , γ -CH ₂	3.78(m), 2.06(m), 2.36(m)
glutamine		α -CH, β -CH ₂ , γ -CH ₂	3.78(m), 2.15(m), 2.46(m)
glycerol		half α,γ -CH ₂ , half α,γ -CH ₂ , β -CH	3.56(dd), 3.64(dd), 3.87(m)
glycine	↓ (d12)	CH ₂	3.55(s)
hypoxanthine		3-CH, 7-CH	8.10(s), 8.11(s)
isoleucine	↑ (d26)	α -CH, β -CH, half γ -CH ₂ , half γ -CH ₂ , δ -CH ₃ , β -CH ₃	3.68(d), 1.93(m), 1.25(m), 1.47(m), 0.99(d), 1.02(d)
lactate		CH, CH ₃	4.12(q), 1.33(d)
leucine	↑ (d8)	α -CH, β -CH ₂ , γ -CH, δ -CH ₃ , δ -CH ₃	3.72(t), 1.96(m), 1.63(m), 1.69(m), 0.91(d), 0.94(d)
lysine		α -CH, β -CH ₂ , γ -CH ₂ , δ -CH ₂ , ϵ -CH ₂	3.77(t), 1.92(m), 1.73(m), 1.47(m), 3.05(t)
methionine		α -CH, β -CH ₂ , γ -CH ₂ , CH ₃	3.87(m), 2.10(m), 2.65(dd), 2.15(s)

Metabolic profiling of an *Echinostoma caproni* infection

<i>myo</i> -inositol		1,3-CH, 2-CH, 5-CH, 4,6-CH	3.53(dd), 4.06(t), 3.28(t), 3.63(t)
phenylacetic acid		CH ₂ , 2,4,6-CH, 3,5-CH	3.52(s), 7.29(t), 7.36(t)
phenylalanine		2,6-CH, 3,5-CH, 4-CH, CH ₂ , CH	7.44(m), 7.39(m), 7.33(m), 3.17(dd), 3.30(dd), 3.99(dd)
proline		α -CH, half β -CH ₂ , half β -CH ₂ , γ -CH ₂ , δ -CH ₂	4.15(dd), 2.05(m), 2.38(m), 2.00(m), 3.39(m)
propionate	↓ (d26)	CH ₂ , CH ₃	2.19(q), 1.06(t)
succinate		2x CH ₂	2.41(s)
threonine		α -CH, β -CH, γ -CH ₃	3.60(d), 4.26(m), 1.33(d)
tryptophan		4-CH, 7-CH, 2-CH, 5-CH, 6-CH, α -CH, half β -CH ₂ , half β -CH ₂	7.79(d), 7.56(d), 7.34(s), 7.29(t), 7.21(t), 4.06(dd), 3.49(dd), 3.31(dd)
tyrosine		2,6-CH, 3,5-CH, CH ₂ , α -CH	7.23(d), 6.91(d), 2.93(t), 3.25(t)
uracil	↑ (d8)	5-CH, 6-CH	5.81(d), 7.59(d)
urocanate		α -CH, β -CH, 5-CH, 2-CH	6.40(d), 7.13(d), 7.41(s), 7.89(s)
valine	↑ (d26)	α -CH, β -CH, γ -CH ₃ , γ' -CH ₃	3.62(d), 2.28(m), 0.98(d), 1.03(d)

In contrast, for the *E. caproni*-infected animals, there was a significant movement from early (day 1) to intermediate time points post-infection (days 5 and 12) in the first component and finally to late time points (days 26 and 33) in the third component (Figure 5.3B). This movement pattern was consistent across the datasets acquired by all three pulse programs.

With regard to the ¹H NMR spectra obtained from stool samples, a clear separation was found at day 5 post-infection in both the PCA and PLS-DA scores plot between *E. caproni*-infected and non-infected control mice, with maximum model fit for the PLS-DA model at day 26 post-infection ($Q^2 = 0.79$). At the final time point (day 33), the two groups were metabolically similar; there was no separation between infected and non-infected mice using PCA, and the PLS-DA model revealed a lower, but still significant Q^2 value than all previous time points. By comparing the time trajectories of the non-infected control with the *E. caproni*-infected group of mice, the controls were more tightly clustered, but showed a significant movement from day 8 post-infection onwards along PC1. In the 2D time trajectory plot of the *E. caproni*-infected mice, all time points were tightly clustered with the exception of days 8 and 12 post-infection, which comprised a separate cluster (Figure 5.3C). Introducing an additional PC brought about clear differentiation of the late time points (days 19, 26, and 33) from day 1 post-infection.

Table 4. List of metabolites found in extracts of an adult *E. caproni*.

Metabolite	Chemical moiety	Chemical shift in ppm and multiplicity
3-hydroxybutyrate	half α -CH ₂ , half α -CH ₂ , β -CH, γ -CH ₃	2.32(m), 2.42(m), 4.16(m), 1.21(d)
acetate	CH ₃	1.91(s)
alanine	α -CH, β -CH ₃	3.81(q), 1.48(d)
betaine	CH ₂ , CH ₃	3.90(s), 3.27(s)
choline	3xCH ₃ , α -CH ₂ , β -CH ₂	3.21(s), 4.07(m), 3.52(m)
formate	CH	8.45(s)
α -glucose	1-CH, 2-CH, 3-CH, 4-CH, 5-CH, half 6-CH ₂ , half 6-CH ₂	5.24(d), 3.56(dd), 3.70(t), 3.40(t), 3.83(m), 3.72(dd), 3.85(m)
β -glucose	1-CH, 2-CH, 3-CH, 4-CH, 5-CH, half 6-CH ₂ , half 6-CH ₂	4.65(d), 3.25(dd), 3.47(t), 3.40(t), 3.47(ddd), 3.78(dd), 3.90(dd)
glutamine	α -CH, β -CH ₂ , γ -CH ₂	3.78(m), 2.15(m), 2.46(m)
glycerophosphocholine	3xCH ₃ , half α -CH ₂ , half α -CH ₂ , half β -CH ₂ , half β -CH ₂ , γ -CH ₂	3.23(s), 4.32(t), 3.60(dd), 3.68(t), 3.89(m), 3.72(dd)
glycine	CH ₂	3.55(s)
histidinol	5-CH, 3-CH, γ -CH ₂ , β -CH, α -CH	7.89(s), 7.12(s), 3.85(dd), 3.67(m), 3.62(m)
homocarnosine	5-CH, 3-CH, half ring-CH ₂ , half ring-CH ₂ , N-CH, N-CH ₂ , CO-CH ₂ , CH ₂	7.90(s), 7.01(s), 3.17(dd), 2.96(dd), 4.48(m), 2.92(m), 2.36(m), 1.89(m), 3.21(t)
isoleucine	α -CH, β -CH, half γ -CH ₂ , half γ -CH ₂ , δ -CH ₃ , β -CH ₃ ,	3.68(d), 1.93(m), 1.25(m), 1.47(m), 0.99(d), 1.02(d)
lactate	CH, CH ₃	4.12(q), 1.33(d)
leucine	α -CH, β -CH ₂ , γ -CH, δ -CH ₃ , δ -CH ₃	3.72(t), 1.96(m), 1.63(m), 1.69(m), 0.91(d), 0.94(d)
lysine	α -CH, β -CH ₂ , γ -CH ₂ , δ -CH ₂ , ϵ -CH ₂	3.77(t), 1.92(m), 1.73(m), 1.47(m), 3.05(t)
methionine	α -CH, β -CH ₂ , γ -CH ₂ , CH ₃	3.87(m), 2.10(m), 2.65(dd), 2.15(s)
phenylalanine	2,6-CH, 3,5-CH, 4-CH, CH ₂ , CH	7.44(m), 7.39(m), 7.33(m), 3.17(dd), 3.30(dd), 3.99(dd)
pipecolate	half 3,4,5-CH ₂ , half 4,5-CH ₂ , half 3-CH ₂ , half 6-CH ₂ , half 6-CH ₂ , 2-CH	1.60-1.66(m), 1.86(m), 2.22(m), 3.02(m), 3.43(m), 3.60(m)
proline	α -CH, half β -CH ₂ , half β -CH ₂ , γ -CH ₂ , δ -CH ₂	4.15(dd), 2.05(m), 2.38(m), 2.00(m), 3.39(m)
propionate	CH ₂ , CH ₃	2.19(q), 1.06(t)
scyllo-inositol	6xCH	3.35(s)
succinate	2xCH ₂	2.41(s)
threonine	α -CH, β -CH, γ -CH ₃	3.60(d), 4.26(m), 1.33(d)
tryptophan	4-CH, 7-CH, 2-CH, 5-CH, 6-CH, α -CH, half β -CH ₂ , half β -CH ₂	7.79(d), 7.56(d), 7.34(s), 7.29(t), 7.21(t), 4.06(dd), 3.49(dd), 3.31(dd)
tyrosine	2,6-CH, 3,5-CH, CH ₂ , α -CH	7.23(d), 6.91(d), 2.93(t), 3.25(t)
uridine	6-CH, 5-CH, 2'-CH, 3'-CH, 4'-CH, 5'-CH, half CH ₂ OH, half CH ₂ OH	7.87(d), 5.90(s), 5.92(d), 4.36(t), 4.24(t), 4.14(q), 3.92(dd), 3.81(dd)
valine	α -CH, β -CH, γ -CH ₃ , γ' -CH ₃	3.62(d), 2.28(m), 0.98(d), 1.03(d)

Pair wise comparison of time points across different types of biofluids. O-PLS-DA was used to extract information on specific metabolic changes induced by an *E. caproni* infection over the duration of the study. Changes in urinary, plasma and faecal metabolites are presented in Figures 5.4-5.6 for selected time points and the complete set are summarized in Figure 5.7. Amongst the most significantly changed urinary metabolites were hippurate (decreased at day 33), 2-ketoisocaproate (decreased from day 8 onwards), trimethylamine (TMA; increased at days 8, 12, 19, and 33), taurine (decreased at days 8, 12, and 19), *p*-cresol glucuronide (increased at days 8, 12, 19, and 26), mannitol (increased from day 5 onwards), TMAO (increased at days 8, and 12), phenylacetyl glycine (increased from day 12 onwards), acetate (decreased at days 8, and 19) and creatine (decreased at days 1, 5, 8, and 12). Plasma from infected mice showed changes in the relative concentration of acetate (increased at all time points except day 5), creatine (decreased from day 8 onwards), lipids (increased from day 8 onwards), formate (decreased at days 1, 8, 12, and 19, but increased at day 33), lactate (decreased at days 1, 8, 12, 19, and 26), glucose (increased at days 1, and 33, but decreased at days 12, 19, and 26), glycerophosphorylcholine (GPC; decreased at days 12, 26, and 33), choline (decreased at days 1, 12, 26, and 33) and branched chain amino acids (BCAAs; decreased at days 12, 26, and 33). The changes in stool samples from infected animals included the BCAAs (increased at days 8, and 26), uracil (increased at day 8), butyrate (decreased at days 12, 19, and 26), propionate (decreased at days 12, 19, and 26) and 5-aminovalerate (increased from day 5 onwards).

Analysis of relative concentrations of key metabolites over study duration. Figure 5.8 shows the relative concentration of some of these metabolites both for control (blue) and infected mice (colored according to biofluid). The error bars signify 2 SDs of the mean. According to this 3 x 3 diagram, the selected plasma and urine metabolites showed a more robust pattern of group separation over time when compared to faecal water extracts. Whereas some overlap was observed in the scores plot relating to the faecal water samples, there was a tendency toward increasing discrimination of urinary metabolites with time over the course of an *E. caproni* infection, whereas the discrimination became smaller toward the end of the experiment in the selected plasma metabolites.

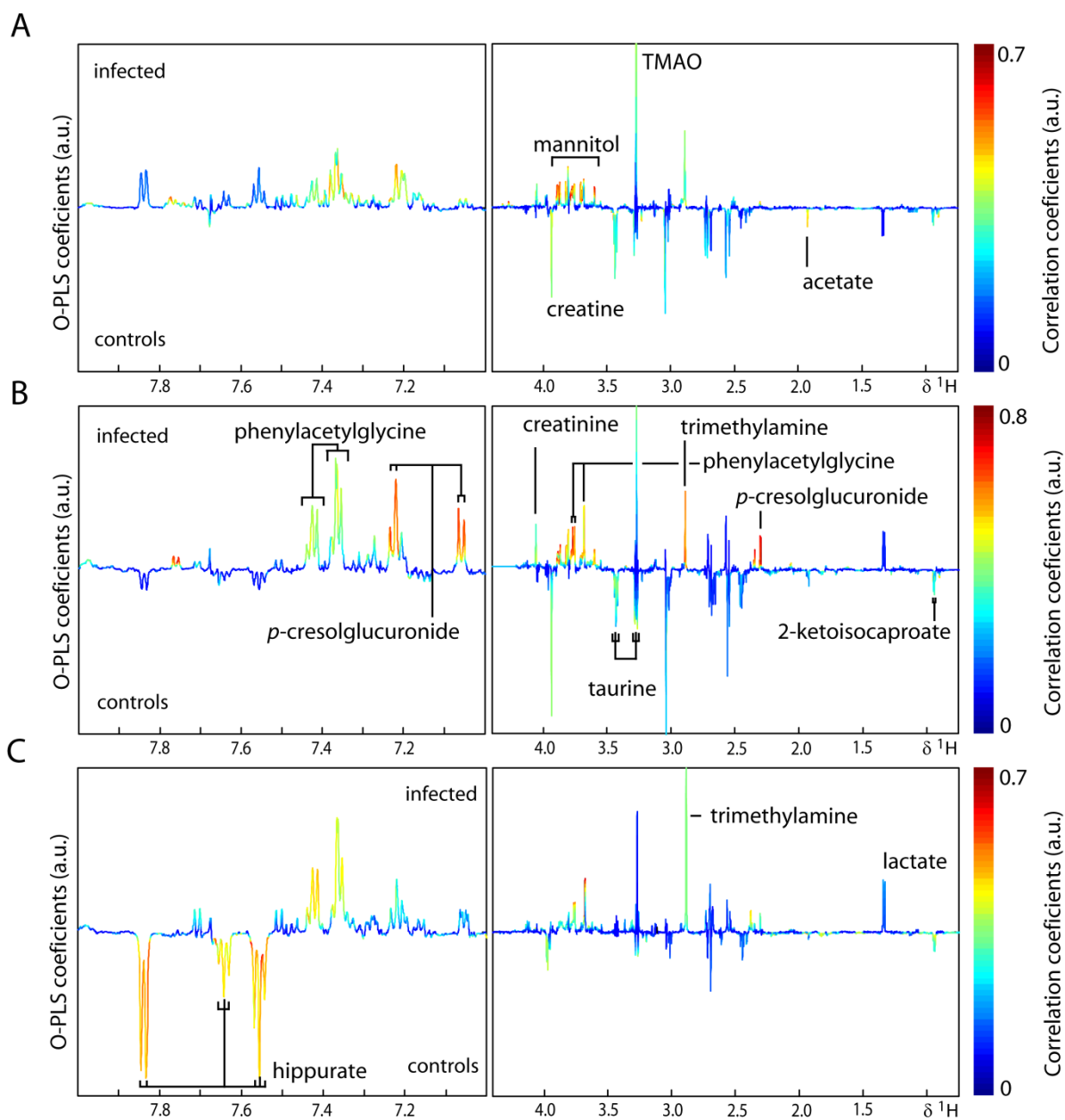


Figure 5.4. O-PLS-DA coefficients plots of urine comparing non-infected control mice (control) with *E. caproni*-infected mice (infected) at 3 different sampling time points, i.e., day 8 (A), day 12 (B), and day 33 (C) post-infection. The color scale indicates the relative contribution of the peak/region to the strength of the differentiation model and the peak intensity is measured relative to the whole peak contribution in arbitrary units (a.u.). Note that the aromatic region (left part) is magnified by a factor 5.

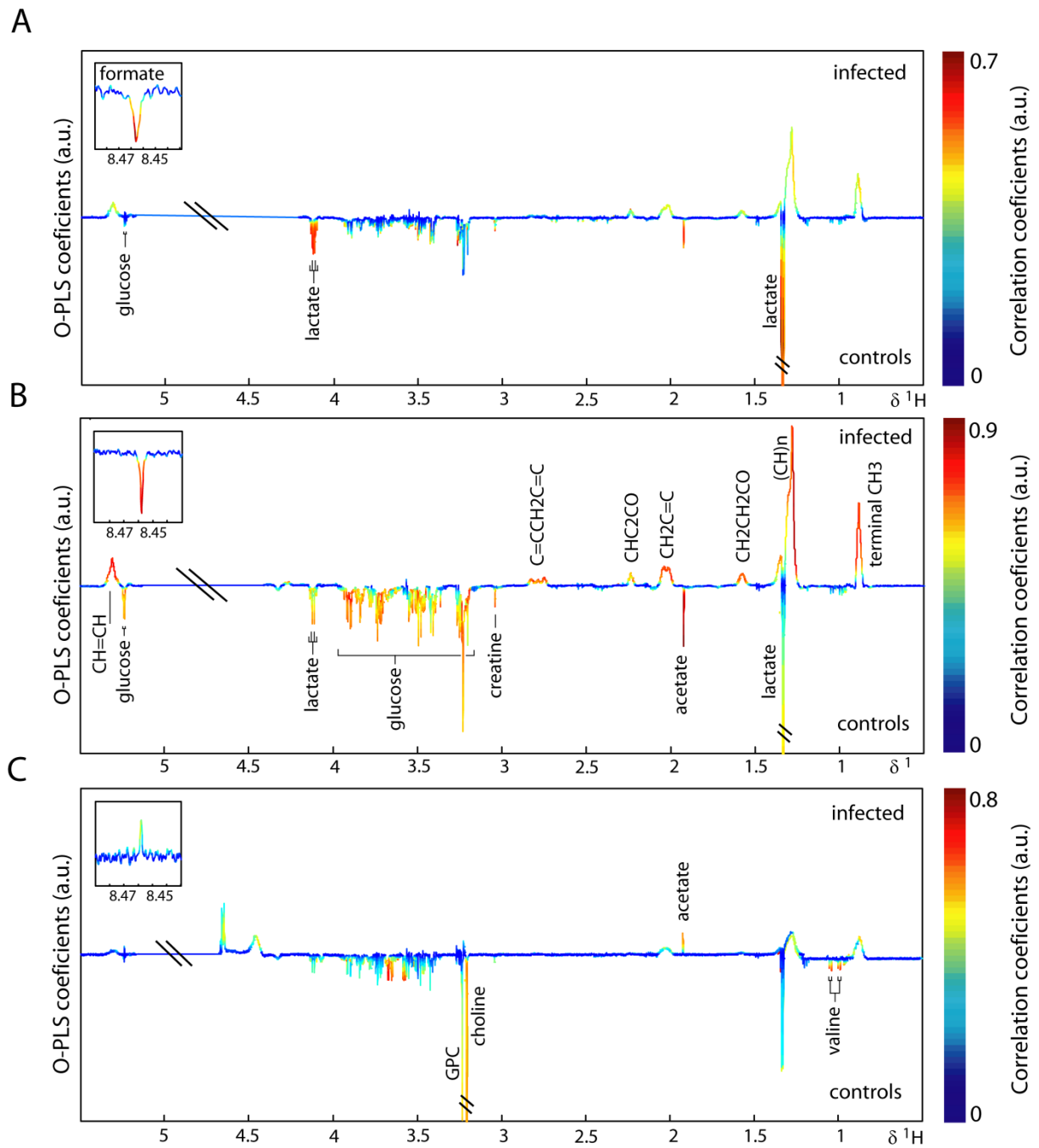


Figure 5.5. Pair-wise comparison *via* O-PLS-DA between non-infected control mice (control) and *E. caproni*-infected mice (infected) at 3 different sampling time points, i.e., day 8 (A), day 12 (B), and day 33 (C) post-infection. The color scale indicates the relative contribution of the peak/region to the strength of the differentiation model and the peak intensity is measured relative to the whole peak contribution in arbitrary units (a.u.). The CPMG spectrum represents small molecular weight components.

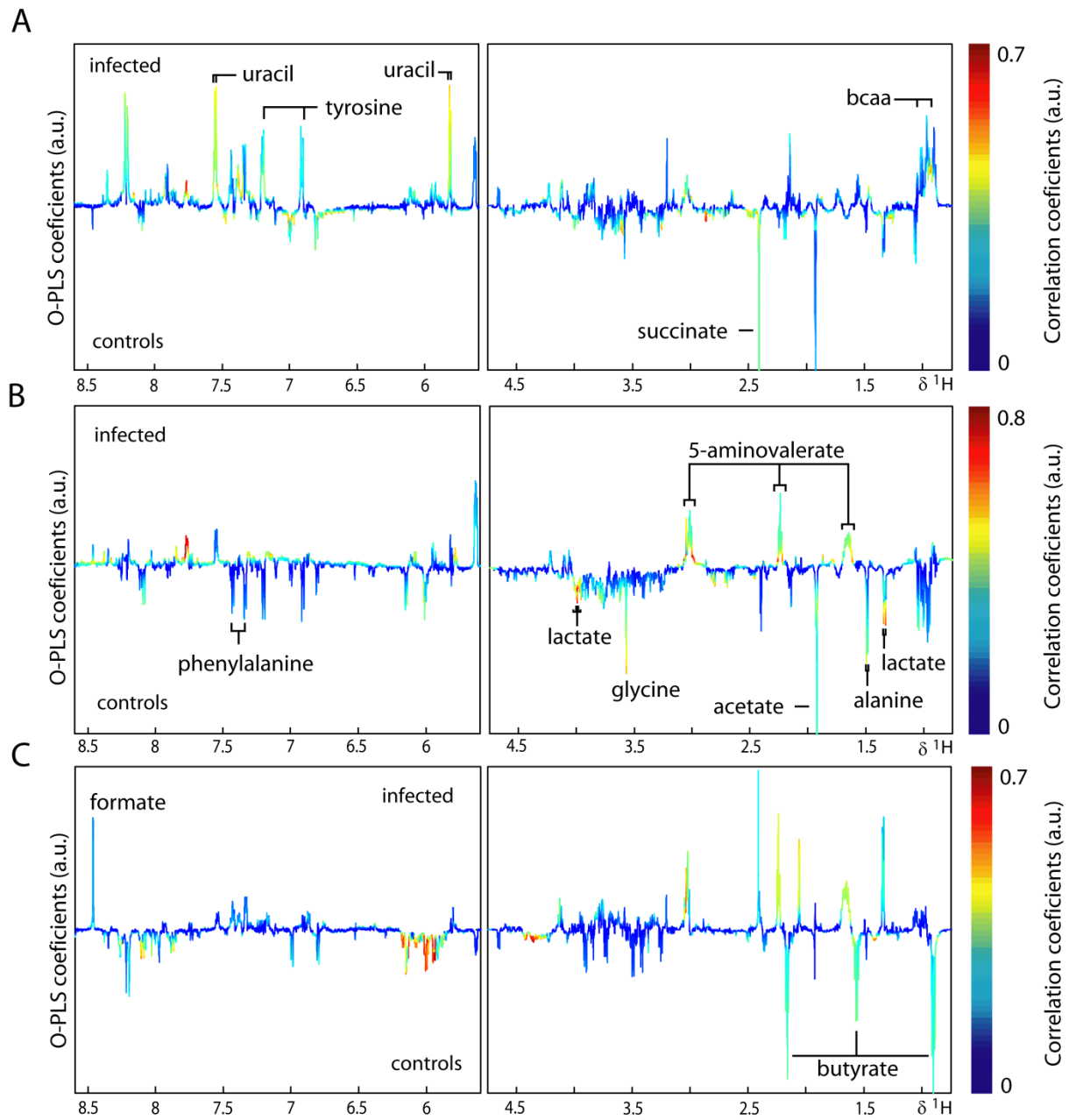


Figure 5.6. O-PLS-DA pair-wise comparison of faecal water comparing non-infected control mice (control) with *E. caproni*-infected mice (infected) at 3 different sampling time points, i.e., day 8 (A), day 12 (B), and day 33 (C) post-infection. The color scale indicates the relative contribution of the peak/region to the strength of the differentiation model and the peak intensity is measured relative to the whole peak contribution in arbitrary units (a.u.). Note that the aromatic region (left part) is magnified by a factor 5.

5.7 Discussion

¹H NMR-based metabolic profiling of biofluids is an established method for deepening our understanding of host-parasite interactions and for investigating disease states in clinical studies [15,19,33]. Sample preparation and spectral acquisition of a biofluid takes little time, and often an overview of the metabolic state of the organism can be obtained by visual assessment of the spectra. Identification of biomarkers from different types of biofluids is similarly convenient, although stool samples need slightly more preparation time and require sonication and an additional centrifugation step, due to the high amount of sediments in the stool-buffer mixture [34].

A number of potential biomarkers for diagnosis of an *E. caproni* infection in the mouse were found here for each of the biofluids employed; 12 in plasma, 10 in urine and 7 in stool. Hence, if for practical purpose, a diagnosis was required based on a single biofluid, either plasma or urine would be the first choice for further development. Stool is the least suitable biological sample not only in terms of a lower number of potential biomarkers, but also because of the more difficult sample preparation, a lower robustness of metabolites (Figures 5.7 and 5.8), and larger inter- and intra-individual variation. The latter issue makes it difficult to determine if the change is related to the actual infection, or results from other factors, e.g., age and/or microbial presence or activity [34]. Although the high degree of individual variation in the faecal metabolite profiles derived from laboratory studies can be overcome with parallel monitoring of metabolic time-related changes in a control group, this issue needs to be addressed in future applications of metabonomics for diagnosis of parasitic infections and disease states, and hence for monitoring disease control programs. If the stability of the urine profiles compared to plasma over the study duration is taken into account, then urine would be the biofluid of choice on which to base a diagnostic. Moreover, urine collection is less invasive than blood collection.

Hence, the systemic movement over time observed in the infected group is most likely to be related to the establishment and progression of the *E. caproni* infection.

In stool and plasma, the time trajectories of the infected animals demonstrated a markedly greater magnitude from the baseline position than the non-infected animals. The greatest differentiation between *E. caproni*-infected mice and non-infected control animals was found in the PC scores plots based on the urine spectral profiles.

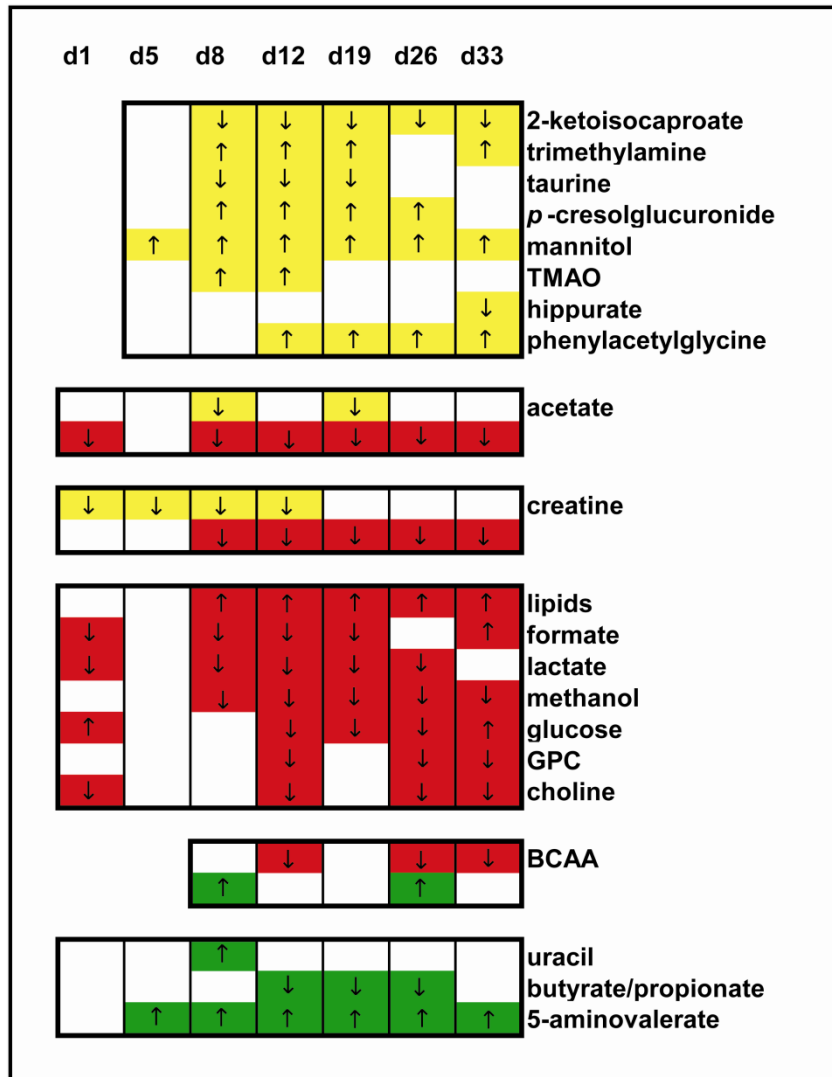


Figure 7. Summary of key *E. caproni* infection-related features for urine (yellow), plasma (red), and faecal water (green). The colored regions show the differences between *E. caproni*-infected mice and non-infected control animals, whereas the changes in direction are indicated by arrows (↑, indicates an increase in the metabolite signal in infected mice with respect to the control group; ↓, indicates a decreased metabolite signal in infected mice).

The smallest differentiation was observed in the stool. From the scale of the PC scores plot axes the trajectory of the infected group occupied a 1.5 and 50 times larger space for stool and plasma, respectively than the non-infected group, whereas in urine, the control trajectory occupied a 10^6 times bigger space, compared to the trajectory of infection. The magnitude of infection-induced metabolic disturbance in the urine profile again clearly points to the greater suitability of urine as a diagnostic biological matrix.

Intestinal re-absorption. The considerable increase in concentration of lipids in the plasma, e.g., fatty acids, triacylglycerols, and lipoproteins, reflects the action of the parasite in the host's gut. In mice harboring a 2-week-old *E. caproni*-infection, an increased breakdown of membrane lipids in the host intestinal tissue has been observed [35], which is consistent with the present findings of a maximum lipid increase on day 12 post-infection [36]. The excretory products of *E. caproni* in the intestinal mucosa are primarily free sterols, triacylglycerols, and free fatty acids [37], but it is unlikely that the amounts excreted by the parasite make a substantial contribution to the host metabolic profile, given that the total parasite mass to host weight ratio is ~1:300.

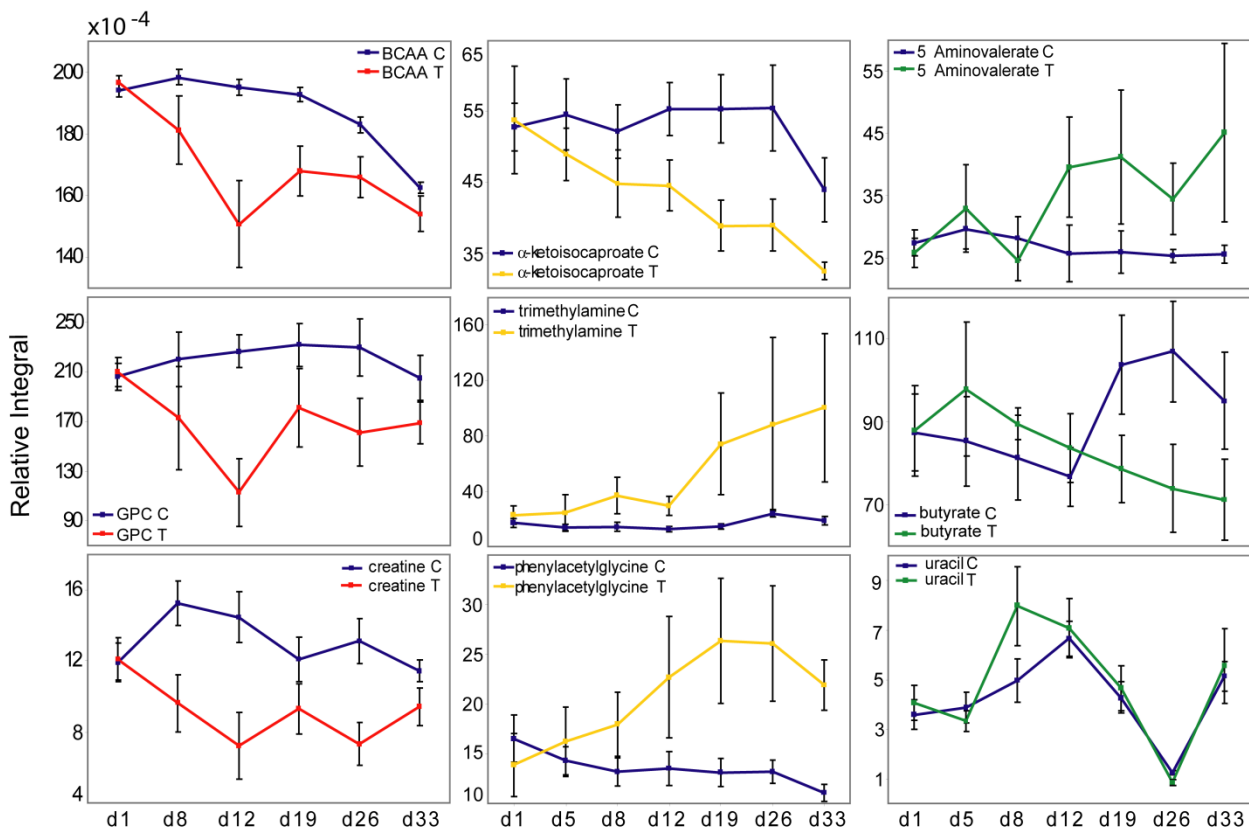


Figure 8. Statistical integration for 3 selected metabolites in the spectra of each of the 3 different types of biofluids (A, urine; B, plasma; C, faecal water). The relative concentration of each of these metabolites is shown for non-infected control mice (blue), and *E. caproni*-infected mice (yellow representing urine, red representing plasma, and green representing faecal water). The error bars signify 2 standard deviations of the mean.

Whilst the simple diffusion of lipid micelles into mucosal cells seems unaffected by the parasite, the Na⁺-dependent active transport of amino acids could be impaired as the increase of the BCAAs in stool and subsequent decrease in plasma suggests. Depletion of the carrier molecules at the brush border of the mucosal cells, or a change of the electrochemical gradient for Na⁺ might explain the selective impact on trans-luminal gut transport [38].

The observed decrease of leucine in plasma, in turn, might induce the significant reduction in levels of 2-ketoisocaproate in urine, which is a transamination product of the former [39]. Taurine is mainly conjugated with cholic acid and chenodeoxycholic acid in the liver to form primary bile salts, and is excreted *via* the urine after deconjugation from the bile salt or it leads into the sulphur- or pyruvate metabolism. Once the taurine conjugated bile salt has transformed the lipids into a micellar form, which is necessary to cross the intestinal wall, taurine is deconjugated by gut bacterial species and reabsorbed into the liver *via* blood circulation [40]. The decreased levels of excreted taurine in the urine of the infected mice may result from the higher demand for increased lipid digestion, resulting from the action of *E. caproni* in the gut.

Gut microbiota. The changes in hippurate, phenylacetyl glycine, *p*-cresol-glucuronide, and TMA in urine, and 5-aminovalerate, and the SCFA levels in stool, are associated with a change in gut microbial presence or activity, as all of these metabolites undergo modification *via* gut microbial species before excretion. For instance, 5-aminovalerate is formed by several different *Clostridium* species which convert ornithine and proline, but to our knowledge, only *C. aminovalericum* degrades 5-aminovalerate further to mainly propionate and acetate [41-43]. This may imply that the presence of *E. caproni* in the gut disturbs the microbial balance resulting in depleted *C. aminovalericum*. The formation of *p*-cresol is likewise known to be performed by a *Clostridium* subspecies (i.e., *C. difficile* and *C. scatologenes*) [44,45], with the bacterium-specific enzyme *p*-hydroxyphenylacetate. It is then conceivable that *p*-cresol is taken up by the bloodstream, bound to serum proteins and glucuronidated in the kidney prior to excretion [46]. Increased excretion of *p*-cresol-glucuronide might be coupled with a higher activity or higher presence of this bacterial strain as the kidney function does not seem to be impaired. PCR analyses on several different *Clostridium* sub-strains are ongoing and will be discussed in forthcoming publications.

The decrease of the SCFAs in stool may also be indicative of an unbalanced microbiota, as dietary carbohydrates (e.g., starches and fibres) are fermented by colonic bacteria to mainly

acetate, propionate, and butyrate. Whilst butyrate serves as main energy source for colonocytes, acetate and propionate pass through the intestinal wall and move *via* peripheral blood to the liver where they have antagonistic functions on the cholesterol synthesis. Whilst the former increases cholesterol synthesis, the latter was shown to act as an inhibitor. The uptake from colon by the blood system is four times higher in the case of acetate, than propionate, which is a possible explanation for depletion of the SCFA, also reflected by the observed decrease in levels of acetate in both urine and plasma [47,48].

The increased concentration of TMA and phenylacetylglucine, and the decrease of hippurate in urine, observed at the later time points of our experiment, are concomitant phenomena of the changed gut microbiota [49,50]. Trimethylammonium compounds like choline and carnitine, which are ingested in the normal diet, are degraded by intestinal bacteria to TMA, and then oxidized in the liver to TMAO in a second step [51,52]. A microbial shift toward choline degrading bacteria might explain the choline/GPC depletion in plasma and the subsequent increase of TMAO in urine.

Specificity of biomarkers for diagnosis. An infection with *E. caproni* induces changes in the concentration of a range of metabolites in urine, plasma, and stool. To be useful as a ‘real’ biomarker, the candidate must be reproducible, robust, specific and, ideally, easy to measure [53]. From the current analyses an anomalous increase in urinary mannitol was noted in infected animals. Mannitol is likely to derive from the diet, since it is not synthesized by vertebrates. However, the higher amounts of urinary mannitol in *E. caproni*-infected mice, reflect the higher intestinal permeability, compared to the control group [54].

To assess the specificity of the biomarkers identified for potential diagnosis of infection, the obtained *E. caproni* fingerprint was compared to altered metabolite patterns, associated with other parasite-rodent models [16-18]. Interestingly, *E. caproni* seems to alter the gut microbiota in a similar way to the biologically-related blood flukes, i.e., *S. mansoni* [16], and *S. japonicum* [17]. Hippurate, phenylacetylglucine, and TMA are modified by several gut microbial species before excretion in urine. In the 3 disease models, hippurate was found to decrease significantly, whereas phenylacetylglucine, *p*-cresol-glucuronide and TMA showed increased levels in infections with all 3 parasites, which suggests a common trematode-inherent influence on gut microbial composition. The change in 2-ketoisocaproate in urine was unique to the infection with *E. caproni* and 5-aminovalerate in stool may also deliver an *E. caproni*-specific marker but, at the time being, cannot be compared to other disease

models, as the metabonomic assessment of stool was applied only in the present parasite-rodent model. The metabolic effect of a nematode infection (*T. spiralis*) in NIH Swiss mice has also been reported by Martin and colleagues [18]. *T. spiralis* has a similar initial mechanism of pathogenicity and also induces a state of inflammation of the gut before it migrates from the intestine to muscle tissue and induces hypercontractility [55]. While comparison between the study conducted by Martin *et al.* [18] and the current study revealed a number of biomarkers, which were the same in both models, the directionality of these metabolites was different. For example, a decrease in choline and creatine concentrations was observed in *E. caproni*-infected mice, whereas the same metabolites were reported to be increased in *T. spiralis*-infected mice compared to non-infected controls. Furthermore, the lipids (e.g., triacylglycerides, saturated and unsaturated fatty acids) which undergo a marked increase in *E. caproni*-infected animals, showed a significant decrease in the mice infected with *T. spiralis*.

Future studies evaluating additional laboratory host-parasite models, and applying complementary metabolic profiling methods, such as ultra performance liquid chromatography (UPLC), in combination with mass spectrometry (MS), will help to confirm the specificity of the metabolic perturbations associated with an *E. caproni* infection. In conclusion, we have shown that metabolic profiling of plasma, urine, and stool delivers a comprehensive fingerprint of an *E. caproni* infection, composed of general as well as highly specific biomarkers (e.g., 2-ketoisocaproate and 5-aminovalerate). Keeping in mind the long-term objective of developing novel diagnostic assays for trematode-borne diseases, one would emphasise the value of further development, particularly based on the urine profiles.

5.8 Acknowledgments

The authors thank Dr. Olivier Cloarec for providing the MATLAB script for O-PLS-DA and STOCSY analysis and Mr. Kirill Veselkov for giving access to his peak alignment and normalization script in MATLAB.

5.9 Author Contributions

Conceived and designed the experiments: JK, EH, and JU. Performed the experiments: JS, JVL, YW, JK, and JU. Analyzed the data: JS, YW, and JGB. Wrote the paper: JS, JK, EH, and JU.

5.10 References

1. Keiser J, Utzinger J (2005) Emerging foodborne trematodiasis. *Emerg Infect Dis* 11: 1507-1514.
2. Keiser J, Utzinger J (2007) Food borne trematodiasis. Current chemotherapy and advances with artemisins and synthetic trioxolans. *Trends Parasitol* 23: 555-562.
3. Halswell-Elkins M, Levri E (2003) Food borne trematodes. In: Manson's Tropical Diseases (21st edn.). Cook GC, Zumla AI, eds. Saunders, London, pp 1471-1486.
4. Fried B, Graczyk TK, Tamang L (2004) Food-borne intestinal trematodiasis in humans. *Parasitol Res* 93: 159-170.
5. Toledo R, Fried B (2005) Echinostomiasis experimental models for interactions between adult parasites and vertebrate hosts. *Trends Parasitol* 21:251-254.
6. Weistein MS, Fried B (1991) The expulsion of *Echinostoma trivolvis* and retention of *Echinostoma caproni* in the ICR mouse: pathological effects. *Int J Parasitol* 21: 255-257.
7. Graczyk TK, Fried B (1998) Echinostomiasis: a common but forgotten food-borne disease. *Am J Trop Med Hyg* 58: 501-504.
8. O'Neill SM, Parkinson M, Strauss W, Angles R, Dalton JP (1998) Immunodiagnosis of *Fasciola hepatica* infection (fascioliasis) in a human population in the Bolivian Altiplano using purified cathepsin L cysteine proteinase. *Am J Trop Med Hyg* 58: 417-423.
9. Le TH, Van DN, Blair D, Sithithaworn P, McManus DP (2006) *Clonorchis sinensis* and *Opisthorchis viverrini*: development of a mitochondrial-based multiplex PCR for their identification and discrimination. *Exp Parasitol* 112:109-114.
10. Fried B, Eyster LS, Pechenik JA (1998) Histochemical glycogen and neutral lipid in *Echinostoma trivolvis* cercariae and effects of exogenous glucose on cercarial longevity. *J Helminthol* 72: 83-85.
11. Keiser J, Xiao SH, Utzinger J (2006) Effect of tribendimidine on adult *Echinostoma caproni* harboured in mice, including scanning electron microscopic observations. *J Parasitol* 92:858-862.

12. Keiser J, Brun R, Fried B, Utzinger J (2006) Trematocidal activity of praziquantel and artemisinin derivatives: in vitro and in vivo investigations with adult *Echinostoma caproni*. *Antimicrob Agents Chemother* 50:803-805.
13. Ordovas JM, Mooser V (2006) Metagenomics: the role of the microbiome in cardiovascular diseases. *Curr Opin Lipidol* 17: 157-161.
14. Holmes E, Tsang TM, Huang JT, Leweke FM, Koethe D, et al. (2006) Metabolic profiling of CSF: evidence that early intervention may impact on disease progression and outcome in schizophrenia. *PLoS Med* 3: e327.
doi:10.1371/journal.pmed.0030327.
15. Nicholson JK, Lindon JC, Holmes E (1999) 'Metabonomics': understanding the metabolic responses of living systems to pathophysiological stimuli *via* multivariate statistical analysis of biological NMR spectroscopic data. *Xenobiotica* 29:1181-1189.
16. Wang YL, Holmes E, Nicholson JK, Cloarec O, Chollet J, et al. (2004) Metabonomic investigations in mice infected with *Schistosoma mansoni*: an approach for biomarker identification. *Proc Natl Acad Sci USA* 101: 12676-12681.
17. Wang YL, Utzinger J, Xiao SH, Xue J, Nicholson JK, et al. (2006) System level metabolic effects of a *Schistosoma japonicum* infection in the Syrian hamster. *Mol Biochem parasitol* 146: 1-9.
18. Martin FPJ, Verdu EF, Wang YL, Dumas ME, Yap IKS, et al. (2006) Transgenomic metabolic interactions of *Trichinella spiralis* infection with dietary *Lactobacillus paracasei* supplementation. *J Proteome Res* 5: 2185-2193
19. Wang YL, Utzinger J, Saric J, Li JV, Burckhard J, et al. (2008) Global metabolic responses of mice to *Trypanosoma brucei brucei* infection. *Proc Natl Acad Sci USA* 105: 6127-6132.
20. Huffman JE, Fried B (1990) *Echinostoma* and echinostomiasis. *Adv Parasitol* 29: 215-269.
21. Wu D, Chen AD, Johnson CS (1995) DOSY processing – introduction and implementation. *J Magn Reson* 115: 260-264.
22. Nicholson JK, Foxall PJD, Spraul M, Farrant RD, Lindon JC (1995) 750 MHz ^1H and ^1H - ^{13}C NMR spectroscopy of human blood plasma. *Anal Chem* 67: 793-811.

23. Foxall PJD, Spraul M, Farrant RD, Lindon LC, Neild GH, et al. (1993) 750 MHz ^1H -NMR spectroscopy of human blood plasma. *J Pharm Biomed Anal* 11: 267-276.
24. Lenz EM, Bright J, Wilson ID, Morgan SR, Nash AF (2003) A ^1H NMR-based metabonomic study of urine and plasma samples obtained from healthy human subjects. *J Pharm Biomed Anal* 33: 1103-1115.
25. Tang H, Wang Y, Nicholson JK, Lindon JC (2004) Use of relaxation-edited one-dimensional and two dimensional nuclear magnetic resonance spectroscopy to improve detection of small metabolites in blood plasma. *Anal Biochem* 325: 260-272.
26. Cloarec O, Dumas ME, Craig A, Barton RH, Trygg J, et al. (2005) Statistical total correlation spectroscopy: an exploratory approach for latent biomarker identification from metabolic ^1H NMR data sets. *Anal Chem* 77: 1282-1289.
27. Hurd RE (1990) Gradient-enhanced spectroscopy. *J Magn Reson* 87: 422-428.
28. Bax A, Davis DG (1985) Mlev-17-based two-dimensional mononuclear magnetization transfer spectroscopy. *J Magn Reson* 65: 355-360.
29. Eriksson L, Johansson E, Kettaneh-Wold N, Trygg J, Wikstrom C, et al. (2001) Multi and megavariate data analysis. Umetrics Academy.
30. Trygg J (2002) O2-PLS for qualitative and quantitative analysis in multivariate calibration. *J Chemom* 16: 283-293.
31. Crockford DJ, Keun HC, Smith LM, Holmes E, Nicholson JK (2005) Curve-fitting method for direct quantitation of compounds in complex biological mixtures using ^1H NMR: application in metabonomic toxicology studies. *Anal Chem* 77: 4556-4562.
32. Salek RM, Maguire ML, Bentley E, Rubtsov DV, Hough T, et al. (2007) A metabolomic comparison of urinary changes in type 2 diabetes in mouse, rat and human. *Physiol Genomics* 29: 99-108.
33. Barton RH, Nicholson JK, Elliott P, Holmes E (2008) High-throughput ^1H NMR-based metabolic analysis of human serum and urine for large-scale epidemiological studies: validation study. *Int J Epidemiol* 37 (Suppl. 1): i31-40.
34. Saric J, Wang YL, Li J, Coen M, Utzinger J, et al. (2008) Species variation in the faecal metabolome gives insight into differential gastrointestinal function. *J Proteome Res* 7: 352-360.

35. Horutz K, Fried B (1995) Effects of *Echinostoma caproni* infection on the neutral lipid content of the intestinal mucosa of ICR mice. *Int J Parasitol* 25: 653-655.
36. Bandstra SR, Fried B, Sherma J (2006) High performance thin-layer chromatographic analysis of neutral lipids and phospholipids in *Biomphalaria glabrata* patently infected with *Echinostoma caproni*. *Parasitol Res* 99: 414-418.
37. Schneck JL, Fried B, Sherma J (2004) Effects of tonicity on the release of neutral lipids in *Echinostoma caproni* adults and observations on lipids in excysted metacercariae. *Parasitol Res* 92: 285-288.
38. Thwaites DT, Anderson CM (2007) H⁺-coupled nutrient, micronutrient and drug transporters in the mammalian small intestine. *Exp Physiol* 92: 603-619.
39. Mitch WE, Chan W (1979) α -Ketoisocaproate stimulates branched-chain amino acid transaminase in kidney and muscle. *Am J Physiol* 236: E514-E518.
40. Bender DA (2002) Introduction to nutrition and metabolism. Taylor & Francis Ltd.
41. Ramsay IR, Pullammanappallil PC (2001) Protein degradation during anaerobic wastewater treatment: derivation of stoichiometry. *Biodegradation* 12: 247-257.
42. Barker HA, D'Ari L, Kahn J (1987) Enzymatic reactions in the degradation of 5-aminovalerate by *Clostridium aminovalericum*. *J Biol Chem* 262: 8994-9003.
43. Hardman JK, Stadtman TC (1960) Metabolism of omega-acids. II. Fermentation of delta-aminovaleric acid by *Clostridium aminovalericum* n. sp. *J Bacteriol* 79: 549-552.
44. Selmer T, Andrei PI, (2001) *p*-Hydroxyphenylacetate decarboxylase from *Clostridium difficile*. A novel glyceryl radical enzyme catalysing the formation of *p*-cresol. *Eur J Biochem* 268:1363-1372.
45. Yu L, Blaser M, Andrei PI, Pierik AJ, Selmer T (2006) 4-Hydroxyphenylacetate decarboxylases: properties of a novel subclass of glyceryl radical enzyme systems. *Biochemistry* 45: 9584-9592.
46. Lesaffer G, De SR, Belpaire FM, Van VB, Van HM, et al. (2003) Urinary excretion of the uraemic toxin *p*-cresol in the rat: contribution of glucuronidation to its metabolization. *Nephrol Dial Transplant* 18:1299-1306.
47. Wong JMW, de Souza R, Kendall CWC, Emam A, Jenkins DJA (2006) Colonic health: fermentation and short chain fatty acids. *J Clin Gastroenterol* 40: 235-243.

48. Cook SI, Sellin JH (1998) Short chain fatty acids in health and disease. *Aliment Pharmacol Ther* 12: 499-507.
49. Nicholls AW, Mortishire-Smith RJ, Nicholson JK (2003) NMR spectroscopic-based metabonomic studies of urinary metabolic variation in acclimatizing germ free rats. *Chem Res Toxicol* 16: 1395-1404.
50. Williams RE, Eyton-Jones HW, Farnworth MJ, Gallagher R, Provan WM (2002) Effect of intestinal microflora on the urinary metabolic profile of rats: a ¹H-nuclear magnetic resonance spectroscopic study. *Xenobiotica* 32: 783-794.
51. Seibel BA, Walsh PJ, (2002) Trimethylamine oxide accumulation in marine animals: relationship to acylglycerol storage. *J Exp Biol* 205: 297-306.
52. Smith JL, Wishnok JS, Deen WM (1994) Metabolism and excretion of methylamines in rats. *Toxicol Appl Pharmacol* 125: 296-308.
53. Bonassi S, Neri M, Puntoni R (2001) Validation of biomarkers as early predictors of disease. *Mutat Res* 480-481: 349-358.
54. Feld JJ, Meddings J, Heathcote EJ (2006) Abnormal intestinal permeability in primary biliary cirrhosis. *Dig Dis Sci* 51: 1607-1613.
55. Barbara G, Vallance BA, Collins SM (1997) Persistent intestinal neuromuscular dysfunction after acute nematode infection in mice. *Gastroenterology* 113: 1224-1232.





6 Trematode-induced modulation of CNS metabolic profiles

Jasmina Saric^{1,2}, Jia V Li^{1,2}, Yulan Wang^{2,‡}, Jennifer Keiser³, Olaf Beckonert², Jürg Utzinger¹, Jeremy K Nicholson² and Elaine Holmes^{2,*}

1 Department of Public Health and Epidemiology, Swiss Tropical Institute, Basel, Switzerland

2 Department of Biomolecular Medicine, Division of Surgery, Oncology, Reproductive Biology and Anaesthetics (SORA), Faculty of Medicine, Imperial College London, London, United Kingdom

3 Department of Medical Parasitology and Infection Biology, Swiss Tropical Institute, Basel, Switzerland

***Corresponding Author:** Professor Elaine Holmes, Department of Biomolecular Medicine, Division of Surgery, Oncology, Reproductive Biology and Anaesthetics (SORA), Faculty of Medicine, Imperial College London, Sir Alexander Fleming Building, South Kensington, London SW7 2AZ, United Kingdom. Tel.: +44 20 7594-3220; Fax: +44 20 7594-3226. E-mail: elaine.holmes@imperial.ac.uk.

‡ Present Address: State Key Laboratory of Magnetic Resonance and Atomic and Molecular Physics, Wuhan Centre for Magnetic Resonance, Wuhan Institute of Physics and Mathematics, Wuhan, People's Republic of China

*Corresponding author:

This article has been submitted to

PLoS Pathogens **2008**

6.1 Abstract

Metabolic effects of three distinct trematode infections, namely *Schistosoma mansoni* and *Echinostoma caproni* in mouse and *Fasciola hepatica* in the rat brain were investigated using ^1H NMR spectroscopy. Twelve rodents were infected with each parasite e.g. 80 *S. mansoni* cercariae in the mouse host (n=12); 30 *E. caproni* metacercariae in the mouse (n=12); 20-25 *F. hepatica* metacercariae in the rat (n=12) and brain samples were obtained at a timepoint where chronic infection had established. Aqueous extracts of the brain were analysed by ^1H NMR spectroscopy coupled with multivariate statistical analysis and compared to brain extracts from corresponding uninfected animals.

Distinct trematode-induced effects on the metabolic profile of the brains of mice and rats infected with *S. mansoni* and *F. hepatica*, respectively, were observed, whereas an *E. caproni* infection did not result in any perturbation of the biochemical profile of the mouse brain. Metabolic changes, induced by *S. mansoni*-infected mice included increased glutamate and decreased γ -aminobutyric acid (GABA) and phosphocholine. These changes were different to the metabolic signature induced by *F. hepatica*, which was characterised by perturbation of the nucleotide balance, e.g. increased levels of inosine and decreased concentrations of adenosine and phosphorylated species of both. Together with the observation of increased plasma levels of IL5 and IL13, and decreased IFN γ suggests modulation of immune reactions towards lowered inflammatory response, which may infer some degree of protection for the parasite. Increased phenylalanine and tyrosine levels were also features of the *F. hepatica*-infected rats possibly reflecting the liver pathology induced by fascioliasis. These findings may contribute to elucidating the mechanism of how a trematode infection impacts on the central nervous system, and warrant further investigations on the impact of parasitic infections on the host brain.

Keywords: brain; *Echinostoma caproni*; *Fasciola hepatica*; inosine; metabonomics; mouse; NMR spectroscopy; rat; *Schistosoma mansoni*; trematode

6.2 Introduction

Trematode infections belong to the neglected tropical diseases and exert a heavy burden on population health and economy in Sub-Saharan Africa and South-East Asia. There is a pressing need to investigate the mechanisms of infection pathology and behaviour to improve surveillance and parasite control. Although the main trematode species share a similar basic physiology, their niches within the mammalian hosts are diverse, as are their pathologic mechanisms¹⁻³. However, many trematode infections have been reported to invoke a response in the central nervous system (CNS) and even to change host behaviour⁴⁻⁷.

The direct contact of a human trematode parasite with the compartments of the CNS can result in overt pathological and biochemical changes. Eggs, secreted by the blood fluke *Schistosoma*, for example, can reach the CNS and cause inflammation in the spinal cord or brain⁸. Serendipitous ectopic worm manifestations in the brain by *Paragonimus westermani*⁹, or *Fasciola hepatica*¹⁰ have also been reported to cause lesions and haemorrhages. However, for most host-parasite interactions, the molecular mechanisms of neurological damage or altered behaviour are less direct and poorly understood.

A series of metabolic profiling experiments employing different host-parasite models, have characterised the direct biochemical consequences of parasite-induced changes in host biofluids (e.g. blood plasma, fecal water and urine) and target tissues (e.g. intestinal tissues, kidney, liver, spleen)¹¹⁻¹⁶. Within the framework of these investigations, we have established three trematode-rodent models, i.e. the blood fluke *Schistosoma mansoni* in the mouse^{11, 17}, the intestinal fluke *Echinostoma caproni* in the mouse¹⁴ and the liver fluke *Fasciola hepatica* in the rat. Here, we extend these investigations by assessing whether any of these trematode infections not only have direct biochemical impact on target tissue but also more remote effects on the host CNS. We compare the metabolic effects across these three phylogenetically similar trematodes, with topographically different locations. It is widely acknowledged that *S. mansoni* causes liver pathology¹⁸, but eggs deposited in the CNS may also cause changes in brain metabolism of the host⁸. While *F. hepatica* induces liver damage prior to settling in the bile ducts¹⁹, to our knowledge, no direct association with the CNS are reported in the extant literature. Since the existence of a bidirectional communication between brain and gut *via* the blood brain barrier interface has been described previously^{20, 21} we also selected an intestinal trematode, e.g. *E. caproni*, for investigation. All infections were

patent prior to removal of the brains of the host animals were removed for subsequent metabolic assessment. Here we implement a multilevel statistical approach combined with ^1H nuclear magnetic resonance (NMR) spectroscopy²⁰⁻²⁵ to obtain an integrative profile of the CNS response of the rodent host to three trematodes, based on differential metabolite, immunological and biometric responses.

6.3 Materials and methods

Animal experiments and trematode-rodent models. All experiments were carried out at the Swiss Tropical Institute (STI; Basel, Switzerland), adhering to local and national guidelines of animal welfare (permission no. 2070 and 2081). Mice and rats were kept under environmentally-controlled conditions (temperature, 22°C; relative humidity, 60-70%; light/dark cycle, 12/12 hours) and had free access to commercially available rodent diet obtained from Nafag (Gossau, Switzerland) and water. Prior to the experiments, all animals were acclimatized for 1-2 weeks.

With regard to the *S. mansoni*-mouse model, 20 female outbred NMRI strain mice (age: ~3 weeks; weight: 20-25 g) were purchased from RCC (Füllinsdorf, Switzerland). Mice were individually marked and group-housed in sizes of 5 animals per cage. Half of the mice were infected subcutaneously with ~80 *S. mansoni* cercariae. We used a Liberian strain of *S. mansoni*, which has been passaged through *Biomphalaria glabrata* (intermediate host snail) and hamster (definitive host) at STI over the past 20 years (Wang et al. 2004, PNAS). The other 10 mice remained uninfected, serving as the control group. Infected mice were sacrificed by cervical dislocation on day 74 post-infection. Uninfected control mice were killed at the same time point.

For the *E. caproni*-mouse model, 24 female outbred NMRI strain mice were obtained from RCC, individually marked and group-housed in sizes of 4 animals per cage. Half of the mice were orally infected with 30 *E. caproni* metacercariae each, after removal from the kidney-pericardial region of infected *B. glabrata* as described before (Keiser et al. 2006, Journal of Antimicrobial Chemotherapy). The remaining mice were left uninfected and served as controls. All mice were euthanised using CO₂ 35 days post-infection and at the same time point for the uninfected control mice,

With regard to the *F. hepatica*-rat model, a total of 24 Wistar female rats, were purchased from RCC. Rats were individually marked and group-housed in sizes of 4 animals per cage. Twelve rats were orally infected with 30 *F. hepatica* metacercariae (Cullompton isolate) obtained from Mr. G. Graham (Addleston, UK). The remaining 12 rats were left uninfected and served as the control group. Rats were killed using CO₂ on day 77 post -infection and at the same time point for the uninfected control rats.

The whole brains of all mice and rats regardless of their infection status were removed upon dissection and the left hemispheres were transferred into cryo-tubes, snap frozen in liquid nitrogen and stored at -80°C pending ¹H NMR spectroscopic data acquisition.

Brain extraction. Each brain sample collected from mice infected with *E. caproni* and rats infected with *F. hepatica* (and from the corresponding uninfected control animals) was placed in a mortar, mashed using a 1 ml mixture of H₂O and acetonitrile (1:1, v:v) and transferred into a glass tube. Another 2 ml of this mixture was used to rinse the mortar twice with the solution and also transferred into the same glass tube. The resulting mixture was centrifuged for 6 min at 10,000 g. The supernatant was collected into a new glass vial, evaporated over night and lyophilized. The dry mass was resuspended into 600 µl of D₂O and transferred into 5 mm-diameter NMR tube for subsequent analyses.

The extraction protocol for the *S. mansoni*-mouse model was slightly extended, in order to gain additional information regarding potential changes in the lipid metabolic profile, as a pharmacological intervention was involved in the original study protocol. Each brain sample obtained from mice infected with *S. mansoni* and the corresponding control mice was transferred into a 2 ml Eppendorf tube containing a metal bead, 0.75 ml of water and 0.75 ml of methanol. The Eppendorf tube was placed in the tissue lyser and shaken for 5 min at the speed of 22 Hz. The resulting homogenate was transferred into a glass tube. A further 0.75 ml of each liquid was used to rinse the Eppendorf tube and transferred into the same glass tube. A total of 1.5 ml of chloroform was added into the mixture and centrifuged at 2,500 g for 30 min. The aqueous and the chloroform phases were transferred into a new glass tube each and both were left to evaporate over night and lyophilized. Prior to ¹H NMR analysis, the powder obtained from the aqueous phase was dissolved in 550 µl phosphate buffer (D₂O:H₂O=9:1, v:v, 0.01% of sodium 3-(trimethylsilyl) propionate-2,2,3,3-*d*₄ [TSP], pH=7.4), whereas the dry mass of the chloroform fraction was dissolved in deuterated chloroform (CDCl₃).

Acquisition of NMR spectral data. All ^1H NMR spectra from mouse and rat brain extracts were recorded on a Bruker Avance 600 NMR spectrometer (Bruker; Rheinstetten, Germany), operating at 600.13 MHz for proton frequency. A 5 mm triple resonance probe with inverse detection was used (Bruker), employing a standard 1-dimensional (1D) NMR experiment with pulse sequence [recycle delay (RD)- 90° - t_1 - 90° - t_m - 90° -ACQ]. Optimal water suppression was achieved by irradiating the water frequency during the RD set to 2 s. The 90° pulse length was adjusted to 10.62 μs for the brain extracts of both the *E. caproni*-mouse and the *F. hepatica*-rat models and 13.5 μs for the *S. mansoni*-mouse model. A total of 128 numbers of scans were acquired for all three models into 32 K data points for each spectrum employing a spectral width of 20 ppm. All free induction decays (FIDs) were multiplied by an exponential function equivalent to a 0.3 Hz line-broadening factor prior to Fourier transformation.

Assignments of the spectral peaks were made from the literature²⁶ and confirmed *via* statistical total correlation spectroscopy (STOCSY)²⁷, or *via* standard 2-dimensional (2D) NMR experiments conducted on selected samples, including correlation spectroscopy (COSY)²⁸, total correlation spectroscopy (TOCSY)²⁹, and J-resolved NMR spectra³⁰. High-performance liquid chromatography (HPLC) was performed in order to separate the brain extract fractions and gain additional information about the previously unknown spectral regions at chemical shifts of δ 6.15 (doublet), δ 8.6 (singlet), δ 8.27 (singlet) and δ 4.02 (multiplet). For this purpose, fractions were separated using an Agilent 1100 HPLC with Eclipse XDB-C18 column, 5 μm , 4.6x150 mm (Agilent, USA), attached to an Esquire 6000 mass spectrometer (MS; Bruker Rheinstetten Germany). An aliquot of 100 μl of brain extract was injected at a flow rate of 1 ml/min and signals were detected by UV at 214nm and by MS in positive mode. A gradient of 98% water to 2% acetonitrile was used for the first 25 min and a standard gradient sequence was applied for the remaining 25 minutes. Fractions were collected over the first 8 min and then lyophilized and resuspended in D_2O for NMR analysis. Inosine, inosine-monophosphate, inosine-diphosphate, inosine-triphosphate, adenosine, adenosine-monophosphate, adenosine-diphosphate and adenosine-triphosphate were confirmed by adding authentic standards purchased from Sigma Aldrich (Gillingham, Dorset, UK).

Data processing and analysis. The raw spectra were corrected with an in-house developed MATLAB script in order to reduce phase and baseline distortions and manually calibrated to the lactate CH_3 signal at δ 1.33 ppm. Although water saturation was efficient, the region

containing the water resonance was removed to avoid any interference with the analysis (i.e., δ 4.65-5.08 in brain extracts in the *E. caproni*-mouse model, δ 4.55-5.40 in brain extracts in the *F. hepatica*-rat model, and δ 4.71-4.90 in the brain extracts in the *S. mansoni*-mouse model). Finally, all spectra were normalized over the total sum of the remaining spectral area.

In an initial stage, principal components analysis (PCA) was applied to the processed spectral data in order to gain an overview of the degree of differentiation or grouping in each parasite-rodent model³¹ between infected and uninfected control animals. PCA reduces the multivariate data to a lower-dimensionality scores plot, without requiring any prior class information and delivers a snapshot of the similarity between observations e.g. brain spectral data, based on the sum of the spectral components. In a second step, projection to latent structure discriminant analysis (PLS-DA) was applied, as a supervised method, which utilizes prior information of class membership and hence optimizes separation³².

Orthogonal (O)-PLS-DA is a further development of PLS-DA applied for optimal recovery of biomarkers³², and removes systematic variation unrelated to infection status *via* an orthogonal filter. The O-PLS-DA model was built by a X-matrix containing all spectral information and a binary dummy matrix, as Y-determining class affiliation. Sevenfold cross validation was applied³³ in order to limit over fitting of the models. The color code in the resulting coefficient plot indicates the strength of association of each data point or signal with differentiation due to infection.

Cytokine multiplex quantification. Plasma from *F. hepatica* infected rats and uninfected control rats from previous spectral preparation (e.g. saline D2O:H2O=1:1), over six different timepoints from 5 individuals each were tested by Mesoscale multiplex assay (MS6000 Rat Demonstration 7-Plex Ultra-Sensitive Kit, Mesoscale Discovery). The rat demonstration 7-Plex Ultra-Sensitivity Kit was used for this purpose which includes IFN- γ , IL-1 β , IL-4, IL-5, IL-13, KC/GRO and TNF- α . Each sample was assessed in duplicates and split in 15 μ l per well in a 96 well plate. The incubation time was extended to 4 hours in order to counteract the 1:1 dilution. The rest of the protocol was followed according to the manufacturer's specifications. A MSD Sector imager was utilized to read the plates. For the *S. mansoni* cytokine assessment, 5 plasma samples were chosen from infected and control animals each and treated the same way as described above. A 96-well multi-spot plate of T_H1/T_H2 cytokines (MS2400 Mouse TH1/TH2 9-Plex Tissue Culture Kit) including TNF- α , MKC, IL-5, IL-4, IL-2, IL-1 β , IL-12, IL-10 and IFN- γ , was selected for the mouse samples.

Table 6.1. List of metabolites found in brain metabolic spectra of female NMRI mice and Wistar rats.

Metabolite	Chemical moiety	Chemical shift in ppm and multiplicity
3-hydroxybutyrate	half α -CH ₂ , half α -CH ₂ , β -CH, γ -CH ₃	2.32(m), 2.42(m), 4.16(tqa), 1.21(d)
acetate	CH ₃	1.91(s)
adenosine	14-CH, 8-CH, 1-CH, 2-CH, 3-CH, 4-CH, half 5-CH, half 5-CH	8.32(s), 8.22(s), 6.05(d), 4.79(dd), 4.44(dd), 4.30(dt), 3.93(dd), 3.85(dd)
adenosine 5' -monophosphate	14-CH, 8-CH, 1-CH, 2-CH, 3-CH, 4-CH, half 5-CH, half 5-CH	8.59(s), 8.25(s), 6.04(d), 4.46(dd), 4.38(dt), 4.01(m)
adenosine 5'-diphosphate	14-CH, 8-CH, 1-CH, 2-CH, 3-CH, 4-CH, half 5-CH, half 5-CH	8.52(s), 8.23(s), 6.14(d), 4.77(dd), 4.63(dd), 4.40(m), 4.24(m)
adenosine 5'-triphosphate	14-CH, 8-CH, 1-CH, 2-CH, 3-CH, 4-CH, half 5-CH, half 5-CH	8.51(s), 8.22(s), 6.12(d), 4.60(dd), 4.40(dt), 4.25 (m)
alanine	α -CH, β -CH ₃	3.81(q), 1.48(d)
asparagine	α -CH, half β -CH ₂ , half β -CH ₂	4.01(m), 2.87(dd), 2.96(dd)
aspartate	α -CH, half β -CH ₂ , half β -CH ₂ ,	3.92(m), 2.70(m), 2.81(m)
choline	3xCH ₃ , α -CH ₂ , β -CH ₂	3.21(s), 4.07(m), 3.52(m)
creatine	CH ₃ , CH ₂	3.04(s), 3.93(s)
formate	CH	8.45(s)
fumarate	CH	6.53(s)
glutamate	α -CH, β -CH ₂ , γ -CH ₂	3.78(m), 2.06(m), 2.36(m)
glutamine	α -CH, β -CH ₂ , γ -CH ₂	3.78(m), 2.15(m), 2.46(m)
glycerophosphocholine	3xCH ₃ , half α -CH ₂ , half α -CH ₂ , half β -CH ₂ , half β -CH ₂ , γ -CH ₂	3.23(s), 4.32(t), 3.60(dd), 3.68(t), 3.89(m), 3.72(dd)
guanosine	14-CH, 1-CH, 3-CH, 4-CH, 5-CH	8.13(s), 5.91(d), 4.41(dd), 4.34(dt), 4.09(AB)
inosine	14-CH, 8-CH, 1-CH, 2-CH, 3-CH, 4-CH, half 5-CH, half 5-CH	8.35(s), 8.23(s), 6.10(d), 4.75(dd), 4.45(dd), 4.30(dt), 3.90(dd), 3.84(dd)
inosine 5' -monophosphate	14-CH, 8-CH, 1-CH, 3-CH, 4-CH, half 5-CH, half 5-CH	8.58(s), 8.23(s), 6.14(d), 4.52(m), 4.37(m), 4.00(m)
inosine 5'-diphosphate	14-CH, 8-CH, 1-CH, 2-CH, 3-CH, CH, half 5-CH, half 5-CH	4- 8.52(s), 8.23(s), 6.16(d), 4.59(d), 4.41(m), 4.24(m), 4.10(s), 3.67(d), 3.37(d)
inosine 5'-triphosphate	14-CH, 8-CH, 1-CH, 2-CH, 3-CH, CH, half 5-CH, half 5-CH	4- 8.48(s), 8.22(s), 6.14(d), 4.60(dd), 4.40(dd), 4.26(m), 4.25(m)
isoleucine	α -CH, β -CH, half γ -CH ₂ , half γ -CH ₂ , CH ₃ , β -CH ₃ ,	δ - 3.68(d), 1.93(m), 1.25(m), 1.47(m), 0.99(d), 1.02(d)
lactate	CH, CH ₃	4.12(q), 1.33(d)
leucine	α -CH, β -CH ₂ , γ -CH, δ -CH ₃ , δ -CH ₃	3.72(t), 1.63(m), 1.69(m), 0.91(d), 0.94(d)
lysine	α -CH, β -CH ₂ , δ -CH ₂ , γ -CH ₂ , ϵ -CH ₂	3.77(t), 1.92(m), 1.73(m), 1.47(m), 3.05(dd)
<i>myo</i> -inositol	1,3-CH, 2-CH, 5-CH, 4,6-CH	3.53(dd), 4.06(t), 3.28(t), 3.63(t)
<i>N</i> -acetylaspartate	α -CH, half β -CH ₂ , half β -CH ₂ , CH ₃ ,	2.03(s), 2.51(dd), 2.70(dd), 4.40(m)
nicotinurate	CH ₂ , 2-CH, 4-CH, 5-CH, 6-CH	3.99(s), 8.94(dd), 8.25(d), 7.60(dd), 8.71(d)
phenylalanine	2,6-CH, 3,5-CH, 4-CH, half β -CH ₂ , half β -CH ₂ , α -CH	7.44(m), 7.39(m), 7.33(m), 3.17(dd), 3.30(dd), 3.99(dd)
phosphocholine	CH ₃ , α -CH ₂ , β -CH ₂	3.24(s), 3.60(m), 4.18(m)
<i>scyllo</i> -inositol	6xCH	3.35(s)
taurine	CH ₂ N, CH ₂ S	3.27(t), 3.43(t)
tyrosine	2,6-CH, 3,5-CH, CH ₂ , α -CH	7.23(d), 6.91(d), 2.93(t), 3.25(t)
uridine	6-CH, 5-CH, 2'-CH, 3'-CH, 4'-CH, 5'-CH(d), half CH ₂ OH, half CH ₂ OH	7.87(d), 5.90(s), 5.92(d), 4.36(t), 4.24(t), 4.14(q), 3.92(dd), 3.81(dd)
valine	α -CH, β -CH, γ -CH ₃ , γ' -CH ₃	3.62(d), 2.28(m), 0.98(d), 1.03(d)
γ -aminobutyrate	α -CH ₂ , γ -CH ₂ , δ -CH ₂	2.30(t), 1.91(m), 3.02(t)
Lipid fractions	CH ₂ CH ₂ C=C, CH ₃ CH ₂ , CH ₃ CH ₂ CH ₂ C=	1.68(m), 0.94(m), 0.88(m)

6.4 Results

Neural metabolite profiles of uninfected control mice and rats. ^1H NMR spectra obtained from the brain removed from the control groups of uninfected mice and rats indicated that these two rodent species shared a similar metabolic profile as expected. Creatine, *N*-acetylaspartate (NAA), lactate, *myo*-inositol, taurine, choline, acetate, glutamate, aspartate and γ -aminobutyrate (GABA) were amongst the dominating metabolites in the aliphatic region of the spectra (Figure 6.1A), whilst inosine and adenosine species and the two aromatic amino acids phenylalanine and tyrosine are characteristic for the aromatic regions in rat and mouse brain profile (Figure 6.1B, Table 6.1).

A

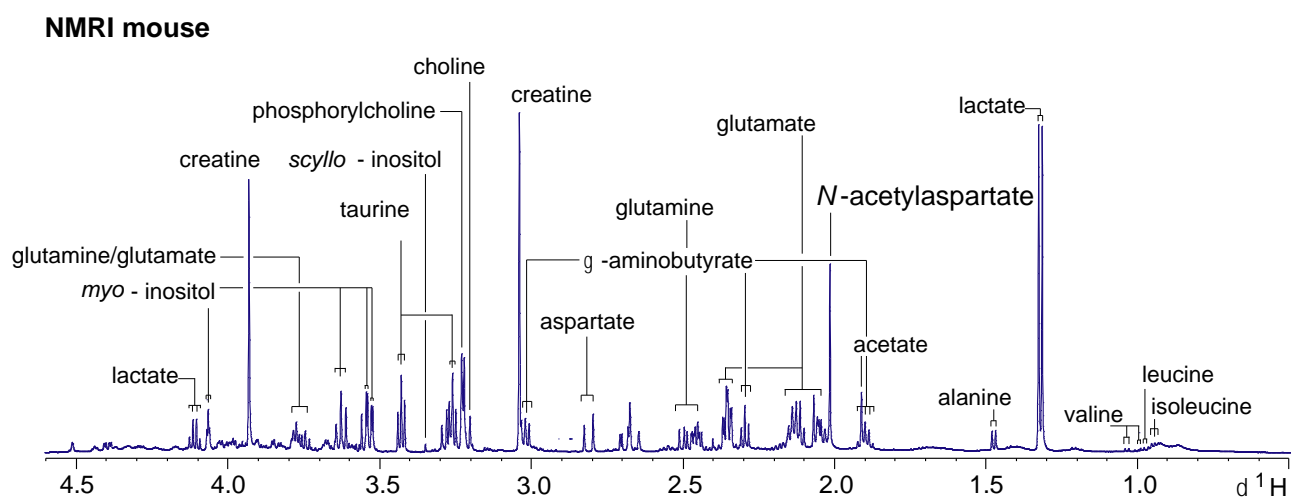
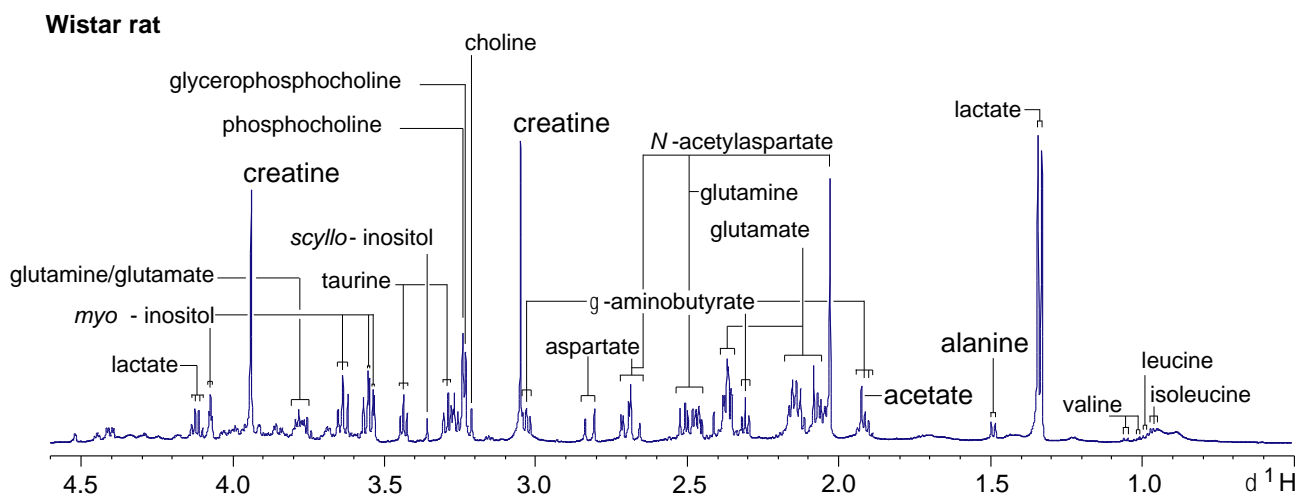
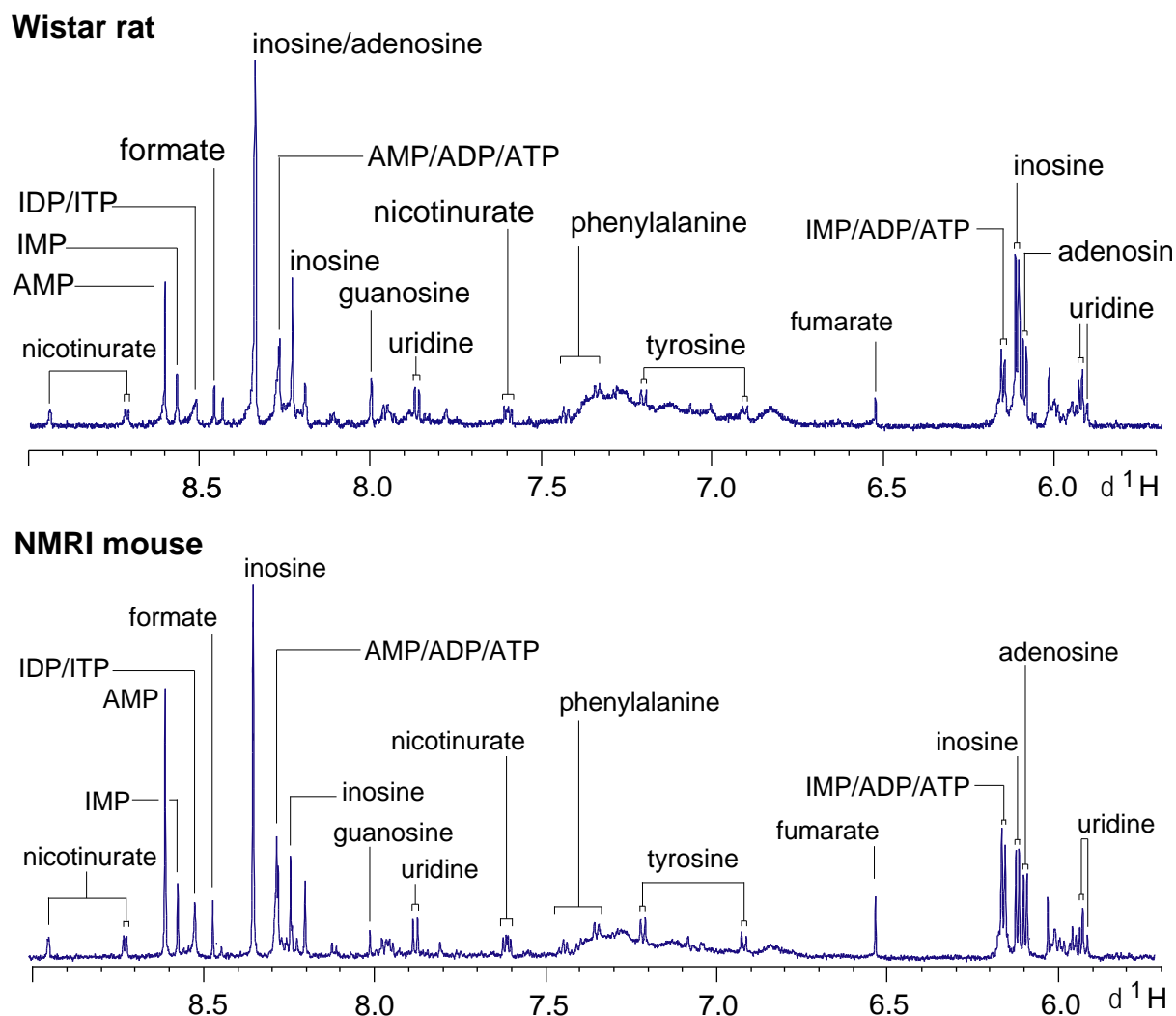


Fig. 6.1. (A) Previous page: Aliphatic region (δ 0.5-4.3) of a typical 600 MHz ^1H NMR spectra of brain extracts obtained from a non-infected control rat and control mouse. (B); Aromatic region (δ 6.5-8.0), magnified 8 fold compared to corresponding spectra in (A).

B



Infection burden and mouse physiology. For each trematode-rodent model, bodyweight and the packed cell volume (PCV) ratio was monitored for each animal at regular intervals. These two measures were used for the overall appraisal of animal wellbeing, with PCV often employed as a proxy for anaemia¹⁵⁹. Upon dissection of experimental animals, *E. caproni* trematodes were removed from the intestine, *F. hepatica* from the bile ducts and *S. mansoni* from both the liver and mesenteric veins in order to confirm infection and assess worm burden^{11, 35}. These description parameters are summarized in Table 6.2.

Table 6.2. Physiological parameters and assessment of wormburden after establishment of chronic infection in all three trematode-rodent models.

	Host number of control (C) and infected (T) animals	Number of animals with established infection	Mean worm burden (range; SD)	PCV at last sampling timepoint
<i>E. caproni</i>	Mouse n(C)=12 n(T)=12	8	26.5 (10-44; 12.0)	C=52.30% T=52.55%
	Rat n(C)=12 n(T)=12			
<i>F. hepatica</i>	Mouse n(C)=10 n(T)=10	8	36 (26-46; 7)	C=54.70% T=33.70%
	Rat n(C)=12 n(T)=12			

Multivariate statistical differentiation. PCA and PLS-DA were initially applied to the brain extract spectra of all three trematode-rodent models. An infection with either *F. hepatica* or *S. mansoni*, induced obvious changes in the metabolic composition of the host brain, as indicated by the clear visual separation of the infected and control animals in the PCA scores plots. Additional PLS-DA analysis confirmed class separation of *F. hepatica*-infected and control rats ($Q^2Y = 0.46$) and *S. mansoni*-infected and control mice, respectively ($Q^2Y = 0.61$). Only *E. caproni*-infected animals were not differentiated from the corresponding control group. The goodness of fit of the PCA model, which is expressed as Q^2X , in a 3 principal component (PC) model was high ($Q^2X = 0.68$) for the *E. caproni* model but visualization of the scores plot did not show clear separation between controls and infected animals, and the model predictivity of the PLS-DA analysis was poor ($Q^2Y = -0.21$) (Figure 6.2). Therefore this group of samples was not explored further.

Pair wise comparison between infected and uninfected control rodents. The O-PLS-DA analysis further underscored whether or not there were remote metabolic changes in the host brain due to a trematode infection. Whereas an *E. caproni* infection in the mouse did not induce any significant differentiation from the healthy state (data not shown), the other two trematodes showed a considerable effect on neurochemical profiles. For instance *F. hepatica* induced significant increase of inosine and the two aromatic amino acids (AAA) tyrosine and

phenylalanine. On the other hand, the concentrations of glycerophosphocholine (GPC), succinate, inosine mono-, di- and triphosphate, adenosine and adenosine mono- di- and triphosphate were relatively lower in the brains of infected animals (Figure 6.3A). Infection with *S. mansoni* was characterised by higher levels of glutamine, but lower concentrations of γ -aminobutyric acid (GABA), choline, phosphocholine and *scyllo*-inositol (Figure 6.4). **Multivariate analyses between physiological compartments.** To reveal systematic effect of the changed brain metabolic profile of the *F. hepatica* infected rats, prominent, but minimally overlapped resonances for all significantly differentiating metabolites were chosen and integrated for all 24 animals. The ^1H NMR urine and plasma spectra obtained immediately prior to the end of the experiment (e.g. day 71) were individually fitted and correlated with 6 brain spectral integrals (Figure 6.5). The results from both analyses are summarized in Table 6.3.

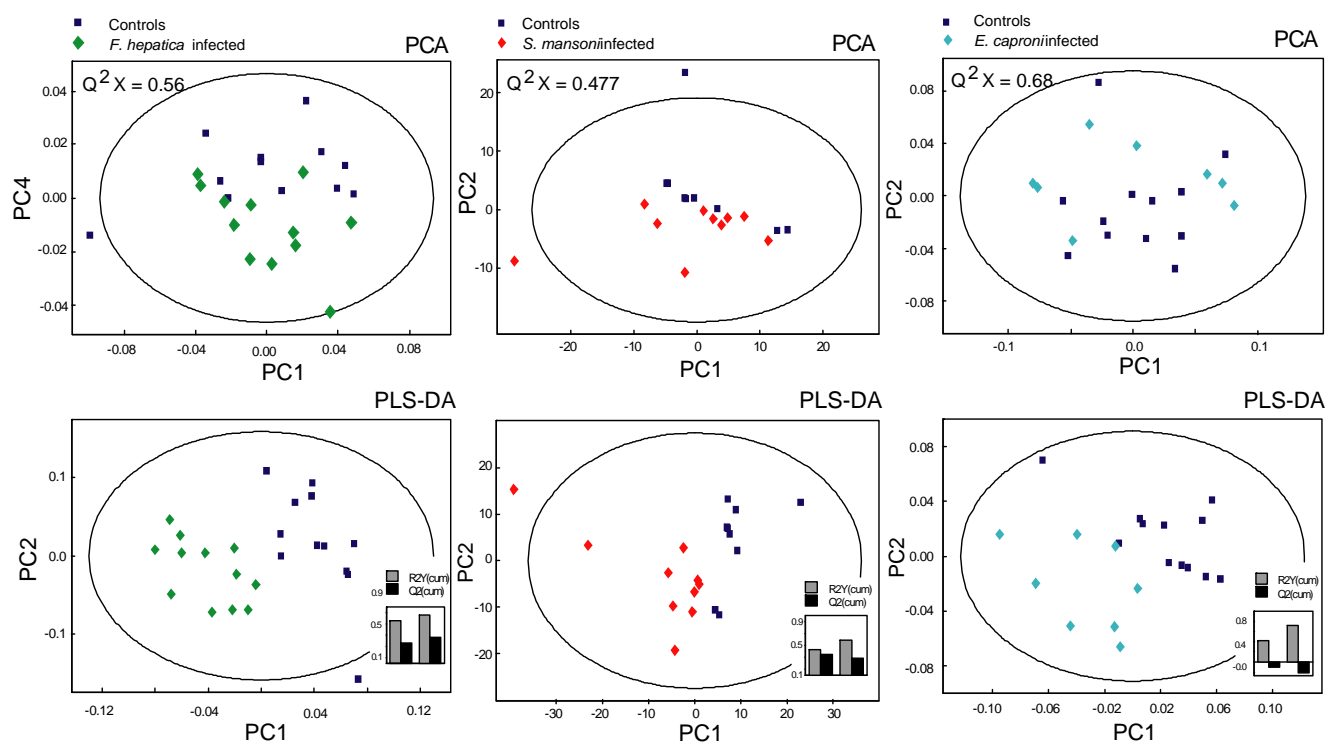


Fig. 6.2. PCA and PLS-DA analysis of (A) *F. hepatica* in the rat, (B) *S. mansoni* in the mouse and (C) *E. caproni* in the mouse. The outlier (T39) died before the timepoint of dissection.

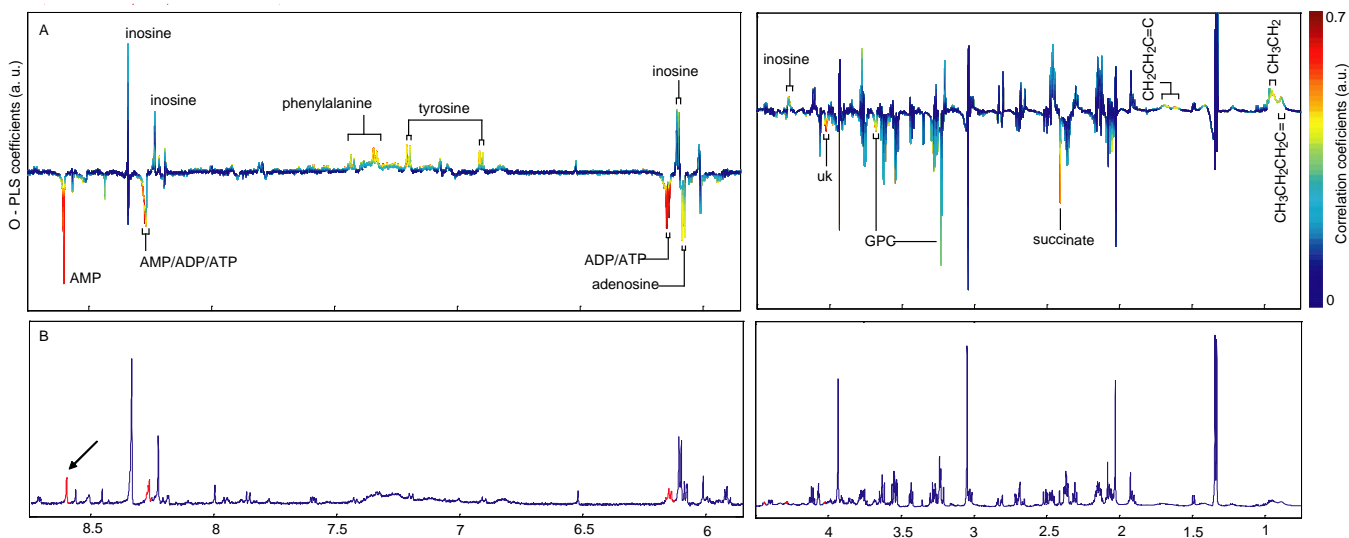


Fig. 6.3. (A) Pair wise comparison *via* O-PLS-DA analysis of *F. hepatica* infected (upwards oriented peaks) and non-infected control animals (downwards oriented peaks). The color scale indicates the magnitude of contribution to the class difference and the peak height is expressed in arbitrary units (a.u.) relatively to the total peak contribution. (B) Statistical Total Correlation Spectroscopy (STOCOSY) of correlated peak regions, revealing spectral regions which belong to the same molecule or close pathway connections.

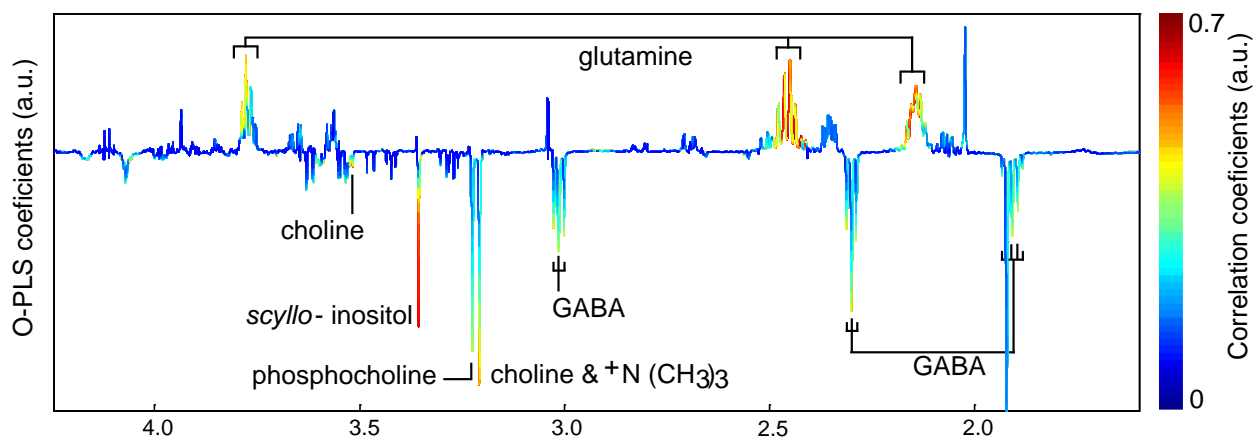


Fig. 6.4. O-PLS-DA differential plot of *S. mansoni* infected (upwards oriented peaks) and non-infected control animals (downwards oriented peaks). The colour scale indicates the weight of contribution to the class differentiation of the data points.

Plasma cytokine level assessment. In order to ascertain whether the metabolic shift from adenosine towards inosine was reflected in the expression of cytokine levels, the concentrations of various cytokines were assessed. Levels of both IL-13 and IL-5 were significantly higher in *F. hepatica* infected rats, compared to the uninfected control group on day 22 post-infection, whereby the former maintained significance on day 43 post-infection (Figure 6.6). Although not statistically significant, a trend towards lower levels in the infected animals during the course of infection was apparent. Comparing the plasma cytokine levels of five *S. mansoni* infected mice with the corresponding control mice, concentrations of IFN- γ , IL-2, IL-12, IL-4 and IL-5, were higher in all infected animals at day 53 post-infection.

Table 6.3. Correlations between neural concentrations of adenosine species, inosine, phenylalanine, succinate and tyrosine and plasma and urinary metabolites, respectively.

plasma	adenosine species	inosine	succinate	tyrosine	phenylalanine
O-acetyl GP	-0.57		-0.62		0.55
N-acetyl GP	-0.53		-0.42		0.57
betaine	-0.50			0.76	
lactate	0.60				
N-acetylcysteine?	-0.48				0.57
creatine			-0.65	0.65	
urine					
α -ketoglutarate	-0.45	0.41		0.60	0.60
taurine		-0.45			-0.51
α -aminoadipate	-0.66	0.52	-0.68		0.66
3-hydroxyphenylpropionic acid	0.55	-0.61		-0.47	
<i>m</i> -hydroxyphenylacetate		-0.54			
succinate			-0.59		
oxaloacetate or pyruvate			-0.61		0.75

6.6 Discussion

S. mansoni and *F. hepatica* both induced a marked perturbation of the neurochemical profiles of the host animals. Interestingly, the third trematode employed (*E. caproni*) was not associated with any clear perturbations in the ^1H NMR spectra obtained from host brain. The patterns of differentiating metabolites in the *S. mansoni*-mouse and the *F. hepatic*-rat models were unique for these two trematode-rodent models apart from exhibiting decrease in

the lipid concentrations of lipid degradation products, such as choline, phosphocholine and GPC, which all have a role in cell membrane formation.

Lipid homoeostasis. Food-derived or *de novo* synthesized choline has three major fates in mammals, (i) further synthesis to phosphocholine, a basic component of membrane anabolism, (ii) oxidation into betaine in the liver and kidney, where it functions as an osmolyte or methyl donor for homocysteine³⁶; or (iii) conversion into acetylcholine³⁷. Choline and phosphocholine were found in lower concentrations in the brains of mice infected with *S. mansoni*, which indicate increased second messenger action, increased membrane maintenance or use of host lipid fractions for parasite lipid anabolism.

The members of the fatty acid binding proteins (FABPs) gene family are also believed to contribute to the decrease in lipid fractions. Esteves *et al.* hypothesised that plathelminthic FABPs play a role in scavenging host membrane lipids, as flatworms are not able to synthesize their own lipids *de novo*, and are dependent on free fatty acid pools³⁸. This hypothesis may explain a global decrease of lipids leading to the observed depletion of cerebral choline and phosphocholine due to a chronic infection with *S. mansoni*, and lower GPC (and the trend in lower choline and phosphocholine) levels after infection with *F. hepatica*.

Parasite specific perturbations of neural profiles. Nucleotide degrading enzymes have been found to be excreted in a variety of ecto- and endoparasitic organisms, such as ticks, blood sucking insects and helminths and serve the primary purpose of minimizing immune reactions in the host organism in order to prolong the survival^{39, 40}. The found shift from adenosine concentrations (decreased) and inosine levels (increased) reflects an attenuated inflammatory response as both nucleotides induce mast cell degranulation, but adenosine is the more potent activator and is converted into the inosine by adenosine deaminase⁴¹. Thus far, adenosine deaminase has been found in secretory channels of *Trichinella spiralis* and *Fasciola gigantica*^{42, 43}. Inosine is mainly formed by intracellular conversion of adenosine *via* adenosine deaminase, or by the 5'-nucleotidase which hydrolyses inosine-monophosphate (Figure 6.6A).

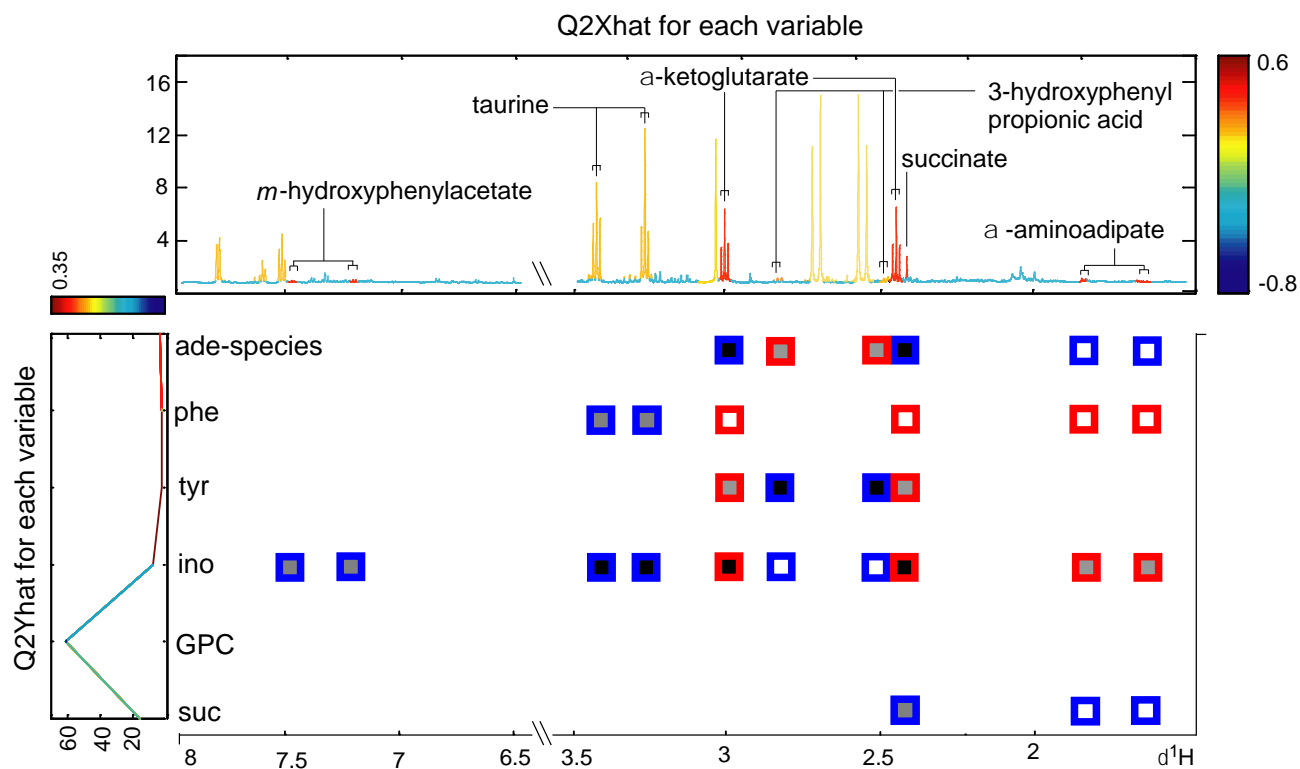


Fig. 6.5. O2-PLS analysis generated using ¹H NMR urine spectra as the x-matrix and the integrals of the control/infection-differentiating metabolites of the brain extracts (ade, adenosine-species; GPC, glycerophosphocholine; ino, inosine; phe, phenylalanine; suc, succinate; tyr, tyrosine;) as the y-matrix. The x-axis shows the most explanatory urine spectral regions, whereas y reveals which descriptor in the y-matrix is best explained by the x-data set, e.g. which metabolite. The resulting cross plot shows the correlation strength of urinary and brain metabolites. Red frame: positive correlation of urinary and brain metabolites; Blue frame: negative correlation of urinary metabolites with increasing brain metabolic integrals; black filled boxes indicate a correlation coefficient of 0.4-0.5; grey fill, 0.5-0.6; white fill, 0.6-0.8.

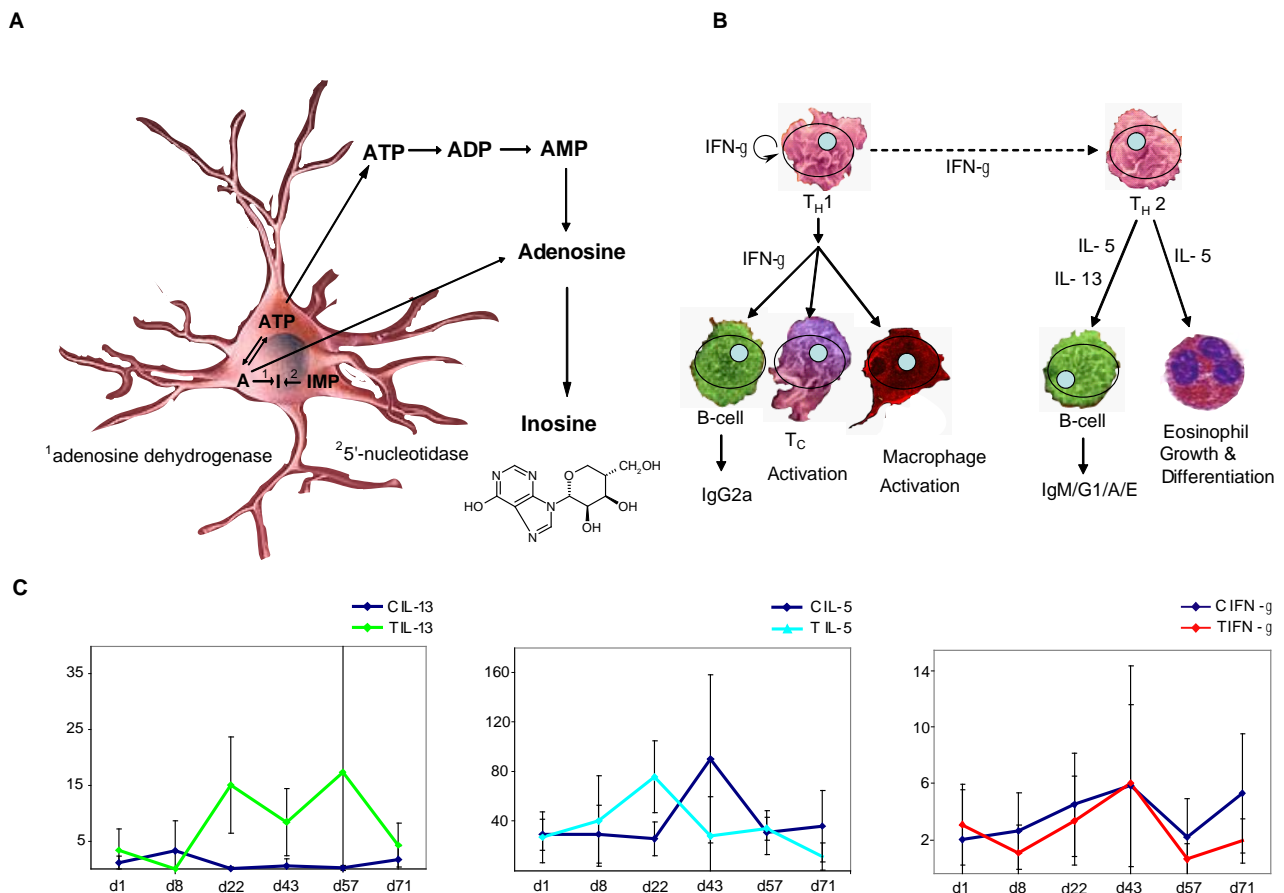


Fig. 6.6. (A) Schematic of: Intra- and extracellular adenosine-inosine interconversion in the brain by two main enzymes, ¹ adenosine dehydrogenase and ² 5'-nucleotidase; A, adenosine; I, Inosine. (B) The shift from adenosine towards inosine leads to T_H2 subset triggered immune mechanisms characterised by relatively higher levels of IL-5, IL-13 and lower concentrations of IFN-γ which acts as T_H2 inhibitor. Plasma concentrations of the three cytokines (C) confirmed significantly lower levels of IL-5 and IL-13 in the *F. hepatica* infected animals (light blue and green) at day 22 post-infection and day 43 post-infection, respectively, and a trend towards lower levels of IFN-γ throughout the main course of infection, compared to the uninfected control animals (blue).

Our data may suggest that *F. hepatica* not only secretes adenosine deaminase but also a 5'-nucleotidase analogue catalytic active molecule. The increased conversion from adenosine, phosphorylated adenosine and phosphorylated inosine species to inosine in the host brain is believed to reflect the systemic state and is potentially beneficial to the parasite as inosine is not only less potent in mast cell activation, but is also known to suppress the synthesis of pro-inflammatory cytokines, such as IFN-γ, IL-1, IL-12 and TNF-α *in vitro*⁴⁴. Indeed, additional

cytokine concentration measurements in the plasma of *F. hepatica*-infected and uninfected control rats at 6 different time points revealed a T_H2 emphasised immune response (Figure 6.6B) with significantly higher levels of IL-5 and IL-13 and a trend toward lower levels of IFN- γ in the infected group (Figure 6.6C). Both, the increase of IL-13 and the enhanced T_H2 immune response counteract mechanisms of inflammation since IL-13 is an important negative regulator of inflammatory cytokines, and the T_H1 cytokine subset is usually associated with tissue injury and excessive inflammation, which would be expectable in a massive liver damage, as caused by *F. hepatica*. Again, minimization of such an intense immune reaction and hence undetected co-existence in the host at earlier stages of infection is obviously beneficial for the survival of the worms.

Characteristic modulation of neurochemical profile following *Schistosoma mansoni* infection. Metabolic alterations associated with a *S. mansoni* infection comprised relatively increased tissue concentrations of glutamine with depleted levels of GABA, choline species and *scyllo*-inositol. Glutamine is a substrate for both excitatory and inhibitory neurotransmitters, including GABA. The inverse association of glutamine and GABA in the current study may indicate an inhibitory mechanism on glutamate decarboxylase, mediated by *S. mansoni*-induced immune reactions in the CNS. It is known that glutamate decarboxylase converts glutamate directly to GABA⁴⁵. It is therefore interesting to note that an infection with the West Nile virus, which induces meningitis and encephalitis, has been associated with the development of anti-glutamate decarboxylase antibodies, leading to motor neurotic disturbances⁴⁶.

The inflammation which *S. mansoni* presence causes is also reflected in the increased concentrations of the pro-inflammatory cytokines IFN- γ and IL-12 in the plasma of infected mice, in contrast to the *F. hepatica* induced attenuation of inflammatory reactions.

GABA has been reported to decrease in the brain of mice with CNS diseases. It is well documented that both GABA and glutamate are associated with inflammatory responses, and hence they may play a role in the cross-talk between immune cells and neurons^{47, 48}.

Interplay of liver pathology and neural profile. Both *S. mansoni* and *F. hepatica* infections cause liver damage, *via* egg induced inflammation⁴⁹, leading to damage of blood vessels, necrosis and structural change of the liver tissue⁵⁰, and direct mechanical damage by the juvenile worm, respectively¹⁹. The inflammation caused by trapped *S. mansoni* eggs in the liver tissue seem to result in malfunction, including failed detoxification of ammonia derived

from the intestinal degradation of nutrients. Compensatory locations for ammonium detoxification are muscle cells and the brain, combining ammonia and glutamate to glutamine^{51, 52}, which could also contribute to the relatively higher levels of glutamine in the brain extracts of *S. mansoni*-infected mice documented in the current investigation. The subsequent decrease of the second messenger GABA indicates that the main fate of glutamate is indeed the detoxification rather than the generation of GABA. The impact of *F. hepatica* on the liver is due on direct, mechanical damage of the tissue by the migration and feeding of the juvenile worm for 5-7 weeks until it reaches maturity and finally resides in the bile duct¹⁹. The consequent hepatic dysfunction in *F. hepatica* infection manifested in increased circulating toxins, such as ammonia, mercaptans and phenols⁵³, which are typically released after hepatic failure, because of failing degradation of aromatic amino acids and ammonia. Animals, infected with *F. hepatica* showed increased neural concentrations of the two aromatic amino acids phenylalanine and tyrosine. Indeed it has been shown that hepatic failure induces an increased passive permeability of the blood-brain barrier for several substances, amongst which phenylalanine and tyrosine were found to increase up to 30% in the brain⁵⁴. Although there is no direct sign of ammonia detoxification in the brain metabolic profiles of *F. hepatica* infected rats, the positive correlation of α -ketoglutarate in the urine with increasing levels of the two aromatic amino acids in the brain indicates potential ammonia degrading capacity with severity of disease, as ammonia is known to inhibit α -ketoglutarate dehydrogenase which accumulates α -ketoglutarate but allows degradation to glutamate and glutamine, respectively⁵⁵.

We have demonstrated a clear effect of two helminth infections on the biochemical composition of the brain whereas a third helminth failed to induce any response in the neural metabolic profile. However, the neurometabolic signature of *S. mansoni* and *F. hepatica* were distinctive with *S. mansoni* indicating markers of inflammation such as increased GABA and glutamate and increased pro-inflammatory cytokines (IFN- γ and IL-12). All other assessed cytokines which underwent increase after infection indicated a mixed T_H subgroup response with IL-2, IL-12 and IFN- γ being characteristic for T_H1 guided immune mechanisms and IL-4 and IL-5 linked to T_H2 responses. *F. hepatica* on the other hand demonstrated a more focussed response primarily associated with the hypothesised worm-induced shift from inosine towards adenosine and the subsequent induction of a T_H2 focussed immune response. Although there is no need to emphasise that the T_H1/T_H2 dogma is not strictly applicable *in*

vivo, and much more complex than the strict categorization to two possible outcomes, we show here that the sum of effects of a helminth infection reflects in the biochemical composition of the biofluids and tissues as response to the trematode antigens, and the direct mechanical effect of larvae and egg which offers a new way to further explore the dynamic action of the immune system and circumvent sub type-assumption.

6.7 Acknowledgment

We thank Dr. O. Cloarec for providing in-house software. This study received financial support from the Swiss National Science Foundation to J.S., J.V.L and J.U. (project no. PPOOB--102883 and PPOOB--119129) and J,K. (project no. xxx). The authors also acknowledge Nestle for provision of funds for Y.W.

6.8 References

1. Liu, Q., Wei, F., Liu, W., Yang, S. & Zhang, X. Paragonimiasis: an important food-borne zoonosis in China. *Trends Parasitol* **24**, 318-323 (2008).
2. Lun, Z.R. et al. Clonorchiasis: a key foodborne zoonosis in China. *Lancet Infect Dis* **5**, 31-41 (2005).
3. Mas-Coma, S., Bargues, M.D. & Valero, M.A. Fascioliasis and other plant-borne trematode zoonoses. *Int J Parasitol* **35**, 1255-1278 (2005).
4. Otranto, D. & Traversa, D. Dicrocoeliosis of ruminants: a little known fluke disease. *Trends Parasitol* **19**, 12-15 (2003).
5. Thomas, F. et al. Biochemical and histological changes in the brain of the cricket *Nemobius sylvestris* infected by the manipulative parasite *Paragordius tricuspidatus* (Nematomorpha). *Int J Parasitol* **33**, 435-443 (2003).
6. Grosman, A.H. et al. Parasitoid increases survival of its pupae by inducing hosts to fight predators. *PLoS ONE* **3**, e2276 (2008).
7. Kennedy, P.G. Human African trypanosomiasis of the CNS: current issues and challenges. *J Clin Invest* **113**, 496-504 (2004).
8. Carod-Artal, F.J. Neurological complications of *Schistosoma* infection. *Trans R Soc Trop Med Hyg* **102**, 107-116 (2008).
9. Kang, S.Y. et al. A case of chronic cerebral paragonimiasis *westermani*. *Korean J Parasitol* **38**, 167-171 (2000).
10. Ying, M., Xiaosu, H. & Wang, B. A case of ectopic parasitism: *Fasciola hepatica* larvae burrow through a human brain and mimic cerebral aneurysm. *Trans R Soc Trop Med Hyg* **101**, 1051-1052 (2007).
11. Wang, Y. et al. Metabonomic investigations in mice infected with *Schistosoma mansoni*: an approach for biomarker identification. *Proc Natl Acad Sci U S A* **101**, 12676-12681 (2004).
12. Wang, Y. et al. System level metabolic effects of a *Schistosoma japonicum* infection in the Syrian hamster. *Mol Biochem Parasitol* **146**, 1-9 (2006).
13. Martin, F.P. et al. Transgenomic metabolic interactions in a mouse disease model: interactions of *Trichinella spiralis* infection with dietary *Lactobacillus paracasei* supplementation. *J Proteome Res* **5**, 2185-2193 (2006).
14. Saric, J. et al. Metabolic profiling of an *Echinostoma caproni* infection in the mouse for biomarker discovery. *PLoS NTD* **2**, e254 (2008).
15. Li, J.V. et al. Global metabolic responses of NMRI mice to an experimental *Plasmodium berghei* infection. *J Proteome Res* **7**, 3948-3956 (2008).
16. Wang, Y. et al. Global metabolic responses of mice to *Trypanosoma brucei brucei* infection. *Proc Natl Acad Sci U S A* **105**, 6127-6132 (2008).

-
17. Li, J.V.H., E.; Saric, J.; Keiser, J.; Dirnhofer, S.; Utzinger, J.; Wang, Y. Metabolic profiling of a *Schistosoma mansoni* infection in mouse tissues using magic angle spinning-nuclear magnetic resonance spectroscopy. Submitted to *Int J Parasitol* (2008).
 18. Manzella, A., Ohtomo, K., Monzawa, S. & Lim, J.H. Schistosomiasis of the liver. *Abdom Imaging* **33**, 144-150 (2008).
 19. Lim, J.H., Kim, S.Y. & Park, C.M. Parasitic diseases of the biliary tract. *AJR Am J Roentgenol* **188**, 1596-1603 (2007).
 20. Banks, W.A. Denial versus dualism: the blood-brain barrier as an interface of the gut-brain axis. *Endocrinology* **147**, 2609-2610 (2006).
 21. Schwartz, G.J. Neural-immune gut-brain communication in the anorexia of disease. *Nutrition* **18**, 528-533 (2002).
 22. Tsang, T.M., Griffin, J.L., Haselden, J., Fish, C. & Holmes, E. Metabolic characterization of distinct neuroanatomical regions in rats by magic angle spinning ^1H nuclear magnetic resonance spectroscopy. *Magn Reson Med* **53**, 1018-1024 (2005).
 23. Holmes, E. et al. Human metabolic phenotype diversity and its association with diet and blood pressure. *Nature* **453**, 396-400 (2008).
 24. Li, M. et al. Symbiotic gut microbes modulate human metabolic phenotypes. *Proc Natl Acad Sci U S A* **105**, 2117-2122 (2008).
 25. Nicholson, J.K., Lindon, J.C. & Holmes, E. 'Metabonomics': understanding the metabolic responses of living systems to pathophysiological stimuli *via* multivariate statistical analysis of biological NMR spectroscopic data. *Xenobiotica* **29**, 1181-1189 (1999).
 26. Nicholson, J.K., Foxall, P.J., Spraul, M., Farrant, R.D. & Lindon, J.C. 750 MHz ^1H and ^1H - ^{13}C NMR spectroscopy of human blood plasma. *Anal Chem* **67**, 793-811 (1995).
 27. Cloarec, O. et al. Statistical total correlation spectroscopy: an exploratory approach for latent biomarker identification from metabolic ^1H NMR data sets. *Anal Chem* **77**, 1282-1289 (2005).
 28. Ernst, R.R.B., G.; Wokaun, A. Principles of nuclear magnetic resonance in one and two dimensions. (1986).
 29. Bax, A. Topics in ^{13}C NMR spectroscopy, Vol. 4. (1984).
 30. Foxall, P.J., Parkinson, J.A., Sadler, I.H., Lindon, J.C. & Nicholson, J.K. Analysis of biological fluids using 600 MHz proton NMR spectroscopy: application of homonuclear two-dimensional J-resolved spectroscopy to urine and blood plasma for spectral simplification and assignment. *J Pharm Biomed Anal* **11**, 21-31 (1993).
 31. Eriksson, L., Johansson, E., Kettaneh-Wold, N., Trygg, J. & Wikstrom, C. in (Umetrics Academy, 2001).
 32. Trygg, J. O2-PLS for qualitative and quantitative analysis in multivariate calibration. *J Chemom* **16**, 283-293 (2002).

-
33. Bro, R., Kjeldahl, K., Smilde, A.K. & Kiers, H.A. Cross-validation of component models: a critical look at current methods. *Anal Bioanal Chem* **390**, 1241-1251 (2008).
 34. Anumudu, C., Afolami, M., Igwe, C., Nwagwu, M. & Keshinro, O. Nutritional anaemia and malaria in preschool and school age children. *Ann Afr Med* **7**, 11-17 (2008).
 35. Keiser, J., Shu-Hua, X., Tanner, M. & Utzinger, J. Artesunate and artemether are effective fasciolicides in the rat model and in vitro. *J Antimicrob Chemother* **57**, 1139-1145 (2006).
 36. Zeisel, S.H. & Blusztajn, J.K. Choline and human nutrition. *Annu Rev Nutr* **14**, 269-296 (1994).
 37. Li, Z. & Vance, D.E. Thematic Review Series: Glycerolipids. Phosphatidylcholine and choline homeostasis. *J Lipid Res* **49**, 1187-1194 (2008).
 38. Esteves, A., Joseph, L., Paulino, M. & Ehrlich, R. Remarks on the phylogeny and structure of fatty acid binding proteins from parasitic platyhelminths. *Int J Parasitol* **27**, 1013-1023 (1997).
 39. Parshad, V.R. & Guraya, S.S. Comparative histochemical observations on the excretory system of helminth parasites. *Z Parasitenkd* **52**, 81-89 (1977).
 40. Ribeiro, J.M. & Francischetti, I.M. Role of arthropod saliva in blood feeding: sialome and post-sialome perspectives. *Annu Rev Entomol* **48**, 73-88 (2003).
 41. Tilley, S.L., Wagoner, V.A., Salvatore, C.A., Jacobson, M.A. & Koller, B.H. Adenosine and inosine increase cutaneous vasopermeability by activating A(3) receptors on mast cells. *J Clin Invest* **105**, 361-367 (2000).
 42. Gounaris, K. Nucleotidase cascades are catalyzed by secreted proteins of the parasitic nematode *Trichinella spiralis*. *Infect Immun* **70**, 4917-4924 (2002).
 43. Ali, E.M. *Fasciola gigantica*: purification and characterization of adenosine deaminase. *Exp Parasitol* **119**, 285-290 (2008).
 44. Hasko, G., Sitkovsky, M.V. & Szabo, C. Immunomodulatory and neuroprotective effects of inosine. *Trends Pharmacol Sci* **25**, 152-157 (2004).
 45. Madsen, K.K., Larsson, O.M. & Schousboe, A. Regulation of excitation by GABA neurotransmission: focus on metabolism and transport. *Results Probl Cell Differ* **44**, 201-221 (2008).
 46. Hassin-Baer, S. et al. Stiff-person syndrome following West Nile fever. *Arch Neurol* **61**, 938-941 (2004).
 47. Vezzani, A. & Granata, T. Brain inflammation in epilepsy: experimental and clinical evidence. *Epilepsia* **46**, 1724-1743 (2005).
 48. Stuckey, D.J. et al. Detection of the inhibitory neurotransmitter GABA in macrophages by magnetic resonance spectroscopy. *J Leukoc Biol* **78**, 393-400 (2005).
 49. Wilson, M.S. et al. Immunopathology of schistosomiasis. *Immunol Cell Biol* **85**, 148-154 (2007).
 50. Goldsby, R.A., Kindt, T.J. & Osborne, B.A. Immunology. (W. H. Freeman and Company, 2000).

-
51. Olde Damink, S.W., Deutz, N.E., Dejong, C.H., Soeters, P.B. & Jalan, R. Interorgan ammonia metabolism in liver failure. *Neurochem Int* **41**, 177-188 (2002).
 52. Kreis, R., Farrow, N. & Ross, B.D. Localized ¹H NMR spectroscopy in patients with chronic hepatic encephalopathy. Analysis of changes in cerebral glutamine, choline and inositols. *NMR Biomed* **4**, 109-116 (1991).
 53. Zaki, A.E., Wardle, E.N., Canalese, J., Ede, R.J. & Williams, R. Potential toxins of acute liver failure and their effects on blood-brain barrier permeability. *Experientia* **39**, 988-991 (1983).
 54. Zaki, A.E., Ede, R.J., Davis, M. & Williams, R. Experimental studies of blood brain barrier permeability in acute hepatic failure. *Hepatology* **4**, 359-363 (1984).
 55. Ott, P., Clemmesen, O. & Larsen, F.S. Cerebral metabolic disturbances in the brain during acute liver failure: from hyperammonemia to energy failure and proteolysis. *Neurochem Int* **47**, 13-18 (2005).



7 Discussion

The ‘-omics-sciences’ have been portrayed as providing new avenues for personalised healthcare in industrial countries (Kusmann *et.al.*, 2006; Martini *et.al.*, 2008; Sigdel and Sarwal, 2008). Metabonomics, which is one of the ‘-omics sciences’ has already established itself as an important contributor for this purpose (Nicholson, 2006; Rochfort, 2005; Yap *et.al.*, 2006). For tropical parasitic diseases, however, approaches that are readily adopted to resource-constrained settings must be found, which implies rapid and inexpensive screening programmes rather than highly optimised personal health care. Comparing efficiency, cost and practicality between proteomics, genomics and metabonomics, we believe that the latter holds particular promise to fulfil some of these prerequisites. The present Ph.D. thesis is part of a longer term investigation with the overarching aim to critically evaluate the scope and limits of ^1H NMR-based metabolic profiling as a new tool to further our understanding of host-parasite interactions, with particular consideration to diagnostic and prognostic potential. In the current thesis, we focussed on the evaluation of potential diagnostic matrices and biomarker recovery and quality assessment issues of a number of trematode infections in selected rodent models.

Of all biological samples, urine has been best characterised by ^1H NMR spectroscopy due to the ease of sample collection and its availability in large quantities (Clayton *et.al.*, 2004; Foxall *et.al.*, 1993; Holmes *et.al.*, 1994; Nicholls *et.al.*, 2003). Another biofluid widely used in metabonomics is blood plasma (Beckonert *et.al.*, 2007; Nicholson *et.al.*, 1995; Tang *et.al.*, 2004). In order to gain the best preparation protocol for faecal water data acquisition, and to conclude on the significance of identified metabolites for eventual diagnosis, we performed a thorough characterisation of faecal water. Based on these findings, a comparison was done on three biofluids (i.e., urine, plasma and faecal water) obtained from *E. caproni*-infected mice and uninfected control mice that were matched for age and sex. Biomarkers were recovered *via* ^1H NMR at several time points post-infection, which included acute and chronic stages of infection. Quantity of biomarkers, stability over time and practicality were assessed to gain an idea over the potential diagnostic range which biofluids can be used for the metabolic assay. In the case of an *E. caproni* infection in the mouse, once the infection had progressed to a chronic stage (i.e. 5 weeks post-infection), mice were killed and a number of different organs recovered for further assessment of disease impact on the murine host. The purpose of this part of the study was to gain further insights into systems level changes due to this intestinal

fluke infection and to uncover subtle changes at a molecular level in different physiological compartments, which had not been chosen for assessment before. The results indeed showed unexpected changes in locations remote from any direct impact of the intestinal fluke, namely in the liver and kidney.

In view of conflicting results of whether or not helminth infections have a negative effect on the cognitive performance of the human host, and whether anthelmintic treatment can revert such effects (Boivin, 1996; de Clercq *et.al.*, 1998; Jukes *et.al.*, 2002; Watkins and Pollitt, 1997), we performed additionally analysis on the brains of *E. caproni*-infected mice, *S. mansoni*-infected mice and *F. hepatica*-infected rats (unpublished data), including age- and sex- matched uninfected control animals. These experiments resulted in revelation of strategic behaviour of *F. hepatica* via immune modulation of the host.

7.1 Potential biological matrices for diagnosis

The main criteria when looking for a suitable template for diagnostics are availability in terms of volume, a non-invasive way of obtaining the sample, inherent stability of the sample, and the potential of offering a quantitatively and qualitatively robust panel of biomarkers.

With view to finding a non-invasive approach, diagnosis based on tissue, spinal and lymph fluid are not considered as an option here, due to obvious practical reasons and the challenge in rural settings in the developing world, respectively. Even if there are medical facilities present to operate tests such as spinal puncture for example, which still needs to be applied to confirm the neuro-encephalitic stage of human African trypanosomiasis (Kennedy, 2004), there is a pressing need to circumvent these highly invasive methods, because of the considerable risk of catching a secondary infections.

There are many available biological samples with potential capacity of disease biomarkers, but some of them are limited in volume (e.g. tears and sweat) and others are difficult to obtain or not accepted, for ethical reasons, such as faeces or sperm, respectively. Apart from the ethical issues in some cultures, stool samples seem to be a suitable candidate for a diagnostic template, due to the ease of sampling and the sheer amount which can be obtained. In-depth assessment of faecal material on species-differences, gender-differences and stability over time showed a high degree of fluctuation over several time-points and species-related grouping of the assessed mouse, rat and human samples, whereas rat and

mouse, as expected, seemed to be closer to each other than the human faecal samples. Furthermore male and female separation was seen due to differences in short chain fatty acid (SCFA) composition. The corresponding loadings revealed differentiation due to concentration differences rather than qualitative differences of all three groups, which indicate certain constancy in the biomarker composition amongst the species. In fact, glycerol and β -alanine were the only two compounds which appeared in a single species only (i.e. human and rat), but apart from that, all species and gender-differences were based on quantitative differences of metabolites.

The main driver to include faecal samples in the biofluid assessment of an *E. caproni*-infection in the mouse was the fact that approximately one-third of all identified urinary biomarkers in the previous parasite-rodent models depend on microbial modification before being excreted. The gut microbiota, which consist of 300-500 different bacterial species is responsible for the production of ~60% of the total faecal mass (Guarner and Malagelada, 2003), hence it would be likely that an intestinal fluke, which is in direct interaction with gut microbial species, would impose some changes in the microbial dynamics.

Evaluating the quantity of the identified biomarkers and stability over time, we focussed – apart from faecal water – on urine and plasma, for which metabolic composition across several species is already well characterised (Foxall *et.al.*, 1993; Nicholson *et.al.*, 1995) and which are obtained easily and in relatively large quantities (>0.25 ml). Comparing quantity and stability over time, as expected, faecal water could not reach the potentially high diagnostic level of urine or plasma but could add valuable information to gut microbial activities. The results indicate the depletion of certain microbial species which are normally responsible for the degradation of 5-aminovalerate (e.g. *Clostridium aminovalericum*) (Barker *et.al.*, 1987; Hardman and Stadtman, 1960) and dietary carbohydrates to SCFAs (Cook and Sellin, 1998; Wong *et.al.*, 2006), but after infection with *E. caproni* failed to do so.

Even though water is not an ideal template for diagnosis, the informative value of this additional data set should not be underestimated, and hence might be included in every future experimental set-up to in order to gain direct correlation of molecular compounds and bacterial strains. Both urine and plasma samples showed a similar quantity of extracted biomarkers for identification of an *E. caproni* infection in mice (ten and 12, respectively) with a very good indication of stability. From day 8 post-infection onwards, when the most significant changes started to manifest, four more time-points were assessed. Five biomarkers

in urine and seven in plasma differentiated the infection-status significantly on, at least four of these five time-points, which is a promising finding. Whereas plasma holds the higher quantity of candidate biomarkers in the experimental measures, urine advances through the easy of sample collection under field conditions (e.g. minimally trained personnel can do it such as school teachers), and would make sterile blood-sampling material redundant. However both, urine and plasma will be given the same attention in future biomarker extraction.

7.2 Specificity of biomarkers

The quality and quantity of the biomarkers are important criteria for choosing a suitable diagnostic template and can be easily assessed in one single parasite-rodent model, but this will not give any conclusion about how well an underlying condition is reflected by the biomarkers. The decisive question of how specific a marker is to a certain infectious-disease is perhaps the most difficult to answer and extensive evaluation over several infection models. Furthermore, parasite-induced pathology can resemble other none infection-related disease states, such as the mechanical liver damage, caused by an infection with the liver fluke *F. hepatica* and alcohol-induced liver cirrhosis, and could potentially generate the same biomarkers. However, it is obvious that different causes of organ damage can induce a similar pathological manifestation but this obstacle can be overcome by creating fingerprints of disease with different subsets of biomarkers, as one health impact is never restricted to a single physiological compartment but rather introduces homeostatic changes in the whole of the system and will also reveal traces of the causative agent, whether it is an invading parasite, a genetic defect or a nutritional ill-condition.

Table 7.1 shows a direct comparison of the complete set of recovered urine biomarkers across five parasite-rodent models, whereas Table 7.2 represents the plasma markers from four of these five models. No urine samples were available of *Trichinella spiralis*-infected mice, and neither plasma from both schistosome models has been sampled, and hence, no biomarkers are listed in the corresponding tables. The markers were evaluated according to a colour code, with red indicating absolute specificity according to parasite-infection, taking directional changes (increased or decreased in infected animals in comparison to corresponding controls) of the markers in account, yellow indicating the up-coming of the

marker in two of the infection models, light blue markers were present in three and dark blue coded markers in all listed parasite-rodent models. Interestingly, the most unspecific urinary markers were all gut microbiota-related, which indicates a general infection-induced impact on the host microbiota. Indeed, bacterial species, which are pathway-linked to hippurate, *p*-cresolglucuronide, phenylacetyl glycine and trimethylamine, seem to be affected the most.

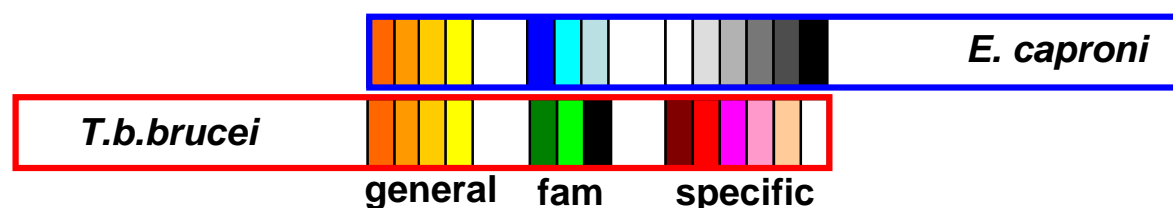


Figure 7.1. Hypothetic disease fingerprint composed of three biomarker sub-panels, which include general markers of infection, family-specific and parasite-specific markers.

Other microbiota-related metabolites, such as SCFAs did not seem to respond to the general infection pattern in such a high degree. In contrast, the more general marker found in plasma were composed of functionally very different metabolites, such as the branched chain amino acids (BCAAs) valine, leucine and isoleucine, which showed depletion in *Trypanosoma brucei brucei* and both intestinal worms, most probably due to their important role in tissue regeneration. Glycerophosphocholine, glucose and lactate also showed high biomarker presence amongst the infection, reflecting the general anaerob metabolism (e.g. glycolysis of parasitic organisms). However, these metabolites were only directly coupled within the protozoan infections, where they showed a clear depletion of glucose and subsequent increase of lactate, which reflects the immense glycolytic turnover of the trypanosomes (Mehta *et.al.*, 2005; Visser and Opperdoes, 1980) and erythrocytes infected by *Plasmodium berghei*, respectively, using mainly glucose as substrate. Although trematodes and other helminths inhabit the same principal pathway, using glucose and glycogen as substrate, the glycolysis does not seem to be particularly efficient and glucose is often not completely catabolised. The end products are composed of mainly lactate but also acetate, succinate and large amounts of SCFA end products (Schmidt, 2000), hence lactate does not come up as a biomarker in the present helminth infections. A combination of the two markers lactate (increased) and glucose (depleted) would be predestined for a second subset of the

hypothetic disease fingerprint for some kind of dipstick that might eventually be developed and used under field conditions. All parasite-host models delivered also a third complementary subset of biomarkers, which were highly parasite specific (Tables 7.1 and 7.2 and Figure 7.1). A three-subset strategy as shown here would optimize diagnostic and circumvent false positive as well as false negative results, by optimized broadness and sensitivity, respectively, through several biomarker subsets.

7.3 Analytical tools

Once the metabolic fingerprints of various single infections in suitable rodent models have been established, obviously the chances of cross-over of biomarkers will increase. In order to counteract this potential problem, the biomarker recovery process has to be further improved. One of the key problems, NMR spectroscopy has to face is the lack of sensitivity, which was indicated by the inability to directly profile parasite derived biomarkers, such as secreted enzymes and peptides and surface molecules, respectively (Hewitson *et.al.*, 2008). In fact only in the *T. b. brucei* model we could be certain, that the increase of lactate in the mouse plasma and urine was directly parasite derived. The missed potential is not to underestimate in a global analysis, because such parasite secreted, low abundant compounds would be highly interesting potential biomarkers in terms of specificity and thus, more sensitive spectroscopic methods have to be emphasised in future metabolic profiling, MS in particular. MS coupled with chromatographic separation methods, such as liquid and gas chromatography or capillary electrophoresis (UPLC-MS, GC-MS or CE-MS or MS-MS), can elevate biomarker recovery to a new level, and e.g. complete the third subset of a disease-specific fingerprint. Highly accurate and mass sensitive mass spectrometers such as the quadrupole-orthogonal Time-of-Flight MS (Q-ToF) (Plumb *et.al.*, 2005; Plumb *et.al.*, 2006; Wilson *et.al.*, 2005) or the Orbitrap mass analyzer, which has got a mass resolution of 100,000 and a mass accuracy of 1 part per million (ppm) (Breitling *et.al.*, 2006; Kamleh *et.al.*, 2008), hold promise for extending mass databases and facilitate recovery and identification of potential biomarkers. Furthermore, the NMR platform is extremely compatible and can be coupled with all the described MS systems, which means that after component separation and mass detection, spectra can be acquired in the same experimental set-up (LC/GC-MS-NMR, MS-MS-NMR), and facilitate identification of unknown compounds.

7.4 Systems integration

Assessment of the biological fluids after an infection with *E. caproni*, gave a comprehensive overview on parasite-impact in the mouse host and could already enable to establish links between liquid compartments for one particular event, such as the disturbance of the microbiota which manifest as various metabolic changes in urine, plasma and also the faeces. Some major disturbances which have not been revealed or have only been hypothesised by looking at the biofluids could be captured by comparing the tissues of *E. caproni*-infected and uninfected mice.

The initial finding of depleted BCAAs valine, leucine and isoleucine in the plasma but increased levels of the same BCAAs in stool of infected animals indicated a malabsorption due to an impaired Na⁺-transporter system. Magic angle spinning (MAS) analysis of all selected tissues revealed relatively lower levels in the ileum (isoleucine, valine) and in the liver, which showed relatively lower levels of all three BCAAs. The malabsorption of various other metabolites in the ileum (e.g. ascorbate, alanine, glutamine, aspartate), confirmed a disturbed intestinal cross-membrane transport of particularly Na⁺-coupled transporters, and indicated a low tonicity in the small intestinal part. The resulting malabsorption of metabolites, in particular the diminished BCAA uptake is not dramatic in an infection with *E. caproni*, but could have serious adverse effects in the case of a concomitant liver damage (e.g. cirrhosis or liver fluke infection), as the liver would depend in this case on the regenerative function of the BCAAs (Nishitani *et.al.*, 2005; Tomiya *et.al.*, 2004).

A variety of additionally recovered biomarkers showed osmolytic activity that could suggest a potential hypertonic state in the liver, by increased betaine and phosphocholine, or hypotonic conditions in the cortical part of the kidney, manifested by decreased GPC and increased *scyllo*-inositol, respectively. However, it is more likely that the increase of phosphocholine and betaine in the liver are the response to the *E. caproni*-induced lipid degradation in the gut, which manifested in increased plasma lipid fractions from day 8 post-infection onwards, whereas the depletion of plasmatic GPC-levels is likely to be responsible for the low renal concentrations.

7.5 Trematode impact on the host central nervous system

A high worm burden and multiple infections with helminths as it is normally found in tropical and sub-tropical regions can lead to a deficient mental development of children and expresses

in cognitive impairment, including speed of information processing and short-term memory (Jukes *et.al.*, 2002). Helminth-induced anaemia, iron-deficiency and malnutrition are the main associated factors for the negative mental performance of heavily infected individuals (Guyatt, 2000; Jasti *et.al.*, 2007; Nokes and Bundy, 1994). The obvious and already well described link of helminth infections and the behaviour of the host encouraged to look for subtle biochemical changes in brain-extracts of three rodent models, i.e. *S. mansoni* and *E. caproni* in the mouse and *F. hepatic* in the rat. Apart from the known negative impact on educational outcome, schistosomes can also induce cerebral complications, particularly in normally non-exposed humans, e.g. travellers, where eggs can get in the central nervous system (CNS) and cause inflammation (Carod-Artal, 2008).

Infection with *E. caproni* did not induce any NMR-detectable changes in the neural profile, which could be either due to the relatively low sensitivity of the spectroscopic method or there was simply no effect. The *S. mansoni*-induced changes reflect an impaired ammonia detoxification by the liver (increased glutamine and decreased γ -aminobutyric acid) and disruption of the host lipid composition (decreased choline/phosphocholine). Also *F. hepatica*-infected rats showed response to liver damage in the neural profile. Whereas the liver damage following a *S. mansoni* infection is triggered by trapped eggs which induce local inflammation and necrosis (Manzella *et.al.*, 2008). *F. hepatica* larvae cause direct mechanical damage while migrating through the hepatic tissue (Lim *et.al.*, 2007). Increased passive permeability of the blood-brain barrier and failed degradation of the aromatic amino acids are likely to have contributed to the relatively higher concentrations of phenylalanine and tyrosine in the brains of the *F. hepatica*-infected rats. The assessment of the brain metabolic profile unravelled a complete systematic network between parasite-secreted enzymes, the neural nucleotide-composition of the host and the host-immunity. The initially found increase of inosine and decrease of adenosine and phosphorylated species of both, are hypothesised to be based on parasite secreted 5-nucleotidase and adenosine-dehydrogenase which convert phosphorylated inosine/adenosine and adenosine, respectively to inosine. The nucleotide shift towards inosine, in turn was believed to result in a T_H2-subtype immune response, with reduced pro-inflammatory activity to increase the host tolerance for worm-co-existence, and could be confirmed with additional cytokine concentration assessment in plasma of *F. hepatica*-infected rats (increased IL-5, IL-13 and decreased IFN- γ).

Whereas the integration of physiological compartments in the *E. caproni*-mouse model gives an overview on metabolite flow through the host system and parasite impact in a holistic manner, the additional cytokine information together with the neural changes revealed by the *F. hepatica*-rat model leads to one step further and opens up interconnection not only on multi-physiological, but also on multidisciplinary level which will ultimately lead to a deeper understanding of host-parasite dynamics, which might be harnessed for discovery of novel diagnostics, drug and vaccine targets.

It will be a challenge to gain direct applicable benefit from the identified neural biomarkers, as it is very difficult to relate metabolite quality and quantity directly to mental processes, but correlation analysis with worm burden, which has been shown to be related to severity of cognitive impairment, could be one way to gain more precise information about the causality. Ideally, one could perform behaviour tests with trematode-infected rodents and related the measures of mental performance to the neural metabolic information.

7.6 Immune response from a metabolic view

Placing the markers of an infection into a biological context, it became clear that also immune features are reflected in the metabolism of the host organism. *N*-acetyl-glycoprotein, for example, showed elevated plasma levels in *T. spiralis*-infected Swiss mice, and is being secreted by the liver as response to pro-inflammatory cytokines. The same metabolite came up again in *F. hepatic* infected Wistar rats. Inter-matrix data integration of the plasma spectra on one hand and the integrals of the neural disease markers on the other hand revealed a positive dependence of *N*- and *O*-acetyl-glycoproteine, on the neural levels of aromatic amino acids (e.g. phenylalanine and tyrosine), which acted as disease specific biomarkers in this trematode-rodent model. In-depth concentration analysis of the cytokine expression pattern introduced by the chronic infection with *F. hepatica* showed increased plasma IL-5 and IL-13 and decreased IFN- γ , which undermined our hypothesised link between the trematode-induced nucleotide imbalance and a shift in the Th-subset towards Th2 and reduced inflammation. Although general patterns can be seen amongst all infectious diseases, protozoan parasites trigger different mechanisms of immune reactions. Whereas *T. b. brucei* also induced increased concentrations of *O*-actetyl-glycoprotein levels in the plasma of infected NMRI mice, there were additional immune features reflected in the metabonome,

based on immune-evasion mechanisms of *T. b. brucei*. Degradation of the plasmatic lipoproteins and phosphatidylcholine with subsequent increase of free choline can be explained by the high turnover of the trypanosome variant surface coat (VSG) and the constant modulation of the glycoprotein (GP) anchor, for which host lipids are known to be utilized by the protozoan.

Early indication of the explanatory role which the metabolism can inhabit in immune mechanisms and our initial success to connect immune measures to metabolic compounds, e.g. cytokine levels, endorse further development towards this interdisciplinary approach and may help resolving important immunological questions in parasite induced immune mechanisms, and finding key triggers for susceptibility/resistance or Th-subset control.

7.7 Conclusion

In the current project, the main tool for metabolic profiling of biofluids and tissues obtained from rodents experimentally infected with either *E. caproni*, *F. hepatica* or *S. mansoni* has been ^1H NMR spectroscopy, because of high throughput and data generation capacities, and excellent reproducibility. Initial exploratory experiments with few sampling time-points and matrices, e.g. urine, showed the scope and potential of this new method applied for purpose of parasite diagnosis, by showing the ease of sample collection, preparation and fast analysis and recovery of biomarkers (Wang *et.al.*, 2004; Wang *et.al.*, 2006).

The present Ph.D. project shows some of the current imitations of the diagnostic potential of metabolic profiling, by evaluating diagnostic templates and technologies and defining biomarker criteria. There are a number of challenges to overcome before metabolic profiling indeed will lead to a rapid, non-invasive and practical diagnostic method, which would be applicable to all or most infectious diseases and safe the multi-diagnostic approach for parasite-infections. An attempt has been made to address potential limitations in this discussion, such as biomarker overlap between different parasitic infections, the transferability to human populations or the relatively low sensitivity of NMR for biomarker recovery, but at the same time I think that we are now in a position to provide a set of reasonable solutions. Even though we already get highly specific and qualitatively as well as quantitatively robust panels of biomarkers, we are confident that we can further enhance biomarker recovery to a higher level with additional spectroscopic methods to gain a broader

palette and detect low-abundant markers, such as parasite secretion products which would be highly disease-specific. The ultimately aim of such a strategy is to collect disease-specific fingerprints from one or two determined biological matrices, for each of the most important tropical parasite diseases, on a portable diagnostic dip-stick, which is cheap, field-applicable.

7.8 Future research

- Expansion of the metabolic profiling approach to other spectroscopic technologies for broader metabolic coverage and higher sensitivity, with preferentially LC-MS, GC-MS and capillary electrophoresis (CE)-MS, using high resolution mass spectrometers.
- Further comprehensive studies on biofluids and tissues in single-species parasitic infections in suitable rodent models with particular emphasis on biomarker extraction in the biofluids and in depth-assessment of the CNS-impact.
- Thorough evaluation of the candidate diagnostic biomarkers.
 - Proposed criteria:
 - Specificity to infection/disease
 - Intra-species transferability
 - Reproducibility
 - Stability over time
 - Transferability through species, human in particular
 - Stability through different infection-intensities
- Extracting biomarkers in well selected human populations and compare to existing rodent database.
- Extensive assessment of co- and multi-infection in suitable rodent models, primarily to assess the impact of additional parasite species to candidate single-infection biomarker, but also to exploring the benefits of different helminths to protozoan infections
- Higher degree of immunological and physiological monitoring of the host, including cytokine-level assessment and gut-microbial co-monitoring of parasitic infections
- Metabolic profiling of parasite and intermediate host *via* NMR and MS-based methods in order to profile different stages and habitats in the parasite life cycle and additionally explore the metabolic features in drug-resistant parasite strains.
- Behaviour tests with trematode-infected rodents, relating the measures of mental performance to the neural metabolic information.
- Assessment of the increased severity of a liver damage in a co-infection of *F. hepatic* and *E. caproni*, compared to *F. hepatica* single-infection.

7.9 References

- Barker H.A., D'Ari L., Kahn J. 1987. Enzymatic reactions in the degradation of 5-aminovaleate by *Clostridium aminovaleericum*. *J Biol Chem* **262**(19):8994-9003.
- Beckonert O., Keun H.C., Ebbels T.M., Bundy J., Holmes E., Lindon J.C., Nicholson J.K. 2007. Metabolic profiling, metabolomic and metabonomic procedures for NMR spectroscopy of urine, plasma, serum and tissue extracts. *Nat Protoc* **2**(11):2692-703.
- Boivin M.J.C., C.; Giordani, B.; Xaisida, S. 1996. Validating a cognitive ability testing protocol with Lao children for community development. *Neuropsychology* **10**(4):588-99.
- Breitling R., Pitt A.R., Barrett M.P. 2006. Precision mapping of the metabolome. *Trends Biotechnol* **24**(12):543-8.
- Carod-Artal F.J. 2008. Neurological complications of *Schistosoma* infection. *Trans R Soc Trop Med Hyg* **102**(2):107-16.
- Clayton T.A., Lindon J.C., Everett J.R., Charuel C., Hanton G., Le Net J.L., Provost J.P., Nicholson J.K. 2004. Hepatotoxin-induced hypercreatinemia and hypercreatinuria: their relationship to one another, to liver damage and to weakened nutritional status. *Arch Toxicol* **78**(2):86-96.
- Cook S.I., Sellin J.H. 1998. Review article: short chain fatty acids in health and disease. *Aliment Pharmacol Ther* **12**(6):499-507.
- de Clercq D., Sacko M., Behnke J., Gilbert F., Vercruyse J. 1998. The relationship between *Schistosoma haematobium* infection and school performance and attendance in Bamako, Mali. *Ann Trop Med Parasitol* **92**(8):851-8.
- Foxall P.J., Parkinson J.A., Sadler I.H., Lindon J.C., Nicholson J.K. 1993. Analysis of biological fluids using 600 MHz proton NMR spectroscopy: application of homonuclear two-dimensional J-resolved spectroscopy to urine and blood plasma for spectral simplification and assignment. *J Pharm Biomed Anal* **11**(1):21-31.
- Guarner F., Malagelada J.R. 2003. Gut flora in health and disease. *Lancet* **361**(9356):512-9.
- Guyatt H. 2000. Do intestinal nematodes affect productivity in adulthood? *Parasitol Today* **16**(4):153-8.
- Hardman J.K., Stadtman T.C. 1960. Metabolism of omega-acids. II. Fermentation of delta-aminovaleic acid by *Clostridium aminovaleericum* n. sp. *J Bacteriol* **79**:549-52.
- Hewitson J.P., Harcus Y.M., Curwen R.S., Dowle A.A., Atmadja A.K., Ashton P.D., Wilson A., Maizels R.M. 2008. The secretome of the filarial parasite, *Brugia malayi*: proteomic profile of adult excretory-secretory products. *Mol Biochem Parasitol* **160**(1):8-21.
- Holmes E., Foxall P.J., Nicholson J.K., Neild G.H., Brown S.M., Beddell C.R., Sweatman B.C., Rahr E., Lindon J.C., Spraul M. and others. 1994. Automatic data reduction and pattern recognition methods for analysis of ¹H nuclear magnetic resonance spectra of human urine from normal and pathological states. *Anal Biochem* **220**(2):284-96.
- Jasti A., Ojha S.C., Singh Y.I. 2007. Mental and behavioral effects of parasitic infections: a review. *Nepal Med Coll J* **9**(1):50-6.
- Jukes M.C., Nokes C.A., Alcock K.J., Lambo J.K., Kihamia C., Ngorosho N., Mbise A., Lorri W., Yona E., Mwanri L. and others. 2002. Heavy schistosomiasis associated with poor short-term memory and slower reaction times in Tanzanian schoolchildren. *Trop Med Int Health* **7**(2):104-17.

- Kamleh A., Barrett M.P., Wildridge D., Burchmore R.J., Scheltema R.A., Watson D.G. 2008. Metabolomic profiling using Orbitrap Fourier transform mass spectrometry with hydrophilic interaction chromatography: a method with wide applicability to analysis of biomolecules. *Rapid Commun Mass Spectrom* **22**(12):1912-8.
- Kennedy P.G. 2004. Human African trypanosomiasis of the CNS: current issues and challenges. *J Clin Invest* **113**(4):496-504.
- Kussmann M., Raymond F., Affolter M. 2006. OMICS-driven biomarker discovery in nutrition and health. *J Biotechnol* **124**(4):758-87.
- Lim J.H., Kim S.Y., Park C.M. 2007. Parasitic diseases of the biliary tract. *AJR Am J Roentgenol* **188**(6):1596-603.
- Manzella A., Ohtomo K., Monzawa S., Lim J.H. 2008. Schistosomiasis of the liver. *Abdom Imaging* **33**(2):144-50.
- Martini S., Eichinger F., Nair V., Kretzler M. 2008. Defining human diabetic nephropathy on the molecular level: Integration of transcriptomic profiles with biological knowledge. *Rev Endocr Metab Disord*.
- Mehta M., Sonawat H.M., Sharma S. 2005. Malaria parasite-infected erythrocytes inhibit glucose utilization in uninfected red cells. *FEBS Lett* **579**(27):6151-8.
- Nicholls A.W., Mortishire-Smith R.J., Nicholson J.K. 2003. NMR spectroscopic-based metabolomic studies of urinary metabolite variation in acclimatizing germ-free rats. *Chem Res Toxicol* **16**(11):1395-404.
- Nicholson J.K. 2006. Global systems biology, personalized medicine and molecular epidemiology. *Mol Syst Biol* **2**:52.
- Nicholson J.K., Foxall P.J., Spraul M., Farrant R.D., Lindon J.C. 1995. 750 MHz ^1H and ^1H - ^{13}C NMR spectroscopy of human blood plasma. *Anal Chem* **67**(5):793-811.
- Nishitani S., Takehana K., Fujitani S., Sonaka I. 2005. Branched-chain amino acids improve glucose metabolism in rats with liver cirrhosis. *Am J Physiol Gastrointest Liver Physiol* **288**(6):G1292-300.
- Nokes C., Bundy D.A. 1994. Does helminth infection affect mental processing and educational achievement? *Parasitol Today* **10**(1):14-8.
- Plumb R.S., Granger J.H., Stumpf C.L., Johnson K.A., Smith B.W., Gaulitz S., Wilson I.D., Castro-Perez J. 2005. A rapid screening approach to metabolomics using UPLC and oa-TOF mass spectrometry: application to age, gender and diurnal variation in normal/Zucker obese rats and black, white and nude mice. *Analyst* **130**(6):844-9.
- Plumb R.S., Johnson K.A., Rainville P., Shockcor J.P., Williams R., Granger J.H., Wilson I.D. 2006. The detection of phenotypic differences in the metabolic plasma profile of three strains of Zucker rats at 20 weeks of age using ultra-performance liquid chromatography/orthogonal acceleration time-of-flight mass spectrometry. *Rapid Commun Mass Spectrom* **20**(19):2800-6.
- Rochfort S. 2005. Metabolomics reviewed: a new "omics" platform technology for systems biology and implications for natural products research. *J Nat Prod* **68**(12):1813-20.
- Schmidt G.D.R., L. S. 2000. Foundations of parasitology.
- Sigdel T.K., Sarwal M.M. 2008. The proteogenomic path towards biomarker discovery. *Pediatr Transplant*.
- Tang H., Wang Y., Nicholson J.K., Lindon J.C. 2004. Use of relaxation-edited one-dimensional and two dimensional nuclear magnetic resonance spectroscopy to improve detection of small metabolites in blood plasma. *Anal Biochem* **325**(2):260-72.
- Tomiya T., Omata M., Fujiwara K. 2004. Branched-chain amino acids, hepatocyte growth factor and protein production in the liver. *Hepatol Res* **30S**:14-8.

- Visser N., Opperdoes F.R. 1980. Glycolysis in *Trypanosoma brucei*. *Eur J Biochem* **103**(3):623-32.
- Wang Y., Holmes E., Nicholson J.K., Cloarec O., Chollet J., Tanner M., Singer B.H., Utzinger J. 2004. Metabonomic investigations in mice infected with *Schistosoma mansoni*: an approach for biomarker identification. *Proc Natl Acad Sci U S A* **101**(34):12676-81.
- Wang Y., Utzinger J., Xiao S.H., Xue J., Nicholson J.K., Tanner M., Singer B.H., Holmes E. 2006. System level metabolic effects of a *Schistosoma japonicum* infection in the Syrian hamster. *Mol Biochem Parasitol* **146**(1):1-9.
- Watkins W.E., Pollitt E. 1997. "Stupidity or worms": do intestinal worms impair mental performance? *Psychol Bull* **121**(2):171-91.
- Wilson I.D., Nicholson J.K., Castro-Perez J., Granger J.H., Johnson K.A., Smith B.W., Plumb R.S. 2005. High resolution "ultra performance" liquid chromatography coupled to oa-TOF mass spectrometry as a tool for differential metabolic pathway profiling in functional genomic studies. *J Proteome Res* **4**(2):591-8.
- Wong J.M., de Souza R., Kendall C.W., Emam A., Jenkins D.J. 2006. Colonic health: fermentation and short chain fatty acids. *J Clin Gastroenterol* **40**(3):235-43.
- Yap I.K., Clayton T.A., Tang H., Everett J.R., Hanton G., Provost J.P., Le Net J.L., Charuel C., Lindon J.C., Nicholson J.K. 2006. An integrated metabonomic approach to describe temporal metabolic dysregulation induced in the rat by the model hepatotoxin allyl formate. *J Proteome Res* **5**(10):2675-84.

Table 7.1

	Biomarkers in Urine					Infections per marker
	<i>Plasmodium berghei</i>	<i>Trypanosoma b. brucei</i>	<i>Schistosoma mansoni</i>	<i>Schistosoma japonicum</i>	<i>Echinostoma caproni</i>	
2-ketoisocaproate					▼	1
2-oxoglutarate			▼			1
2-oxoisocaproate	▲		▼			2
2-oxoisovalerate	▲	▲	▼			3
3-carboxy-2-methyl-3-oxopropanamine		▲				1
3-hydroxybutyrate		▲				1
3-methyl-2-oxovalerate	▲	▲				2
4-hydroxyphenylacetic acid		▲				1
acetate	▲		▼	▲	▼	4
alanine			▼			1
butyrate			▼			1
citrate			▼	▼		2
creatine			▲		▼	2
creatinine	▲					1
dimethylamine	▲			▼		2
formate	▲					1
glucose					▼	1
glycerol				▲		1
hippurate		▼	▼	▼	▼	4
lactate		▲		▼		2
malonate			▼			1
mannitol					▲	1
methylcrotonic acid		▼				1
<i>p</i> -cresolglucuronide			▲	▲	▲	3
phenylacetylglucine	▲		▲	▲	▲	4
pipecolic acid	▲					1
propionate			▼	▼		2
pyruvate			▲	▲		2
succinate			▼	▼	▲	3
taurine	▲		▼		▼	3
trimethylamine		▲	▲	▲	▲	4
trimethylamine-N-oxide	▼				▲	2
tryptophan		▲	▲			2
β-alanine			▲			1
Number of disease specific markers	7	5	8	3	6	

Table 7.2

	Biomarkers in Plasma				Infections per marker
	<i>Plasmodium berghei</i>	<i>Trypanosoma b. brucei</i>	<i>Echinostoma caproni</i>	<i>Trichinella spiralis</i>	
3-hydroxybutyrate				▲	1
acetate	▼	▲	▲	▼	4
acetoacetate				▲	1
alanine				▲	1
arginine				▲	1
cholesterol		▲		▼	2
choline		▲	▼	▲	3
citrate	▲			▲	2
creatine	▼	▲	▼	▲	4
ethanolamine				▲	1
formate			▲		1
glucose	▼	▼	▼		3
glutamate				▲	1
glutamine		▼		▲	2
glyceophosphocholine	▼		▼	▼	3
glycerol				▲	1
isoleucine		▼	▼	▼	3
lactate	▲	▲		▲	3
leucine		▼	▼		2
lipid fractions		▼	▲	▼	3
lysine		▲		▲	2
methionine				▲	1
<i>N</i> -acetyl-glycoproteine				▲	1
<i>O</i> -acetyl-glycoproteine		▲			1
oxaloacetate		▲			1
phosphatidylcholine		▼			1
phosphocholine				▲	1
pyruvate	▲				1
tyrosine				▲	1
valine		▼	▼		2
Number of disease specific markers	1	5	3	13	



Curriculum vitae

Personal data

Full name Jasmina Saric
Place, date of birth Neuhausen, 31.07.1978
Marital status Single
Nationality Swiss

Address Work Swiss Tropical Institute
Department of Public Health and Epidemiology
Socinstrasse
4051 Basel, Switzerland

Tel.: (office) +41 (0)61 284 8226
Fax +41 (0)61 284 8101
E-mail jasmina.saric@stud.unibas.ch

57

Current position

01.10.2005 – 06.11.2008 **Ph.D.-Student**
System-level metabolic effects of trematode infections in rodent models
Swiss Tropical Institute, Basel – Switzerland

Education

1993-1998 High School
Kantonsschule Schaffhausen
C-Matura; Equivalent to **A-levels** with Emphasis in Sciences

1998 - 2004 **MSc**
Eidgenössisch Technische Hochschule Zurich, ETH Zurich (Swiss Federal Institute of Technology)

Main Subjects Biochemistry *Immunology
Medical Parasitology Pharmacology
Toxicology Cancer Genetics

*Diploma work Establishment and evaluation of techniques for assessing HIV-specific CD4⁺ T-cell frequency.

Computer literacy MS Office, Matlab, Simca, Masslynx, Markerlynx, AMIX, MZmine, XWIN-NMR, Topspin, Adobe Illustrator, ISIS Draw

Languages

German:	Mother tongue
English:	Very good (written/spoken)
French:	Basic (written/spoken)
Serbo-Croatian:	Basic (written/spoken)

Driving licence Category B (cars)

Professional Membership: **Member of the British Society of Parasitology**

Presentations, Prizes and organisational activities

January 2006 **Lecture**, Swiss Tropical Institute, Basel, **High resolution NMR spectroscopy in the field?**

June 2007 **Lecture**, Three Country Parasitology Meeting, Faculté de Médecine de l'Université Louis Pasteur, Strasbourg, **Experimental infection in mice with the intestinal fluke *Echinostoma caproni*. Does metabonomics offer a new approach in parasite diagnostic?**

November 2007 **Lecture**, METAGRAD Meeting, Imperial College, **Specificity of biomarkers: Review of 7 parasite-animal models in metabonomics.**

June 2006 **Poster Presentation**, Systems Biology Meeting, Imperial College London, **Metabonomic Profiling of *Fasciola hepatica* infection in the rat.**

1.-5. October 2007 **Organisation of workshop and symposium, Metabonomics Workshop 2007**, Imperial College London

4. June 2008 **Lecture**, Imperial College London, **Biomarker Discovery in Infectious Diseases**

21.-27. June 2008 **Poster Presentation**, Gordon Conference, Host-Parasite Interactions, Salve Regina University, Newport, US, **Trematode induced changes in the brain metabolic profile**

03. September 2008 **Lecture & organisation of symposium**, "Metabolic profiling of infectious diseases – New technologies in biomarker recovery", Imperial College London, **Trematode induced alterations of brain metabolism in the rodent host**

October 2008 **Travelgrant**, obtained from Basel University

08. Dezember 2008 **Lecture** at ASTMH - The American society of tropical medicine and hygiene - annual meeting, 7.-11 Dec., New Orleans, **Trematode induced alterations of brain metabolism in the rodent host**

Work and Laboratory Experience

Research Assistant: Plantphysiology ETH Zürich

Diploma Thesis: **Class 3 Bio safety** (cultivation of HIV, ETH Zurich and Zürich University Hospital)

Diploma Thesis: **Class 3 Bio safety** (cultivation of HIV, ETH Zurich and Zürich University Hospital)

Diploma Thesis: **Cell biology** (cultivation and generation of dendritic cells, **FACS**, **MACS**)

Eprova AG Merck: **Sterile** Work hoods (Eprova, Water quality control; cultivation of bacteria)

PhD: ^1H , ^1H - ^{13}C , ^1H - ^1H **NMR spectroscopy** (Imperial College London) on 400, 600 and 800 MHz Spectrometers of Imperial College Facility

PhD: **UPLC-MS** (AstraZeneca Macclesfield, Manchester) on Q-ToF

PhD: **Animal Course 2006** (Zürich University)

PhD: **Animal Work** (Swiss Tropical Institute, Parasite-Rodent models)

PhD: **Microbiology**; Gen extraction, PCR and DGGE (Cork University, Cork, Ireland)

Current Research

My PhD project research is focused on NMR spectroscopic based approaches to profiling perturbations in biofluids and tissues from rodent-parasite models with a view to characterising the metabolic responses that reflect host-parasite interactions and find a new angle in parasite diagnostic. Particular consideration has been given to food-borne trematodiasis (intestinal fluke *Echinostoma caproni*) with further investigations pertaining to *Schistosoma mansoni*, *Plasmodium berghei* and *Trypanosoma brucei brucei* in suitable rodent models. The metabolic signature of these infections are unique to each host-parasite model and the aim of future research is to evaluate whether the panel of diagnostic biomarkers detected in the experimental models can be extrapolated into human – parasite disease, and further to establish if any of these changes will provide a reliable metric for evaluating response to therapeutic interventions. In addition to the metabolic profiling, conventional measures of parasitic infection were applied, such as histopathological monitoring of the structural damage in tissues and microbiological techniques (gene extraction, PCR and DGGE) on the stool samples obtained from experimentally infected animals. The latter aimed to explore the interaction between parasitic infection and consequential changes in the host microbiota, since gastrointestinal symptoms are a well documented effect of many parasitic infections.

PhD supervisors:

Prof. Juerg Utzinger
Swiss Tropical Institute
Department of Epidemiology
and Public Health
Socinstrasse 57
4002 Basel, CH

Prof. Elaine Holmes
Imperial College
Department of Biomolecular
Medicine
SAF, South Kensington,
London, UK

Publications

1. **Saric, J**; Wang, Y; Li J.V; Coen M; Utzinger J; Marchesi J.R; Keiser J; Veselkov K; Lindon J.C; Nicholson J.K; Holmes E; Species variation in the fecal metabolome gives insight into differential gastrointestinal function. *J Prot Res* 7(1): 352-360 (2008)
 2. Keun H.C; Athersuch T.J; Beckonert O; Wang Y; **Saric J**; Shockcor J.P; Wilson I.D; Holmes E; Nicholson J.K; Heteronuclear (^{19}F - ^1H) Statistical total correlation spectroscopy as a new tool in drug metabolism: a study of flucloxacillin biotransformation. *Anal Chem* 80:1073-1079 (2008)
 3. Wang Y; Utzinger J; **Saric J**; Li J.V; Nicholson J.K; Singer B.H; Brun R; Holmes E; Global metabolic responses of mice to *Trypanosoma brucei brucei* infection. *PNAS* 105(16): 6127-32 (2008)
 4. **Saric, J**; Li J.V; Wang, Y; Keiser J; Dirnhofner S; Marchesi J.R; Holmes E; Utzinger J; (2008) Metabolic profiling of an *Echinostoma caproni* infection in the mouse for biomarker discovery. *Plos NTD* 2(7):e254 (2008)
 5. **Saric, J**; Li J.V; Wang, Y; Holmes E; Utzinger J; Keiser J; Use of *Echinostoma* spp. in studies on chemotherapy and metabolic profiling. To be published in “*The Biology of Echinostomes*”, Fried B and Toledo R., Springer Science
 6. Yap I.K.S; Li J.V; **Saric J**; Martin F.P; Davies H; Wang Y; Wilson I.D; Nicholson J.K; Utzinger J; Marchesi J.R; Holmes E; Metabonomic and microbiological analysis of the dynamic effect of vancomycin-induced gut microbiota modification in the mouse. *J Prot Res* 7(9):3718-3728 (2008)
 7. Li J.V; Wang Y; **Saric J**; Nicholson J.K; Dirnhofner S; Singer B.H; Tanner M; Wittlin S; Holmes E; Utzinger J; Global metabolic responses of NMRI mice to an experimental *Plasmodium berghei* infection. *J Prot Res* 7(9):3948-3956 (2008)
 8. Li J.V; Holmes E; **Saric J**; Keiser, J; Dirnhofner S; Utzinger J; Wang Y; Metabolic profilig of a *Schistosoma mansoni* infection in mouse tissues using magic angle spinning-nuclear magnetic resonance spectroscopy. submitted to *Int J Parasitol* (2008)
 9. **Saric J**; Li J.V; Wang Y; Keiser, J; Beckonert, O; Utzinger J; Nicholson J.K; Holmes E; Trematode-induced modulation of CNS metabolic profiles. submitted to *PLoS Pathogens* (2008)
 10. Li J.V; **Saric J**; Wang Y; Utzinger J; Balmer, O; Holmes E; Metabolic profiling of co-infection of *Trypanosoma brucei brucei* strains in mice. submitted to *PLoS Pathogens* (2008)
-

Introduction

To my scientific Family

“Quand tu veux construire un bateau, ne commence pas par rassembler du bois, couper des planches et distribuer du travail, mais reveille au sein des hommes le desir de la mer grande et large.”

Antoine de Saint-Exupéry

“If you want to build a ship, don't drum up people together to collect wood and don't assign them tasks and work, but rather teach them to long for the endless immensity of the sea”

Antoine de Saint-Exupéry

